

University of Bath



PHD

Synthesis of Redox-Active Probes for the Multiplex Detection of DNA

Sharp, Jonathan

Award date:
2013

Awarding institution:
University of Bath

[Link to publication](#)

General rights

Copyright and moral rights for the publications made accessible in the public portal are retained by the authors and/or other copyright owners and it is a condition of accessing publications that users recognise and abide by the legal requirements associated with these rights.

- Users may download and print one copy of any publication from the public portal for the purpose of private study or research.
- You may not further distribute the material or use it for any profit-making activity or commercial gain
- You may freely distribute the URL identifying the publication in the public portal ?

Take down policy

If you believe that this document breaches copyright please contact us providing details, and we will remove access to the work immediately and investigate your claim.

Download date: 23. May. 2019

Synthesis of Redox-Active Probes for the Multiplex Detection of DNA

Jonathan Oliver Sharp

A thesis submitted for the degree of Doctor of Philosophy

University of Bath

Department of Chemistry

September 2012

COPYRIGHT

Attention is drawn to the fact that copyright of this thesis rests with the author. A copy of this thesis has been supplied on the condition that anyone who consults it is understood to recognise that its copyright rest with the author and that they must not copy it or use material from it except as permitted by law or with consent of the author.

This thesis may not be consulted, photocopied or lent to other libraries without the permission of the author / Atlas Genetics for two years from the date of acceptance of the thesis.

J. O. Sharp

Dedicated to
Dorothy Gardiner

Acknowledgements

First of all I would like to thank my supervisor Prof. Chris Frost for all his help, support and guidance during the course of my studies. I would also like to extend a big thank you to all the folks at Atlas Genetics for the highly interesting project. Special thanks to David Pearce, Dan Shenton and Marc Green for all their guidance and help in the realms of a biology lab.

Cheers to all the Frost group members past and present who have made my time here in the lab enjoyable. I would like to thank Dr. Barrie Marsh for his help, guidance and proof-reading during the writing of Thesis.

I would like to say a big thank you to Dr. Joseph Allen, Dr. Jimmy (Hobbit) White for the good but normally strange conversation, beers, help and support.

I would like to say a special thank you to Dr. Steve (Old man river) Flower and Sean Goggins for your some times extremely strange conversations, laughs and being the co-founders of chair cricket.

Contents

1	Introduction : Electrochemical DNA Sensors	1
1.1	DNA Structure and Function	2
1.2	DNA hybridisation and Detection Assays.....	4
1.3	Polymerase chain reaction.....	6
1.4	DNA Hybridisation Sensors <i>via</i> Electrochemical transducer methods	8
1.4.1	Direct hybridisation analysis	8
1.4.2	Non Covalent Label Detection Approaches	11
1.4.3	Covalently Labelled Probes.....	18
1.4.4	Nanoparticle Based DNA Detection	27
1.4.5	Enzymatic Based DNA Detection	29
1.5	Nanopore Electrochemical DNA Detection.....	31
1.6	Introduction of Ferrocene in DNA sensing.....	35
1.7	Conclusions	56
2	Chapter 2: The Synthesis of Mono-ferrocenyl Labels for the use as DNA Probes.....	57
2.1	Atlas Genetics, T7 exonuclease assay	57
2.2	Aims and Previous work.....	61
2.3	Results and Discussion	64
2.4	Conclusion.....	90
3	Chapter 3: The synthesis of Di-ferrocenyl labels for the use as DNA Probes	93
3.1	Background	93
3.2	Results and Discussion	99
3.3	Conclusion.....	116
4	Chapter 4: The Analysis of Unique Redox-Active DNA probes in the Atlas DNA Detection Assay.....	119
4.1	Background	119
4.2	Results and Discussion	120
4.3	Conclusion.....	140
5	Chapter 5: The synthesis of 2-Oxazolines and The Ring-Opening Reaction for the use as an Analytical Tool for Carboxylic Acids	143
5.1	Background	143
5.2	Ring-opening reactions of 2-oxazolines	146
5.3	Aims and Objectives.....	153
5.4	Results and Discussion	154
5.5	Conclusion.....	168

6	Future Work	169
7	Experimental	171
7.1	General Considerations.....	171
7.2	General electrochemical procedure	172
7.3	Synthesis of mono-ferrocenyl redox active labels.....	173
7.4	Synthesis of di-ferrocenyl redox active labels	207
7.5	Synthesis of Oxazolines.....	227
8	References	251
9	Appendix	260

Abstract

The research presented within this thesis is concerned with the design and synthesis of redox-active derivatives for the use as labels for DNA probes to be used in a commercial DNA detection assay.

Chapter 1: Introduces the area of electrochemical DNA sensing, the methods used and the transducer derivatives used. Also included within this chapter is the discussion on the use of ferrocene and its derivatives as redox-active transducer moieties and their use in a DNA sensing capacity.

Chapter 2: Introduces the sponsoring company, Atlas genetics, and the DNA detection assay they are developing for use in a point of care device (POC). The chapter also details the design, synthesis and electrochemical analysis *via* differential pulse voltammetry of mono-ferrocenyl derivatives for the use as redox-active labels for DNA sensing. The chapter outlines the development of labels containing a variety of functionality as well as possessing a range of oxidation potentials from 95 to 610 mV (vs Ag/AgCl).

Chapter 3: Introduces and details the sensitivity issues between mono-ferrocenyl and di-ferrocenyl labels and the effect this could have on the commercial DNA detection assay. Within this chapter there are the details of the design, synthesis and electrochemical analysis *via* differential pulse voltammetry of the di-ferrocenyl labels. The chapter shows the synthesis of di-ferrocenyl labels containing a wide range of functionality on both the ferrocene core as well as the linker unit, with the labels possessing a range of oxidation potentials from 242 to 500 mV (vs. Ag/AgCl).

Chapter 4: Discusses the use of the labels designed and synthesised in chapters 2 and 3 in the commercial DNA detection assay developed by Atlas genetics. The development of the labels used as DNA probes in the DNA detection assay and their ability to be used in multiplex DNA detection assays are also described. Demonstrated within this chapter is the use of the labels synthesised in this thesis that give both a duplex between two different probes and also the development of a triplex assay using three different labels to detect for two different target DNAs as well as provide an internal control.

Chapter 5: Introduces the synthetic methods towards the synthesis of 2-oxazolines and discusses their use within ring-opening reactions. This chapter details the optimisation of the ring-opening reaction of phenyl-2-oxazoline with a range of carboxylic acid derivatives. The synthesis of a range of 2-oxazolines with various functionality aimed towards the analytical detection of carboxylic acids through the direct conjugation with 2-oxazolines. The ring-opening reaction was found to tolerate a wide range of carboxylic acid derivatives as well as a variety of functionality on the 2-oxazolines such as ferrocene-2-oxazolines and also 3,5 – *bis*(trifluoromethyl)phenyl-2-oxazoline. The use of ferrocene-2-oxazoline allowed for the electrochemical detection of carboxylic acids and the 3,5 – *bis*(trifluoromethyl)phenyl-2-oxazoline allows for the detection of carboxylic acids through its ring-opened form *via* ^{19}F NMR. These two functionalised 2-oxazolines were used to further analyse the reactions viability as a possible analytical tool for the detection of carboxylic acids by carrying out the ring-opening reaction conditions for the detection of ibuprofen from an over the counter tablet.

Abbreviations

δ Chemical shift in ppm

A Adenosine

AIBN azobisisobutronitrile

anhyd. Anhydrous

app. Apparent

aq. Aqueous

AQMS anthraquinone monosulfonic acid

ATP adenosine triphosphate

BMS borane dimethylsulfide

Bn Benzyl

Boc *tert*-Butyloxycarbonyl

br Broad

C deoxycytidine

CDI 1,1'-carbonyldiimidazole

CH₂Cl₂ dichloromethane

Co(bpy)₃³⁺ Tris(2,2'-bipyridyl)cobalt

Cp Cyclopentadienyl

CROP cationic ring-opening polymerisation

CuBr copper bromide

d Doublet

dsDNA double-stranded DNA

DBU 1,8-diazabicyclodec-7-ene

DCC Dicyclohexylcarbodiimide

DIPEA *N,N*-Diisopropylethylamine

DNA deoxyribonucleic acid

DMF *N,N*-dimethylformamide

DMSO Dimethyl sulfoxide

DMT dimethoxytrityl

EDCI/EDC 1-ethyl-3-(3-dimethylaminopropyl) carbodiimide

FAD flavin adenine dinucleotide

Fc Ferrocene, or, in combination: Ferrocenyl

Fc⁺ ferrocenium ion

G Guanosine

g Gram(s)
GOD glucose oxidase
H₂O water
HOBT hydroxybenzotriazole
hr Hour(s)
HPLC high-performance liquid chromatography
HRP horse raddish peroxidase
Hz Hertz
J Coupling constant in Hz
KOH potassium hydroxide
MeCN Acetonitrile
Mes Mesylate
min Minute(s)
mol Mole(s)
MsCl methane sulfonyl chloride
NHS *N*-hydroxy succinimide
NMR nuclear magnetic resonace
NP nanoparticle
PCR polymerase chain reaction
PHPB pyridinium hypobromide
PNA peptide nucleic acid
q Quartet
r.t. Room temperature
s Singlet
SAM self-assembled monolayer
ssDNA single-stranded DNA
T thymidine
t Triplet
TBAF tetrabutylammonium fluoride
TEA triethyl amine
TFA trifluoroacetic acid
THF Tetrahydrofuran
TMS Trimethylsilyl
U uridine

1 Introduction : Electrochemical DNA Sensors

The development of novel biosensors is a field of great interest, due to the wide range of applications that have a use for biosensors such as; the food industry,¹ defence against biological weapons,² environmental applications,³ biological and pharmacological research and medical diagnostics.⁴ A biosensor can be described as a compact analytical device that contains a biologically derived sensor component that is closely linked with a physicochemical transducer (Figure 1.1), the physicochemical transducer can involve a range of methods⁵⁻⁷ such as electrochemical (e.g. potentiometric)⁸ or optical.⁹

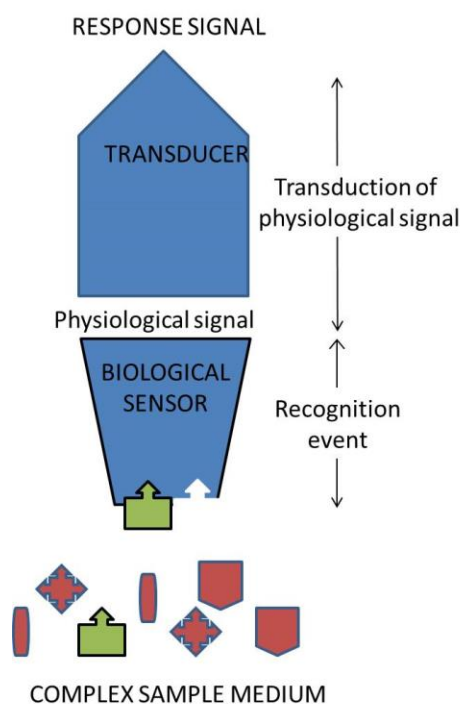


Figure 1.1: Schematic of a biosensor

The common aim that all biosensors share is to produce a digital signal that is quantitative and is directly related to a single analyte or related family of analytes.¹⁰ The biological component could be an enzyme,¹¹ antibody¹² or nucleic acid¹³ and in some cases a whole cell.¹⁴

The ability to detect specific sequences of DNA is at the heart of the diagnosis of both genetic diseases and infectious disease causing pathogens. Fluorescent and colorimetric detection methods are the most established transducer approaches.¹⁵⁻¹⁶ The use of optical detection methods such as fluorescence has a number of disadvantages for the development of biosensors. The main disadvantage is that optical detection methods require expensive, often large and sophisticated equipment that usually requires a trained operator to run and maintain the system. Fluorescent detection methods are also susceptible to photobleaching of the reporter moiety, which is the inactivation of the reporter moiety. This has an effect on the sensitivity of the technique and also on the life-time of the reporter moieties. However using electrochemical detection methods holds a number of advantages over these detection methods. Advantages such as the simplicity at which the systems can be miniaturised and the fact that a direct electrical response is received, therefore no further analysis of the signaling response is required.

1.1 DNA Structure and Function

Deoxyribonucleic acid (DNA) consists of two chains of deoxyribonucleotides that are joined together *via* a phosphodiester bonds from the 5 carbon of one nucleotide and the 3 carbon of another nucleotide. The individual strands are labelled at each end as either 5' or 3' depending on which end groups terminates the ends of the chains (Figure 1.2).

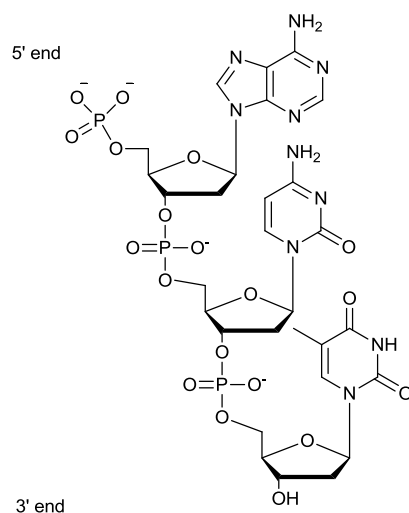


Figure 1.2: Structure of DNA

Deoxyribonucleotides are made up of deoxyribose sugars with a nitrogenous base substituents. DNA contains four different nitrogenous bases: adenine (A), Cytosine (C), Guanine (G) and Thymine (T). These four bases are further divided into two subgroups purines (A and G) and pyrimidines (C and T), this is due to the difference in the structures of the nucleoside bases. Purines are made up of bis-heterocycle rings whereas pyrimidines are made up of only one heterocycle ring. Within double stranded DNA the nucleotide bases interact through hydrogen bonding and pair up into specific base pair units adenine and thymine and the other pair of cytosine and guanine (Figure 1.3).

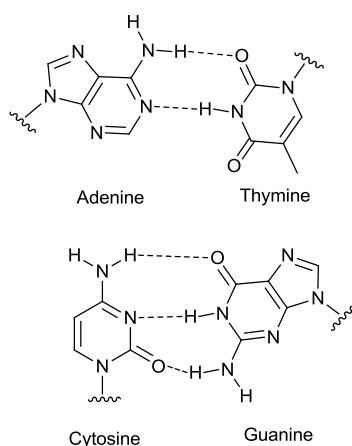
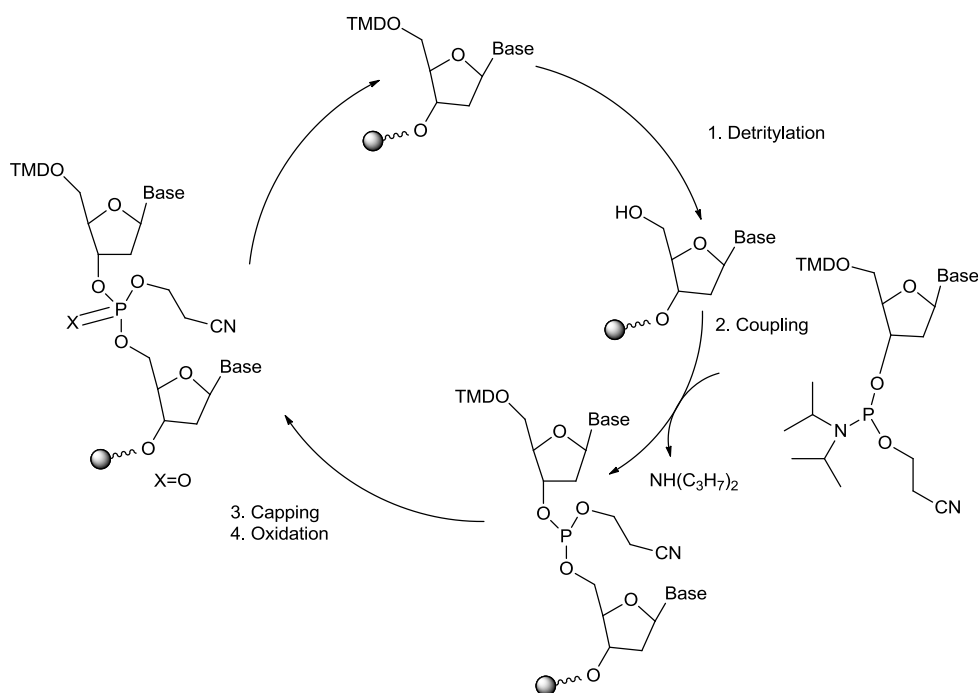


Figure 1.3: H-bonding between the bases

1.2 DNA hybridisation and Detection Assays

In a DNA assay the hybridisation between a target DNA and a DNA probe is followed by a detection event. Single-stranded DNA (ssDNA) is used as a probe due to the specificity of DNA hybridisation, which can also be controlled by stringency. Stringency has an effect on the selectivity of the hybridisation, if the DNA hybridisation conditions are carried out under high stringency such as high temperature and low salt concentration in the buffer solution this leads to only highly complementary DNA strands hybridising. Whereas with lower stringency strands that are not fully complementary are able to hybridise, leading to base-pair mismatches. The hybridisation can be detected by a wide range of techniques. The DNA probe is usually a shorter DNA strand which is complementary to a specific region on the target DNA. These DNA probes are typically synthetic oligonucleotides, which are usually synthesised with the desired sequence and normally the probes are labelled with the reporter moiety. Probe oligonucleotides are normally shorter strands of synthetically made DNA which are usually between 20-40 nucleotides in length, the use of longer oligonucleotides does form duplexes with higher stability however their hybridisation with the target DNA takes longer than shorter oligonucleotide probes. Oligonucleotides are typically synthesised using an automated solid supported oligonucleotide synthesiser, this enables the oligonucleotides to be synthesised with the desired sequence. The oligonucleotides are built up from the 3' end of the strand which is loaded on the solid support. The oligonucleotides are built up one nucleotide at a time, with each nucleotide addition going through a synthetic cycle (Scheme 1.1). The synthetic cycle goes through four main steps; Detritylation, coupling, capping and oxidation. The detritylation step can also be known as de-blocking, it is the deprotection of the DMT protecting group. The deprotection is carried out under acidic conditions in an inert organic solvent. The coupling is then carried out between the now deprotected hydroxyl group at the 5'terminal of the strand and the 3'-terminal phosphoramidite of the next nucleoside. The coupling is typically carried out in acetonitrile (MeCN) in the presence of an acidic azole catalyst such as 1*H*-tetrazole. Post the coupling step in the synthetic cycle there is a capping step, in which the solid supported strand is treated with acetic anhydride and usually 1-methylimidazole as the catalyst. The capping step

serves to permanently block off any un-reacted 5'-hydroxyl groups, to guarantee that only the successfully coupled products are able to continue in the synthesis of the oligonucleotide. The capping is done by the acetylation of the un-reacted hydroxyl groups. The formed tricoordinated phosphite triester linkage is then oxidised through the treatment with iodine, water and a weak base such as 2,6-lutidine. This treatment oxidises the phosphite triester to the phosphate triester, which is a protected precursor to the natural phosphate diester found in the backbone of DNA strands.



Scheme 1.1: Oligonucleotide synthetic cycle

There are two main procedures used in DNA hybridisation assays; surface hybridisation and solution based assays. Surface probe hybridisation involves a capture probe being immobilised on a surface such as an electrode. Surface immobilisation of DNA probes led to the development of DNA chip sensors. There are a range of methods utilised for the immobilisation of the probe DNA, such as direct adsorption, covalent attachment to the electrode surface, affinity binding, and chemisorption. Direct adsorption methods rely on the electrostatic interaction between the electrode surface and the DNA probe.¹⁷⁻¹⁸ Covalent attachment of DNA probes to an electrode surface require the functionalisation of the electrode surface,

different methods for covalently attaching the DNA probe to the electrode surface are used depending on what electrode is being used in the assay (Figure 1.4).

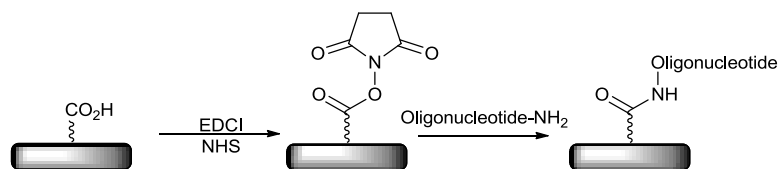


Figure 1.4: Example of surface immobilisation of oligonucleotide

DNA hybridisation detection methods are usually classified by the detection method utilised and also the target they are designed to detect. The detection methods used often require different labels. There are three main methods used to label probes with reporter derivatives: covalent labelling, non-covalent labelling and direct detection techniques. A DNA sensor should be both sensitive and specific, therefore allowing the assay to detect a low concentration of the target DNA and only detect that specific target DNA.

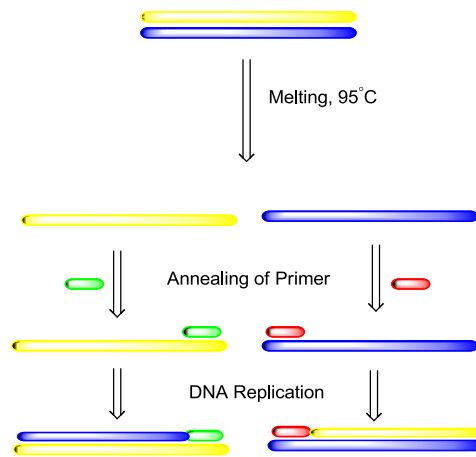
1.3 Polymerase chain reaction

Polymerase chain reaction (PCR) is a biological technique that is routinely used to increase the number of copies of target DNA present in DNA detection assays. PCR was first developed in 1983 by Mullis,¹⁹ it was first used as a detection method for sickle cell anaemia.²⁰

An important aspect of any DNA detection assay is having a sufficient quantity of target DNA present in the assay system. PCR is an enzyme based reaction which utilises the function of polymerase enzymes. Polymerase enzymes copy genetic materials and synthesise new single-strands of the specific region of the DNA. For the PCR reaction to function it requires two things, the target DNA strand and also the two primers. Two primers are required a forward primer and a reverse primer.

These two primers bind to opposite ends of the two strands of DNA. PCR primers are made up of short nucleotide sequences of usually four bases in length. The primers are chosen so that they are able to bind either side of the sequence of interest, this guarantees that only this region of the strand between the two primers will be replicated and amplified.

There are three main steps involved in the PCR mechanism. First of all the DNA is denatured which causes separation of the two strands of DNA. This is usually carried out between 90-96°C. This stage is known as melting. The next step is the annealing of the primers that bind to their complementary base sequences on the single-stranded DNA. The DNA polymerase enzyme works on single-stranded DNA, however it requires a short region of double-stranded DNA to initiate the replication hence why the primers are required. The final stage is the synthesis of new DNA by the polymerase enzyme (Scheme 1.2).



Scheme 1.2: Schematic of PCR

1.4 DNA Hybridisation Sensors *via* Electrochemical transducer methods

Electrochemical DNA sensing is a vast field, the sections following will highlight and discuss the recent advances made in the approaches for the electrochemical detection of DNA.

1.4.1 Direct hybridisation analysis

DNA can be detected electrochemically in solution²¹ as well as on the electrode surface.²² DNA itself is redox-active through the purine bases; adenine and guanine (Figure 1.5).²³ Guanosine is the most readily oxidised nucleoside.

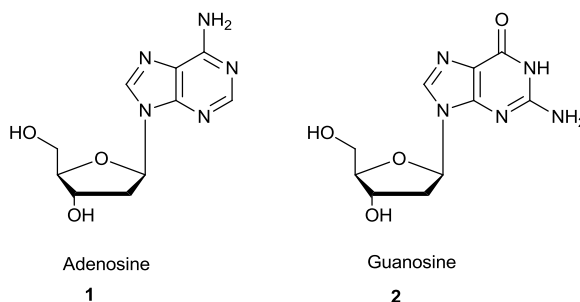
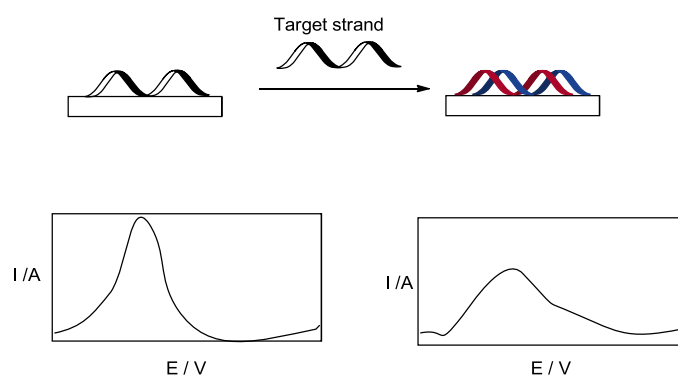


Figure 1.5: Redox-active nucleoside bases

De-los-Santos-Alvarez *et al.*,²⁴ published work into the redox processes associated with the oxidation of an immobilised probe on a graphite electrode. It was shown that it was possible to directly measure the oxidation of adenine bases of ssDNA immobilised on the electrode surface. When the immobilised DNA strand was hybridised with a complementary target strand there was a reduction in the oxidation signal of adenine (Scheme 1.3).



Scheme 1.3: Direct DNA detection at the electrode surface

Due to the higher volume of DNA present at the electrode surface post hybridisation there is a higher background current observed, this leads to issues with the sensitivity of this assay method. Wang *et al.*,²⁵ also showed that it was possible to directly measure the oxidation of guanine bases present in the immobilised DNA. However this method also suffered from the higher background current due to the increased volume of DNA present at the electrode surface. Wang *et al.*,²⁶ further published work into the electrochemical analysis of guanosine on the immobilised DNA probe strand and into the guanosine in the strand being replaced by inosine which is identical to guanosine just without the amine group (Figure 1.6).

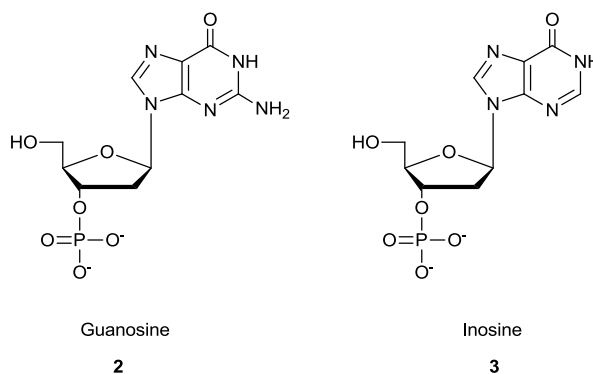


Figure 1.6: Guanine and inosine

The use of inosine increased the sensitivity as the oxidation potential for inosine can be distinguished from that of guanosine, therefore reducing the effect of the post hybridisation increased background current.

Yang *et al.*,²⁷ reported the use of ruthenium complexes as a mediator for guanine oxidation and adenine oxidation. Two different ruthenium complexes were used in the assay Ru(dmb)_3^{2+} and Ru(bpy)_3^{2+} (Figure 1.7). The two different ruthenium complexes carry out selective oxidisations. Out of the two complexes used in this assay Ru(dmb)_3^{2+} , selectively oxidises the guanine derivative and Ru(bpy)_3^{2+} is able to carry out the oxidation of both guanine and adenine. The use of the ruthenium mediators improves the sensitivity of the direct detection method.

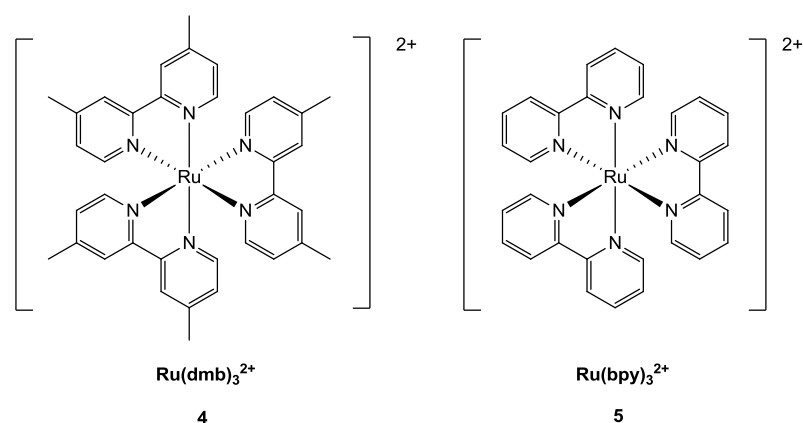


Figure 1.7: Ru complexes used as mediators

Travas-Sejdic *et al.*,²⁸ developed a sensitive label-free DNA sensor using a polymer coated electrode. The use of an electrochemically conductive polymer has a number of benefits, the polymer coating aids the transfer of electrons to the electrode surface and also improves the surface conjugation of the capture probe to the electrode surface. The assay uses the ferro/ferricyanide redox-couple as a mediator (Figure 1.8), which is used for the detection of the hybridisation of the capture probe with the target DNA.

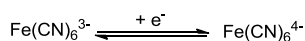


Figure 1.8: Ferricyanide redox-couple

1.4.2 Non Covalent Label Detection Approaches

The most common form of label used in non-covalent label based DNA assays are modified DNA intercalators. Electrochemical intercalators are small electrochemically active compounds which have a high binding affinity to DNA. DNA intercalators bind in the grooves in the double-stranded DNA (dsDNA) and between the nucleotide bases. DNA intercalators must have a very high affinity for dsDNA and a much lower binding affinity for ssDNA to be suitable for use as a label in the detection of target DNA (Figure 1.9). Electrochemical DNA intercalators also require both the oxidised and the reduced form of the compound to be stable.

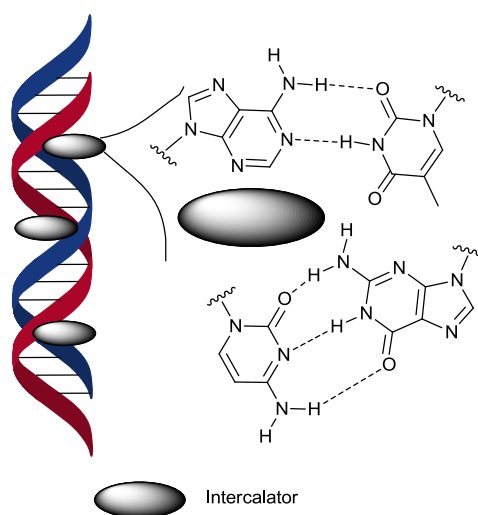


Figure 1.9: Example of DNA intercalation

Mikkelsen *et al.*,²⁹ reported the first electrochemically active DNA intercalators for the use in DNA detection assays. The cobalt complex $\text{Co}(\text{bpy})_3^{3+}$ was shown to have a high activity as a DNA intercalator for double stranded DNA (Figure 1.10).

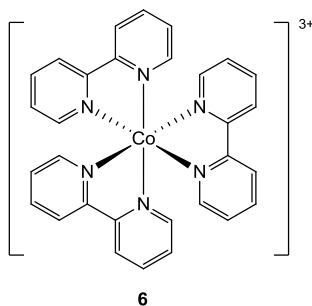


Figure 1.10: Cobalt complex as DNA intercalator

Lorenzo *et al.*,³⁰ synthesised a bifunctional redox-active intercalator probe (Figure 1.11), which contains a fluorescently active portion and also a redox-active ruthenium complex.

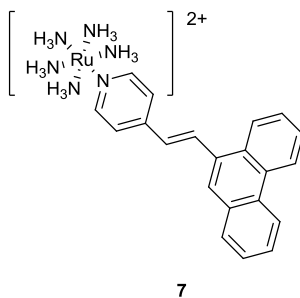
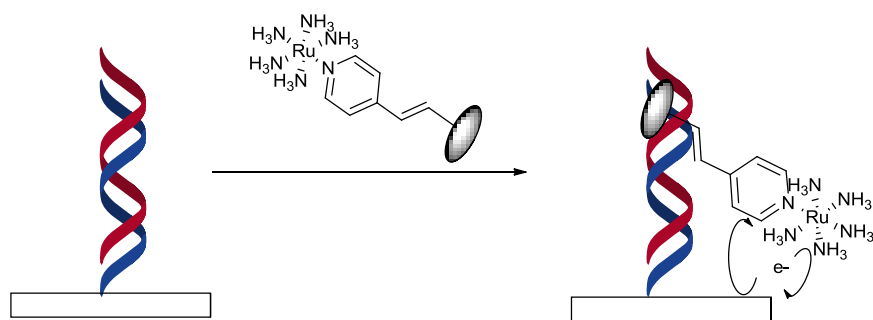


Figure 1.11: Lorenzo's DNA intercalator

The conjugated phenyl ring portion of the compound is able to act as a DNA intercalator with the ruthenium complex region acting as a redox-active label. The ruthenium complex can be analysed *via* differential pulse voltammetry to distinguish between ssDNA and dsDNA (Scheme 1.4).



Scheme 1.4: DNA intercalation and switch on of electrochemical signal

Acridine – DNA interactions are well understood,³¹ they have been used as a tool in the modelling of dsDNA.³² Acridine's themselves are not redox-active (Figure 1.12).

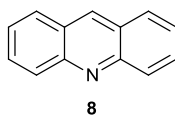
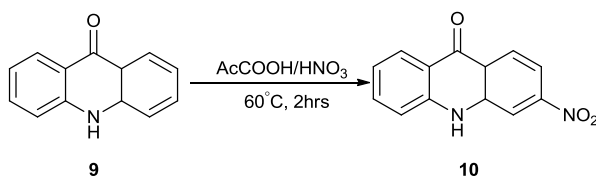


Figure 1.12: Acridine

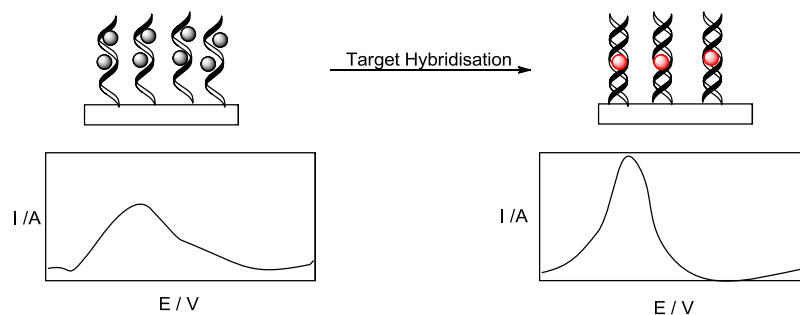
Chen *et al.*,³³ reported work into the modification and use of acridine derivatives as redox-active intercalator labels for the use in DNA detection assays. 9-Acridone **9** was modified *via* the substitution of a nitro group onto one of the aromatic rings (Scheme 1.5).



Scheme 1.5: Nitro functionalisation of 9-acridone

The addition of the nitro functionality transformed **9** into a redox active compound **10** which was found to have an oxidation potential of approximately -116 mV. This

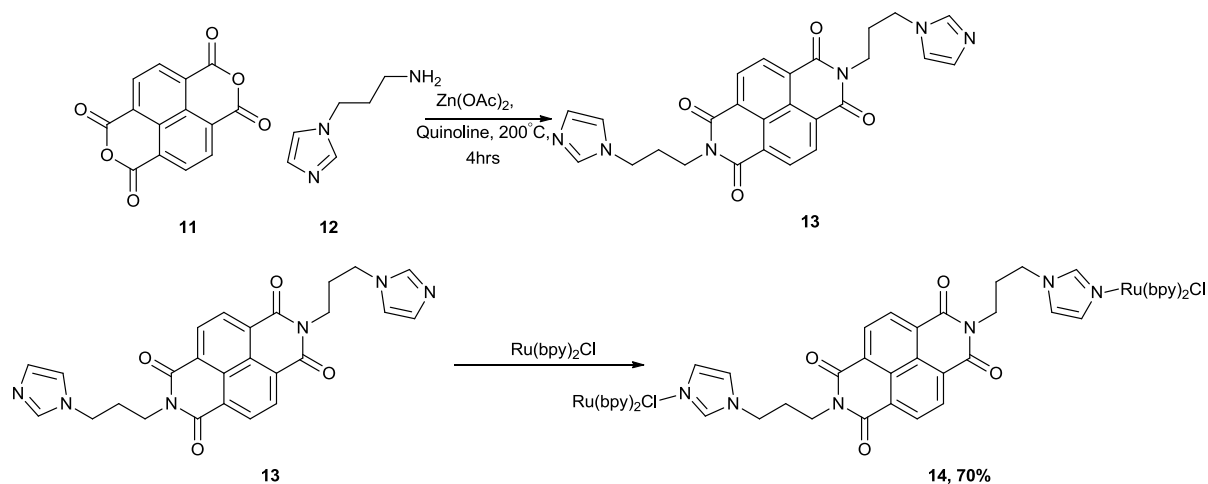
simple intercalator was able to electrochemically distinguish between ssDNA, complementary dsDNA and mismatched oligomer targets (Scheme 1.6).



Scheme 1.6: Increase in electrochemical signal from intercalator between ssDNA and dsDNA

10 was found to form a 2 : 1 complex with dsDNA and had a binding constant of 3.19×10^5 L/mol. Upon analysis *via* cyclic voltammetry there was shown to be an increase in the intensity of the signal for **10** when it was intercalated with dsDNA.

Tansil *et al.*,³⁴ designed and synthesised a ruthenium modified threaded DNA intercalator for an electrochemical DNA biosensor. The backbone of the intercalator *N,N'*-bis[(3-propyl)-imidazole]-1,4,5,8-naphthalene diimide **13** (PIND), which was synthesised from 1,4,5,8-naphthalenetetracarboxylic dianhydride **11** and *N*-(3-aminopropyl)-imidazole (Scheme 1.7).



Scheme 1.7: Synthetic route to intercalator 14

The imidazole rings present in **13** are then complexed with $Ru(bpy)_2Cl$. A PNA capture probe was immobilised onto an indium tin oxide electrode surface, which forms the bio-recognition event of the biosensor with the target DNA. The target DNA is then hybridised with the immobilised capture probe. The PIND-Ru intercalator **14** is then added to the assay mixture, **14** is selective only for dsDNA. the intercalated dsDNA was found to be a highly stable complex with reversible electrochemical oxidation/reduction processes. The peak currents exhibited from the intercalator can be directly related to the target DNA concentration in the assay matrix. The high affinity PIND-Ru has for dsDNA has a high significance in the design of a sensitive DNA biosensor. This was demonstrated when Tansil *et al*, carried out the assay in an amine-containing buffer solution, in which the electrocatalytic activity of the $[Ru(bpy)_2Cl]$ moieties on the intercalator. This electrocatalytical activity and the current observed from the interaction between the Ru complex and the amine compounds in the buffer solution increased the sensitivity to a level that as low as 3 attomoles of target DNA could be detected in the assay solution.

Gooding *et al*,³⁵ described the development of an electrochemical DNA intercalator for the detection of DNA hybridisation in real time *via* the method of monitoring the

charge transfer through dsDNA. The utilisation of anthraquinone monosulfonic acid (AQMS) **15** as the DNA intercalator (Figure 1.13).

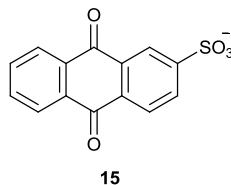


Figure 1.13: anthraquinone monosulfonic acid

15 has been proposed to intercalate into dsDNA at the top of the duplex. **15** was found to have an oxidation potential of -540 mV and upon intercalation to dsDNA the oxidation potential of **15** undergoes a positive redox potential shift. The oxidation potential of **15** shifts from -540 mV to -480 mV.

Buttry *et al.*,³⁶ reported the synthesis and use of a bis-intercalative electrochemical probe **16** (Figure 1.14).

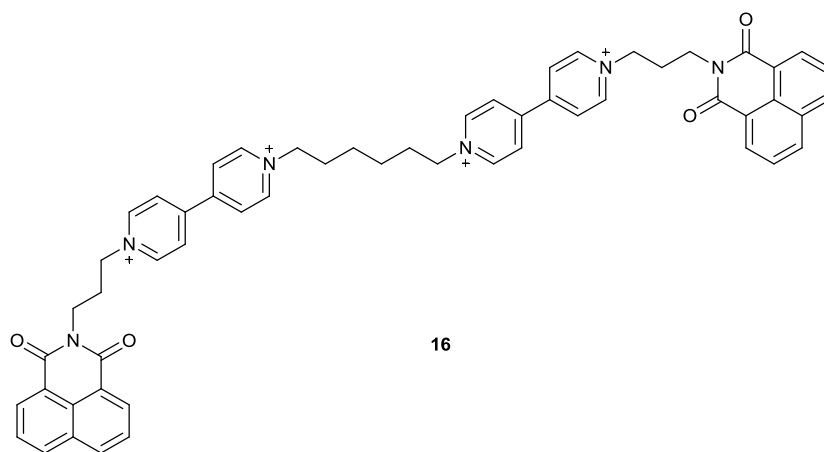
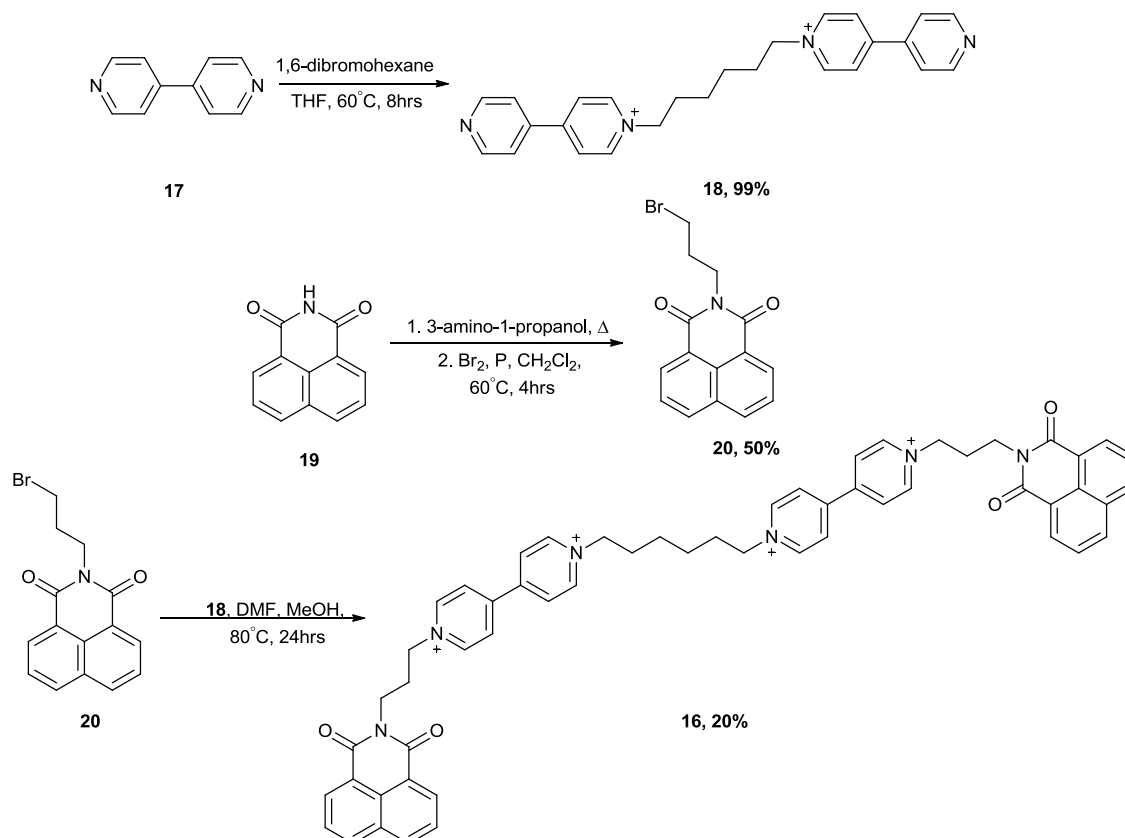


Figure 1.14: DNA intercalator synthesised by Buttry *et al*

16 was used to distinguish between ssDNA and dsDNA in a DNA detection assay. **16** was found to have a strong binding affinity for dsDNA, due to a very low

dissociation rate from dsDNA. **16** was synthesised from a 4-4'-bipyridine linked backbone with 1*H*-benzo[de]isoquinoline-1,3(2*H*)-dione at each end of the intercalator molecule **16** (Scheme 1.8).



Scheme 1.8: Synthetic route to **16**

The high binding affinity for dsDNA of **16** allows for the detection at the electrode surface, even when the electrode has been moved to a non saline solution. As some intercalators show a strong interactions with ssDNA,³⁷⁻³⁸ which would lead to a false positive in a sensing capacity. However the higher binding affinity of **16** with dsDNA provided a method for distinguishing between ssDNA and dsDNA in a sensing capacity.

The use of electrochemical DNA intercalators have the main advantage of the probe not having to be covalently attached to the probe strand in the assay, as this requires some sensitive reagents and specific reaction conditions. However due to the difficulties sometimes exhibited in distinguishing between ssDNA and dsDNA, this leads to the assays not being of a high enough sensitivity level to be used in a sensing capacity.

1.4.3 Covalently Labelled Probes

This approach requires the covalent labelling of a redox-active reporter moiety to one of the oligonucleotides used in the detection assay. It is usually the probe or the captive probe that are labelled rather than the target strand itself. The labelling of the oligonucleotide with a reporter moiety enables an electrochemical signal to be produced post hybridisation. There are two main groups of reporter derivatives that are used as labels for the oligonucleotide probes; organometallic derivatives³⁹⁻⁴⁰ and redox-active organic derivatives.⁴¹⁻⁴³ Ferrocene and its derivatives are the most commonly used reporter derivatives in the covalently labelling of DNA, which will be covered later in this chapter. After ferrocene the next most common family of redox-active labels to be used as transducer moieties are ruthenium complexes are ruthenium complexes.⁴⁴ These ruthenium complexes also undergo a reversible one-electron oxidation as well as being highly stable.

Metzler-Nolte *et al.*,⁴⁵ published the synthesis of transition metal labelled PNA strands for the use in DNA detection assays. The PNA strands were synthesised through the standard solid supported peptide synthesis methods.⁴⁶⁻⁴⁷ The PNA strands were labelled with a ruthenium complex (Figure 1.15).

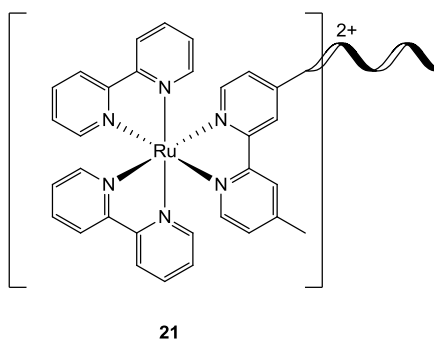


Figure 1.15: Ru complex labelled to PNA conjugate

The stability of the ruthenium labelled PNA conjugate and its binding to a complementary strand of DNA, which was found to be slightly less than the unlabelled PNA strand. This therefore allows for the metal labelled PNA strand to act as a reporter probe for the detection of DNA, through the binding of PNA and DNA.

Grinstaff *et al.*,⁴⁸ reported the design and synthesis of nucleobase labelled with $\text{Ru}(\text{bpy})_3^{2+}$ complex and then incorporated into an oligonucleotide (Figure 1.16).

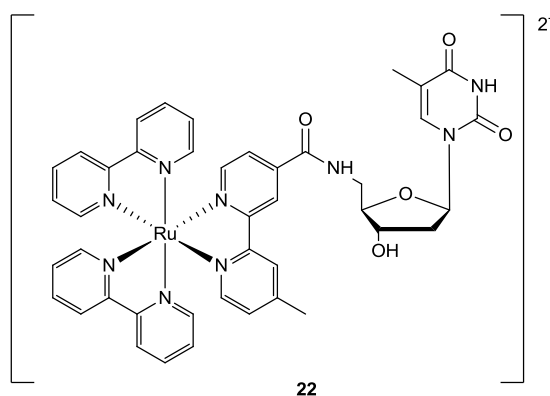
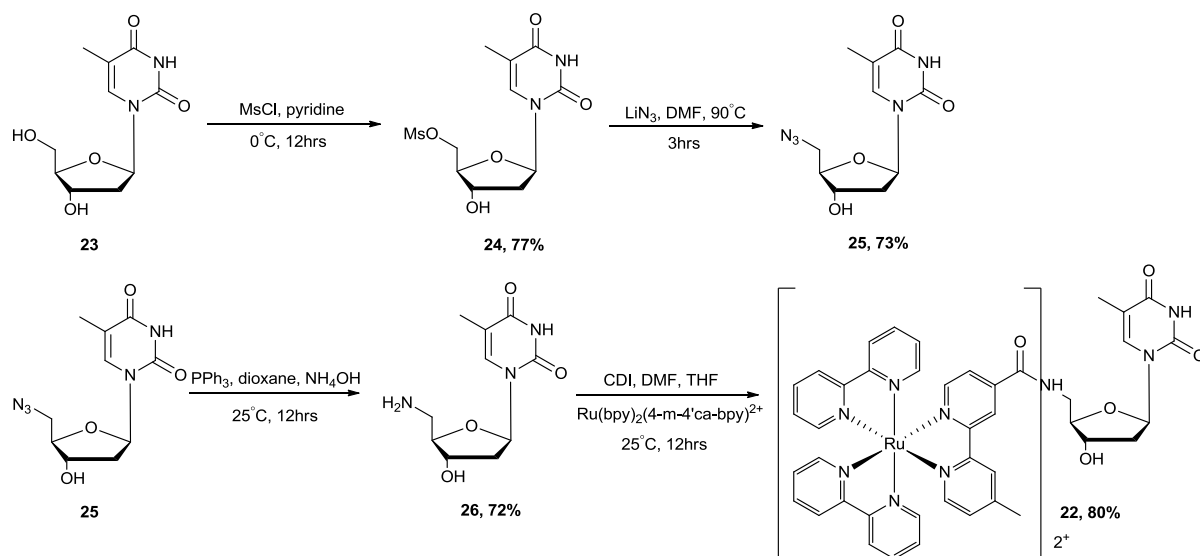


Figure 1.16: Nucleobase labelled with $\text{Ru}(\text{bpy})_3^{2+}$

The ruthenium complex $\text{Ru}(\text{bpy})_3^{2+}$ was conjugated to the nucleotide on the deoxyribose sugar backbone of a thymidine moiety (Scheme 1.9).



Scheme 1.9: Synthesis of Ru labelled thymine nucleotide

The labelling of the thymine nucleotide on the sugar back bone of the base post hybridisation was shown not to have any effect on the dsDNA duplex structure or stability. It was also shown that the ruthenium complex post labelling does not lose any of the properties that make the complex desirable as a label.

Zhang *et al.*,⁴⁹ developed a highly selective biosensor for the detection of target DNA, utilising a hairpin DNA probe as the recognition section which was labelled with the ruthenium complex $\text{Ru}(\text{bpy})_2(\text{dcbpy})\text{NHS}$ (Figure 1.17).

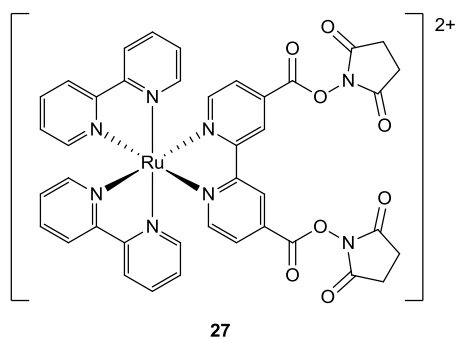
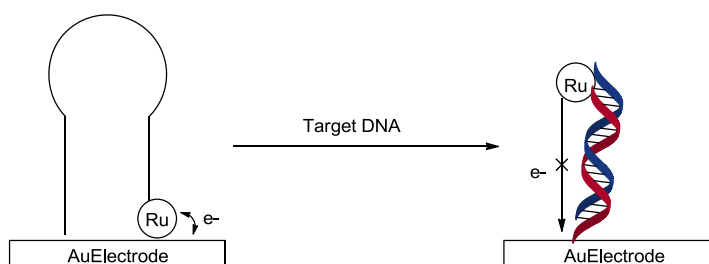


Figure 1.17: Ru complex used for labelling oligonucleotide

The hairpin probe is immobilised onto a gold electrode, when there is no target DNA present the ruthenium labelled probe is in the folded conformation. Therefore the ruthenium complex is held in close proximity to the electrode surface leading to a high signal intensity. Whereas when there is target DNA present the stem-loop probe is converted to linear dsDNA, therefore the ruthenium complex is no longer in close proximity to the electrode surface causing a decrease in the signal intensity generated by the ruthenium complex (Scheme 1.10). With a high enough concentration of target DNA, there is a switch off event leading to no signal being produced at the electrode.



Scheme 1.10: Switching off electrochemical signal post target hybridisation

A range of metal-free redox active labels have been used in DNA detection assays, such as; anthraquinone,⁵⁰⁻⁵¹ phenothiazine⁵² and thionine.⁵³ Grinstaff *et al*,⁵⁴ reported the development of the facile and automated procedure for the synthesis of oligonucleotides which have been labelled at the 5' end of the oligonucleotide in a high yield. The oligonucleotides were labelled with organo-reporter moieties 9-fluorene-4-carboxylic acid **28**, 2-anthraquinone carboxylic acid **29** and phenothiazine **30** (Figure 1.18).

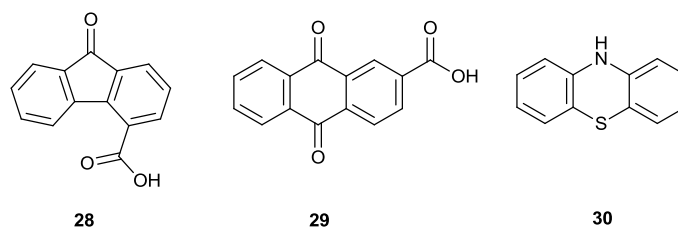
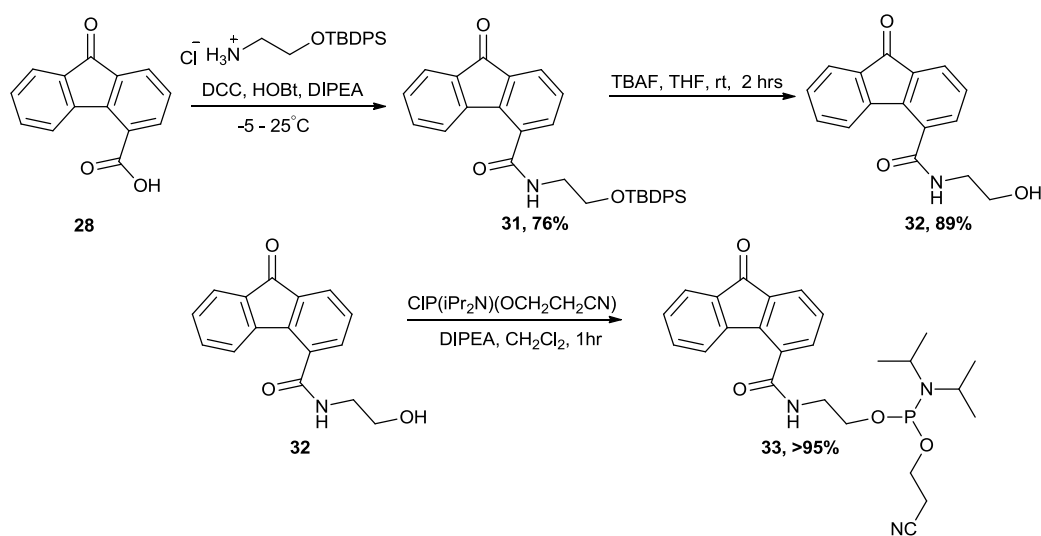


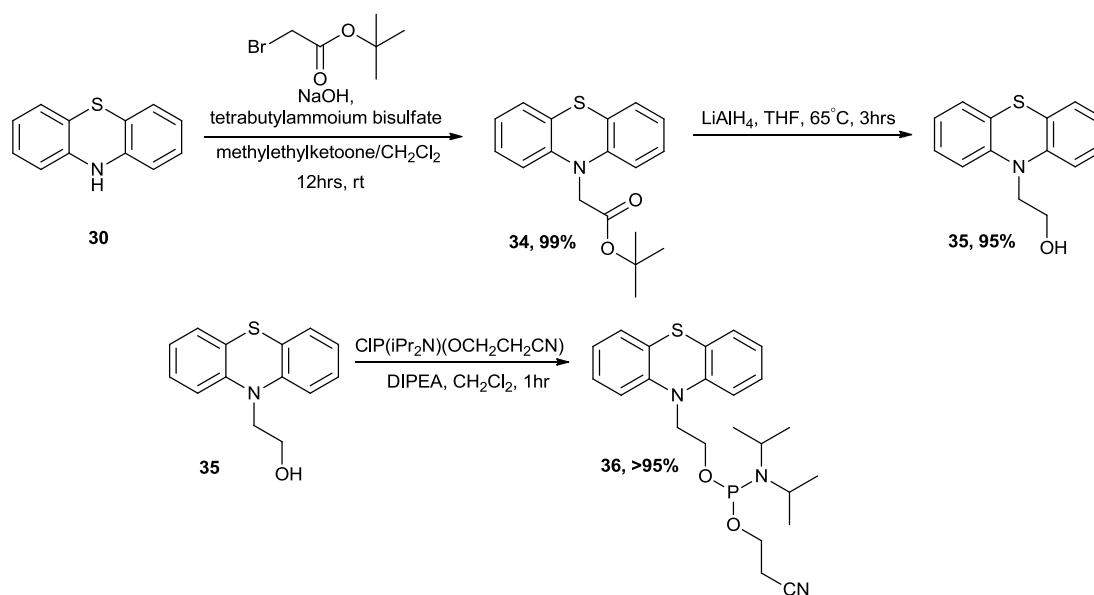
Figure 1.18: organo-reporter derivatives 28, 29, 30

The redox-active derivatives were labelled onto the oligonucleotides *via* the synthesis of their corresponding phosphoramidite derivatives. The phosphoramidites of **28** and **29** were synthesised through an amide coupling with aminoethanol to instill the required hydroxyl group, which in turn is conjugated to the phosphoramidite (Scheme 1.11).



Scheme 1.11: Functionalisation and phosphoramidite synthetic route used for 28 and 29

The phosphoramidite of **30** was synthesised by reacting the amine group with *tert*-butylbromoacetate which was reduced to yield the necessary hydroxyl group required for phosphoramidite conjugation (Scheme 1.12).



Scheme 1.12: Functionalisation and phosphoramidite synthesis of 30

The duplexes formed with the 5' labelled oligonucleotides and a target strand were shown to be as stable or have increased stability in comparison to the duplex formed between the un-labelled oligonucleotide and the target DNA. These labelled oligonucleotide probes were designed for use in the electrochemical sensing of DNA.

Plaxco *et al.*,⁵⁵ reported the development of a surface immobilised methylene blue labelled capture probe for the detection of target DNA (Figure 1.19)

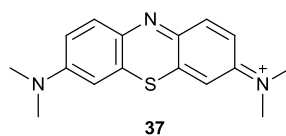
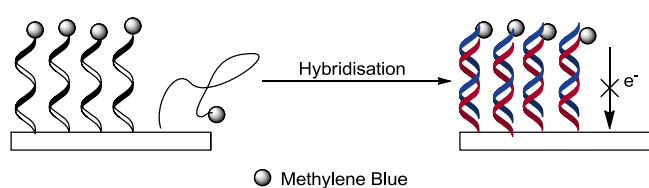


Figure 1.19: Methylene blue

The sensor was designed around the immobilisation of a 27-base probe sequence onto an electrode surface. The probe was labelled at the 5'-terminal with the

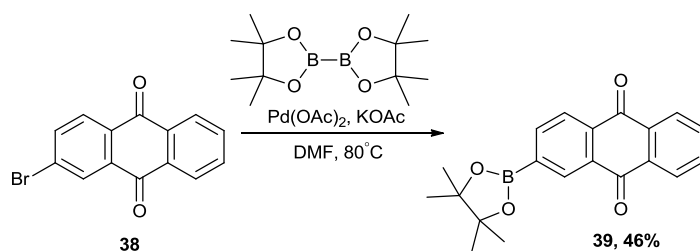
methylene blue reporter moiety. The flexibility of ssDNA allows for the methylene blue to reach the electrode surface, the methylene blue probe was found to have an oxidation potential of ~ -260 mV and an intensity of $6.9 \mu\text{A}$. However when the complementary target DNA strand was present in the assay mixture and hybridisation occurred a significant drop in the signal from the methylene blue was observed, this change in the signal at the electrode is due to the more rigid structure of dsDNA leading to less of the methylene blue probe being able to reach the electrode surface (Scheme 1.13).



Scheme 1.13: DNA detection assay using methylene blue labelled probe

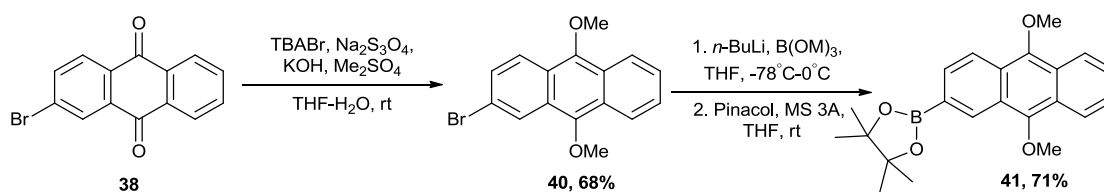
Plaxco *et al*, showed that the same drop in signal intensity could be exhibited in a blood serum solution which had been spiked with the target DNA, this proves that the assay could be used as a functioning biosensor. However there is a drop in the signal intensity for the methylene blue labelled capture probe prior to hybridisation.

Gothelf *et al*,⁵⁶ reported the synthesis of a 2'-deoxyuridine nucleoside labelled derivative. The nucleosides were labelled with an anthraquinone moiety. The synthesis was started from 2-bromoanthraquinone **38**, which was converted to the pinacol protected boronic ester derivative **39** via a Miyaura coupling reaction (Scheme 1.14).



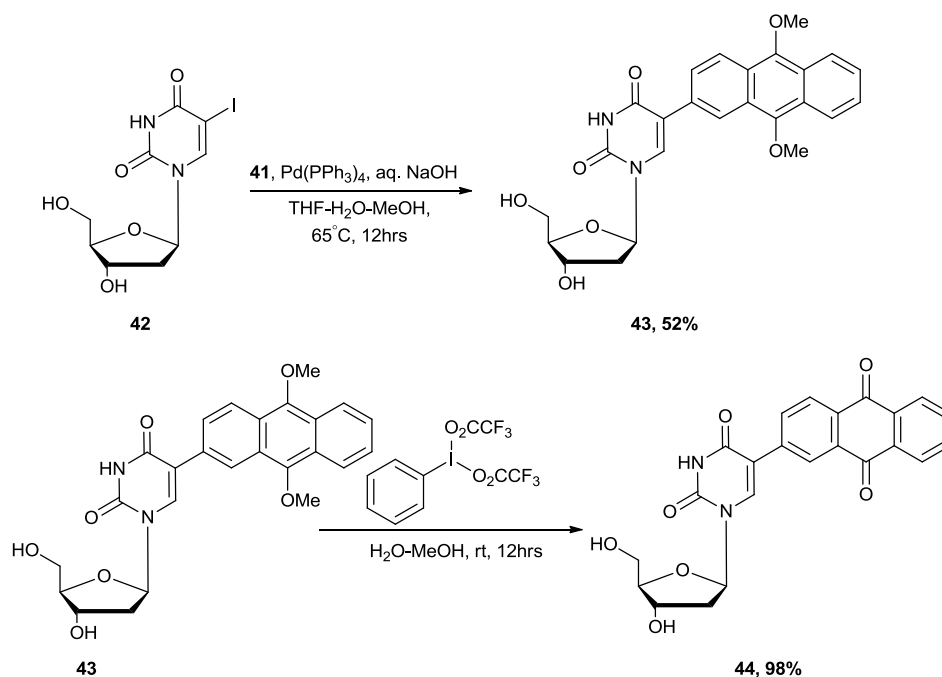
Scheme 1.14: Synthesis of boronic ester derivative 39

However the Suzuki coupling reaction of **39** with 2'-deoxy-5-iodouridine **42** did not yield any product and caused decomposition of the nucleoside. A protected form of **38** was then synthesised (Scheme 1.15), to afford the dimethyl protected anthraquinone pinacol boronic ester species **41**.



Scheme 1.15: Synthesis of protected boronic ester derivative 41

41 did yield the desired product **43** in the Suzuki coupling reaction, however after the Suzuki reaction a demethylation step followed by an oxidation is required to deprotect the anthraquinone derivative (Scheme 1.16).



Scheme 1.16: Suzuki coupling of 41 and deprotection of labelled nucleoside

Grothelf *et al*, showed that the labelled uridine nucleosides could be incorporated in stable oligonucleotides. The inclusion of the anthraquinone derivative directly onto the nucleoside base did not have an effect on the stability of the duplexes formed. The anthraquinone labelled nucleoside base was found to have an oxidation potential of -422 mV and when **44** was included into an oligonucleotide which was loaded onto a gold electrodes surface an oxidation potential of -414 mV was observed, therefore showing that the inclusion into the oligonucleotide did not have a large shift on the labelled bases oxidation potential.

Fang *et al*,⁵⁷ reported the development of an electrochemically active solution based molecular beacon assay for the detection of target DNA, using a molecular beacon probe that is labelled at both the 5' and the 3' ends of the strand with a carminic acid derivative (Figure 1.20).

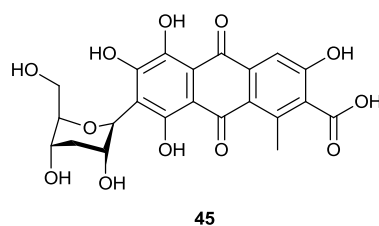
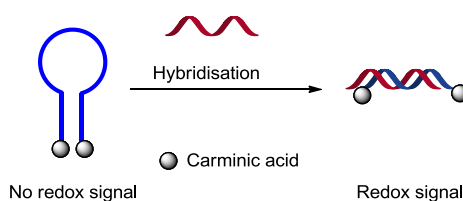


Figure 1.20: Carminic acid derivative 45

When the molecular beacon is in the closed form the electrochemical signal from the two carminic acid derivatives is switched off, this is due to the two compounds being in close enough proximity to form a dimer. When complementary target DNA was present in the assay solution there was a change in the conformation of the molecular beacon from the closed hairpin conformation to the open linear form of the dsDNA, post hybridisation with the target DNA. The change in the conformation leads to the two redox-active derivatives being separated at either end of the duplex formed which in turn causes the switching on of the electrochemical signal (Scheme 1.17).



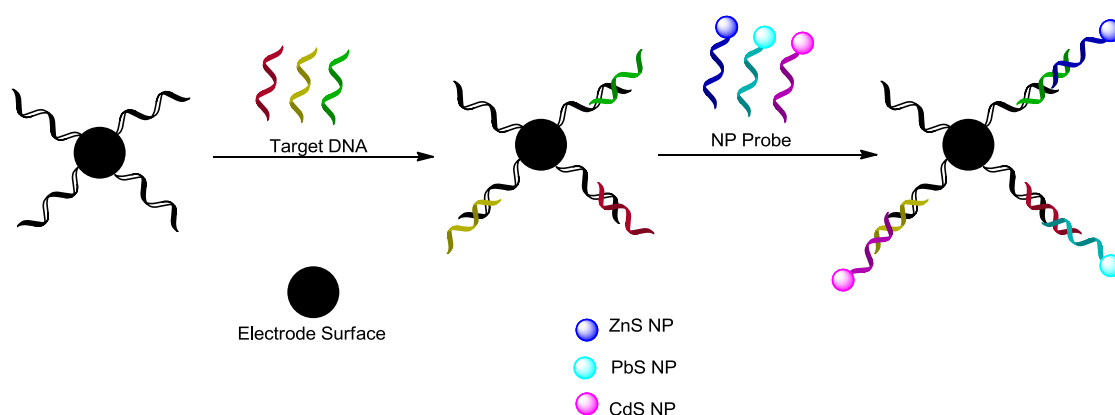
Scheme 1.17: Molecular beacon assay using 45 as redox-reporter

1.4.4 Nanoparticle Based DNA Detection

Metal nanoparticles (NPs) have been used in a wide-range of applications due to their large surface area and the nanoparticles size inherent optical properties.⁵⁸ NPs have been regularly used in the field of biosensors in the role of signal amplification,⁵⁹⁻⁶⁰ or as solid supports which increase the surface area of the sensor.

There are a wide range of different NPs used in the field of sensing. The most common of which are gold nanoparticles,⁶¹⁻⁶² however silver, zinc, palladium and cadmium NPs have all been used in the field of biosensing.

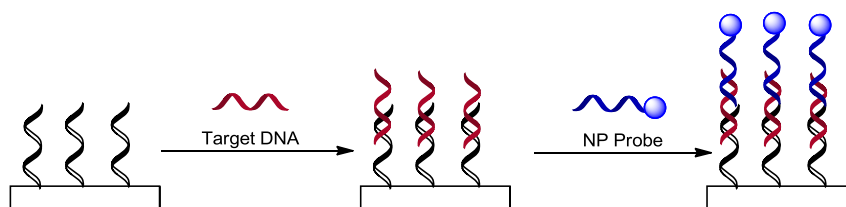
Wang *et al.*,⁶³ developed a nucleic acid hybridisation assay using three different NP labelled probes. The three NP reporter moieties are based around three inorganic sulfide complexes that make up the NPs; zinc sulfide, lead sulfide and cadmium sulfide. Capture probes are immobilised onto a mercury-coated glassy-carbon electrode, three different capture probes are used in the assay. The capture probes all have sequences that are unique to a specific region on different strands of target DNA. The NP labelled probes are then added to the assay mixture to hybridise with the trapped target DNA. The three different NP labelled probes are each labelled with a different metallic nanoparticle each probe has a different sequence that is complementary to a specific region of its complementary target DNA (Scheme 1.18).



Scheme 1.18: Multi-target detection using NP labelled probes

The hybridisation of the NP labelled probes with the target DNA is detected using stripping voltammetry with the different metal containing NPs were found to have unique oxidation potentials of -1.12 V for the zinc NP, -680 mV for the cadmium NP and -530 mV for the lead NP. This method can be used for the simultaneous detection of three different DNA targets. Wang *et al.*, used this assay for the simultaneous detection of the genes related to BCRA1 breast-cancer genes in a single assay.

Bard *et al.*,⁶⁴ reported the development of a highly sensitive DNA sensing mechanism for the detection of low volumes of target DNA. The assay is based around a sandwich assay. A capture probe is immobilised onto a gold electrode surface, to which the target DNA is added to this assay mixture and hybridised. The hybridisation of the target DNA with the capture probe allows for the hybridisation of the reporter labelled probe, in this case the reporter moiety is a platinum NP (Scheme 1.19).



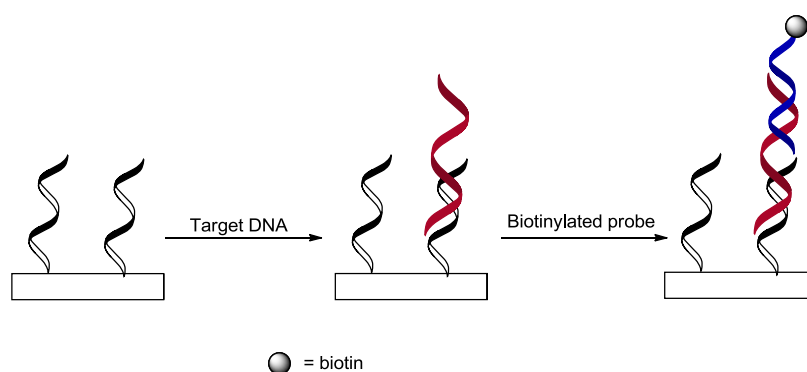
Scheme 1.19: Bard's DNA detection assay using platinum labelled probe in sandwich assay

The hybridisation of the labelled probe to the bound target strand allows for the platinum NP to get to the electrode surface and carry out the oxidation of hydrazine.

1.4.5 Enzymatic Based DNA Detection

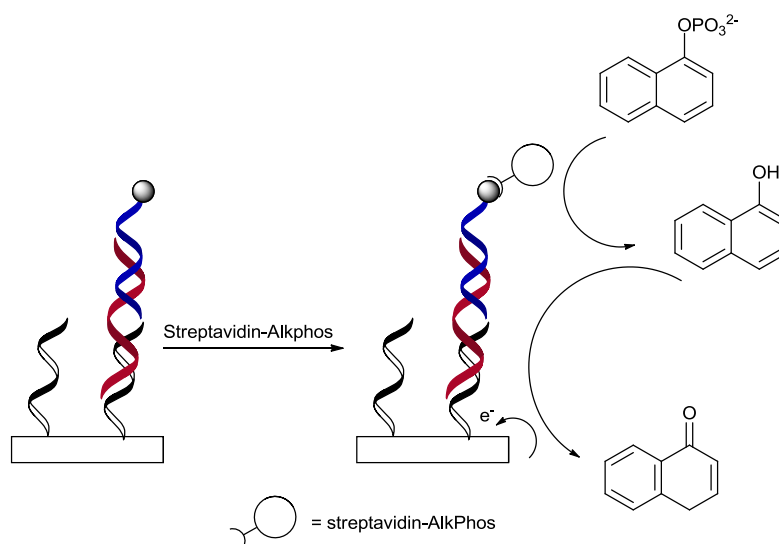
Oligonucleotides can also be labelled with an enzyme, such as horse radish peroxidase (HRP). The probe bound enzymes can function in two different methods.⁶⁵ The enzyme can either directly detect the hybridisation of the probe and the target DNA or they can be used indirectly, where the enzyme reacts with a substrate to a redox-active components.⁶⁶

Tuñón-blanco *et al.*,⁶⁷ developed a hairpin based biosensor for the enzymatic electrochemical detection of target DNA. A capture probe was immobilised onto the electrode surface, the capture probe was designed and synthesised to be complementary to a region on the target DNA. A secondary probe which was labelled with biotin, which is complementary to another region on the target DNA (Scheme 1.20).



Scheme 1.20: Sandwich assay with alkaline phosphatase labelled probe

Once the secondary probe had been hybridised to the target DNA, to the assay mixture a streptavidin bead which was labelled with alkaline phosphatase was added. Due to the very high binding affinity of biotin and streptavidin the duplex is now labelled with the alkaline phosphatase. The progress of the assay was analysed by the enzymatic conversion of 1-naphthyl phosphate to 1-naphthol (Scheme 1.21). The 1-naphthol is oxidised at the electrode to give 1-naphthalenone.



Scheme 1.21: Function of alkaline phosphatase on 1-naphthylphosphate

Xu *et al.*,⁶⁸ developed an array biosensor, also utilising the action of avidin-alkaline phosphatase to convert 1-naphthyl phosphate into a redox-active species. The DNA capture probes for the biosensor were immobilised on a photolithographically gold array electrode *via* standard chemical conjugation techniques. The assay developed by Xu works along a very similar principle as the assay developed by Tuñón-Blanco as both the assays are sandwich based assays involving the trapping the target DNA between two probes.

1.5 Nanopore Electrochemical DNA Detection

A nanopore is a very small hole in a thin membrane. Nanopores are usually formed by pore-forming proteins such as α -hemolysin and MspA porin.⁶⁹ The proteins form the pores in lipid bilayers (Figure 1.21). More recently nanopores have been made in thin synthetic membranes, produced from silicon and graphene.⁷⁰⁻⁷¹ Silicon nitride is one of the most common silicon compounds in which nanopores are produced in. Nanopores in synthetic membranes can be produced by several techniques such as ion-beam sculpting and electron beams.⁷²

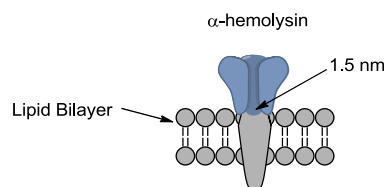


Figure 1.21: Example of nanopore in lipid bilayer

Nanopores can be used to detect and identify analytes directly or electronically. The detection of analytes is possible by the formation of a nanopore in an electrochemically resistant membrane, the membrane is suspended in a physiological solution. The membrane then has a voltage applied across it, this results in an ionic current to be passed through the nanopore. This ionic current is disrupted when the analyte of interest passes through the pore (Figure 1.22).

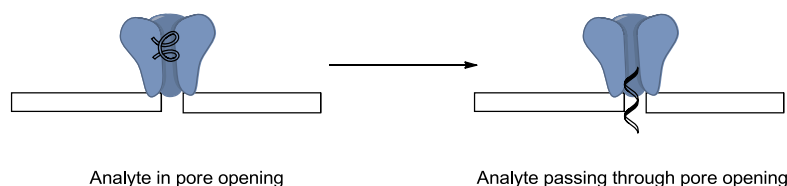


Figure 1.22: SsDNA passing through a nanopore

The use of nanopores in sensing was first proposed in the mid 90s. They have been studied for the possible sensing applications for a wide range of analytes; small molecules,⁷³⁻⁷⁴ the identification of biomarkers,⁷⁵⁻⁷⁶ the studying of ion channels⁷⁷ and for DNA sequencing and sensing. Nanopore sequencing and sensing of DNA is of interest due to no analytical reporter label being required, it does not require an amplification method such as PCR and the fact that the single molecule methods can be scaled up for high-throughput DNA analysis. The use of nanopores to sequence DNA was first proposed by Church *et al.*⁷⁸ The concept for the sequencing of ssDNA as it passes through the nanopore, works on the principle that each nucleotide base has a different structure and will interact with the nanopore in a different way. Therefore there would be a different shift in the residual ionic current depending on

which nucleotide is in the nanopore at that moment (Figure 1.23). Deamer *et al.*,⁷⁹ carried out proof of principle experiments using two naturally produced nanopores by the enzymes α -haemolysin and *Mycobacterium smegmatis* porin, which showed that there was a difference in the residual ionic current when a nucleotide base was present in the pore. Also it was shown that there was a unique shift in the residual current for each of the four nucleotide bases that make up DNA.

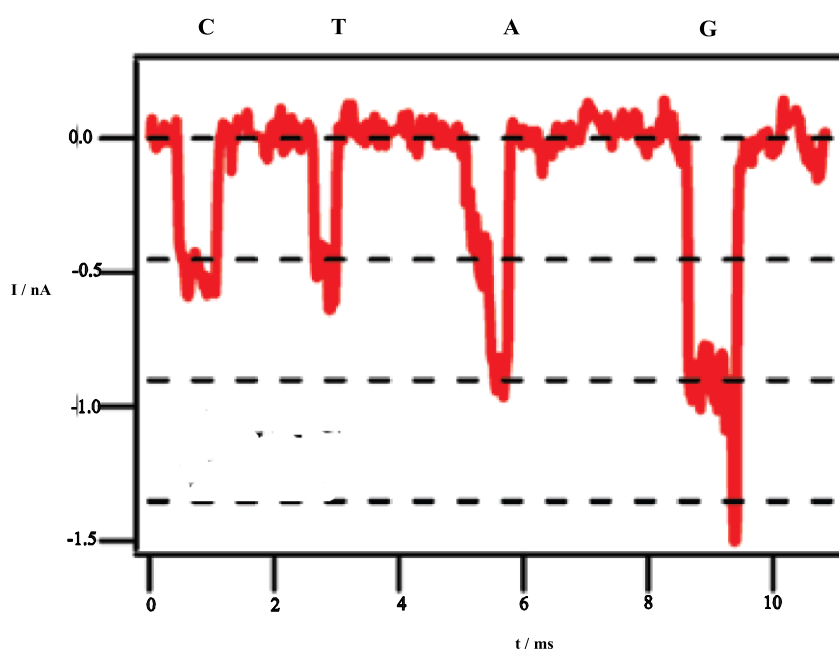


Figure 1.23: Shift in ionic current exhibited by different nucleotides passing through the nanopore

Martin *et al.*,⁸⁰ described the development of a nanopore based resistive-pulse sensing of ssDNA up to 7250 bases in length and also to a lesser level the sensing of dsDNA. The development of conically shaped nanopores in a polycarbonate membrane was carried out using anisotropic chemical etching. The conical had an opening diameter at the tip of 40 nm and an opening diameter of 1.5 μm at the base of the nanopore. The polycarbonate films were placed in an U-tube cell, an etch solution of KOH (9M) was added to one half of the U-tube cell and a stop solution of formic acid was added to the other half of the cell. The etching process continued until the etching solution broke through the membrane into the stop solution. The break through was detected *via* an increase in current from the Pt wires that were in each half of the cell and the potential difference of 15 V was applied to the cell during the

etching process. The cell was set up so that the anode was in the side of the U-tube cell with the etch solution.

During the DNA sensing application of these conical nanopores, ssDNA was driven electrophoretically through one of the nanopores. This translocation event results in the transient current-blocking events as the pore is filled with the strand of ssDNA. The frequency of which these current-blocking events is linearly related to the concentration of ssDNA. The current-blocking effects of dsDNA was also investigated, however due to dsDNAs larger size and its poor flexibility of the dsDNA can not enter the tip opening of the nanopore or translocate through the nanopore. Therefore the shorter duration of the current-blocking event and the lower levels of current shift observed were believed to be due to the dsDNA bumping against the tip opening of the conical nanopore.

The use of graphene membranes for the fabrication of nanopores is of interest due to the mechanical, electrical and thermal properties of the graphene membranes.⁸¹ Another benefit to the use of graphene membranes is that the thickness of a single layer of graphene membrane is the same thickness as the spacing between the nucleotides in DNA. Drndic *et al*,⁸² were the first to produce nanopores and nanopore arrays in suspended graphene films and study the nanopore formation kinetics as well as the edge stability of these nanopores.

Golovchenko *et al*,⁸³ reported the use of atomically thin graphene conducting membranes containing single nanopores for the use in DNA sensing and sequencing. The graphene membranes used in this study were as thin as one or two atomic layers thick, even at this thickness the graphene membranes were found to be very efficient ionic insulators. Electrical analysis of these graphene membranes with a single nanopore, showed that the effective insulating thickness of these membranes was less than a nano meter. The fact that the effective insulating thickness of the graphene membrane is so small makes them ideal membranes for the high resolution nanopore-based single molecule detectors. Govovchenko *et al*, studied the effect of

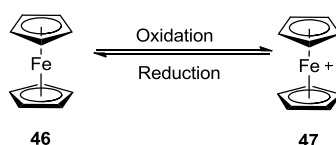
electrophoretically driving negatively charged DNA through the nanopores. As each nucleotide base passes through the nanopore it transiently reduce or block the ionic current in a way that eludes to the size of the DNA strand and also the conformation of the strand.

Drndic *et al.*,⁸⁴ reported research into the translocation of DNA through nanopores created in graphene membranes of a thickness between 1-5 nm. Using electron-beaming techniques nanopores of between 5-10 nm in diameter were etched into the graphene membrane. With the thinness of the graphene membranes used in this study, larger blocked ionic currents were observed in comparison to traditional solid-state nanopores. However, at this thinness of membrane the ionic current background noise levels are larger than for silicon nitride based nanopores. The background noise levels of the device were shown to be reduced by the atomic layer deposition of a 5 nm layer of titanium dioxide over the whole device. Unlike nanopores in silicon nitride based membranes, nanopores in graphene membranes opens up the possibility of a new style of device in which the electronic sensing and control can be carried out directly at the nanopore.

1.6 Introduction of Ferrocene in DNA sensing

Ferrocene was first discovered and characterised in the 1950's, thereafter there has been a large interest in the chemical characteristics and chemistry of the transition metal sandwich complexes. Ferrocene itself is used in a wide range of chemistry from chiral ligands for catalysis⁸⁵⁻⁸⁶ to its use as a transducer compound in a sensing capacity.⁸⁷

The redox couple between ferrocene (Fc) and the oxidised ferrocenium ion (Fc⁺) is well known and understood (Scheme 1.22).



Scheme 1.22: Ferrocene redox couple

The reduced form of ferrocene and its derivatives is the most stable form, therefore a lot of the work is carried out into the oxidation of ferrocene to the ferrocenium ion. This oxidation provides the oxidation potential of the ferrocene derivative. The oxidation potential of ferrocene can be altered by affecting the overall electronics of the metallocene itself, this is carried out *via* the substitution of the cyclopentadienyl rings (Cp). Ferrocene can be affected by inductive and mesomeric affects *via* the Cp rings which are a conjugated ring system (Figure 1.24).⁸⁸

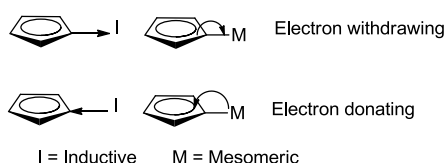
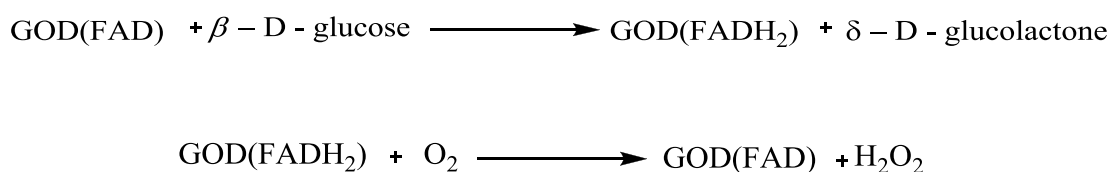


Figure 1.24: Showing the effects of EWG and EDG on Cp ring

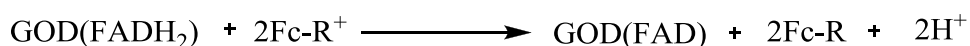
The inductive and mesomeric effects can be electron donating or electron withdrawing, substitution on to the Cp with an electron donating group (EDG) can stabilise the formation of the ferrocenium ion. Conversely, substitution using an electron withdrawing group (EWG) does not favour the formation of the oxidised ferrocenium ion. This is due to the electron withdrawing group pulling electron density from the metallocene core, therefore a higher oxidation potential is required to remove the electron and oxidise the ferrocene derivative. Ferrocene and its derivatives are used in a wide array of roles in sensing assays. Ferrocene can be used as a mediator or an electron shuttle. In the field of medical diagnostics, the key example of ferrocene being used as a mediator in a biosensor is in the glucose biosensor. The glucose biosensor was developed for the personal monitoring of blood glucose levels in diabetics. The biosensor utilises the biological response of

the oxidation of β -D-glucose to δ -D-glucolactone by the enzyme glucose oxidase (GOD). The oxidation of glucose is a two electron process, the oxidation is carried out by the redox-active centre of GOD along with a cofactor. Flavin adenine dinucleotide (FAD) is the cofactor, within the oxidation process FAD is converted to FADH₂ (Scheme 1.23). FAD is then regenerated by dioxygen to produce hydrogen peroxide as a biproduct.



Scheme 1.23: Oxidation of glucose by GOD

In converting this biological process into a biosensor the inclusion of a physicochemical transducer is required, in this case an electrochemical transducer utilising ferrocene. The ferrocene is utilised as a mediator between the biological response and the electrode. GOD was directly labelled using a ferrocene carboxylic acid derivative *via* an EDC coupling reaction. The ferrocene derivatives replace the requirement for dioxygen leading to no side products being produced (Scheme 1.24). The ferrocene derivative allows for the electron transfer from FADH₂ to the electrode to regenerate the FAD. This is possible as the ferrocene moiety would become oxidised to the ferrocenium ion by the electrode, making it receptive to electrons from the cofactor. Work into developing the biosensor was carried out in 1986 by a number of groups independently.⁸⁹



Scheme 1.24: Ferrocene as a mediator in the glucose biosensor

Ferrocene derivatives have also been used as redox-active reporter moieties for studies into DNA structure and to investigate the H-bonding between the nucleotide bases.⁹⁰

Tucker *et al.*,⁹¹ reported the synthesis and characterisation of four ferrocenyl nucleobases, the ferrocenyl nucleobases contained a linker group that was either unsaturated or saturated connecting the ferrocene moiety and either adenine or thymine (Figure 1.25).

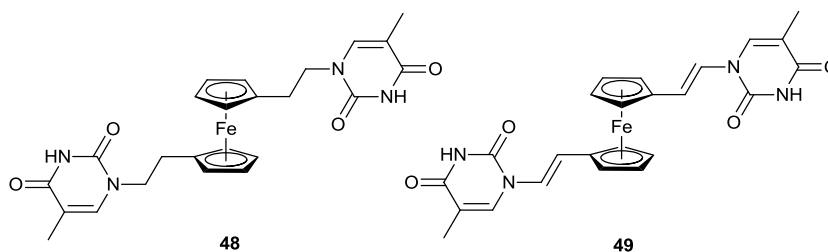
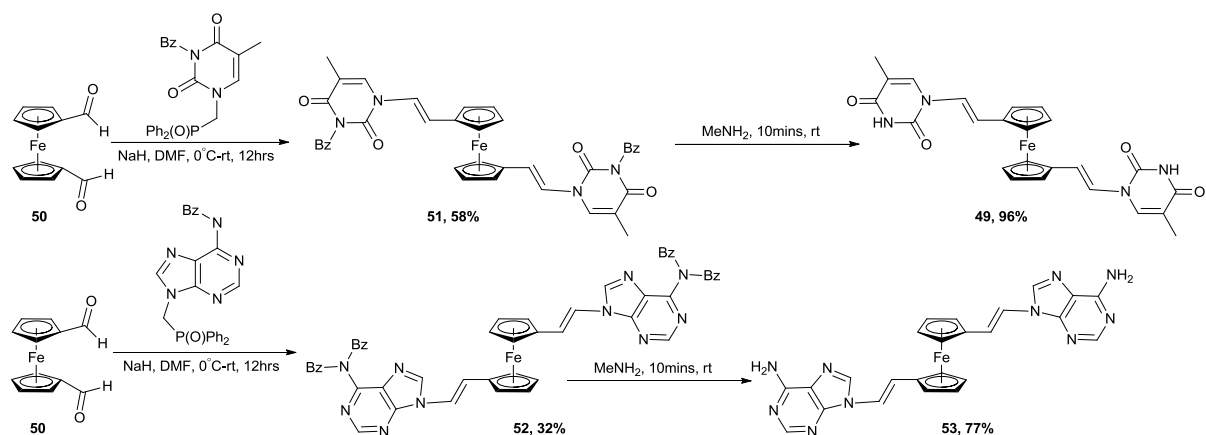


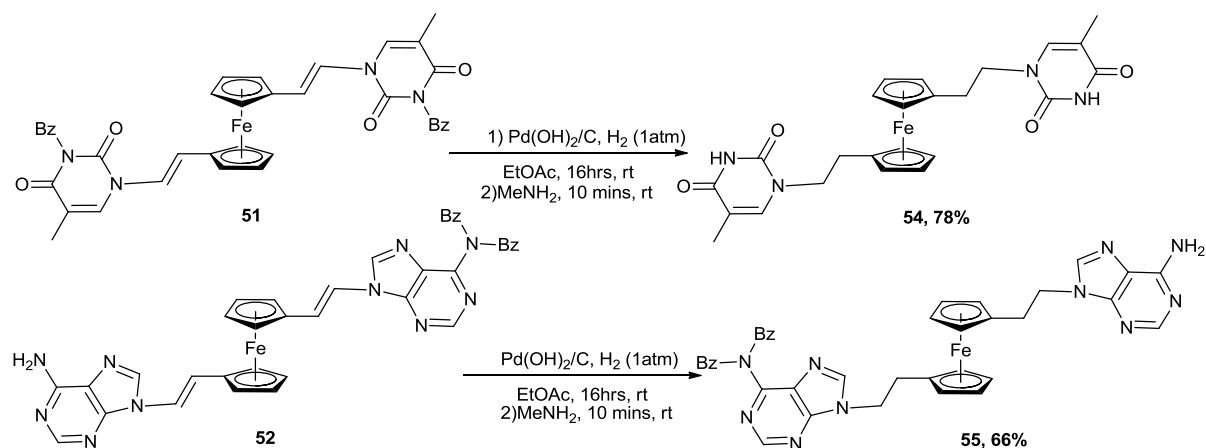
Figure 1.25: Examples of the synthesised nucleobase derivatives

The starting material for all four of the desired products was ferrocene-1,1'-dicarboxaldehyde **50**. **50** was reacted with the benzoyl protected phosphonates of either adenine or thymine *via* a Horner-Wadsworth-Emmons reaction (Scheme 1.25), the benzoyl protecting groups were removed to afford the desired products.



Scheme 1.25: Synthetic route to 49 and 53

For the saturated linker containing derivatives the alkene bonds were reduced *via* hydrogenation with Pd(OH)₂/C and hydrogen gas (1 atm) (Scheme 1.26).



Scheme 1.26: Hydrogenation reaction to afford 54 and 55

Tucker *et al*, studied the four derivatives *via* electrochemical analysis and to further the understanding of their behaviour during solid-state aggregation studies. The four derivatives were analysed *via* cyclic voltammetry and there was found to be a large difference in the redox potentials between the saturated derivatives: **54** (525 mV) and **55** (552 mV) and the unsaturated derivatives: **49** (765 mV) and **53** (770 mV).

Ferrocene derivatives have also been used as the redox-active labels for the use in DNA intercalators.⁹² Takenaka *et al.*,⁹³ reported the synthesis of a ferrocene modified naphthalene diimide intercalator (Figure 1.26). The intercalator is a threading intercalator, these intercalators contain a region of planar functionality that intercalates between dsDNA bases and a reporter moiety that is threaded through the DNA.

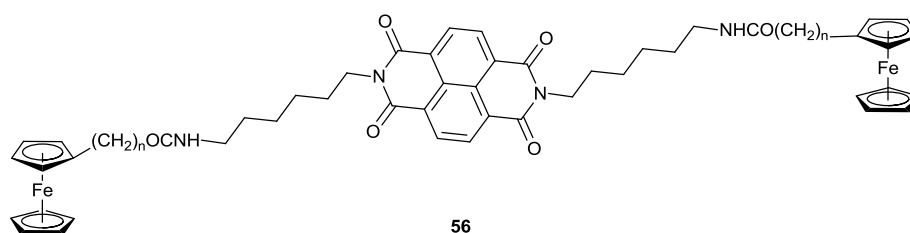
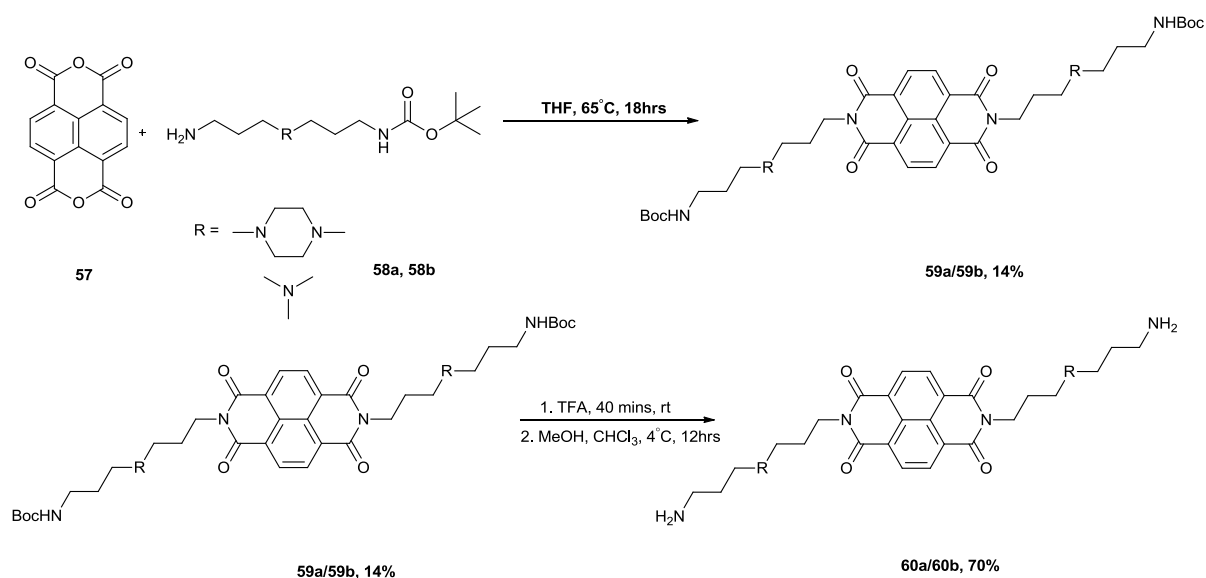


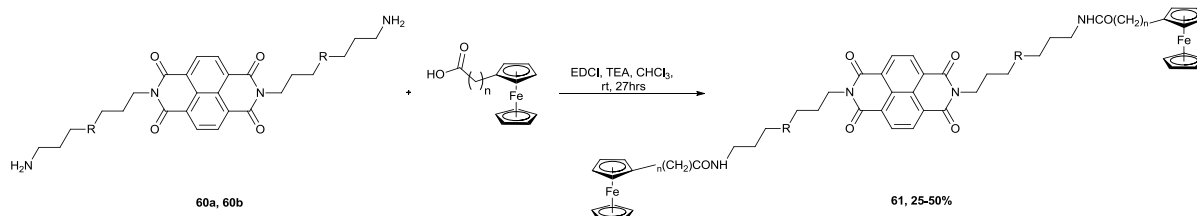
Figure 1.26: Takenaka DNA intercalator

The intercalator **56** was found to have an oxidation potential of ~250 mV. Takenaka *et al.*,⁹⁴ later published improvements of their original intercalator **56**. The intercalator modifications were based around the length of the linker and the linker structure (Scheme 1.27).



Scheme 1.27: Synthesis of intercalator backbone and linker

60a and **60b** were then labelled with a range of ferrocene derivatives to produce a range of redox-active DNA intercalators (Scheme 1.28).



Scheme 1.28: Functionalisation of Intercalator with ferrocene moiety

The ferrocene derivatives used to label naphthalene diimide linker ferrocenecarboxylic acid, ferrocene acetic acid and ferrocenepropionic acid. The labelled intercalators were found to have a range of oxidation potentials from 180 mV – 440 mV depending on which ferrocene derivative was used.

Oligonucleotides can be tagged with ferrocene labels in two main ways: post-labelling and nucleobase incorporation. The post-labelling approach involves the synthesis of the complete oligonucleotide strand, to which the ferrocene containing label is conjugated to complete the DNA probe. The conjugation of the transducer label to the oligonucleotide normally is carried out on the 5' end of the oligonucleotide (Figure 1.27).

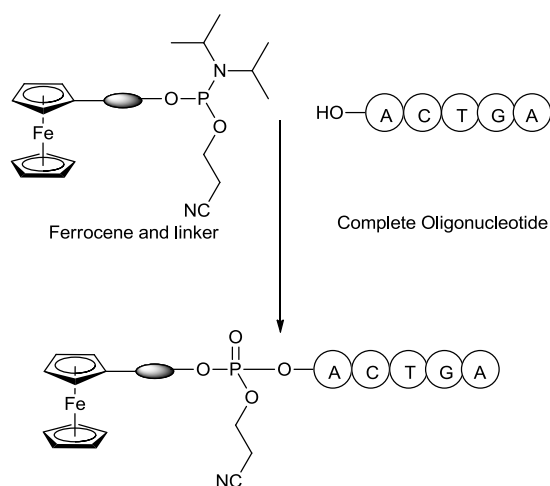
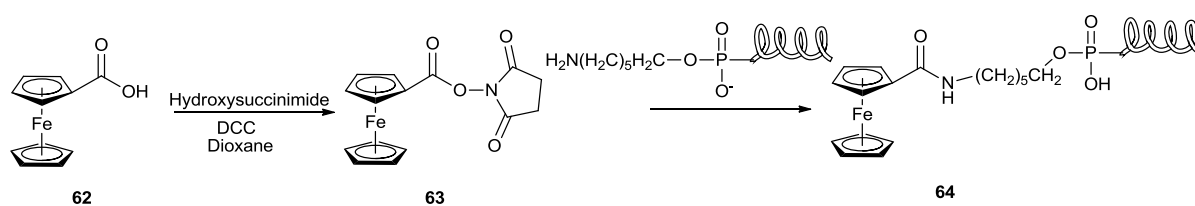


Figure 1.27: Representation of post-labelling approach

Synthetic post-labelling is one of the most common methods used in post-labelling of probes. This involves the synthesis of an oligonucleotide probe which has been labelled with a linker and once purified the oligonucleotide is then further reacted with an activated form of the desired ferrocene derivative such as an *N*-hydroxysuccinimide ester (NHS). This method was first reported in the literature using the NHS ester of ferrocenecarboxylic acid, which was reacted with an oligonucleotide that had been labelled with a carbon chain with a terminal amine group (Scheme 1.29).

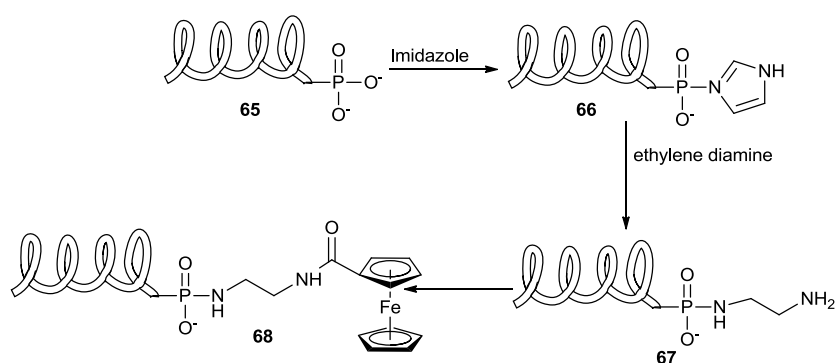


Scheme 1.29: Conjugation to oligonucleotide via NHS ester

The labelled probe was used for a DNA hybridisation based assay as a sensor, the ferrocene probe was added to a solution that contains a complementary target strand of DNA. The hybridised DNA is injected into an HPLC column that allows dsDNA to pass through the column to the electrochemical detector. The assay is calibrated

using certain concentration of the ferrocene probe, this allows for quantitative analysis of concentration of target DNA.⁹⁵

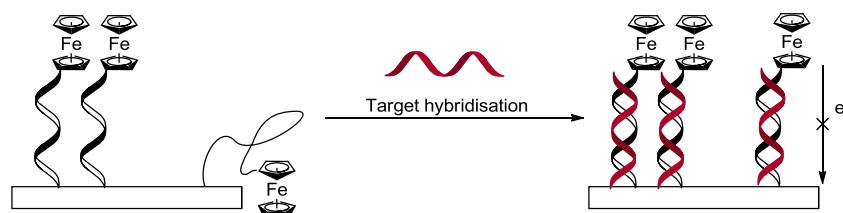
Fang *et al.*,⁹⁶ functionalised the free phosphate groups on the oligonucleotide by reacting it with imidazole, then ethylene diamine and finally, *via* an EDCI coupling reaction, with ferrocenecarboxylic acid (Scheme 1.30).



Scheme 1.30: Example of covalently labelling an oligonucleotide probe

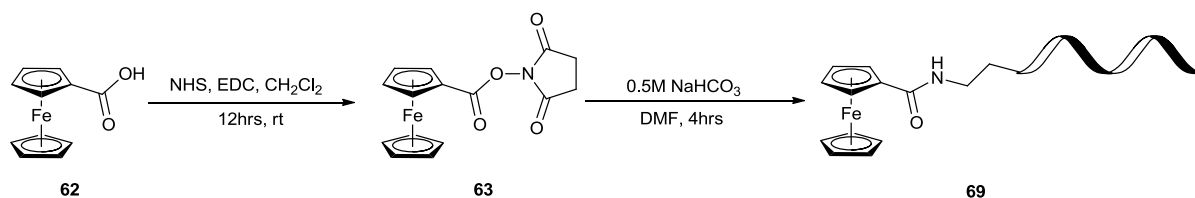
The assay developed works *via* target DNA being adsorbed onto the surface of a carbon electrode, to which the DNA probe was added and hybridisation occurs and a signal is produced, however no signal is observed when a mismatch in sequence is observed.

White *et al.*,⁹⁷ developed a biosensor for the detection of target DNA using an electrode immobilised capture probe that was labelled with a ferrocene moiety at the 3'-terminal of the oligonucleotide. When the target DNA is present and hybridisation with the labelled capture probe has taken place there is an 87% decrease in the electrochemical signal exhibited from the label at the electrode (Scheme 1.31).



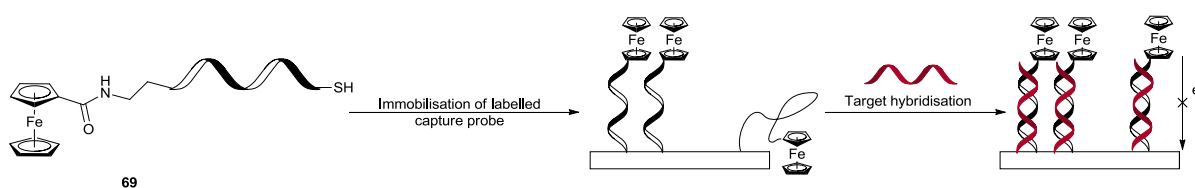
Scheme 1.31: Schematic of White's DNA detection assay

Ferrocenecarboxylic acid is used as the redox-active moiety. The ferrocenecarboxylic acid was converted to the activated NHS ester which was coupled to the amine labelled 3'-terminal of the oligonucleotide (Scheme 1.32).



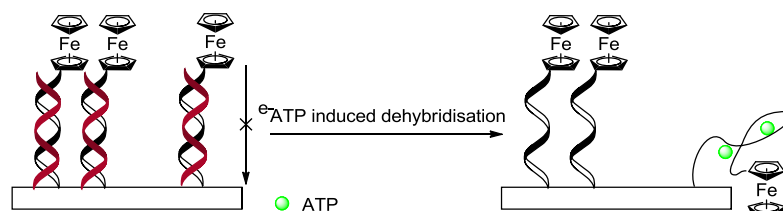
Scheme 1.32: Labelling of oligonucleotide probe with ferrocene NHS ester

Fan *et al.*,⁹⁸ reported the development of a target responsive electrochemical switch assay to be used in the development of a biosensor. In this assay an oligonucleotide was labelled at the 5'-terminal with a reporter moiety, in the case of this assay a ferrocene derivative was used. The 3'-terminal of the oligonucleotide was thiolated for the immobilisation of the probe to the surface of a gold electrode (Scheme 1.33). The immobilised capture probe is able to hybridise with the target DNA, which causes a reduction in the signal at the electrode from the reporter moiety.



Scheme 1.33: Immobilisation of Ferrocene labelled capture probe followed by hybridisation

Adenosine triphosphate (ATP) is used in the assay to separate the complementary strand from the immobilised capture strand which switched on the electrochemical signal at the electrode (Scheme 1.4).



Scheme 1.34: Switching on of electrochemical signal by dehybridisation via ATP

The assay developed by Fan *et al*, has a number of advantages, like most DNA detection assays it is largely resistant to non-complementary DNA strands and was shown to be functional in a complex reaction matrix.

Farkas *et al*,⁹⁹ produced a system for electrochemical detection of nucleic acids via micro arrays, also providing a selective detection method for molecular diagnostics. Gold electrodes were printed on circuit boards and coated with a self-assembled monolayer (SAM) containing DNA capture probes. Target nucleic acids are immobilised on the surface of the electrode via SAM using the capture DNA oligonucleotide. Another oligonucleotide containing ferrocene-modified nucleotide complementary to another section of the target DNA is introduced. The ferrocene labelled oligonucleotides binding site is near to the surface of the SAM layer (Figure 1.28).

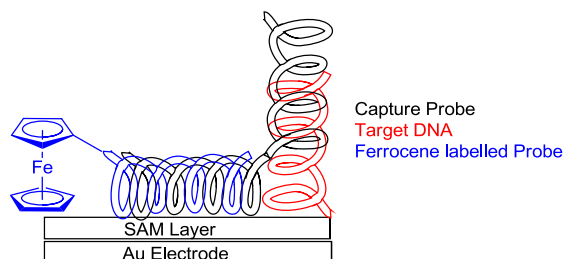
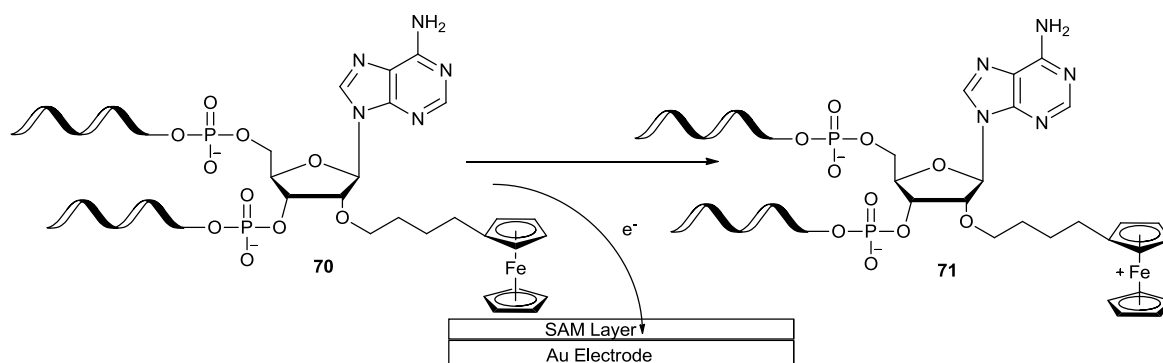


Figure 1.28: Example of Farkas SAM assay

The SAM layer allows for the electron transfer to the electrode and also has the benefit of blocking the electrode from other redox active species in the solution – including the unbound probe (Scheme 1.35).

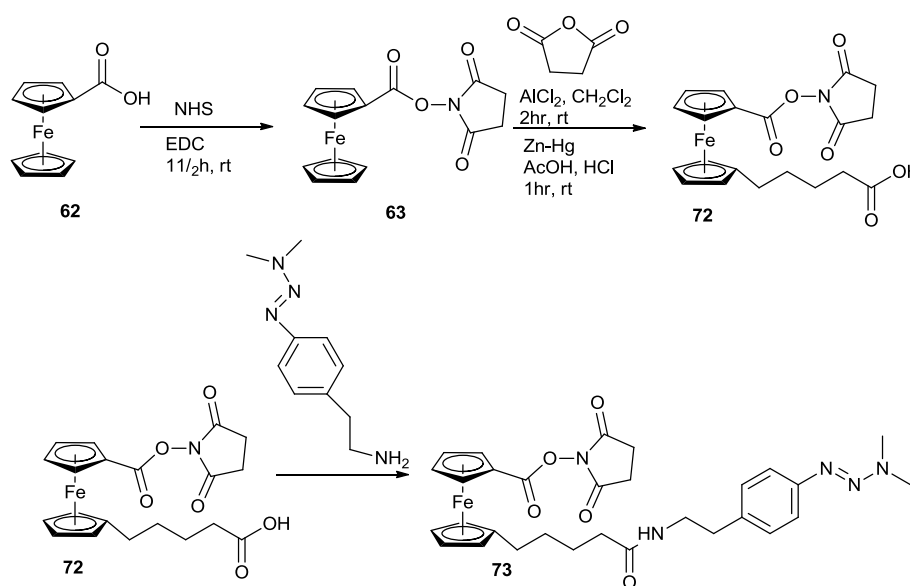


Scheme 1.35: Reaction at the electrode surface

Through the use of PCR and oligonucleotides this method shows high sensitivity for the target DNA. Also high sensitivity towards a positive sample due to only the bound redox centre being able to interact with the electrode.

Gothelf *et al.*,¹⁰⁰ carried out work using a ferrocene derivative as an electron mediator in the detection of DNA hybridization in the study and characterisation of oligonucleotides. Gothelf *et al.* present work showing the trapping of a ferrocene derivative between a single strand of DNA and an electrode, either a gold or glassy carbon electrode. DNA that has been fixed to an electrode has been shown to have

interesting hybridisation properties that can be seen through the reversible redox potential shift of a mediator, in this case a ferrocene based derivative. This redox shift is detected during the hybridisation and denaturation process. The ferrocene derivative Gothelf studies was synthesised from ferrocene carboxylic acid. It was modified with a triazene moiety on one of the cyclopentadienyl rings, this group is used in the fixation of the ferrocene mediator to the electrode. The carboxylic acid derivative is converted to an active ester which is then conjugated to an aminated DNA strand (Scheme 1.36).

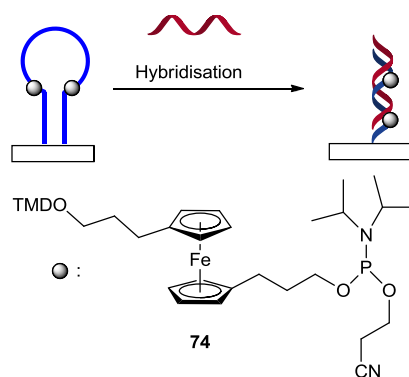


Scheme 1.36: Synthesis of ferrocene linker unit 73

Using a target strand of DNA that had been labeled with methylene blue, the hybridisation between the mediator immobilised DNA and the methylene blue labeled target strand DNA can be observed.

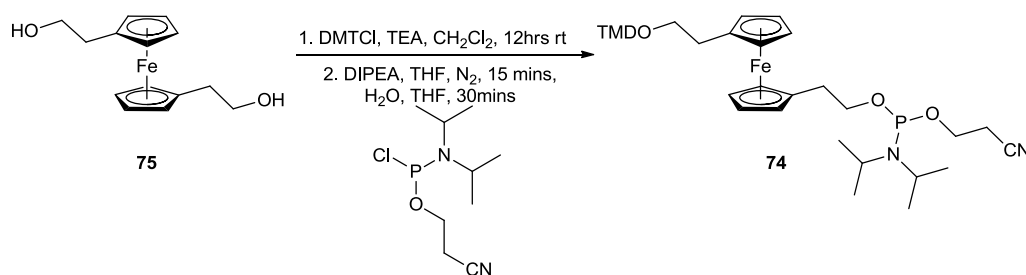
Chaix *et al.*¹⁰¹ reported the development of electrochemical probes for nucleic acid detection, using a ferrocene phosphoramidite derivative **74**. **74** was incorporated into a stem-loop structure. Stem-loop structures are often used in fluorescent detection methods of DNA.¹⁰²⁻¹⁰³ Oligonucleotides used in the synthesis of these stem-loop structures are often functionalised at either the 5' end or the 3' end with the transducer reporter moiety. Chaix *et al.*, developed a functionalised stem-loop with the ferrocene derivative **74** being incorporated into the stem-loop structure

itself, between the stem region and the loop moiety. The assay works on the detection of a shift in the redox properties of **74**, between the closed stem-loop structure and the opening of the stem-loop during the hybridisation with target DNA. The ferrocene derivative used as the label in this assay was ferrocene-1,1'-bispropanol (Scheme 1.37).



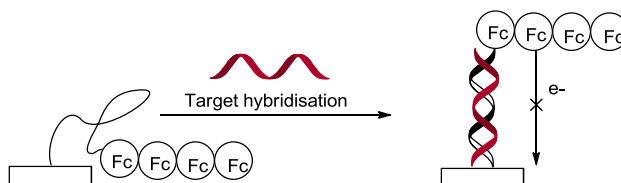
Scheme 1.37: Stem-loop assay developed by Chaix *et al*

Chaix *et al*,¹⁰⁴ further reported the development of a ferrocene modified stem-loop probe for the detection of target DNA and even a single-base mismatch. Ferrocene bis propanol **75** was used as the ferrocene derivative in this assay, in which four ferrocenes were labelled onto the 5' end of the stem-loop with the 3' end being trapped onto the surface of a gold electrode. The use of the four ferrocenes in a row allowed for the detection of target DNA in concentrations as low as in the 1 pM. The ferrocene bis propanol was activated for the use in an automated oligonucleotide synthesiser with both a trityl protecting group and a phosphoramidite (Scheme 1.38).



Scheme 1.38: Synthesis of ferrocene derivative **74**

When there was no target DNA present the hairpin remained intact and therefore allowed the ferrocenes to reach the electrode and a signal was observed, however when the target DNA was present there was a decrease in the signal observed or the signal was completely shut off (Scheme 1.39).



Scheme 1.39: Chaix DNA detection assay

Bertin et al,¹⁰⁵ reported the development of electroactive self-assembled monolayers as platform for biosensors. Specifically ferrocenyl molecules with functional groups suitable for bioconjugation and immobilisation with SAMs. This paper describes the synthesis of novel redox active biofunctional crosslinkers from unsymmetrical 1,1'-disubstituted ferrocenes (Figure 1.29).

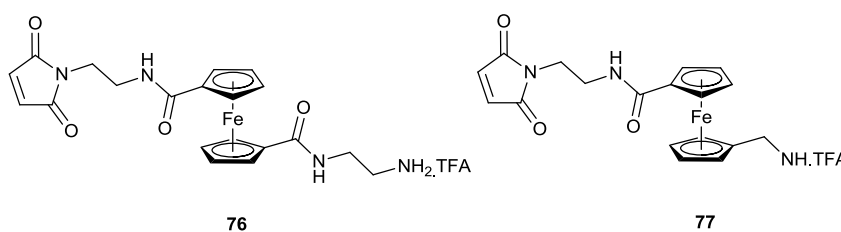


Figure 1.29: Ferrocene derivative for incorporation into SAM layer

The derivatives were analysed *via* cyclic voltammetry, the derivatives were first tested as *N*-*boc* protected derivatives. Both of the derivatives exhibited reversible one electron redox reaction. **78** was found to have an oxidation potential at 338 mV compared to **79** was found at 178 mV (Figure 1.30).

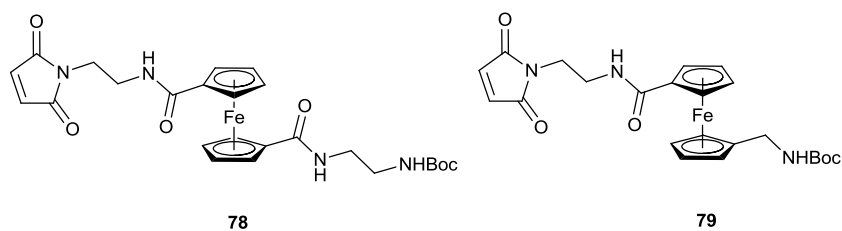


Figure 1.30: Boc-protected versions of 76 and 77

The deprotected derivatives were found at **76** 392 mV and **77** 297 mV (Figure 1.29). The difference in oxidation potential exhibited between the protected and deprotected derivatives can be explained by the electron withdrawing effects of the amine TFA salts in the deprotected compounds and the effect this has over the electrochemistry of ferrocene. The preparation of novel metal containing peptide nucleic acids (PNA) is an area of great interest in the field of sensing. PNA's are unnatural nucleic acids with a back bone made of *N*-(2-aminoethyl)glycine units. They are bound together *via* methylene carbonyl to the nucleobases. The sequence of PNA have to hold up to the values of the Watson-crick base pairing rules. The modification of PNA's with the incorporation of metal containing groups has been carried out for a number of different reasons such as biosensors, development of artificial nucleases and proteases and also increase the cell uptake of PNA strand.

Metler-Nolte *et al*,¹⁰⁶ reported the development of a duplex PNA based biosensor for the detection of two different sequences of target DNA. The synthesis of two differently sequenced oligonucleotides was carried out using solid supported methodology with the 3' end being built of a PNA linker, which is present to tether the oligonucleotide to the surface of an electrode. The 5' end of the oligonucleotide was labelled with an acetyl azide derivative. Two electrochemically unique ferrocene alkyne derivatives were used (Figure 1.31), in the post oligonucleotide synthesis labelling.

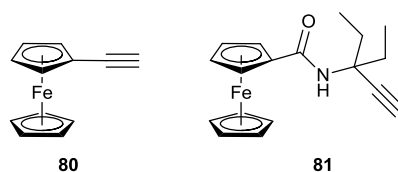


Figure 1.31: Ferrocene derivatives used by Metler-Nolte

The ferrocene derivatives **80** and **81** were conjugated to the oligonucleotides *via* click chemistry with the terminal azide group on the oligonucleotides (Scheme 1.40).

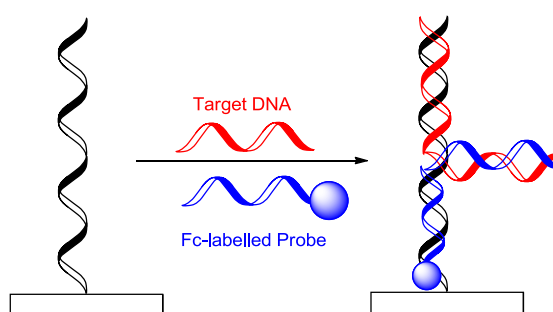


Scheme 1.40: Post-synthesis labelling *via* click chemistry

The two labelled oligonucleotides **83** and **84** both produce a signal at the electrode when neither of the target DNA strands are present, this is thought to be due to the flexibility of the oligonucleotides. Both the ferrocene derivatives have different oxidation potentials with **83** having an oxidation potential of approximately 350 mV and **84** having an oxidation potential of approximately 500 mV. However when the target DNA was added there was an approximate 60% decrease in intensity of the signal from the ferrocene labelled oligonucleotide. The drop in intensity was caused by the hybridised DNA being less flexible than the single-stranded oligonucleotide, therefore the ferrocene end group can not as readily reach the electrode surface.

Li *et al.*¹⁰⁷ described the development of an electrochemical DNA biosensor based around the proximity-dependent surface assay. The biosensor assay involved the immobilisation of a capture probe onto the surface of a gold electrode, through a 3'-thiol group. The sequence of the capture probe is complementary to both half the strand of the target DNA and the labelled end of the ferrocene labelled probe. The ferrocene probe was labelled at the 5'-end through an EDC coupling reaction

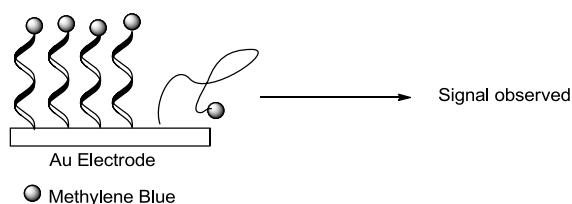
between ferrocenecarboxylic acid and the 5'-terminal amine on the oligonucleotide. The ferrocene labelled probe is also complementary to the other half of the target DNA, this leads to the 5'-labelled ferrocene being trapped close to the gold electrode surface (Scheme 1.41)



Scheme 1.41: Li biosensor assay

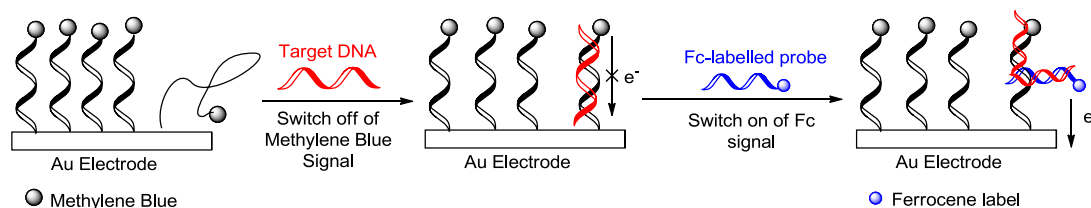
Li *et al.*, showed that they could detect target DNA in as lower concentration as 1 fM as well as the assay being able to distinguish between complementary DNA compared to mismatch hybridisation. This would allow for the assay to be used as an electrochemical DNA biosensor, for the detection of a specific target DNA in a complex medium.

Lai *et al.*,¹⁰⁸ reported the development of an electrochemical DNA sensor which involves two different redox-active labels, methylene blue and ferrocene are the two redox-active moieties used. The assay functions as both a signal-off and a signal-on probe based assay. The assay involves the immobilisation of the capture probe onto the gold electrode surface. The capture probe is immobilised onto the gold electrode surface *via* a 5'-alkanethiol group. The capture probe was also labelled at the 3'-end with the redox-active label methylene blue, when no target DNA was present in the assay mixture the methylene blue moiety was able to reach the electrode surface and a signal was observed. Lai *et al.*, found the methylene blue moiety to have an oxidation potential of approximately -270 mV (Scheme 1.42).



Scheme 1.42: Methylene blue labelled capture probe on gold electrode surface

When the target DNA is present in the assay medium there is a drop in intensity of the signal exhibited from the methylene blue labelled capture probe. A ferrocene labelled probe is also used in the assay, which is partially complementary to the target DNA as well as the methylene blue labelled capture probe. The ferrocene labelled probe becomes captured with the ferrocene label moiety being in close proximity to the electrode surface ‘switching-on’ the signal from the ferrocene label (Scheme 1.43).



Scheme 1.43: 'Switch off' - 'switch on' assay developed by Lai *et al*

Lai *et al*, showed that not only could the assay protocol be used as a DNA sensor for a specific target DNA but the assay could also be used to determine specific mismatches between the capture probe and the target, through the comparison of the signal intensities observed for the two redox-active labels used in the assay.

Nucleobase incorporation uses ferrocene modified nucleobases in the synthesis of the oligonucleotide probe, this allows the label to be positioned in the probe at a specific location (Figure 1.32).

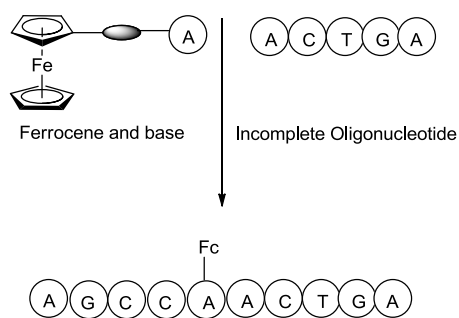


Figure 1.32: Representation of nucleobase incorporation approach

The most common method for nucleobase incorporated probes is *via* a solid supported synthesiser. This method is widely used in the preparation of DNA chips for surface modification. Labelling nucleobases with ferrocene has the advantage of being able to incorporate the ferrocene labelled nucleobase anywhere in the sequence.

Meade *et al*, developed a ferrocene modified nucleobase for the use in nucleobase incorporation **85** (Figure 1.33).¹⁰⁹

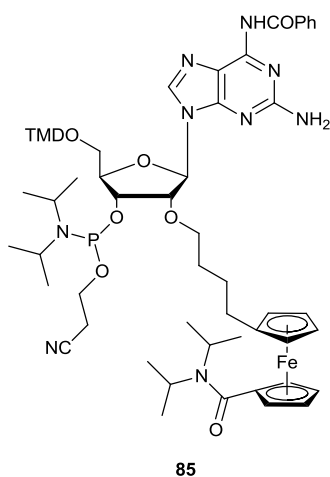
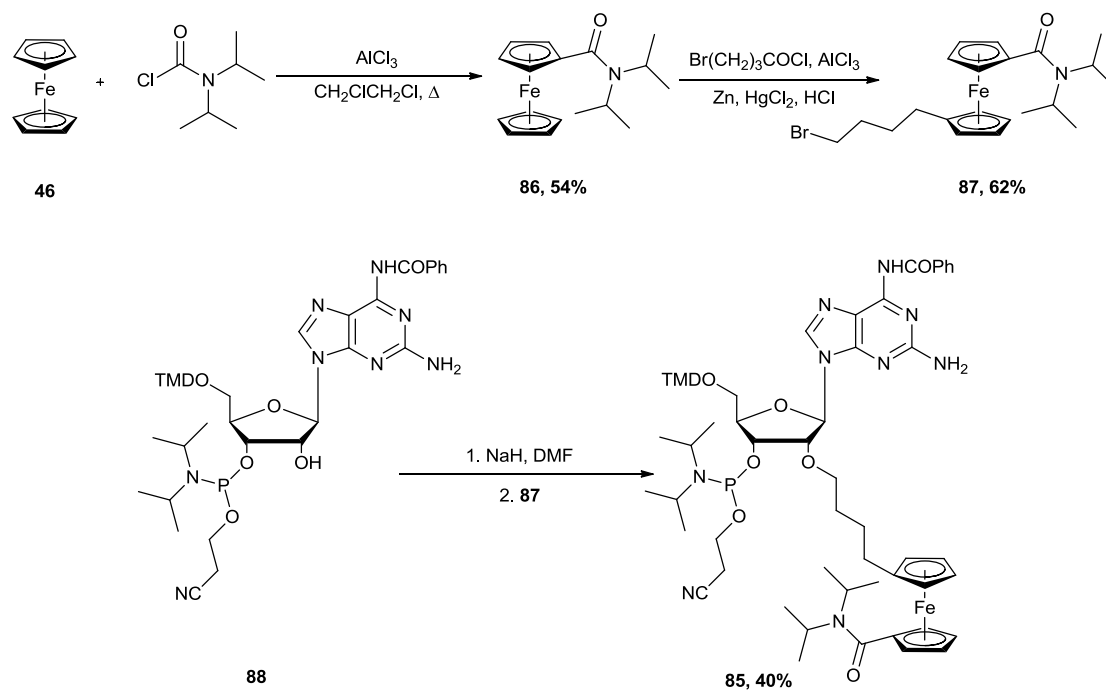


Figure 1.33: Ferrocene modified nucleobase

The electrochemical moiety is synthesised from ferrocene *via* a Friedel-Crafts acylation followed by a Clemmensen reduction (Scheme 1.44), which was then coupled to adenosine.

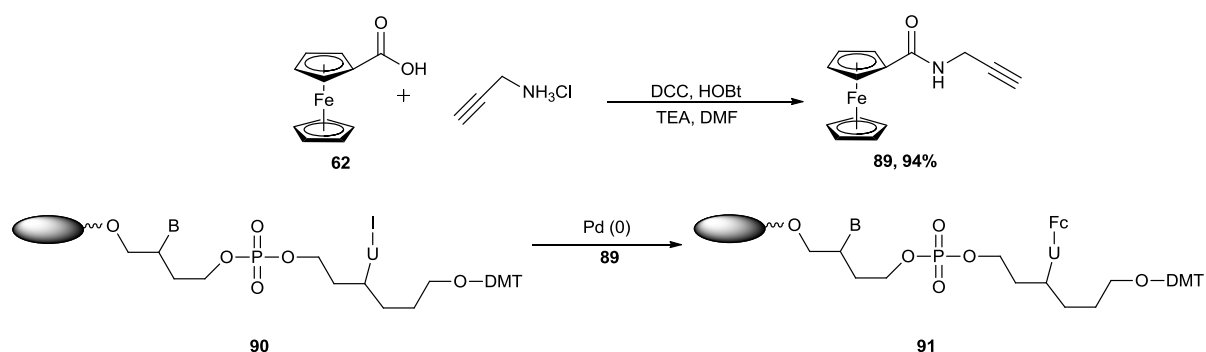


Scheme 1.44: Synthetic route to ferrocene labelled adenosine 85

The ferrocene modified adenosine was incorporated into an oligonucleotide at various locations along the strand. The incorporation of the ferrocenyl modified nucleotide into the oligonucleotide was found to have little destabilisation of the oligonucleotide or the duplex.

Electrochemical analysis of the labelled oligonucleotides containing ferrocene showed that the oligonucleotides can be used as a signalling probe for the electrochemical detection of nucleic acids. This was carried out *via* the incorporation of the ferrocene modified oligonucleotides into a CMS-DNA chip, to detect single base mismatches using a second labelled oligonucleotide with a previously synthesised ferrocene labelled nucleotide base.

Grinstaff *et al.*,¹¹⁰ reported the synthesis of oligonucleotides with ferrocene derivatives at specific sites within the oligonucleotides. The oligonucleotides were synthesised containing halogenated bases within the oligonucleotide, which were labelled with a ferrocene derivative *via* a sonagashira cross-coupling reaction (Scheme 1.45). The structure and stability of hybridised DNA is not altered by the addition of ferrocene derivatives.



Scheme 1.45: Synthetic route to ferrocene derivative used for Sonagashira cross-coupling reaction

1.7 Conclusions

The field of DNA sensing is a large area of research that covers a range of different transducer methods. The most common transducer method used in DNA sensors are optical detection methods, however since the 1990 there has been a large amount of interest in the use of electrochemical reporter moieties for the use in DNA detection. A range of these methods have been outlined in this chapter, from the more established methods such as; redox-active DNA intercalators and the labelling of DNA probes with a redox-active reporter moiety to the relatively newer methods such as the use of nanopores for DNA sensing and sequencing. Ferrocene and its derivatives are the most common redox-active moieties used in a wide range of applications in the field of DNA sensing, ferrocene derivatives have been used as mediators, in redox-active DNA intercalators and labels for DNA probes.

2 Chapter 2: The Synthesis of Mono-ferrocenyl Labels for the use as DNA Probes

Summary of Chapter 2

This chapter details the synthesis of a range of monoferrocenyl derivatives for the use as redox-active labels and application in a DNA detection assay. The monoferrocenyl derivatives were analysed *via* differential pulse voltammetry to provide the oxidation potentials for the range of labels synthesised.

2.1 Atlas Genetics, T7 exonuclease assay

Atlas genetics are a UK-based diagnostics company producing an *in vitro* point-of-care device for the use in doctors surgeries and hospital wards. Atlas genetics are particularly focused on sexually transmitted diseases where quick diagnosis is required for treatment and control of the disease. Point-of-care devices have to be rapid in detection of the target compared to the standard laboratory testing methods, which in some cases can take up to a week to get the results back to the patient. They are also required to be extremely selective and sensitive. Atlas aim to cut the waiting time down to 30 minutes from sample extraction to being able to give the patient the results. The point-of-care device being developed by Atlas is based around one-use disposable cartridges, in which the whole assay is carried out. The clinical sample is injected into the cartridge, which is then loaded into the instrument (Figure 2.1).



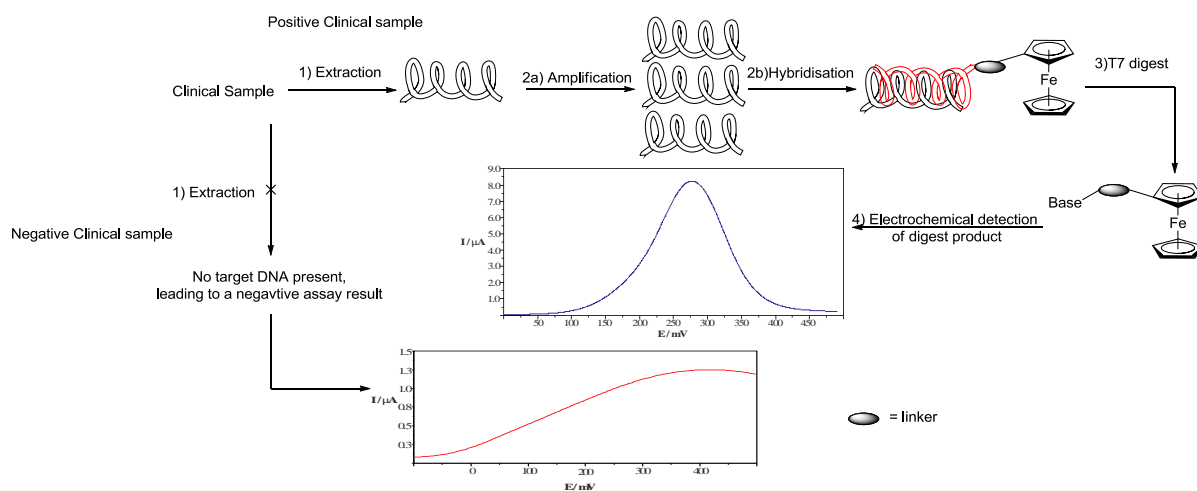
Figure 2.1: Atlas Genetics Point-of-care device

Once the cartridge is loaded into the instrument there is no further operator interaction required until the end of the testing process. The cartridges contain all the necessary reagents required to carry out the assay. The sample and the assay are processed through the card *via* pneumatically controlled fluidic movements. The assay cartridges contain multiple channels for the assay to be processed through with each channel leading to an electrode (Figure 2.2), the use of multiple channels sets the cartridge up for the multiplex detection of different pathogenic targets in the same cartridge.



Figure 2.2: Multichannel cartridge developed by Atlas Genetics

Atlas have developed a highly selective assay for the detection of pathogenic bacterial DNA. The Atlas assay can be broken down into four main sections: 1) extraction of the clinical sample, 2) amplification of target DNA and hybridisation, 3) a T7 exonuclease digest reaction and 4) electrochemical detection of digest product (Scheme 2.1).¹¹¹



Scheme 2.1: Schematic of the Atlas assay

The amplification step of the Atlas assay is carried out *via* PCR, this allows for the accurate detection of target DNA from a clinical sample in which there could be as few as five copies of the target DNA. The PCR method that Atlas are using amplifies a specific region of sequence in the target DNA, this region is unique to the particular bacterial pathogen of interest. The PCR amplification is able to be selective for a specific region in the target DNA due to the forward and reverse phase primers that are being used in the amplification step. Through the use of PCR the sensitivity of the assay is increased due to the higher volume of target DNA being present in the assay mixture post amplification.

Atlas are pairing the PCR amplification of a specific region of target DNA with the use of labelled oligonucleotide probes that are synthesised to have a complementary sequence to the target DNA. The oligonucleotide probes are labelled at the 5' end of

the strand with an electrochemically active molecule (Figure 2.3), in the case of the Atlas assay a ferrocene label is used.

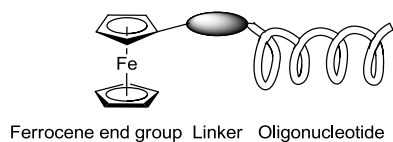


Figure 2.3: Structure of the labelled oligonucleotide probes

After PCR amplification the ferrocene labelled probe is hybridised with the target DNA. The dsDNA is then exposed to T7 exonuclease. T7 exonuclease is an enzyme that cleaves the phosphodiester bonds between nucleotides in nucleic acids. T7 is selective for dsDNA only and cleaves the DNA from the 5' end of the DNA (Figure 2.4).

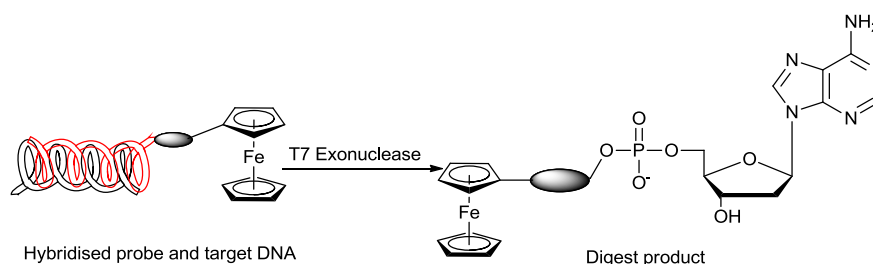


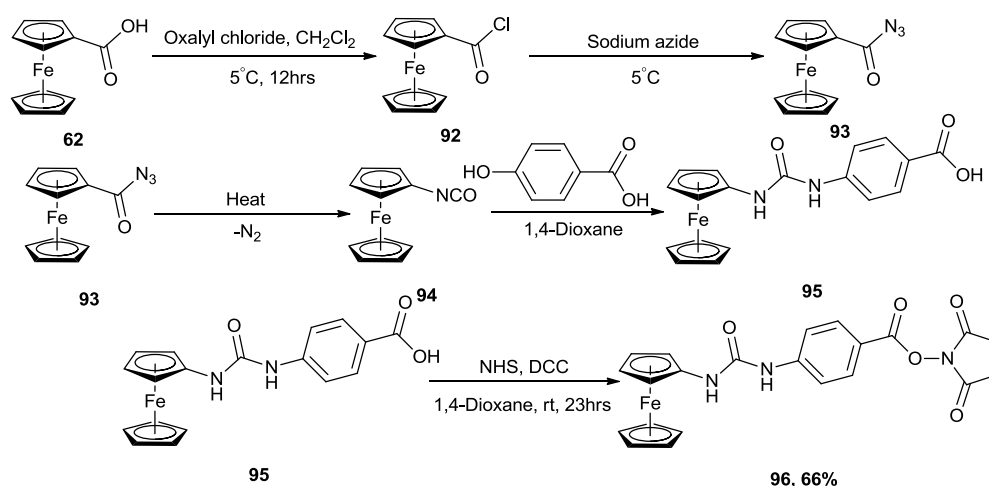
Figure 2.4: Action of T7 leaving single labelled nucleotide digest product

The digest product from the T7 exonuclease reaction is a single nucleotide with the ferrocene label attached. It is this digest product which is analysed on the electrode *via* differential pulse voltammetry. However if the sample is a negative and there is no target DNA present for the labelled probe to hybridise with, the T7 enzyme does not cleave the ssDNA and no signal is observed on the electrode.

2.2 Aims and Previous work

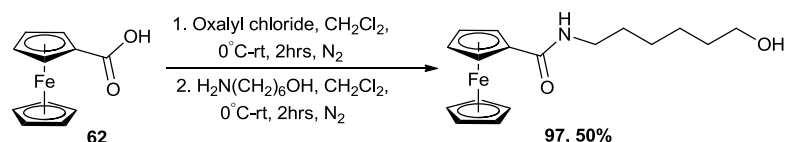
Previous work in the group focused on the synthesis of ferrocene containing DNA probes for the detection of gene sequences using an exonuclease enzyme based assay, developed by Atlas Genetics (previously Molecular Sensing).

Hillier *et al.*,¹¹² synthesised a ferrocene label **96** that could be readily coupled to an oligonucleotide post synthesis *via* a coupling reaction using a 5' amine-labelled oligonucleotide. **96** was found to have an oxidation potential of 150 mV vs. Ag/AgCl (Scheme 2.2).



Scheme 2.2: Synthetic route to label **96** developed by Hillier *et al*

Hillier *et al.*,¹¹³ developed a ferrocene containing label for the detection of target DNA. The previous label **96** by Hillier *et al* was synthesised to be covalently labelled post oligonucleotide synthesis, whereas **97** was designed to be conjugated to the oligonucleotide *via* the phosphoramidite derivative. Ferrocenecarboxylic acid was used as the starting material for the synthesis of label **97**. Ferrocenecarboxylic acid was taken through an amide coupling *via* the *in situ* generation of the acid chloride, which was reacted with 6-aminohexan-1-ol to afford **97**, which was found to have an oxidation potential of 400 mV vs. Ag/AgCl (Scheme 2.3)



Scheme 2.3: Amide label 97 synthesised by Hillier *et al*

There is a large difference in the oxidation potentials of the two compounds synthesised, this is due to the urea functionalities in **96** being able to stabilise the ferrocenium ion, therefore leading to a lower oxidation potential compared to amide **97**. Flower *et al*, designed and synthesised a label containing two identical ferrocene moieties (Figure 2.5). **98** was found to have an oxidation potential of 250 mV vs. Ag/AgCl and is the current label being used in the assay developed by Atlas Genetics. **98** has an increased sensitivity in the assay in comparison to **96** and **97**, due to **98** containing two ferrocene moieties.

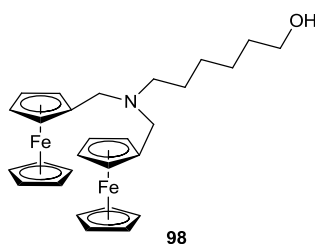


Figure 2.5: Label developed by Flower *et al*

The primary aim of the work presented within the thesis is to design and synthesise a range of redox-active compounds for the use as labels in a multiplex Atlas DNA detection assay *via* the conjugation of the labels to an oligonucleotide probe. The aim was to synthesise redox-active compounds based around ferrocene with unique oxidation potentials in comparison to each other and the current label **98** being used by Atlas. The main aim of the project is to utilise the range of labels synthesised in duplex or multiplex assays with **98** for the detection of more than one pathogen. The detection of more than one pathogen in the same assay is required due to the fact that a number of infectious diseases co-infect (such as Chlamydia and Gonorrhoea) or that

there can be a number of different strains of the bacterial pathogen like *Staphylococcus aureus* (such as in hospital acquired infections).

2.3 Results and Discussion

The development of new labelled oligonucleotide probes for the use in the multiplex DNA detection assay can be separated into three areas; 1) the design and synthesis of the redox-active label component of the overall probe, 2) the synthesis of the oligonucleotides and the conjugation of the activated label to the oligonucleotide post-synthesis and 3) analysis of the DNA probe in the DNA detection assay itself (Figure 2.6)

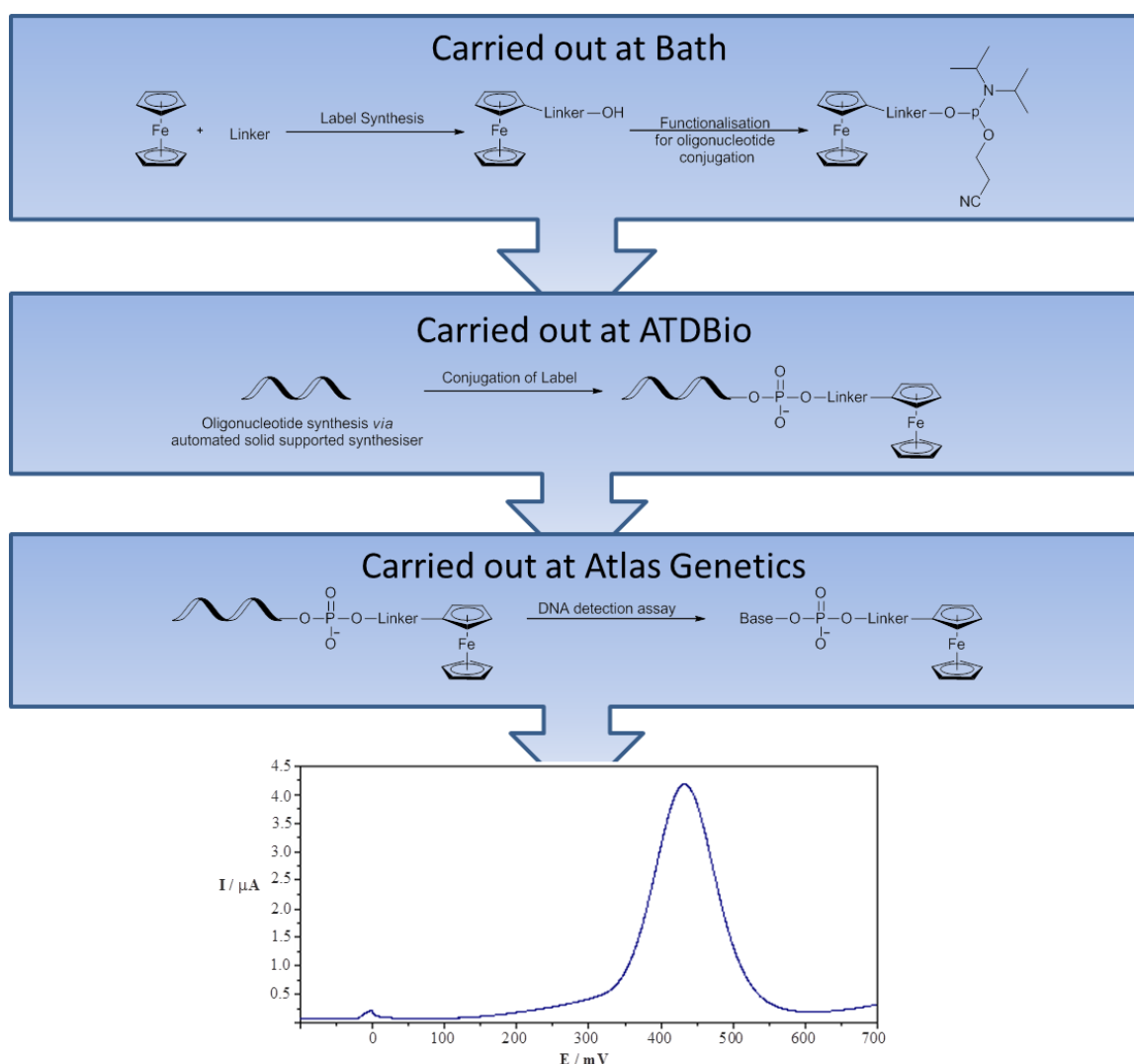


Figure 2.6: Flow chart of the synthesis and testing of redox-active DNA probes

For the Atlas assay these three areas are carried out at three different locations. The area that concerns the work carried out in Chapter two and three, is the design and synthesis of the redox-active labels and their functionalisation for conjugation to the oligonucleotide. When designing a new redox-active label for the use in the synthesis of probe oligonucleotides there are three main sections to consider; the redox-active moiety, the linker structure and functionality and the conjugation technique going to be used. The redox-active moiety of the labels to be designed and synthesised in this thesis are based around ferrocene. Ferrocene was chosen due to the ferrocene/ferrocenium ion redox couple being well understood as well as the ability to alter the oxidation potential of ferrocene *via* the functionalization of the Cp rings of the ferrocene.¹¹⁴⁻¹¹⁵ The ability to synthesis ferrocene based redox-active labels with different oxidation potentials is of importance in the development of a multiplex detection assay. As the linker portion of the label will be directly substituted onto the ferrocene, the functionality on the linker that is in close proximity to the ferrocene moiety will also have an effect on the oxidation potential of the ferrocene moiety. Therefore a range of linkers were targeted that contain a variety of functionalities such as; amine, amide, triazole and ether groups. A range of target labels were identified involving various levels of substitution on the ferrocene, as well as the utilisation of the linker moieties mentioned previously (Figure 2.7).

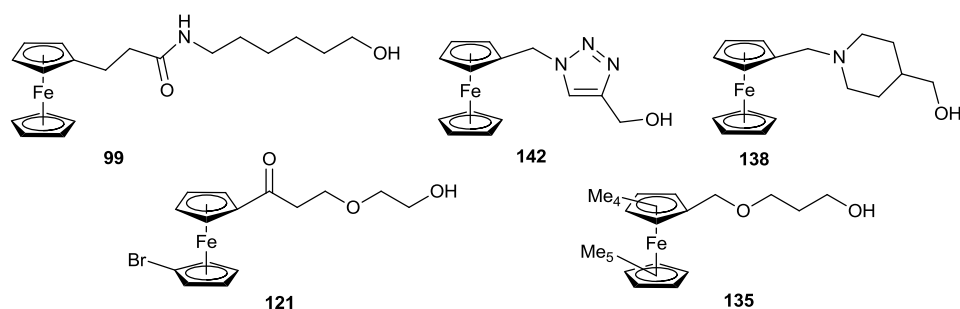


Figure 2.7: Range of target labels

The first of the target labels to be synthesised was **99**, the proposed synthetic route to 3-ferrocenyl-*N*-(6-hydroxyhexyl)propanamide **99** (Figure 2.8) was a four step synthesis.

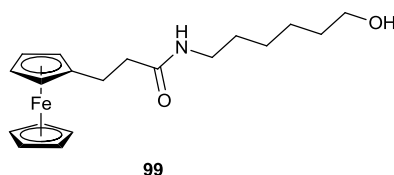
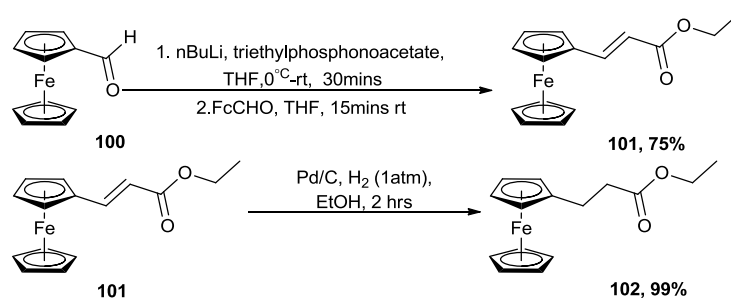


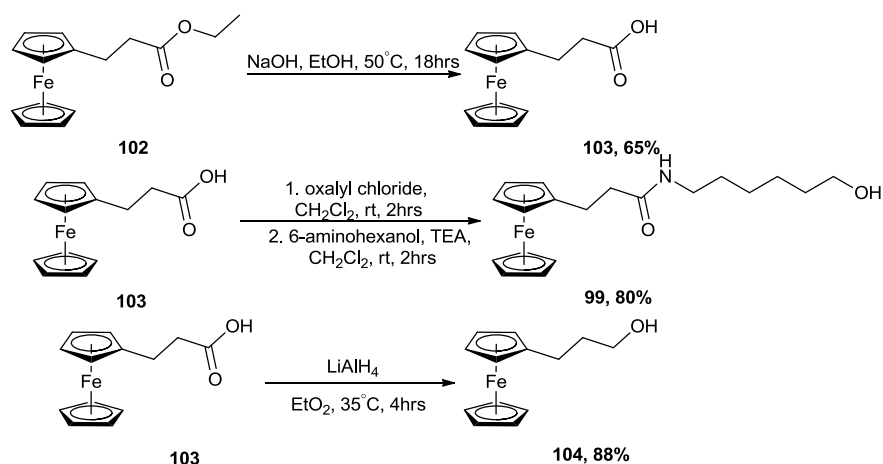
Figure 2.8: 3-Ferrocenyl-*N*-(6-hydroxyhexyl)propanamide

The label was synthesised starting from ferrocenecarboxaldehyde. First, a Horner-Wadsworth-Emmons reaction was carried out (Scheme 2.4) to afford the enone **101** in a good yield. The enone **101** was then reduced to the corresponding saturated ester under standard hydrogenation conditions using palladium on carbon to afford **102** in a high yield.



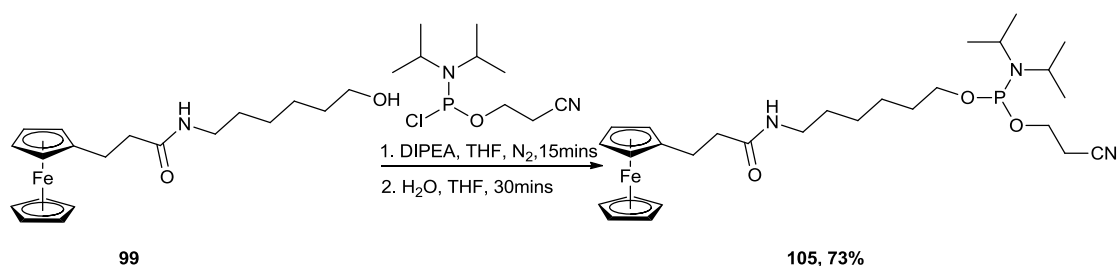
Scheme 2.4: Synthetic route to 102

The final steps of the synthesis of **99** was a saponification of ester **102** to yield carboxylic acid **103**, followed by an amide coupling with 6-aminohexanol. The carboxylic acid **103** was subsequently used for the synthesis of another label *via* a reduction of the carboxylic acid to the alcohol (Scheme 2.5).



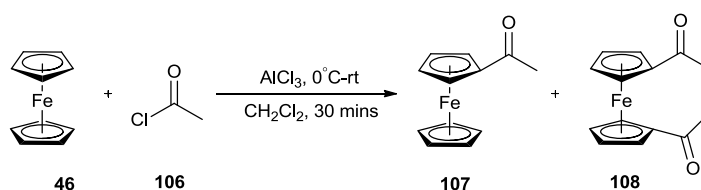
Scheme 2.5: Synthetic route to 3-ferrocenyl-N-(6-hydroxyhexyl)propanamide

3-Ferrocenyl-N-(6-hydroxyhexyl)propanamide **99** was easily synthesised on a relatively large scale and in a good yield over 4 steps. **99** was then analysed *via* differential pulse voltammetry under the standard conditions, showing it to have an oxidation potential of 85 mV vs. Ag/AgCl. The oxidation potential for **99** was found to be in a unique region of the electrochemical range, with comparison to **98**. Therefore the corresponding phosphoramidite was synthesised (Scheme 2.6). **104** was analysed *via* DPV and was found to have an oxidation potential of 85 mV vs. Ag/AgCl. However the label was not taken any further at this stage as the linker was believed to be too short for efficient coupling to oligonucleotide, being only a three carbon distance between the ferrocene and the hydroxyl group.



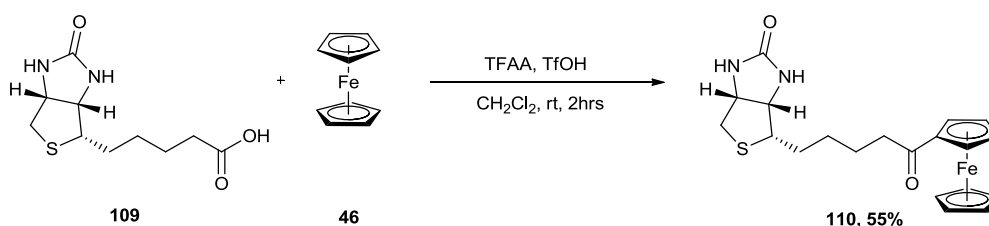
Scheme 2.6: Phosphoramidite synthesis of 105

Woodward *et al*,¹¹⁶ during their study of the structure of ferrocene, demonstrated that the reactivity of ferrocene was analogous to the reactivity of benzene rings. The cyclopentadienyl rings of the sandwich complex are electronically the same as a benzene ring. Therefore ferrocene can readily undergo aromatic electrophilic substitution reactions such as the Friedel – Crafts acylation reaction. One of the most common examples of ferrocene undergoing a Friedel – Crafts acylation reaction is in the synthesis of acetylferrocene (Scheme 2.7).¹¹⁷



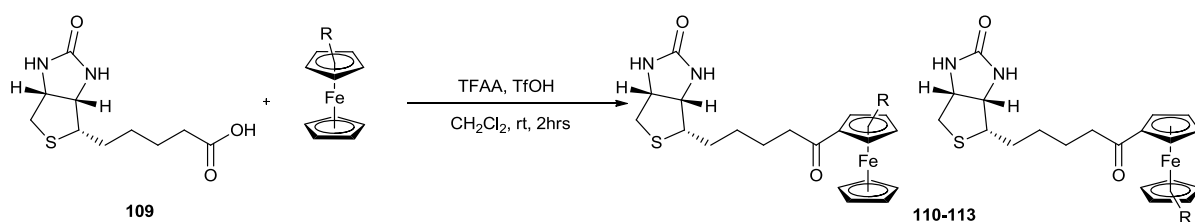
Scheme 2.7: Synthesis of acetylferrocene via Friedel-Crafts acylation

When the reactivity of ferrocene was compared to that of anisole in the Friedel – Crafts acylation reaction it was shown that ferrocene reacted at a much higher rate than the anisole. The reason for the higher rate of reaction for ferrocene is due to the electron density of ferrocene. The Cp ring has a higher electron density than that of a corresponding benzene ring. Salmain *et al*, published work on the use of biotin as an acylating agent in the Friedel – Crafts reactions with aromatic compounds, they showed an example using ferrocene as the aromatic derivative (Scheme 2.8).¹¹⁸ It was decided to utilise the reaction developed by Salmain *et al*, in the design and synthesis of a range of redox-active labels.



Scheme 2.8: Salmain Friedel - Crafts reaction with Biotin

Using a modified version of Salmain's conditions the reaction was repeated, using trimethylsilyl trifluoromethanesulfonate (TMS triflate) instead of triflic acid. The reaction proceeds by the formation of the acyltrifluoroacetate of biotin which then undergoes the Friedel – Crafts reaction in the presence of TMS triflate and ferrocene. It was discovered that through the use of TMS triflate there was an increase in yield to 95 %, compared to the 55% yield of product **110** when triflic acid is used. The scope of this reaction was explored using a range of ferrocene derivatives (Scheme 2.9, Table 2.1).

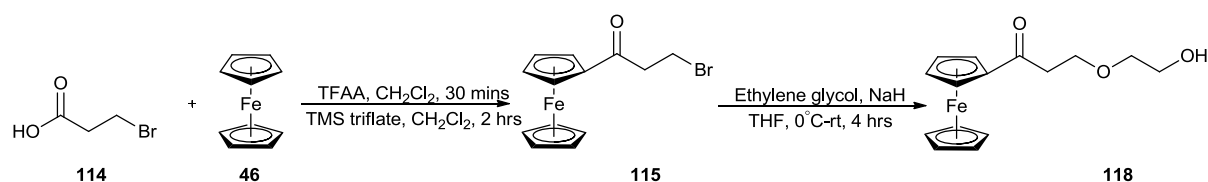


Scheme 2.9: Synthetic route to Friedel - Crafts products 110-113

Table 2.1: Yields from Friedel – Crafts reaction with a range of ferrocene derivatives

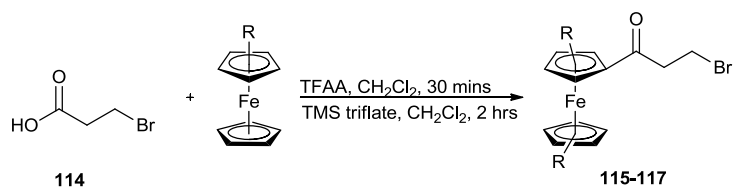
No.	Product	Yield
110		95
111		84
112		78
113		82

As shown in Table 2.1 the reaction works in good yield for the various substituted ferrocene derivatives. The majority of the products from the reaction substitution on the substituted Cp ring giving a 1,3-disubstituted ferrocene, however with the bromoferrocene derivative substitution was observed on the unsubstituted cyclopentadienyl ring giving a 1,1'-disubstituted ferrocene. The result was proven by the proton NMR spectra, in which there are four individual peaks for the protons on the Cp rings compared to the free Cp ring which all the protons come as a 5H singlet. The positive results from this reaction lead to the use of this methodology in the design and synthesis of a range of ferrocenyl derivatives to be used as labels for DNA probes. The carboxylic acid used in place of biotin had to have a functionality in the molecule that could be further functionalised either pre or post the Friedel – Crafts reaction to instill the free hydroxyl group needed for the conjugation of the label to the oligonucleotide probe, the compound chosen for such a task was 3-bromopropionic acid. 3-Bromopropionic acid was then utilised as the starting material for the synthesis of compound **118**. The route to **118** was to go through two synthetic steps, firstly a Friedel – Crafts reaction to give the desired ketone **115** followed by an etherification to give the target compound **118** (Scheme 2.10).



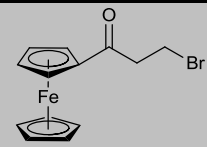
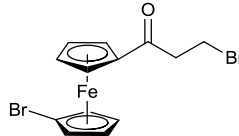
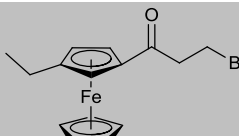
Scheme 2.10: Proposed synthetic route to labels using Friedel - Crafts methodology

The Friedel – Crafts reaction gave similar yields to the previous reactions carried out with biotin (Scheme 2.11, Table 2.2).

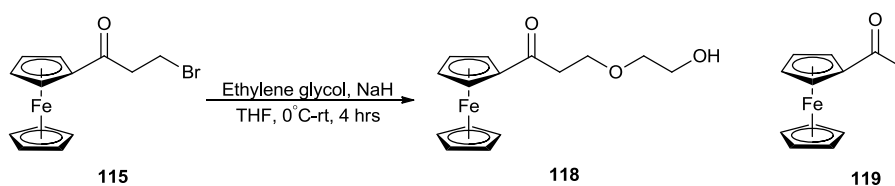


Scheme 2.11: General synthetic route to products 115-117

Table 2.2: Friedel – Crafts reaction with 3-bromopropionic acid

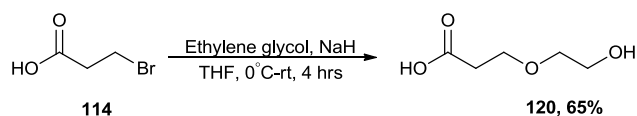
No	Product	Yield
115		95
116		65
117		65

However when the Friedel – Crafts reaction was carried out on a larger than 1 mmol scale, a significant side product was observed from the reaction. This second product was isolated and found to be the acrylate of the ferrocene species **118** (Scheme 2.12).



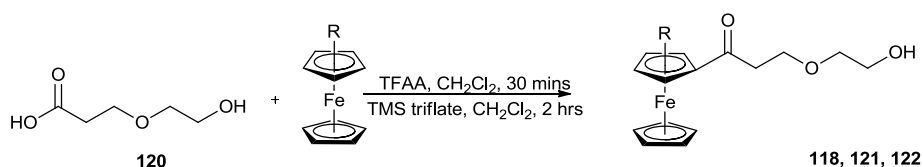
Scheme 2.12: Etherification reaction and acrylate by-product

Upon discovery of this result it was necessary to redesign the synthetic route towards these labels in an attempt to limit the formation of the acrylate. The first proposed strategy was carried out by synthesising the linker unit prior to the Friedel – Crafts reaction (Scheme 2.13).



Scheme 2.13: Synthesis of linker unit prior to Friedel - Crafts reaction

The synthesis of the linker was successful without the presence of any acrylate being formed, the linker was then exposed to the Friedel – Crafts conditions and this afforded the compounds **118**, **121** and **122** in good yield (Scheme 2.14 and Table 2.3).



Scheme 2.14: Friedel - Crafts reaction between linker 120 and a range of ferrocene derivatives

Table 2.3: Friedel - Crafts reaction with linker 120

No.	Product	Yield
118		65
121		68
122		64

This group of labels were analysed *via* differential pulse voltammetry to calculate their oxidation potential. The labels exhibited a range of oxidation potentials from 150 mV to 610 mV vs. Ag/AgCl, with **118** having an oxidation potential of 433 mV vs. Ag/AgCl which is due to the electron – withdrawing effects of the linker group

itself. The electron-withdrawing effects of the linker can be seen from the shift that has been exhibited on the oxidation potential of the ferrocene, which is usually at 160 mV and shifted to 433 mV (Figure 2.9).

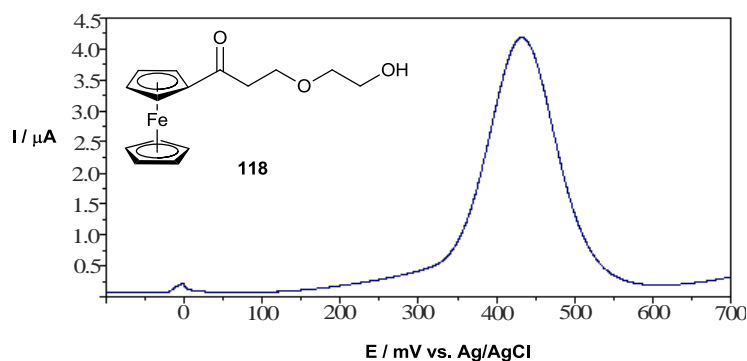


Figure 2.9: Voltammogram of the DPV scan of 118

The further electron – withdrawing effects of the bromide in compound **121** can be seen by its oxidation potential being 610 mV vs. Ag/AgCl, therefore the formation of the ferrocenium ion of this derivative is more difficult and requires a considerably higher voltage to oxidise the ferrocene (Figure 2.10).

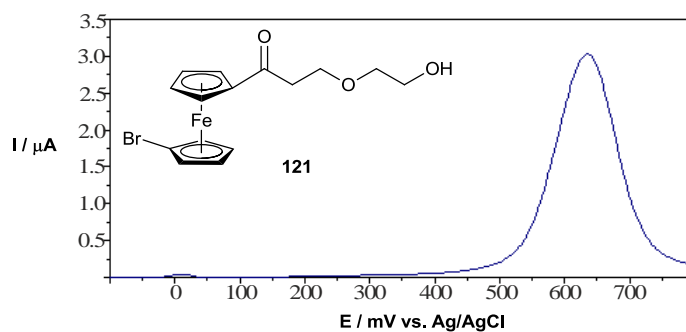


Figure 2.10: Voltammogram of the DPV scan of 121

The electron-donating ethyl group of **122** counteracts the electron-withdrawing nature of the linker group and an oxidation potential of 150 mV vs. Ag/AgCl is observed (Figure 2.11).

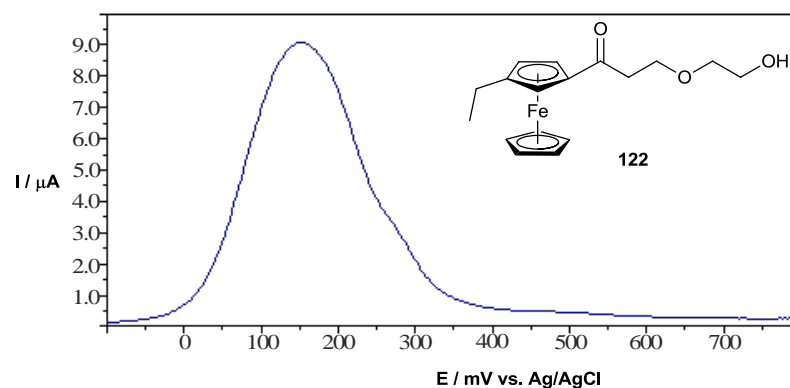


Figure 2.11: Voltammogram of the DPV scan of 122

All the oxidation potentials of these compounds come in unique regions compared to compound **98**, therefore they are all viable for a multiplex assay for the detection of target DNA. **118** was used for a duplex assay at the free hydroxyl stage, to assess the viability of using these monoferrocenyl labels in an assay with **98** (Figure 2.12, Table 2.4). It can be seen from the positions of the peaks **98** at 275 mV vs. Ag/AgCl and **118** at 433 mV vs. Ag/AgCl, there is definite separation between the two signal peaks.

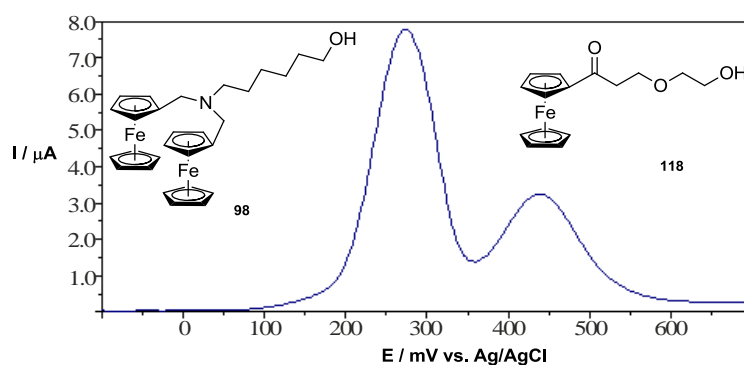


Figure 2.12: Voltammogram of the DPV scan of the duplex between 98 and 118

Table 2.4: Showing comparison of **98** and **118** via DVP

Label	Peak position (mV)	Peak height (μA)
98	275	7.5
118	433	3.2

However as can be seen from the Figure 2.12 the signal produced for **118** is considerably lower in intensity than that for **98**. While it would be expected for **98** to produce a signal of higher intensity as it is a label containing two ferrocene moieties whereas **118** only contains one ferrocene moiety (Figure 2.13).

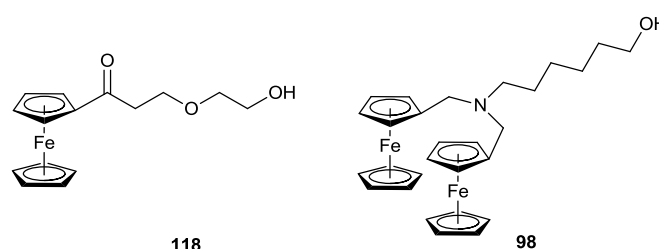
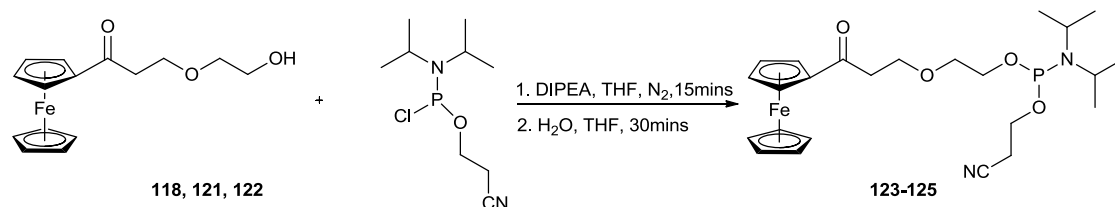


Figure 2.13: Labels **118** and **98** used in duplex

It would be expected that a label with half the number of redox-active components to produce a signal with half the intensity of a label containing double the number of redox-active components such as **98**. What is actually being observed in this case is that **118** is giving a signal with a third of the intensity compared to the signal received for **98**. With **98** giving a peak height of around 7.5 μA and **118** giving a peak height of 3.2 μA (Table 2.4).

The labels are then converted to the phosphoramidite *via* the free hydroxyl group for the conjugation to an oligonucleotide. First of all however all the labels are subjected to the conditions for the oligonucleotide cleavage from the solid support, these are to expose the compounds to 5 M NH_4OH solution at both room temperature and at 50°C. All of the compounds survived under these conditions overnight, therefore they were taken forward to the corresponding phosphoramidite, the synthesis of the

phosphoramidites **123**, **124** and **125** all worked in satisfactory yields (Scheme 2.15, Table 2.5).



Scheme 2.15: General synthetic route to phosphoramidite 123-124

Table 2.5: Yields and phosphorous peaks for 123-125

No.	³¹ P NMR	Yield
123	147.16	78%
124	147.24	20%
125	147.27	74%

Once the phosphoramidites had been synthesised and prior to the conjugation to an oligonucleotide the compounds were subjected to a range of stability tests as the oligonucleotide synthesis is both expensive and was undertaken offsite so survival of the compound during transportation is necessary. The stability of the phosphoramidites was followed by ³¹P NMR analysis, if the phosphoramidite began to decompose the growth of a second peak in the phosphorus NMR can be seen. The second peak corresponds to the phosphine oxide of the phosphoramidite (Figure 2.14).

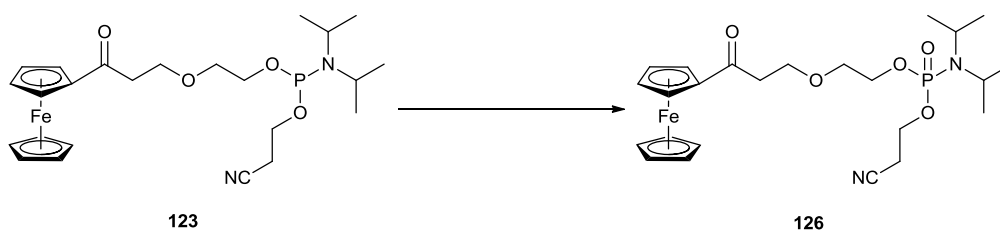


Figure 2.14: Decomposition of phosphoramidite to the corresponding phosphine oxide

The stability tests were carried out at room temperature, with an aliquot being kept at room temperature neat and another aliquot being dissolved in deuterated acetonitrile. Acetonitrile was used as it is the most common solvent used to load phosphoramidites into the oligonucleotide synthesiser. ^{31}P NMRs were then taken of the aliquots after 12 hrs, 24 hrs, 48 hrs and one week. If the labels passed the stability tests over 48 hrs they were then sent off to be conjugated to an oligonucleotide for testing in an assay.

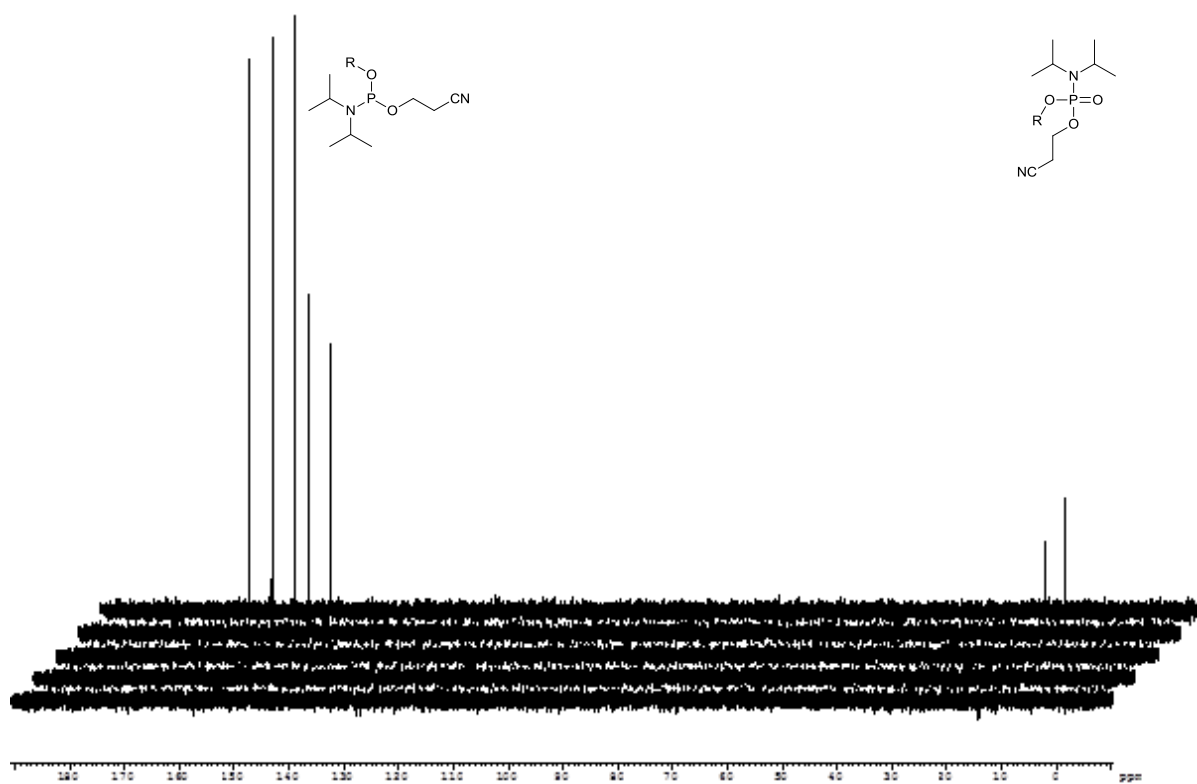
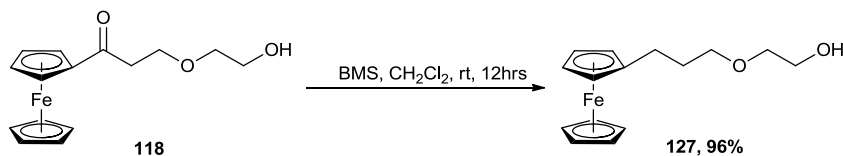


Figure 2.15: ^{31}P NMR of the stability test of **123** run over 1 week in CD_3CN

Stability testing of **123** showed that the phosphoramidite was stable at room temperature in MeCN over 24 hours (Figure 2.15). The phosphoramidite did start to decompose to the phosphine oxide after 48 hours at room temperature, the level of decomposition was found to be 13% and after a week 24%. From the effect of the

linker on the oxidation potential of ferrocene exhibited in **118** it was decided to reduce the ketone to the alkane using borane dimethylsulfide (BMS) (Scheme 2.16).



Scheme 2.16: BMS reduction of 118

The reduced compound **127** exhibited a difference in oxidation potential compared to the parent compound **118**, the elicited change is due to the reduced form of the being less electron – withdrawing due to the reduction of the ketone moiety. The oxidation potential of **127** was found to be 114 mV vs. Ag/AgCl (Figure 2.16).

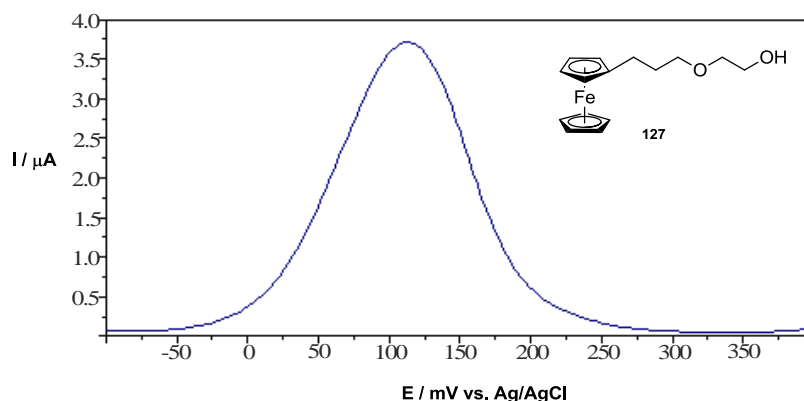
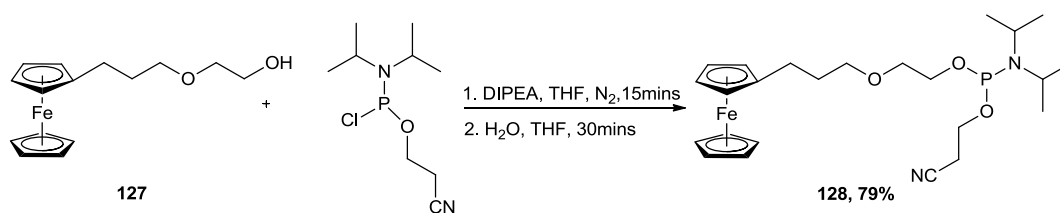


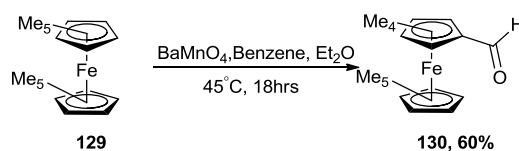
Figure 2.16: Voltammogram of the DPV scan of 127

This compound was then taken through to the phosphoramidite in a 79% yield (Scheme 2.17), **128** was found to be stable under the conditions of the stability test over a week.



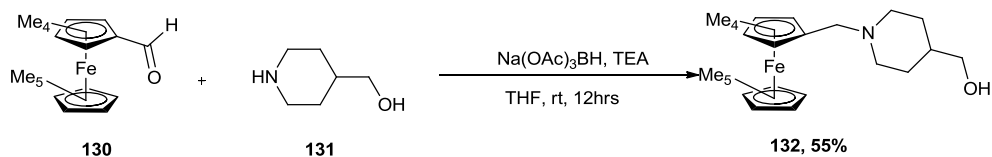
Scheme 2.17: Synthesis of phosphoramidite 128

Electron rich ferrocene derivatives have lower oxidation potentials due to an increased electron density, therefore a lower voltage is required to oxidise the ferrocene moiety. Therefore the synthesis of a highly electron rich label is a logical progression in the design of labels for the use in multiplex detection assays. Using decamethylferrocene as an electron rich ferrocene starting material was likely to give a label in a unique region of the electrochemical spectrum. Nonamethyl ferrocenecarboxaldehyde **130** was prepared by a selective oxidation of a single methyl group on decamethylferrocene using barium manganate *via* the procedure developed by James *et al* (Scheme 2.18).¹¹⁹



Scheme 2.18: Selective oxidation of methyl group to aldehyde 130

The aldehyde **130** provides a useful functional handle for the synthesis of labels containing an electron rich ferrocene moiety. The aldehyde could be taken through a functional group transformation such as the reduction of the aldehyde to the corresponding alcohol or reacted as the aldehyde itself *via* a reductive amination such as in the synthesis of **132** (Scheme 2.19).



Scheme 2.19: Synthetic route to 132

132 was analysed *via* DPV to ascertain its oxidation potential. Analysis showed it to have a low oxidation potential of -105 mV vs. Ag/AgCl. The negative oxidation potential is due to the ferrocene being electron rich, this is due to the nine methyl groups on the cyclopentadienyl rings which have an inductive electron donating (Figure 2.17).

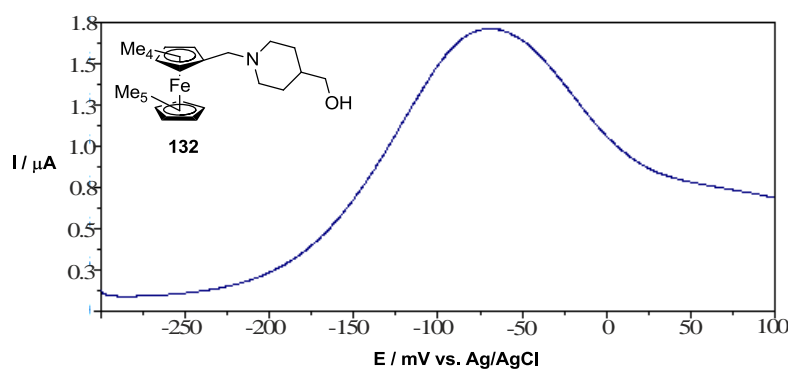
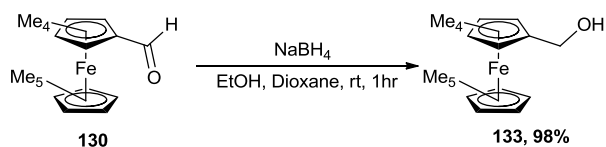


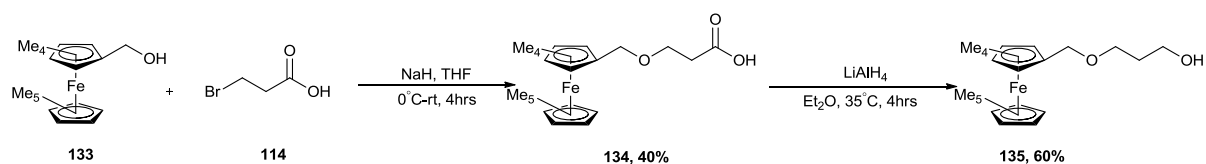
Figure 2.17: Voltammogram of the DPV scan of 132

Figure 2.17 shows that the peak observed for this derivative is very broad, this could be an issue when it comes to using this as a label in a multiplex assay. This led to the design of the synthesis of another label starting from the nonamethylferrocenecarboxaldehyde derivative. The first step of the synthesis is the reduction of the aldehyde to the alcohol through the use of sodium borohydride (Scheme 2.20).



Scheme 2.20: Sodium borohydride reduction of 133

The next step of the synthesis was a nucleophilic substitution reaction with 3-bromopropionic acid, in which the bromide is displaced by the nonamethylferrocene methanol **133** to form the ether **135** (Scheme 2.21). The next step is then to incorporate the free hydroxyl group into the compound, this was carried out through the reduction of the carboxylic acid to afford **135**.



Scheme 2.21: Synthetic route to 135

Analysis was carried out to ascertain the oxidation potential of **135**, which was found to be -85 mV vs. Ag/AgCl (Figure 2.18). Figure 2.18 shows that the peak observed for **135** is a lot sharper than the peak observed for **132**.

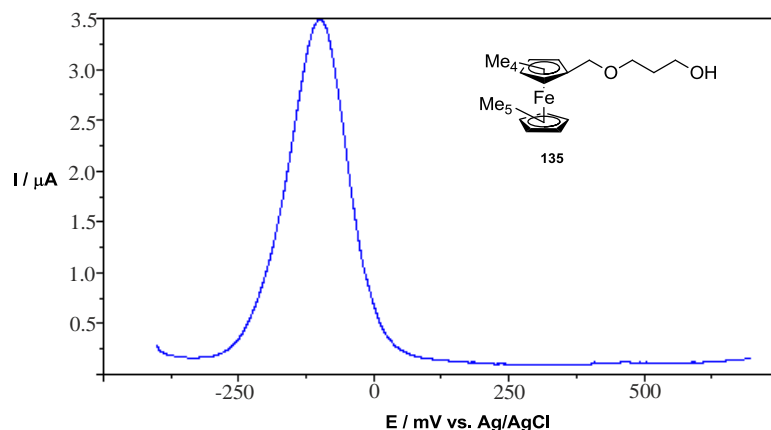
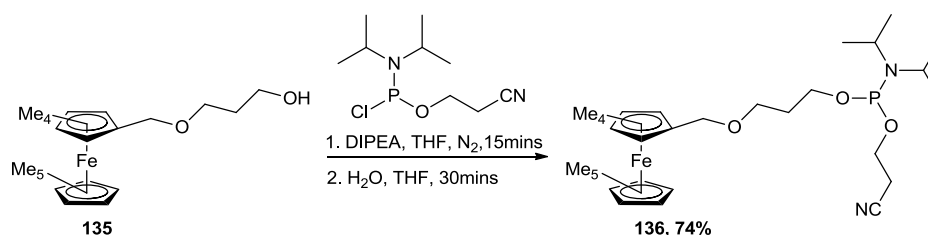


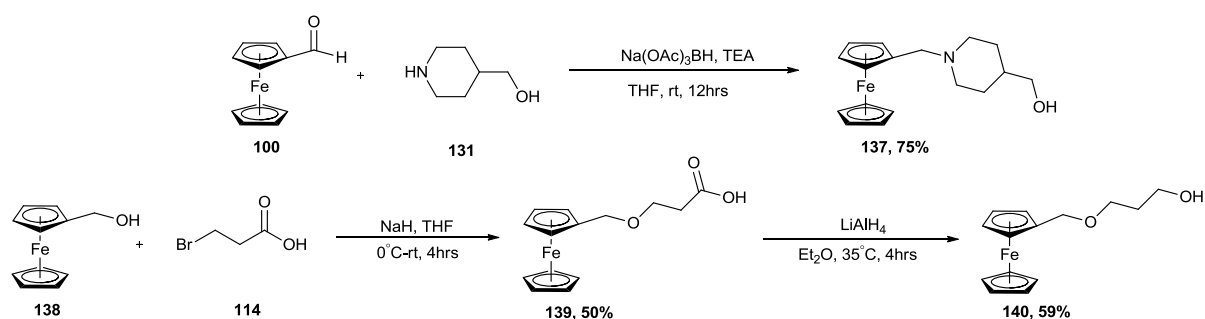
Figure 2.18: Voltammogram of the DPV scan of 135

The phosphoramidite **136** was then synthesised and stability tests were carried out (Scheme 2.22). **136** was found to be stable upon testing under the standard stability conditions both for the solid support cleavage conditions and also the phosphoramidite transport conditions.



Scheme 2.22: Synthesis of phosphoramidite **136**

From the development of the two nonamethylferrocenyl labels **132** and **135** which are electron rich species and where found to have negative oxidation potentials, it was decided to synthesise the standard ferrocene derivative versions of the labels to compare the oxidation potentials with the electron-rich labels. The non-substituted ferrocene labels were also synthesised for the investigation of the possibility of the duplex between the different label species. Both **137** and **140** were synthesised through the same respective synthetic routes either starting from ferrocenecarboxaldehyde or ferrocene methanol (Scheme 2.23).



Scheme 2.23: Synthetic routes to **137** and **140**

137 and **140** have oxidation potentials of 250 mV and 179 mV vs. Ag/AgCl respectively (Table 2.6).

Table 2.6: Comparison of oxidation potentials of electron rich ferrocene derivatives and standard ferrocene derivatives

No	Oxidation potential (mV vs. Ag/AgCl)
132	-105
137	250
135	-80
140	179

The same observation can be made between the voltammograms of **137** and **140**, with **137** having a broader peak (Figure 2.19) than the later compound.

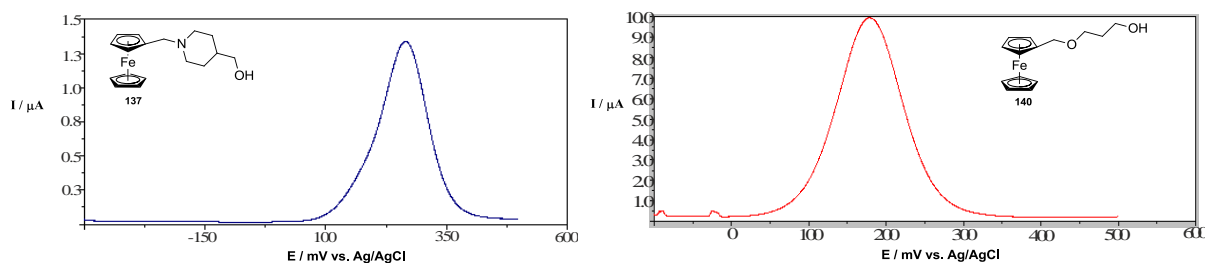


Figure 2.19: Voltammogram of the DPV scan of 137 and 140

The fact that the electron-rich ferrocene labels **132** and **135** come in a unique location compared to their standard ferrocene derivatives and therefore they are an ideal pair to be used in a duplex assay. A duplex was run of **132** and **137** (Figure 2.20) and it can be seen from the figure 2.20 that the signal peaks for both the labels are clearly distinguishable from each other and also of the same intensity at equal concentrations to one and other.

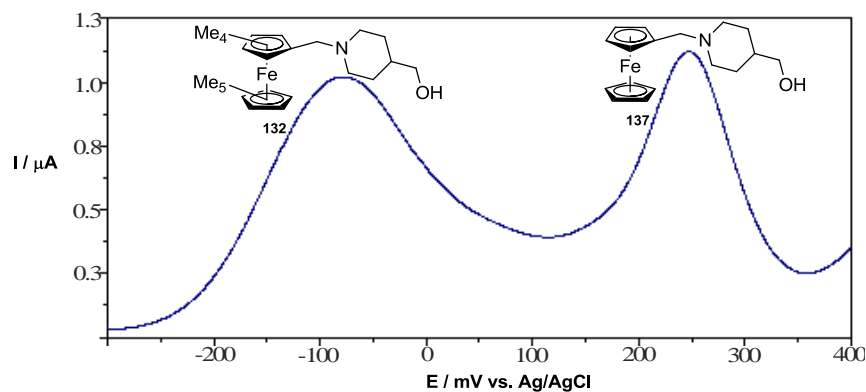


Figure 2.20: Voltammogram of the duplex of 132 and 137

Having clear separation is important in a duplex assay as when using two different labels to detect different targets in the same solution it is vital to have clear separation as not to get a false negative or positive from one of the labels. However with this duplex the signal from **132** does not make it back down to the base line and the signal from **137** starts to grow in at the same time, this leads to a broadening of the signal peaks of these two labels. When **135** was duplexed with **140** at equal molar concentration in the duplex solution there can be seen a greater separation between the two peaks than exhibited between **132** and **137** (Figure 2.21), which follows on from the observation that both **135** and **140** have sharper signal peaks than the broader peaks exhibited by **132** and **137**.

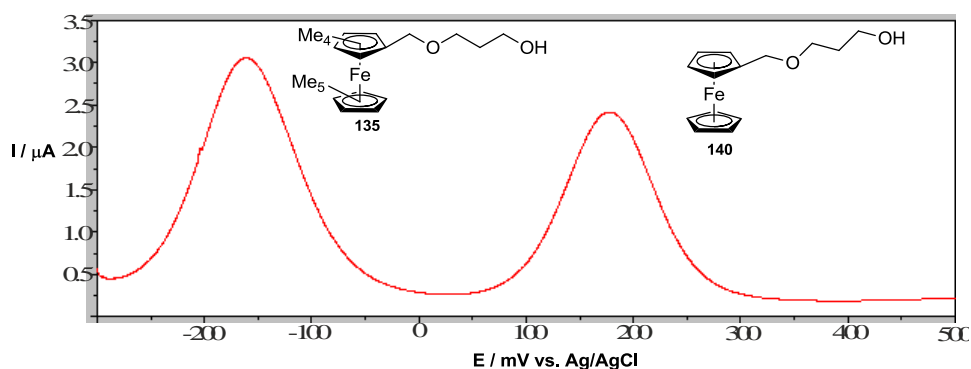


Figure 2.21: Voltammogram of the duplex between 135 and 140

Figure 2.21 shows that there is not only good separation between the two peaks exhibited from **135** and **140** but there is also no overlap observed between the two peak signals as the tail of the signal for **135** returns to the baseline level before there is the growth in of the peak exhibited for **140**. Therefore the duplex between **135** and **140** possesses more desirable characteristics than that of the duplex between **132** and **137**, these being sharper signals for the two labels in the duplex and also a higher level of separation between the two peaks.

As mentioned previously a range of functionalities on the linker have been targeted, one specific linker functionality that was outlined as a target was a triazole containing linker which can be achieved *via* click chemistry. Click chemistry reactions have been used for the post-labelling of functionalised oligonucleotides.¹²⁰ It was proposed to utilise click chemistry in the synthesis of redox-active labels. This could be carried out either by having the azide moiety situated on the ferrocene derivative or the alkyne moiety situated on the ferrocene derivative (Figure 2.22)

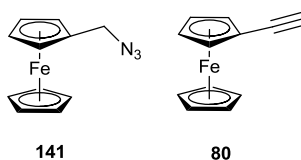


Figure 2.22: Ferrocene derivatives for the click reactions

The click reaction will be used to tie together the redox-active ferrocene moiety and the free hydroxyl containing moiety in the synthesis of triazole containing linkers. (1-(Ferrocenylmethyl)-1*H*-1,2,3-triazol-4-yl)methanol **142** (Figure 2.23), was the first proposed label to be synthesised.

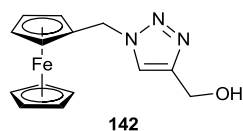
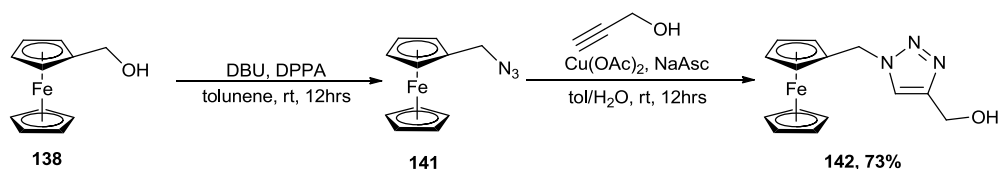


Figure 2.23: label 142

Starting from ferrocenemethyl azide **141**, which was synthesised from ferrocene methanol **138** using 1,8-diazabicycloundec-7-ene (DBU) and diphenylphosphoryl azide (DPPA) (Scheme 2.23).



Scheme 2.23: Synthetic route to 142 via click reaction

142 was used without isolation or purification, the *in situ* generated azide was then reacted with propargyl alcohol in the presence of copper acetate and sodium ascorbate solution to afford **142**. The triazole product was found to have an oxidation potential of 250 mV vs. Ag/AgCl (Figure 2.24). This shows that the triazole ring in the linker is having an electron withdrawing effect on the ferrocene core, shifting the ferrocenes' oxidation potential by approximately 90 mV.

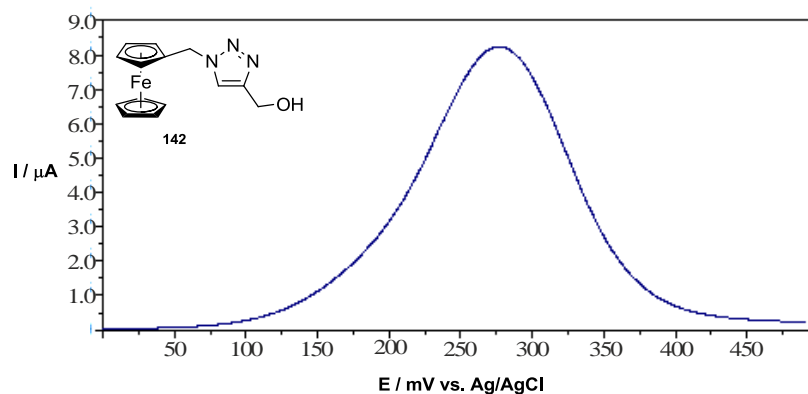


Figure 2.24: Voltammogram of the DPV scan of 142

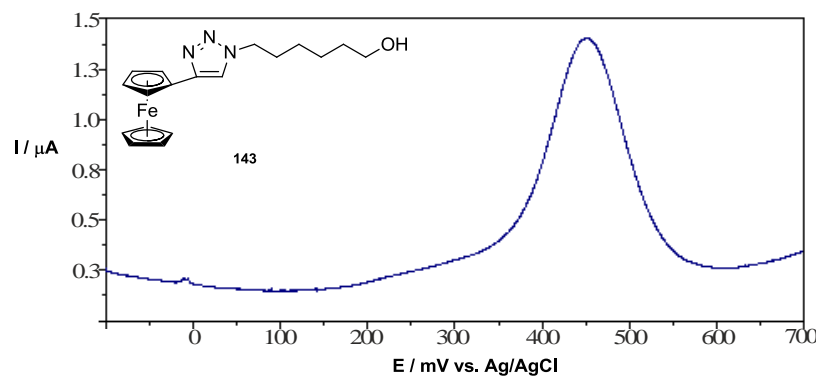


Figure 2.26: Volammogram of the DPV scan of **143**

The comparison of the oxidation potentials of **142** (250 mV vs. Ag/AgCl) and **143** (450 mV vs. Ag/AgCl) shows that there is a stronger electron withdrawing effect on the ferrocene moiety at the four position due to the ferrocene being directly bound to the conjugated triazole ring, whereas in the one position there is a carbon between the ferrocene and the triazole ring therefore the electron withdrawing effect on the ferrocene is lower.

From the previous work done in the group by Hillier *et al*, on the synthesis of **97** (Figure 2.27). **97** was found to have an oxidation potential of 400 mV vs. Ag/AgCl.

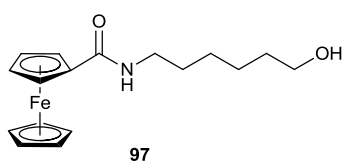


Figure 2.27: **97** synthesised by Hillier *et al*

Along with the synthesis of **99** which was found to have an oxidation potential of 85 mV vs. Ag/AgCl (Figure 2.28), it was decided to study the effect of the number of carbon atoms between the ferrocene moiety and the amide group has on the oxidation potential of the labels themselves.

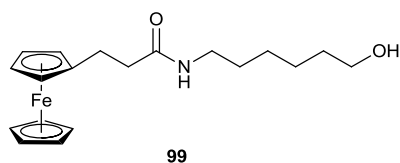
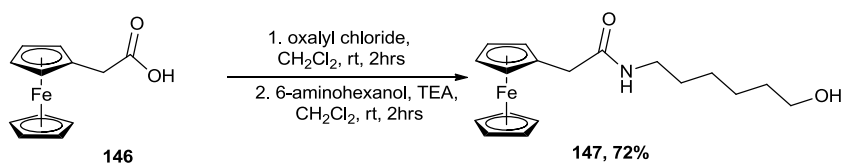


Figure 2.28: Compound 99

There is an approximate shift of approximately 300 mV in the oxidation potential between **97** with the amide being directly situated on the amide and **99** in which there is a two carbon linker between the ferrocene and the amide group. 2-Ferrocenyl-*N*-(6-hydroxyhexyl)acetamide **147** was therefore proposed to be synthesised, the starting material was ferrocene acetic acid. The synthesis of the label **147** was carried out *via* the *in situ* generation of the acid chloride, which was reacted with 6-aminohexanol (Scheme 2.25).



Scheme 2.25: Synthetic route to 147

147 was found to have an oxidation potential of 269 mV vs. Ag/AgCl, which is just over halfway between the other two labels (Figure 2.29). This shows that there is a decrease of approximately 150 mV for every carbon added between the ferrocene and the amide group.

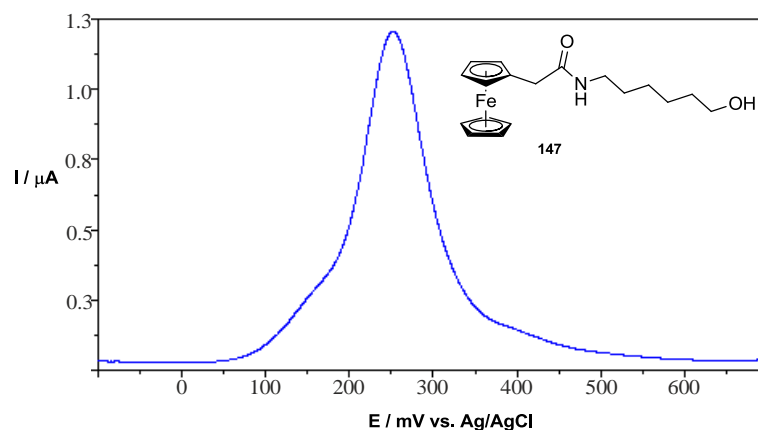
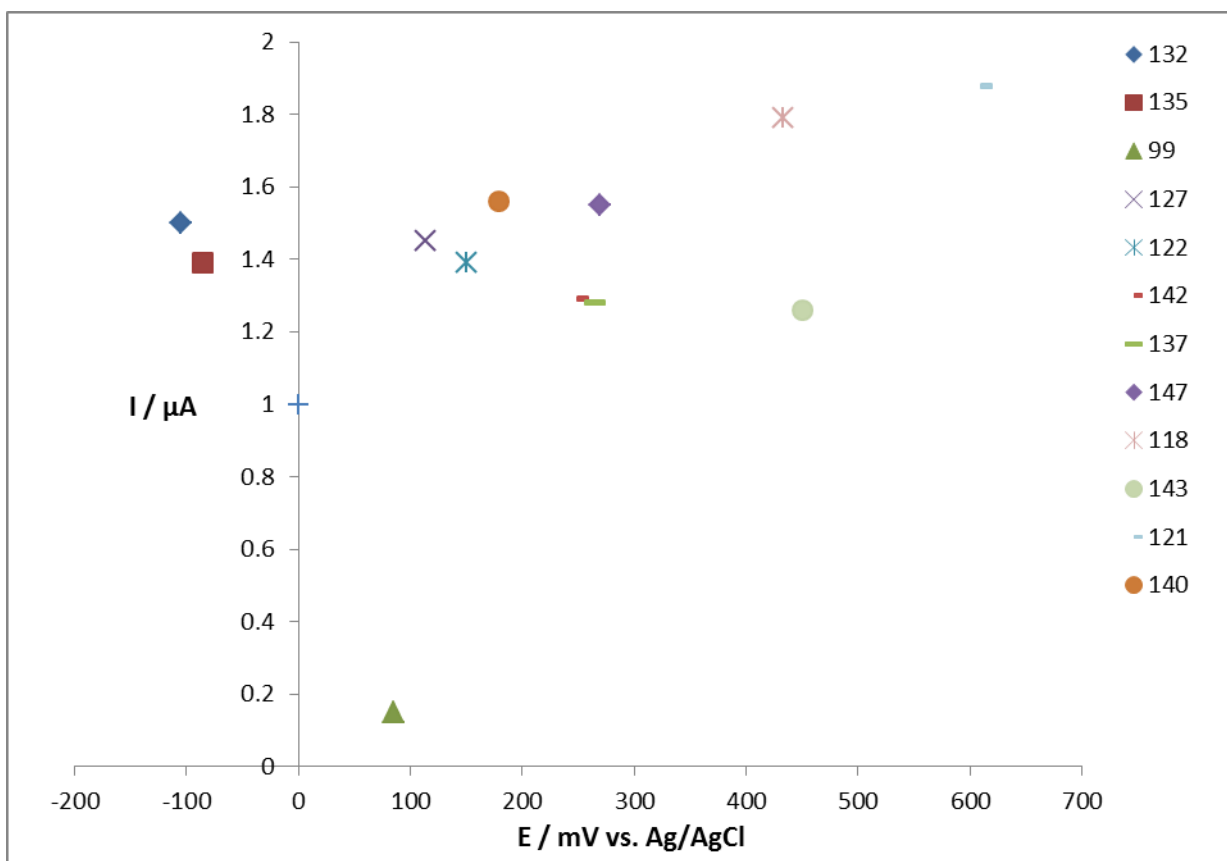


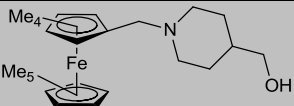
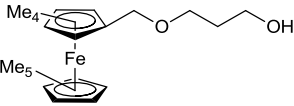
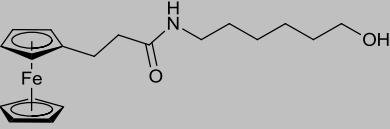
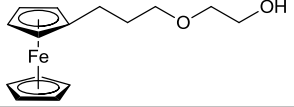
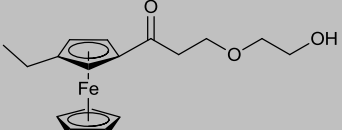
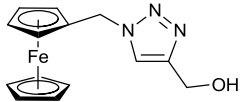
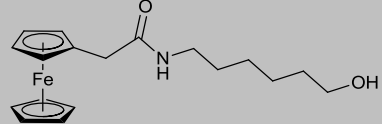
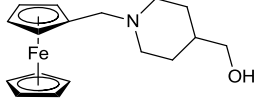
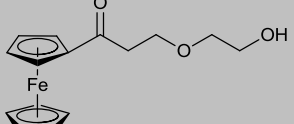
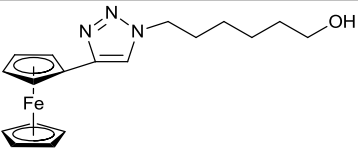
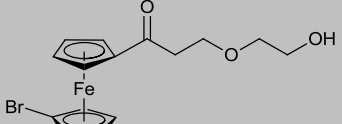
Figure 2.29: Voltammogram of the DPV scan of 147

2.4 Conclusion

This chapter has shown the synthesis of a range of mono-ferrocenyl derivatives for the use as redox-active labels in the synthesis of DNA probes, to be used in a DNA biosensor. The compounds synthesised were analysed *via* differential pulse voltammetry, which showed a range of oxidation potentials have been achieved (Graph 2.1). However, the sensitivity of the mono-ferrocenyl labels was shown to be lower than that of di-ferrocenyl label currently being used in the biosensor assay. Labels with unique oxidation potentials were activated for bioconjugation *via* the synthesis of their equivalent phosphoramidite.



Graph 2.1: Range of mono-ferrocenyl labels showing their oxidation potentials vs intensity

Label	Oxidation potential (mV vs. Ag/AgCl)
	132 -105
	135 -80
	99 85
	127 114
	122 150
	142 250
	147 269
	138 265
	118 433
	143 450
	121 610

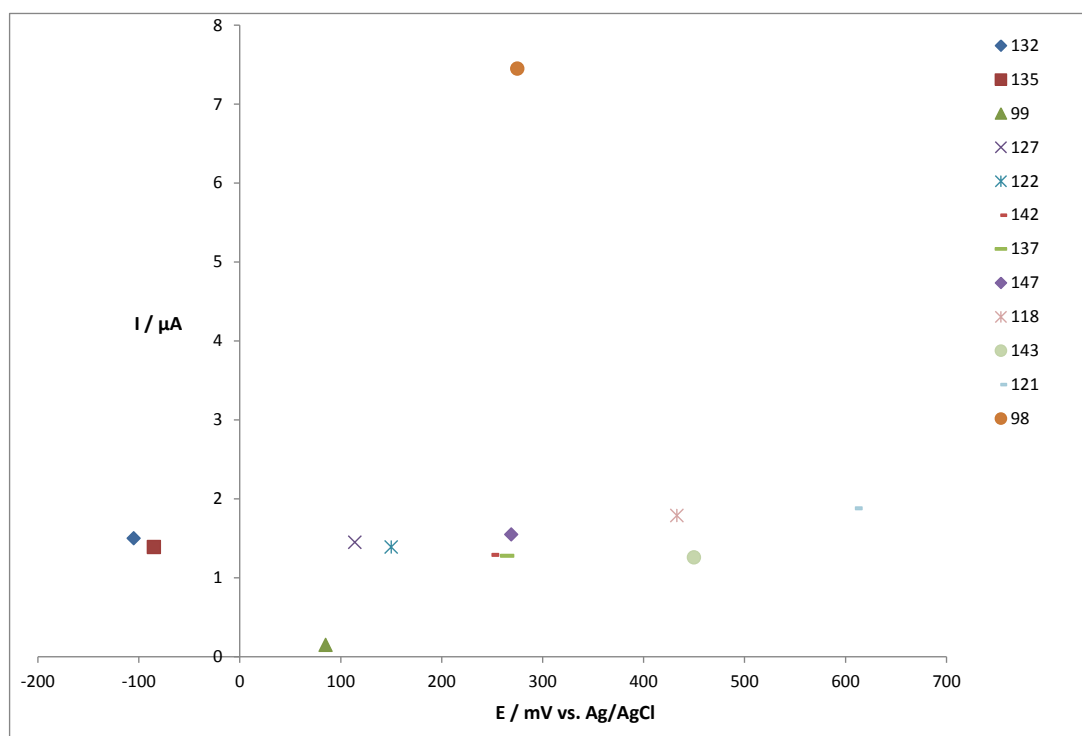
3 Chapter 3: The synthesis of Di-ferrocenyl labels for the use as DNA Probes

Summary of Chapter

This chapter details the design and synthesis of redox-active labels containing more than one redox-active moiety present in the label. All the redox-active components are symmetrical, so that there is only one oxidation potential for the label and not separate peaks for the individual redox-active components. The ferrocene containing redox active labels described in this chapter are to be used in the Atlas DNA detection assay, in a multiplex capacity with current labels in use.

3.1 Background

From the work presented in chapter 2 on the synthesis of mono-ferrocenyl labels it became apparent that the mono-ferrocenyl derivatives have a lower sensitivity in comparison to **98** which is currently the main redox-active label used as a probe in the Atlas assay. This lower level of sensitivity at the electrode can be seen in graph 3.1 (Graph 3.1).



Graph 3.1: Graph depicting the difference between the di-label **98** and the mono-labels synthesised

The difference in the sensitivity was highlighted in the duplex assay between **98** and **118** (Figure 3.1), the signal intensity of **118** was found to be lower in comparison to the intensity of the signal for **98** when each of the labels were in equimolar concentration within the duplex assay mixture.

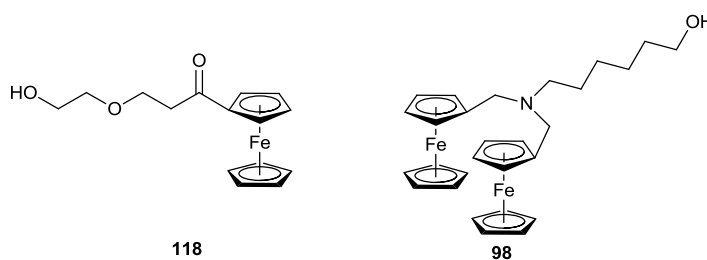


Figure 3.1: Redox-active labels used in the duplex assay

A lower intensity of signal between the two compounds would be expected due to **118** containing one ferrocene moiety compared to two ferrocene moieties in **98**, from this information the intensity at the electrode for **118** would be expected to be

approximately half the intensity of **98**. However in practise the signal intensity for **118** was found to be approximately a third of the signal intensity of **98**. The result was reproducible as seen in Table 3.1, where **118** was found to have an average signal intensity of 2.6 μA and **98** having an average intensity of 6.9 μA , over the three runs carried out on the duplex assay (Table 3.1)

Table 3.1: Duplex at equal concentration of **98** and **118**

Run	Label	Peak Position (mV vs. Ag/AgCl)	Peak Height (μA)
1	98	272	7.47
	118	440	2.70
2	98	275	6.49
	118	440	2.43
3	98	274	7.45
	118	441	2.53

The difference between the two labels can be clearly seen from the overlays of the three duplex runs on Figure 3.2 (Figure 3.2).

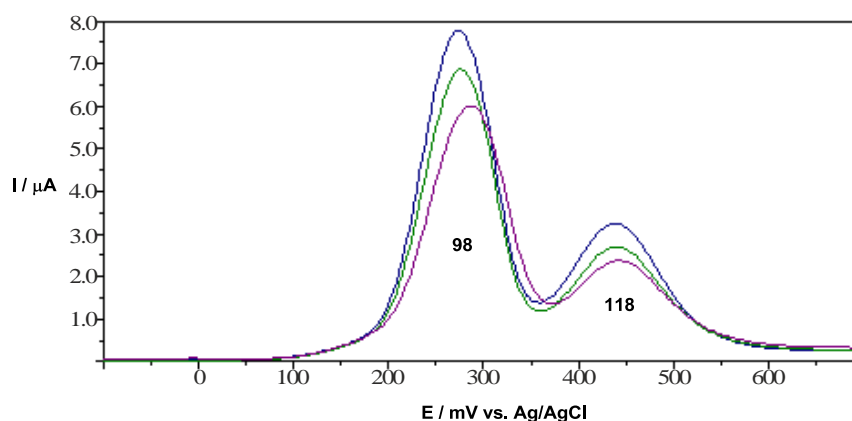


Figure 3.2: Overlay of the DPV voltammograms of the duplex run between **98** and **118** at equal concentrations

A further experiment was undertaken, the concentration of **118** was doubled in the duplex solution with the concentration of **98** being kept constant, therefore effectively equalising the number of redox-active moieties with regards to the two labels. When the duplex solution was analysed *via* differential pulse voltammetry it was shown that there was an increase in the intensity of the signal for **118**, the signal intensity was increased from a third of the intensity to a signal intensity of two thirds of the intensity in comparison to the signal for **98** (Figure 3.3).

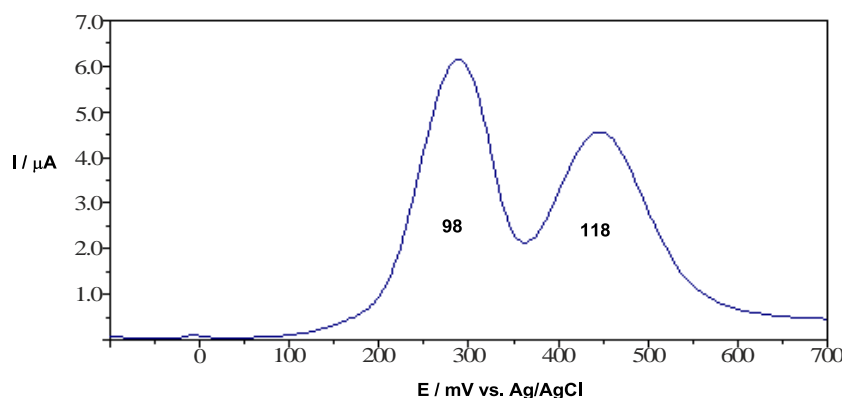


Figure 3.3: Voltammogram of the duplex run between 98 and 118 with 118 at double the concentration

With the redox-active moieties for the two labels in the duplex being equal it would have been theoretically perceived that the signal intensity for both labels **98** and **118** would be equal. However in practise this is not the case, the signal intensity for **118** was shown to be two thirds of the intensity of **98** (Table 3.2).

Table 3.2: Duplex of 118 and 98 at a 2:1 ratio

Run	Label	Peak Position (mV vs. Ag/AgCl)	Peak Height (μA)
1	98	288	5.77
	118	446	4.31
2	98	282	6.17
	118	446	3.80
3	98	275	7.17
	118	443	3.71

At double the concentration label **118** has the average peak height of 3.9 μA whereas label **98** has the average peak height of 6.4 μA . The results of the duplex at this concentration mix in the duplex are repeatable (Figure 3.4).

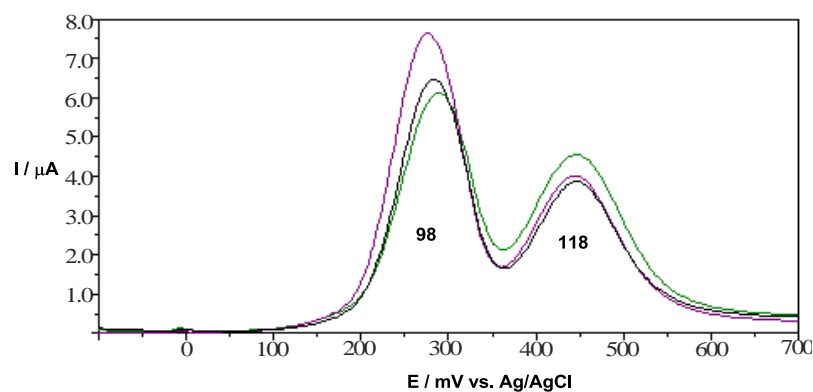


Figure 3.4: Overlay of the voltammograms of the duplex run between **98** and **118** with **118** at double the concentration

A final experiment was conducted, the concentration of **118** was triple in comparison to **98** (Figure 3.5). At this ratio it was found that the intensities of the peaks for **98** and **118** were found to be equal.

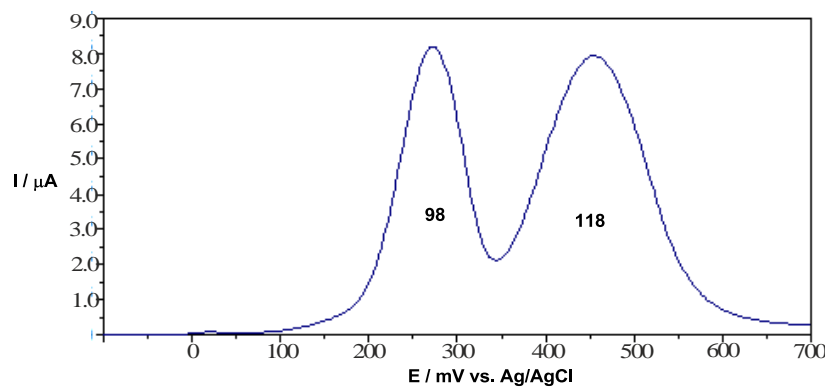


Figure 3.5: Voltammogram of the duplex run between **98** and **118** with **118** at triple the concentration

As can be seen from Figure 3.5 the intensity of the signal produced by **118** is now equal in intensity to the signal produced by **98**, for which the concentration of the label has stayed the same in all of the duplex assay systems (Table 3.3).

Table 3.3: Duplex of 118 and 98 at a 3:1 ratio

Run	Label	Peak Position (mV vs. Ag/AgCl)	Peak Height (μA)
1	98	285	5.75
	118	455	5.53
2	98	272	7.66
	118	455	7.39
3	98	288	5.88
	118	455	5.31

As shown in the Table 3.3 the results for this duplex were found to be constant across all of the three runs of the duplex system (Figure 3.6).

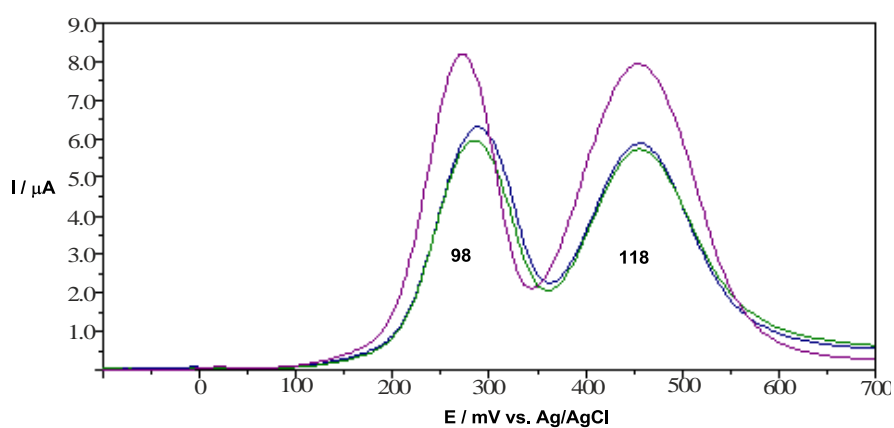


Figure 3.6: Overlay of the voltammograms of the duplex between 98 and 118 with 118 at triple the concentration

3.2 Results and Discussion

From the synthesis and electrochemical analysis *via* DPV of the monoferrocenyl labels presented in chapter 2, it was shown that the mono labels were less sensitive than **98**. Therefore the design and synthesis of a range of redox-active labels containing more than one redox-active moiety present in the label structure was proposed. The first targeted range of labels are derivatives of the label developed by Flower *et al* **98**, which is the current label used in the Atlas DNA detection assay. The labels targeted were either derivatives of **98** which were either further substituted on the Cp rings or with the alteration of the functionality of the linker unit (Figure 3.7).

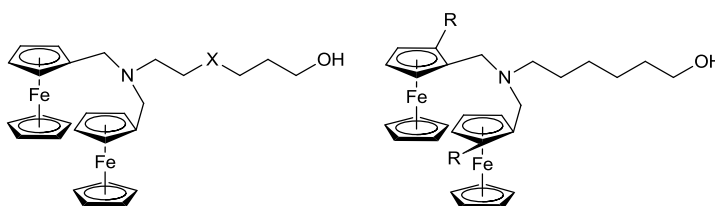
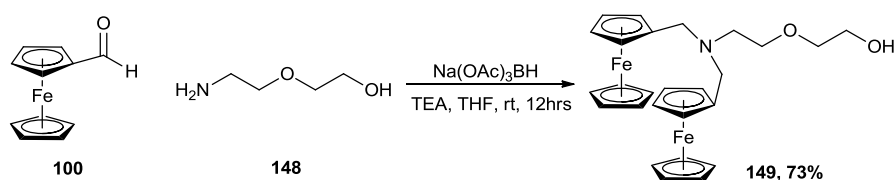


Figure 3.7: Structures of labels targeted based around **98**

The first label designed for synthesis containing more than one ferrocene moiety was a direct derivative of **98** using an ether containing linker moiety, with the aim of improving the labels solubility in aqueous media. The solubility of the labels synthesised is important due to the DNA detection assay being carried out in an aqueous buffer medium. Solubility however becomes less of an issue when the labels are conjugated to the oligonucleotide. **149** was synthesised using a reductive amination procedure, starting from ferrocenecarboxaldehyde and (aminoethoxy)ethanol (Scheme 3.1).



Scheme 3.1: Synthesis of 149

Upon electrochemical analysis it was found that **149** had an oxidation potential of 242 mV vs. Ag/AgCl (Figure 3.8). The oxidation potential of **149** was found to be very similar to the oxidation potential of **98** which is the current label used in the DNA detection assay, which has an oxidation potential of 275 mV vs. Ag/AgCl. **149** was synthesised to investigate the effect of the ether group in the linker unit has on the behaviour and oxidation potential of the label in the DNA detection assay.

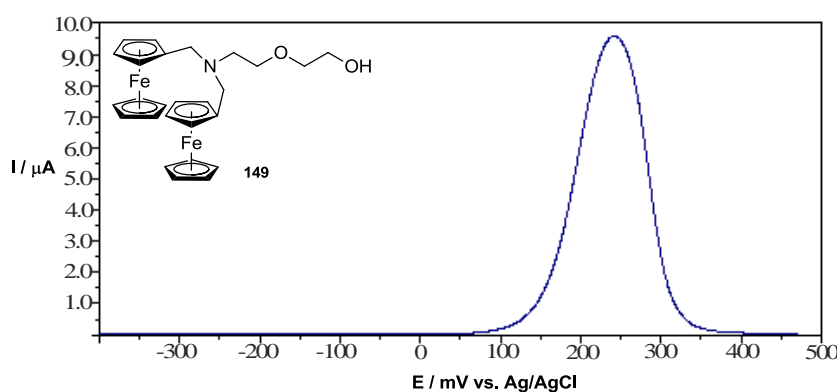
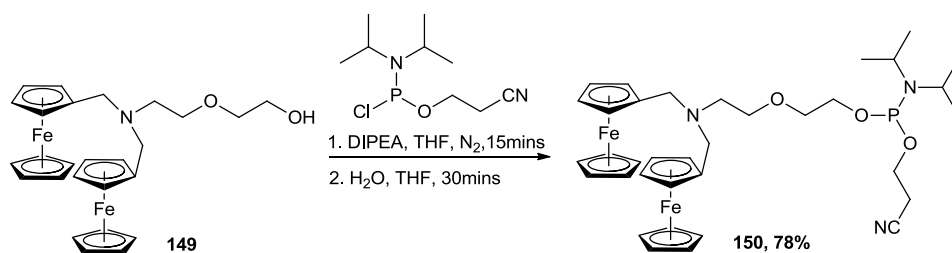


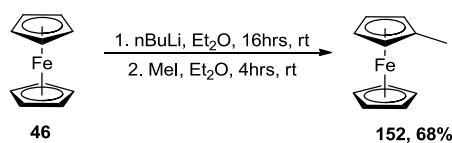
Figure 3.8: Voltammogram of the DPV scan of 149

The phosphoramidite of **149** was then synthesised (Scheme 3.2), which proved to be stable under the standard stability test conditions.



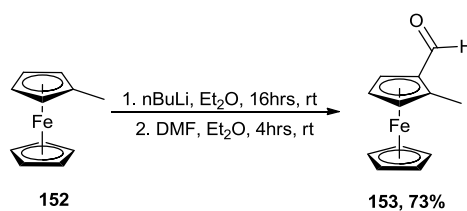
Scheme 3.2: Synthesis of phosphoramidite 150

The first substituted derivative of **98** proposed for synthesis was 6-(bis((2-methylferrocenyl)methyl)amino)hexan-1-ol **151** which has a methyl group substituted onto one of the Cp rings. The starting material for this label is methyl ferrocene **152** which was synthesised from ferrocene *via* the deprotonation of ferrocene with *n*-butyl lithium giving the lithioferrocene derivative, the reactive lithioferrocene derivative was reacted with methyl iodide to instil the desired methyl group in a good yield (Scheme 3.3).



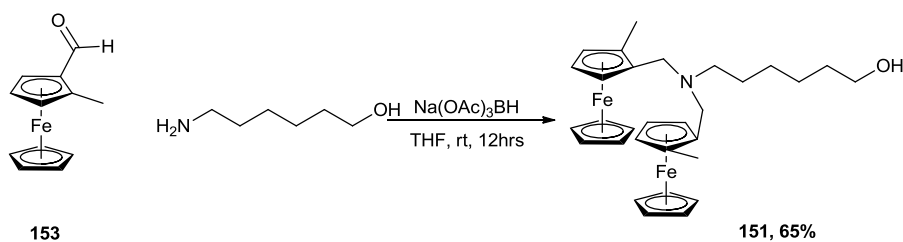
Scheme 3.3: Synthesis of methylferrocene

The next step of the synthesis was to instil the aldehyde functionality onto the ferrocene Cp ring, this was also carried out *via* the generation of the lithioferrocene species, which was reacted with DMF to afford the methylferrocenecarboxaldehyde **153** in a 73% yield (Scheme 3.4)



Scheme 3.4: Formylation of methylferrocene

The final step in the synthetic route to **151** was a reductive amination reaction with 6-aminohexan-1-ol, to instill the desired nitrogen containing bridge head unit and the linker moiety (Scheme 3.5).



Scheme 3.5: Synthesis of **151** via reductive amination

Upon running the differential pulse voltammetry of **151** it was found that it processes an oxidation potential of 330 mV vs. Ag/AgCl (Figure 3.9). This shows the effect of the linker nitrogen bridge unit between the two ferrocene moieties on the oxidation potential. With regards to **151** it can be seen clearly the effect the linker has on the oxidation potential of the ferrocene itself. The incorporation of an *ortho*-methyl group on the ferrocene results in an increase in the oxidation potential, this could possibly be due to steric effects. An interesting observation to make from **151** is that the substitution of a methyl group on to the cyclopentadienyl ring as well as the linker moiety the oxidation potential is 330 mV, with the electron donating effect of the methyl group it could be argued that the oxidation potential should be closer to the oxidation potential of ferrocene itself.

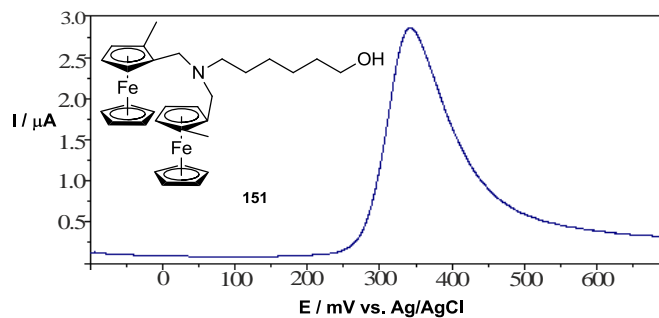


Figure 3.9: Voltammogram of the DPV scan of **151**

The next label targeted was a label that incorporated amine functionality onto the ferrocene as well as the nitrogen containing linker moiety. The amine functionality was targeted as the amine functionality of the linker in label **98** was shown to shift the oxidation potential of the ferrocene by approximately 135 mV, therefore it was theorised that the inclusion of another amine group onto the ferrocene core would have a similar effect on the oxidation potential of the label compound. The label targeted was bis((dimethylamino)methylferrocenyl)-6-aminohexan-1-ol **154**, the starting material for the synthesis of **154** was (dimethylamino)methyl ferrocene **155** (Figure 3.10).

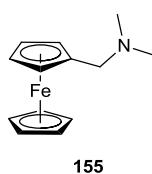
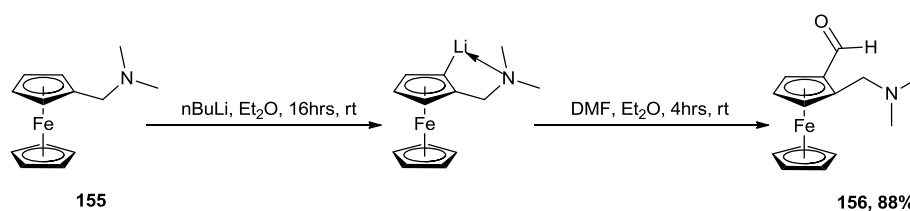


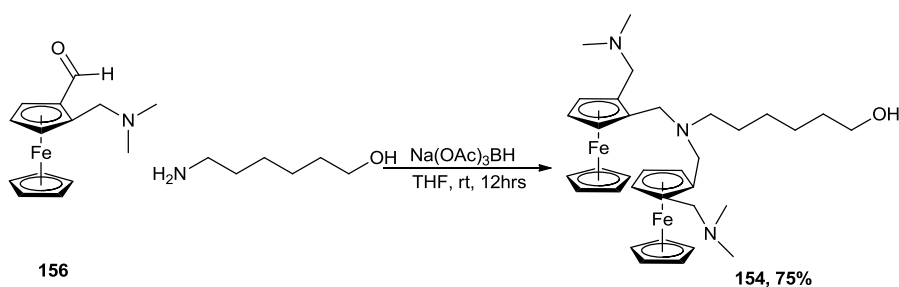
Figure 3.10: (dimethylamino)Methyl ferrocene **155**

The dimethylamine group on **155** has the ability to stabilise the lithioferrocene species generated *via* the lone pair on the nitrogen, therefore keeping the lithioferrocene species around for longer in the reaction mixture.¹²¹ The lithioferrocene intermediate was then *in situ* reacted with DMF to instil the aldehyde functionality required for the next step in the label synthesis (Scheme 3.6).



Scheme 3.6: Synthesis of aldehyde **156**

The aldehyde generated was afforded in a higher yield of 88% rather than that of the aldehyde **153** which was afforded in a 68% yield. This is due to the lithioferrocene species generated in the synthesis of **153** being less stable than the lithioferrocene species generated in the synthesis of **156**, which is stabilised by the presence of the amine functionality. Aldehyde **156** was used in a reductive amination with 6-aminohexanol to afford the desired label **154** in 75% yield (Scheme 3.7).



Scheme 3.7: Synthesis of **154**

154 was then analysed *via* DPV and was found to have an oxidation potential of 380 mV vs. Ag/AgCl (Figure 3.11). As can be seen from Figure 3.11 the peak exhibited for **154** is broader than the peaks exhibited by **98**.

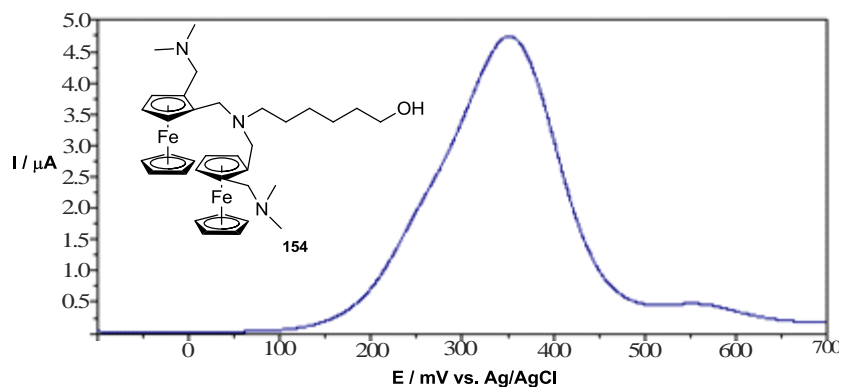
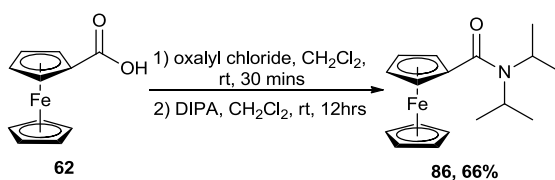


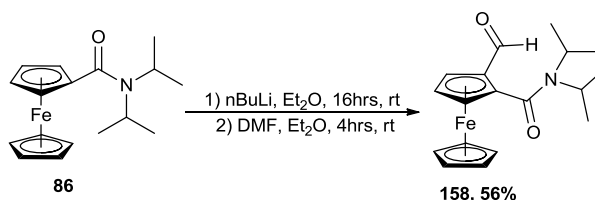
Figure 3.11: Voltammogram of the DPV scan of 154

It has been shown by previous work in the group and work presented in chapter 2 that amides have an effect on the oxidation of the ferrocene derivative, the effect has been shown to vary depending on the distance between the ferrocene moiety and the amide moiety. Hiller *et al*, showed that having the amide situated directly on the Cp ring shifted the oxidation potential of the ferrocene moiety to 400 mV vs. Ag/AgCl. Therefore the next label targeted would be substituted with an amide group on the Cp ring. 2,2-(6-Hydroxyhexylazanedy)bis(methylene)bis(*N,N'*-diisopropylferrocenecarboxamide) **157** was the amide containing label designed, the proposed synthetic route to **157** started from ferrocenecarboxylic acid **62**. The first step of the synthetic route to **157** was the *in situ* generation of an acid chloride by reacting ferrocenecarboxylic acid with oxalyl chloride. The generated acid chloride was then reacted with diisopropyl amine (DIPA) to incorporate the amide functionality onto the Cp ring to afford the desired amide derivative (Scheme 3.8).



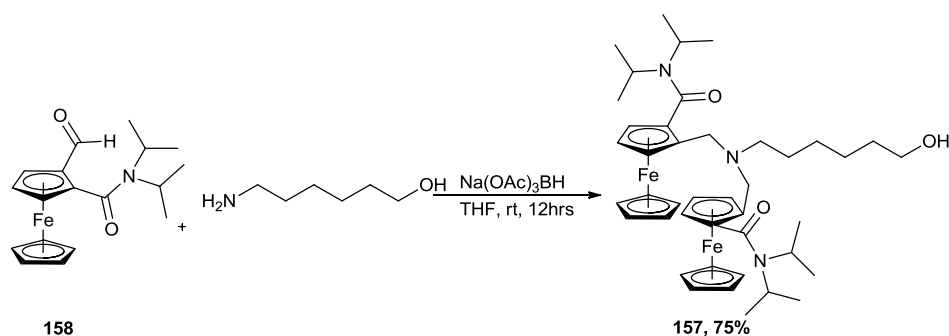
Scheme 3.8: Synthesis of amide 86

86 was then reacted with *n*-butyl lithium to generate a lithioferrocene species, which was quenched with DMF to afford the desired aldehyde functionality **158** into the compound that is required for the final step of the synthesis of **157** (Scheme 3.9).



Scheme 3.9: Synthesis of aldehyde **158**

With aldehyde **158** in hand, the final step of the synthetic route to **157** was a reductive amination reaction of **158** with 6-aminohexan-1-ol (Scheme 3.10). This gave the desired compound **157** in a good yield.



Scheme 3.10: Synthesis of **157**

157 was analysed *via* DPV and was found to have an oxidation potential of 350 mV vs. Ag/AgCl (Figure 3.12).

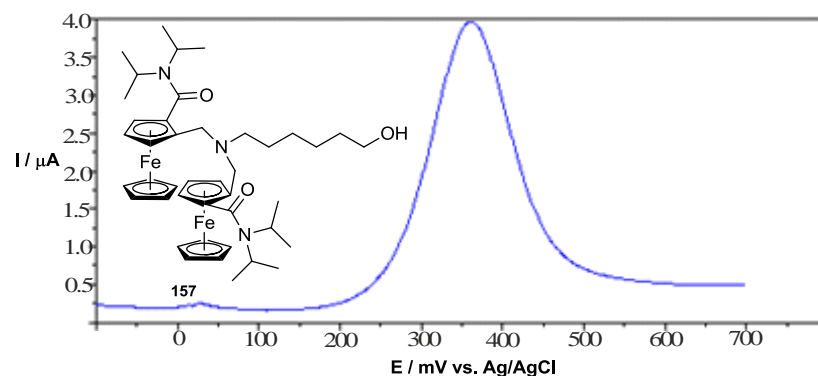
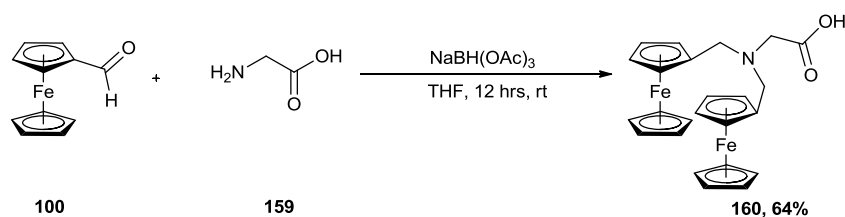


Figure 3.12: Voltammogram of the DPV scan of 157

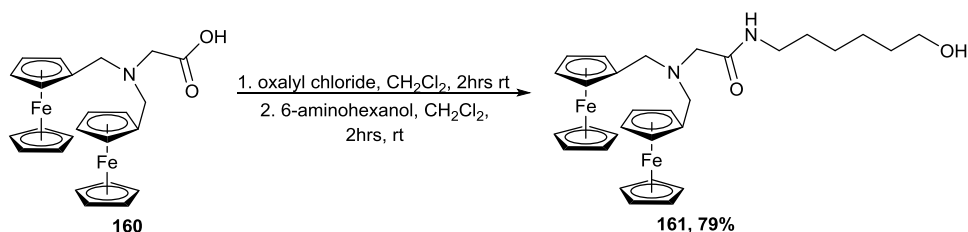
As labels **151**, **154** and **157** all have oxidation potentials that are in close proximity to **98** they were not taken any further at this stage. It has become apparent from the synthesis of **151**, **154** and **157** that the linker moiety of the derivatives has an effect on the oxidation potential of the labels as well as any substitution on the Cp rings.

Therefore it was decided to analyse the effect of further functionality within the linker moiety has on the oxidation potential of the labels. The nitrogen containing bridging unit between the two ferrocene moieties was kept the same and the functionality was installed into the compound between the bridged ferrocene moieties and the free hydroxyl group. The functionality targeted within the linker unit was an amide functional group. Therefore a label was designed around the linker unit being in two halves to instil the desired functionality into the linker unit. The ferrocene end of the label was designed to still contain the same nitrogen containing bridging unit between the two ferrocene derivatives as in **98**. The use of glycine as the first half of the linker was proposed, this would lead to an amide functional group in the linker. Starting from ferrocenecarboxaldehyde and glycine, which were taken through a reductive amination reaction to afford the di-ferrocenyl head group **160** in a good yield (Scheme 3.11).



Scheme 3.11: Synthesis of 160 from glycine

160 was then reacted with oxalyl chloride to generate the acid chloride *in situ* which was then further reacted with 6-aminohexan-1-ol (Scheme 3.12), to afford 2-(bis(ferrocenylmethyl)amino)-*N*-(6-hydroxyhexyl)acetamide **161**.



Scheme 3.12: Amide coupling to afford 161

161 was analysed *via* DPV and was found to have an oxidation potential of 500 mV vs. Ag/AgCl (Figure 3.13). The inclusion of the amide moiety in the linker increases the electron-withdrawing effect of the linker on the ferrocenes themselves, therefore a higher oxidation potential is required to oxidise the ferrocenes to their ferrocenium ions.

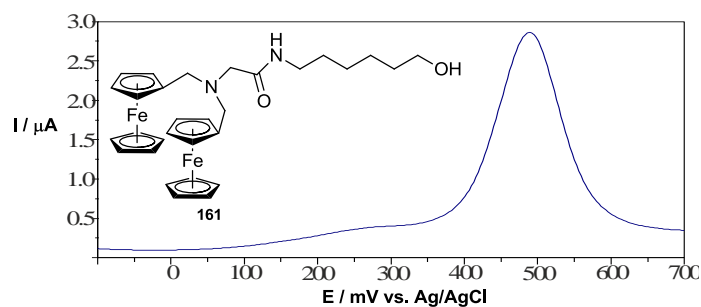
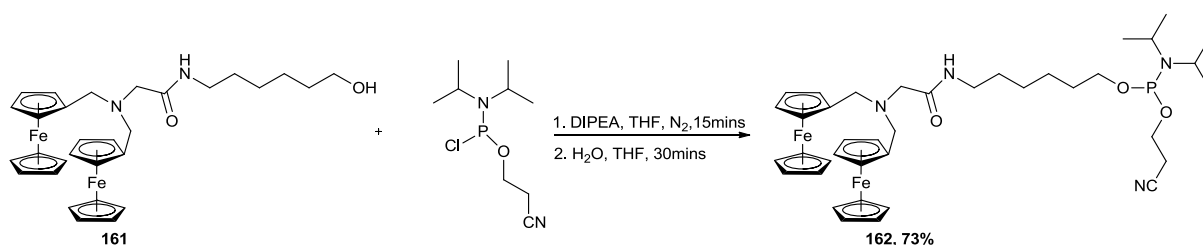


Figure 3.13: Voltammogram of the DPV scan of 161

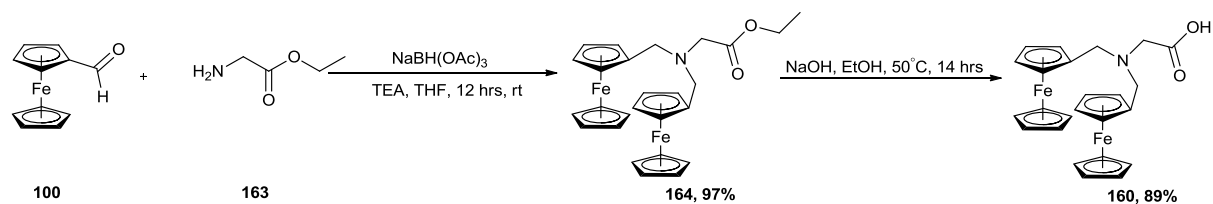
The oxidation potential of **161** was found to be considerably different to that of **98**, therefore the phosphoramidite **162** was then synthesised for the use as a duplex label with **98** (Scheme 3.13). However upon stability analysis on **162** as well as attempted conjugation to oligonucleotide there were some issues with the labels stability. A possible reason for this unstability the amide in the linker still has a free proton, which could lead to deprotonation and possible decomposition of the label due to the 5M ammonium hydroxide that is used in the final step of the oligonucleotide synthesis.



Scheme 3.13: Synthesis of phosphoramidite **162**

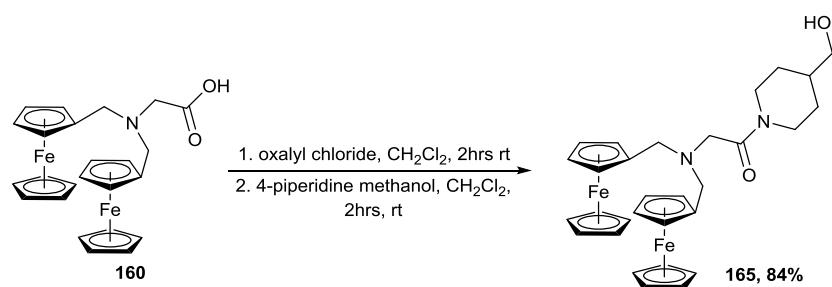
Therefore it was decided to change the primary amine used to a secondary amine to analyse the effect the removal of the amide proton has on the stability of the label. The secondary amine chosen was 4-piperidine methanol to be used as the amino alcohol moiety.

The synthetic route to 2-(bis(ferrocenylmethyl)amino)acetic acid **160** was altered to increase the yield of the desired compound. The first step was still a reductive amination starting from ferrocenecarboxaldehyde **100**, however instead of glycine the ethyl ester protected derivative of glycine **159** was used as the amine source for the reaction. The use of the ethyl ester increased the yield of the reductive amination from 64% to 97%. The next step of the synthesis was a saponification under basic conditions to afford **160** in an 89% yield (Scheme 3.14).



Scheme 3.14: Synthesis of 160 through altered route

The final step of the synthetic route to **165** was an amide coupling reaction carried out *via* the *in situ* generation of the acid chloride of **160** which was further reacted with 4-piperidine methanol to afford the desired product 2-(bis(ferrocenylmethyl)amino)-1-(4-(hydroxymethyl)piperidin-1-yl)ethanone **165** (Scheme 3.15).



Scheme 3.15: Synthesis of amide 165

165 was analysed *via* DPV and was found to have an oxidation potential of 410 mV vs. Ag/AgCl (Figure 3.14).

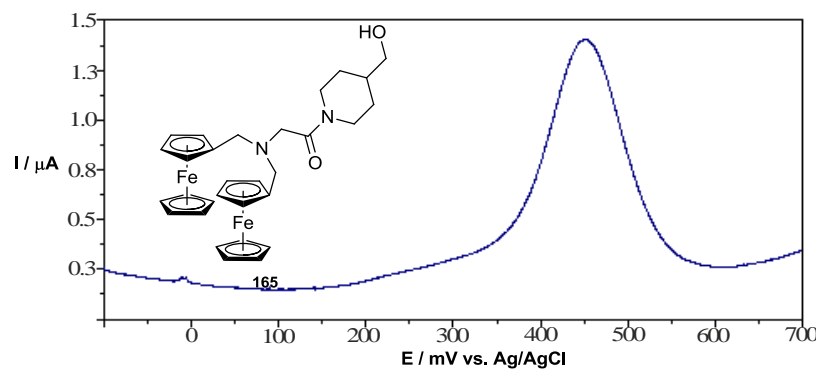


Figure 3.14: Voltammogram of the DPV scan of 165

The oxidation potential of **165** is in a unique region of the scan width compared to **98** which is the current redox-active label being used in the Atlas DNA detection assay, therefore a duplex assay was carried out between **165** and **98** (Figure 3.15, Figure 3.16).

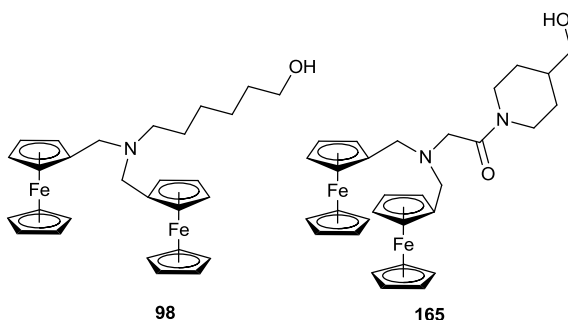


Figure 3.15: Labels **98** and **165** used in duplex assay

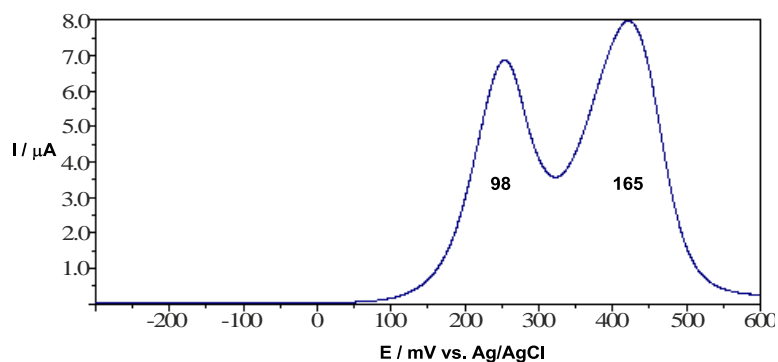


Figure 3.16: Voltammogram of the duplex run between **98** and **165**

The duplex assay was run with equal molar concentration of the two labels **98** and **165**. As Figure 3.16 shows there is separation between the two signals for the two labels. However there is not complete separation between the two signals from the labels, this can be seen as the tail of the peak for **98** does not reach the baseline before the signal for **165** grows in. This could become an issue if the labels were used in a DNA detection duplex assay as it could lead to a false negative result if one of the targets associated to one of the labels was in lower concentration to the other.

It was decided following the result of this duplex to analyse the capability of these two labels being combined with a third label in a multiplex assay. The third label chosen for this was **135** which has an oxidation potential of -80 mV vs. Ag/AgCl, this label was chosen for the multiplex assay as the region from zero down to -300 was smooth and the label would have clear separation from the other two labels (Figure 3.17).

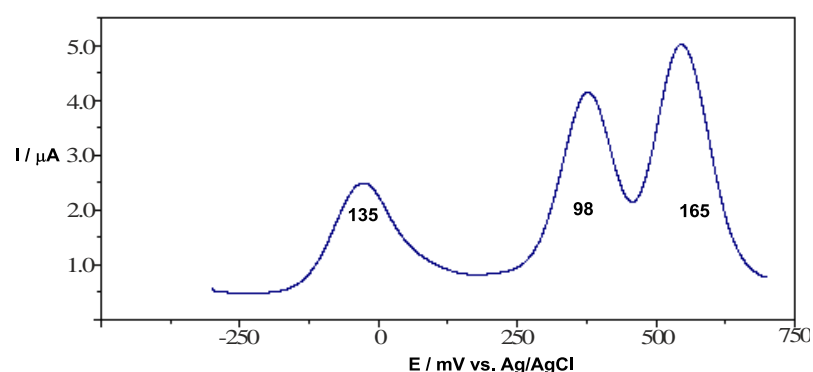


Figure 3.17: Voltammogram of the triplex run between 98, 135 and 165

As Figure 3.17 shows that labels **135**, **98** and **165** are able to be used in a multiplex assay and the fact that all three of the labels can be individually identified. There is clear separation between the peaks of **135** and **98** with there being no overlap between the two signals observed for these two labels. However there is some overlap observed between the signals for **98** and **165**, this could lead to a sensitivity issue in the assay.

From the work presented in chapter 2 it has been shown that labels developed with an ether group in the linker moiety are stable, therefore it was decided to design and synthesise a di-ferrocenyl label containing an ether linkage, 1,1,1-tris(hydroxymethyl)ethane **166** was targeted as the linker moiety for the synthesis of an ether linkage containing di-label (Figure 3.18).

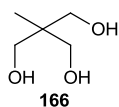


Figure 3.18: Triol 166 to be used as linker moiety

The label 3-ferrocenylmethyl-2-(ferrocenylmethyl)-2-methyl propan-1-ol **167** was designed to be synthesised utilising the linker **166** along with ferrocene methanol **139** as the redox-active moiety of the label (Figure 3.19).

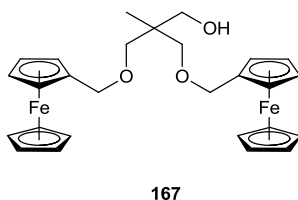
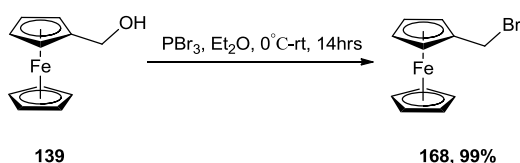


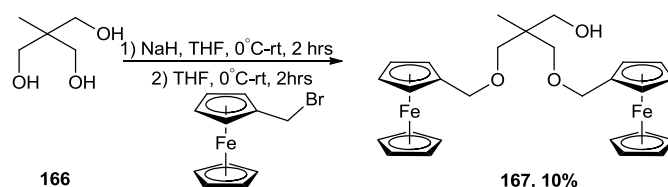
Figure 3.19: 3-ferrocenylmethyl-2-(ferrocenylmethyl)-2-methylpropan-1-ol 167

The initial proposed synthetic route to **167** was three steps with ferrocene methanol being the starting material, the primary synthetic step was the halogenation of the hydroxyl group to afford (bromomethyl)ferrocene **168** via the use of phosphorous tribromide (Scheme 3.16).



Scheme 3.16: Synthesis of 168

The next step was the *in situ* generation of the di-sodium salt of **166** using sodium hydride, the generated sodium salt was then reacted with two equivalents of **168** to afford the desired label species (Scheme 3.17).



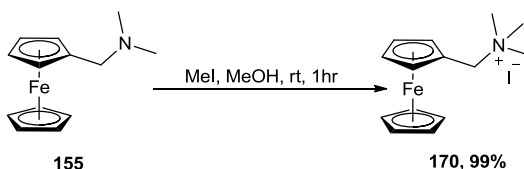
Scheme 3.17: Synthesis of **167**

The yield for this reaction was poor for the desired product, however a higher yielding biproduct was observed. The biproduct was found to be the mono-substituted triol **169**, following this discovery the mono-substituted triol was re-exposed to the reaction conditions to attempt to reach **167** (Scheme 3.18).



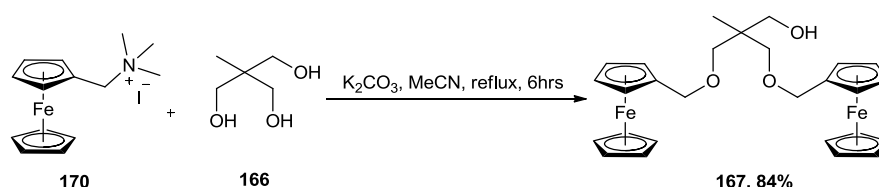
Scheme 3.18: Synthesis of **167** via re-exposure of **169** to reaction conditions

However as the synthesis of **167** was still found to be low yielding after exposing **169** to the reaction conditions for a second time a new synthetic route to **167** was designed. In the new proposed synthetic route the starting material was (dimethylamino)methyl ferrocene **155**, which was converted to the trimethylaminium iodide salt **170** by the reaction with methyl iodide (Scheme 3.19).¹²²



Scheme 3.19: Synthesis of trimethylaminium iodide salt **170**

The formation of salt **170** makes the ferrocene derivative more electrophilic at the benzylic carbon. Therefore this makes the ferrocene derivative more susceptible to nucleophilic attack from nucleophiles such as the triol in this example (Scheme 3.20).



Scheme 3.20: Synthesis of **167** via trimethylaminium iodide salt

The re-design of the synthetic route to **167** proved to be successful as the only product observed from this reaction was the desired product **167**. **167** was analysed via DPV and was found to have an oxidation potential of 360 mV vs. Ag/AgCl (Figure 3.20).

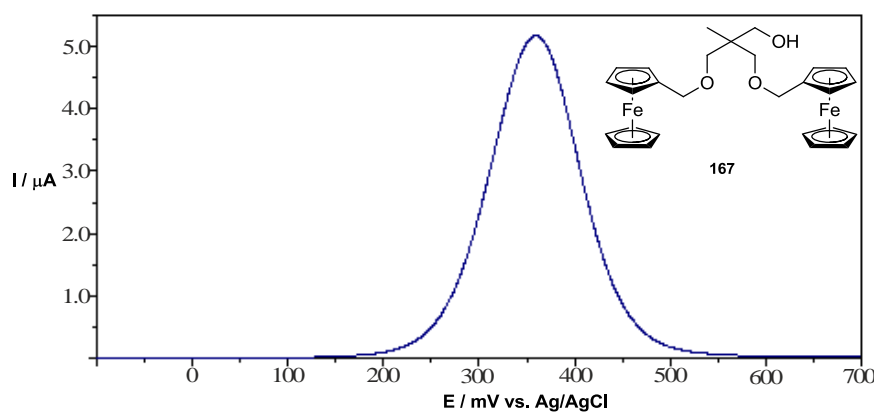


Figure 3.20: Voltammogram of the DPV scan of **167**

The oxidation potential of **167** is close to the oxidation potential of **98** which is the current label being used in the DNA detection assay, therefore a duplex of **98** and **167** was run to analyse the capability of using **167** as a redox-active label for the use

in a DNA detection assay. The duplex was run with **98** and **167** at equal concentration to each other in the assay medium (Figure 3.21).

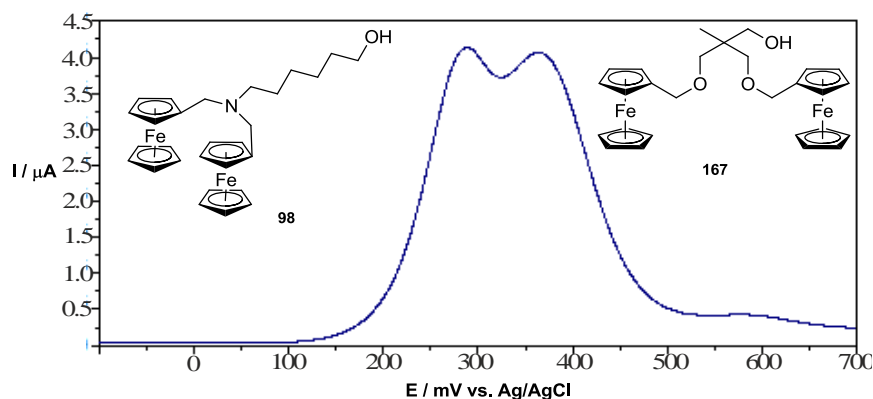


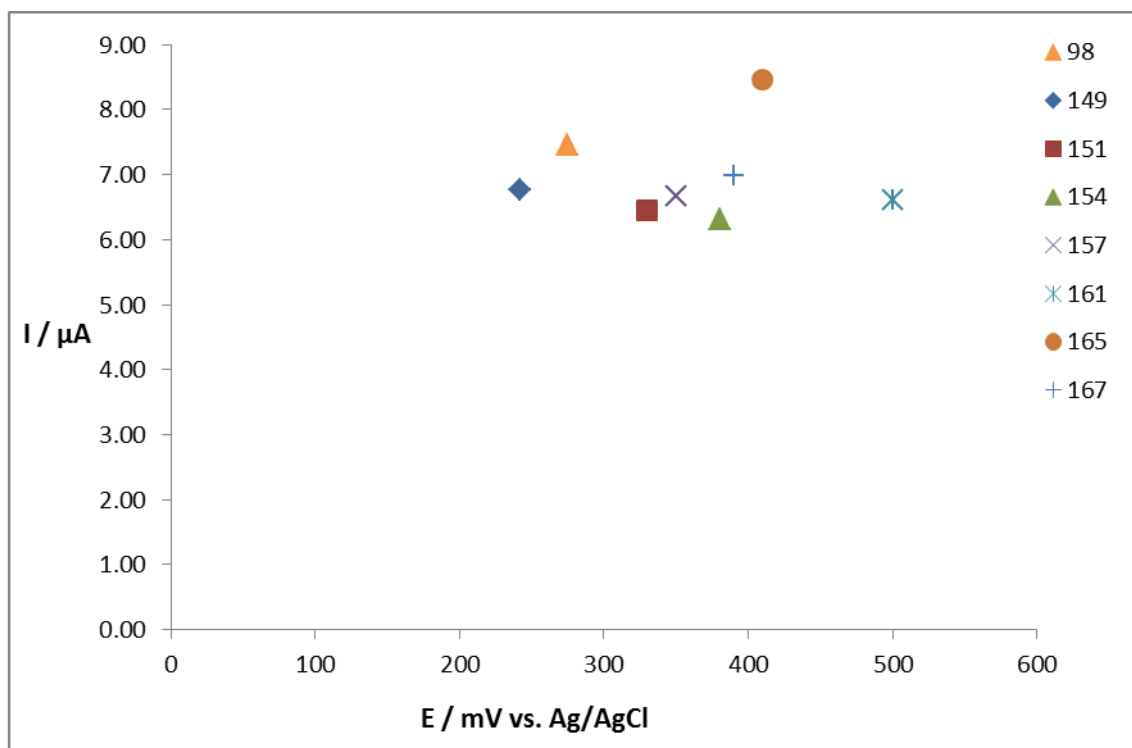
Figure 3.21: Voltammogram of the duplex run between **98** and **167**

As Figure 3.21 shows the two compounds oxidation potentials are too close together to be used as a successful duplex detection assay, as there is no clear separation between the oxidation potentials of the two compounds **98** and **167**. Therefore these two labels would not be suitable for the use in a duplex DNA detection assay, as one of the most important requirements for a successful duplex assay is clear separation between the two labels oxidation potentials so that if the targets are in different concentrations in the assay mixture therefore both labels would be able to be picked up. However with labels **98** and **167** this would not be possible as if either of the labels were at a lower concentration to the other there signal peak would be lost underneath the other labels peak. This would lead to just one peak being exhibited as a broad signal and therefore could lead to a false negative in respect to the assay.

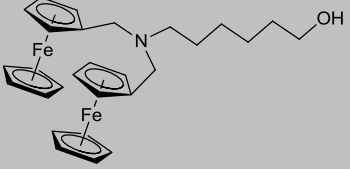
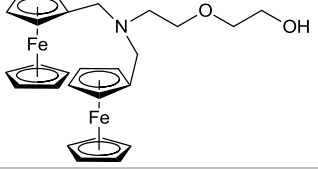
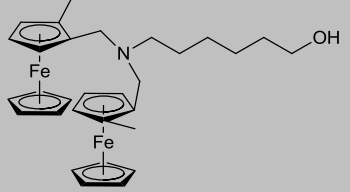
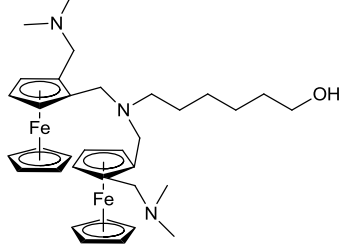
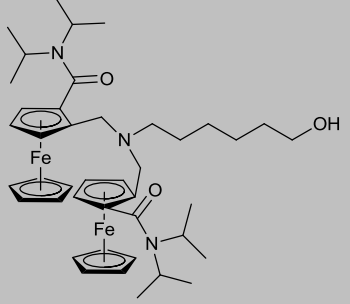
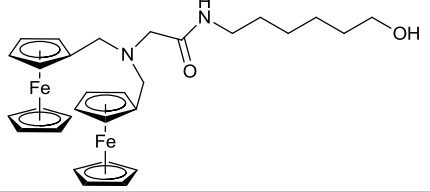
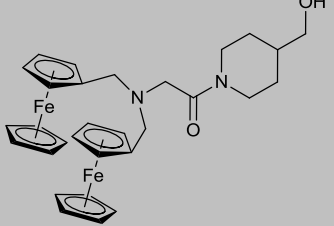
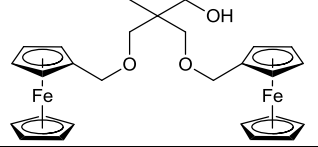
3.3 Conclusion

This chapter has shown the synthesis of a range of di-ferrocenyl derivatives for use as redox-active labels in the synthesis of DNA probes, for use in a DNA biosensor. The compounds synthesised were analysed *via* DPV to ascertain their oxidation potentials and show that a range of oxidation potentials has been achieved (Graph 3.2). Graph 3.2 shows that the di-ferrocenyl derivatives synthesised have similar

signal intensities to that of the current label being used in the biosensor developed by Atlas. It has also been shown that there is the capability through the use of the labels synthesised in this chapter along with chapter 2 for the development of duplex and multiplex assays.



Graph 3.2: Range of di-ferrocenyl labels showing their oxidation potentials vs intensity

Label	Oxidation Potential (mV vs. Ag/AgCl)
	98 275
	149 242
	151 330
	154 380
	157 350
	161 500
	165 410
	167 390

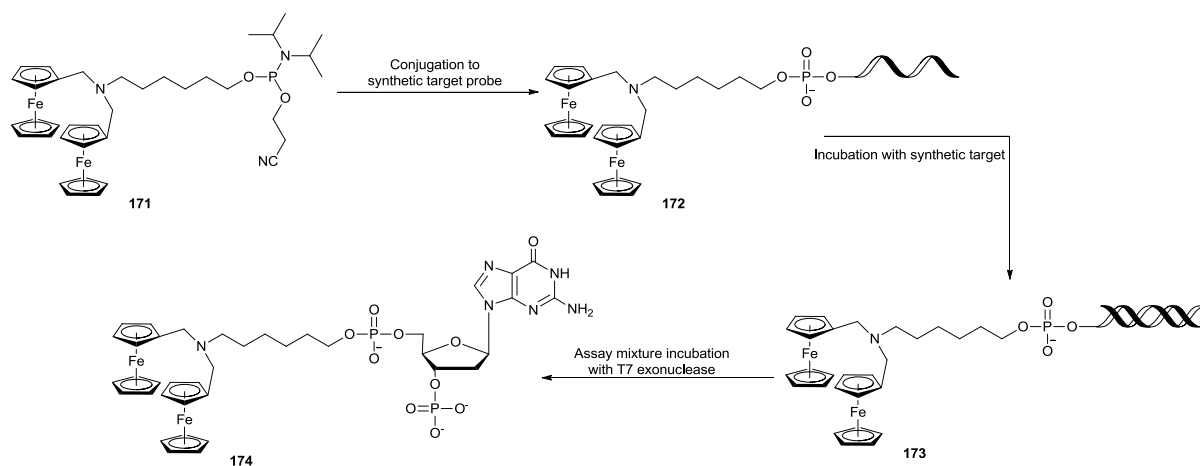
4 Chapter 4: The Analysis of Unique Redox-Active DNA probes in the Atlas DNA Detection Assay

Summary of Chapter

This chapter details the use of the labels synthesised in chapters 2 and 3 in the commercial DNA detection assay set up by Atlas for use in medical diagnostics.

4.1 Background

The development of redox-active labels presented in this thesis in chapters two and three were designed and synthesised to be used in the DNA detection assay developed by Atlas Genetics, with the aim for the redox-active labels to be used in a multiplex detection assay. Once the labels designed have been synthesised and functionalised for conjugation they are sent to ATDBio who carry out the synthesis of the oligonucleotides for use in the assay as well as the labelling of the oligonucleotides with the specific redox-active label. The labelled oligonucleotide probes are then sent to Atlas for testing in the DNA detection assay. The primary testing carried out on a new label is usually the synthetic target assay. A synthetic target assay involves not only the labelled probe being a synthetic strand of DNA but also the target strand is a synthetic oligonucleotide strand. The synthetic target assay is used for the primary analysis of new redox-active probes as the assay contains a higher level of operator control, as the target DNA concentration in the reaction can be controlled by the operator as no PCR amplification of the target DNA is required (Scheme 4.1).

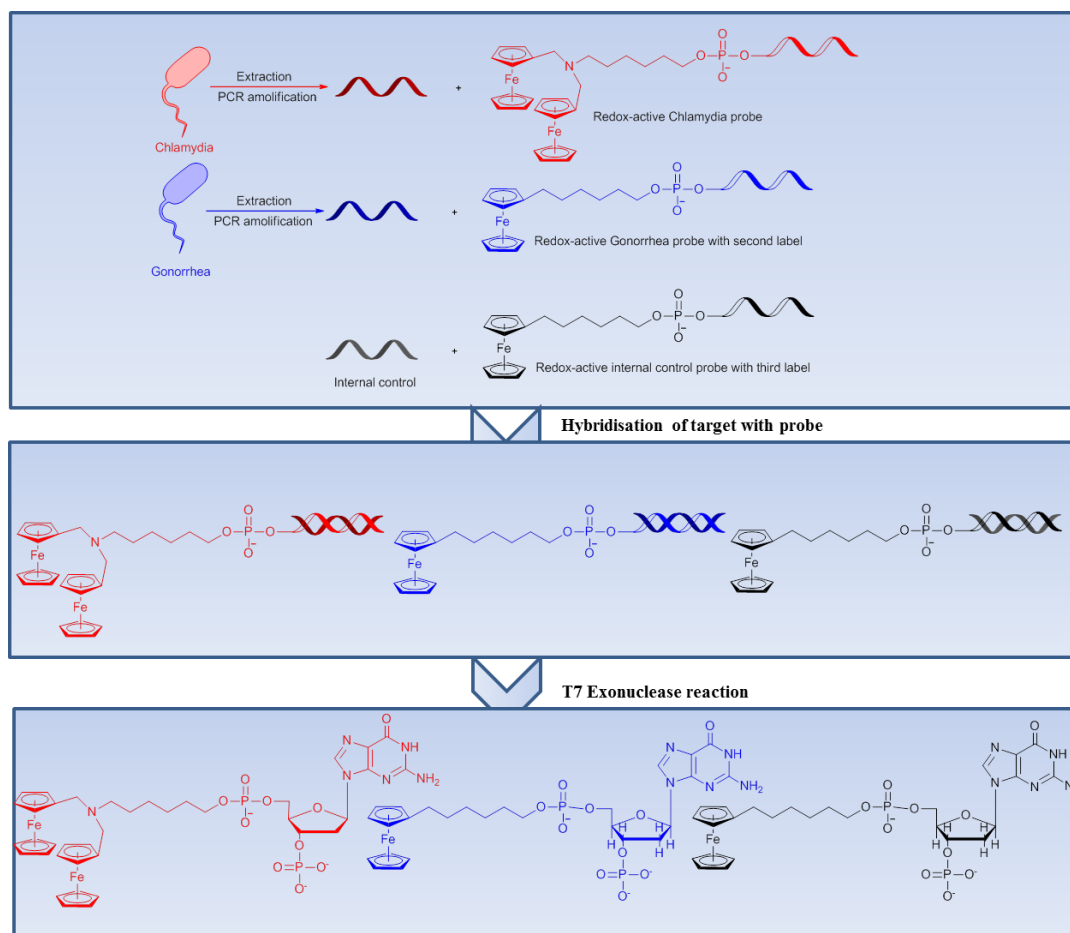


Scheme 4.1: Synthetic target assay schematic

Once a probe has been tested through the synthetic target assay the probe is then analysed in the commercial DNA detection assay developed by Atlas. In the current commercial DNA detection assay the probe **172** is used in the assay as the Chlamydia probe, with the aim to use the labels developed in this thesis as an internal control probe and another labelled probe for the detection of a secondary target in this case a Gonorrhoea probe.

4.2 Results and Discussion

The major aim of the work presented in this thesis has been the design and synthesis of redox-active labels for the use as DNA probes in the Atlas T7 DNA detection assay. More specifically the synthesis of labels for the development of a multiplex DNA detection assay, with the probe that is currently being used in the DNA detection assay by Atlas **172** (Scheme 4.2).



Scheme 4.2: Schematic of targeted multiplex DNA detection assay

The phosphoramidite **150** was conjugated to an oligonucleotide probe, even though **149** was found to have a similar oxidation potential to that of **98** which is the current label being used in the DNA detection assay (Figure 4.1, Table 4.1). As the oxidation potential of **149** is in close proximity to the oxidation potential of **98**, therefore a duplex assay between these two labels would not be possible. **150** was conjugated to an oligonucleotide probe to investigate the effect the ether linker in **149** had on the oxidation potential of the DNA digest product and also the effect on the solubility of the probe digest product.

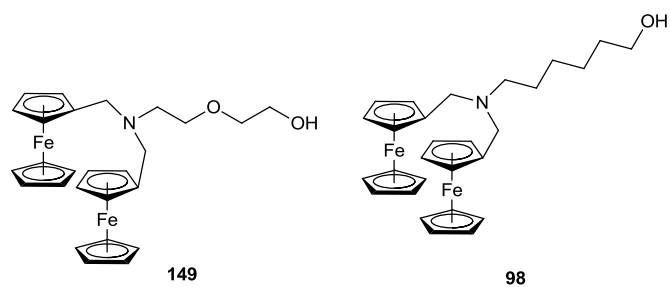


Figure 4.1: Labels 149 and 98

Table 4.1: Oxidation potential and intensity of 98 and 149 vs. Ag/AgCl

Label	Peak Position (mV vs. Ag/AgCl)	Peak height (μA)
98	279	12.5
149	242	10.4

From the electrochemical analysis of **149** via DPV it was observed that at the free alcohol label stage the signal for **149** was found to be sharper than the signal for **98** (Figure 4.2). This observation can be seen on Figure 4.2, which is an overlay of the DPV scans of **98** and the DPV scan of **149**.

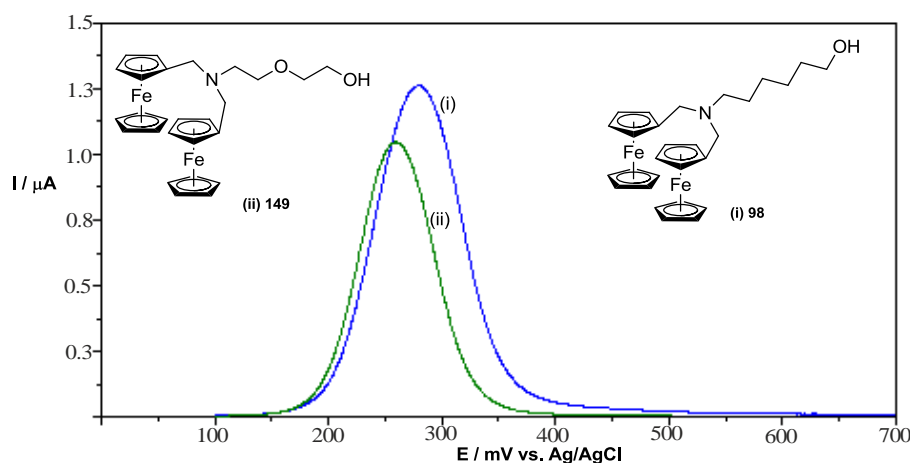
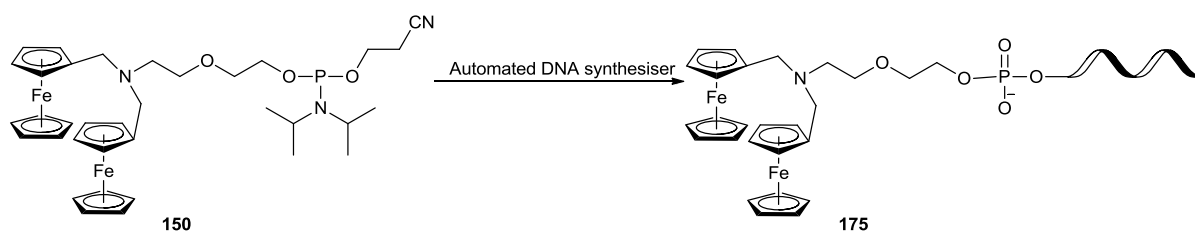


Figure 4.2: Voltammogram showing the overlay of DPV scans for 98 (i) and 149 (ii)

As can be seen from the peaks on Figure 4.2 both the peaks are symmetrical in shape as well as both peaks starting to grow in at the same point at approximately 180 mV. Both peaks start to grow in at the same voltage however the peak for **149** (ii) has a steeper gradient than the peak of **98** (i). This leads to a broader peak being exhibited for **98**, this can be seen from the Figure 4.2 as the peak for **98** (i) starts at the same point as **149**, however it does not return to the baseline until approximately 400 mV. When designing a duplex or multiplex assay the use of a label that possess a sharp signal *via* DPV analysis has a number of benefits, primarily being the fact that the pairing of the label with another is made easier by the fact that there is more of the range free. Also the use of a label with a sharp signal also lowers the chance of any overlap between the two peaks, which can affect the sensitivity of the assays being run.

The phosphoramidite label **150** was conjugated to an oligonucleotide, the probe synthesis was carried out with high coupling efficiency (Scheme 4.3).



Scheme 4.3: The synthesis of probe 175

150 was conjugated to the synthetic target probe, this is an oligonucleotide probe that was synthesised to be complementary in sequence to that of another synthetic target strand. The volumes of reagents needed for one assay volume were calculated, the assays are always repeated in triplicate this is to confirm the results is accurate and also to discount for any false positives or negatives (Table 4.2). When the volumes for the triplicates are calculated they are calculated for both positive and negative assay runs. The triplicate volumes are calculated for four assay runs as the extra assay volume guarantees that there will be the same volume in each assay run and

also that each assay run will contain the correct volumes of all the reagents necessary for an effective assay.

Table 4.2: Reaction volumes for the synthetic target assay

Reagent	1 x rxn (μL)	Positive 4 x rxn (μL)	Negative 4 x rxn (μL)
175	0.6	2.4	2.4
Synth target DNA	1	4	/
MgCl₂	4	16	16
10x Atlas PCR buffer	2	8	8
T7	0.2	0.8	0.8
H₂O	12.2	46.4	52

The assay was then run and following the incubation with T7, the reaction volumes were read on the electrodes (Table 4.3, Figure 4.3).

Table 4.3: DPV analysis of 176 in the assay solution

Run No.	Positive		Negative	
	Peak Position (mV vs. Ag/AgCl)	Peak Height (μA)	Peak Position (mV vs. Ag/AgCl)	PH (μA)
1	175	3.57	/	/
2	178	3.20	/	/
3	175	2.96	/	/

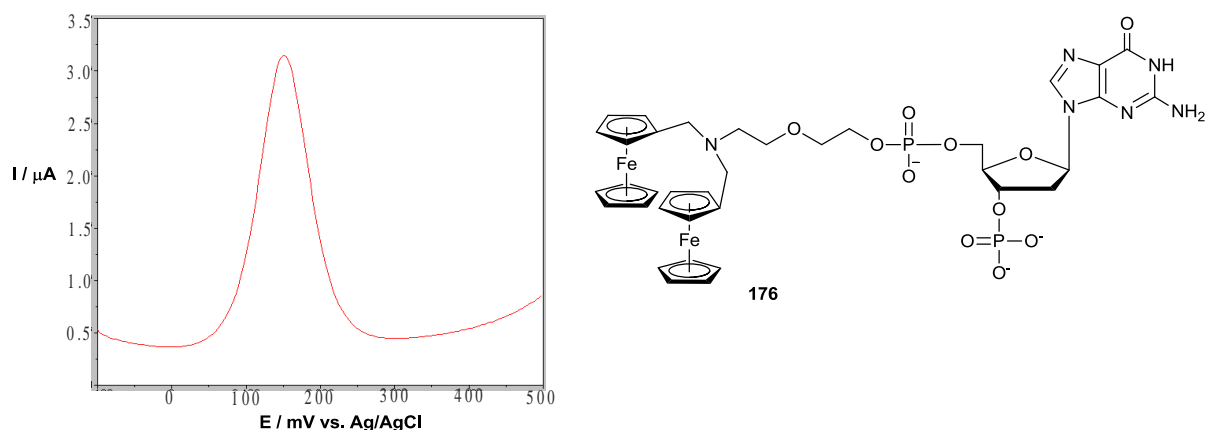


Figure 4.3: Voltammogram of the DPV scan of the digest product **176**

One observation that can be made from Figure 4.3 is that the oxidation potential of **149** has shifted from 242 mV vs. Ag/AgCl as the free alcohol to 175 mV vs. Ag/AgCl for the digest product **176** (Figure 4.4).

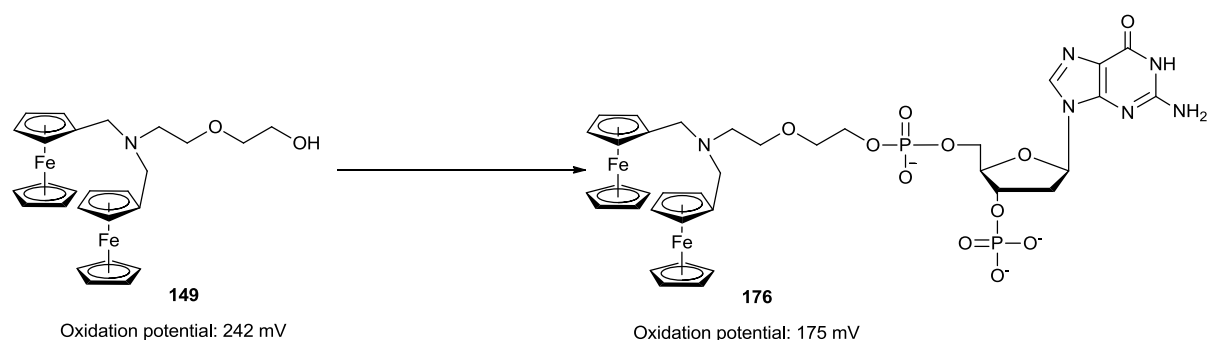


Figure 4.4: Oxidation potentials of label **149** and **176** digest product

First of all the development of a duplex between the current probe **172** that is conjugated to a Chlamydia oligonucleotide probe and a secondary label with an oxidation potential that is different to that of **98** and with a high degree of separation between the two labels oxidation potentials. The second label being added to the assay is initially going to be the internal control probe. The first label targeted for use in a duplex detection assay with **98** was **99** (Figure 4.5).

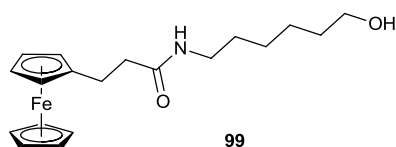
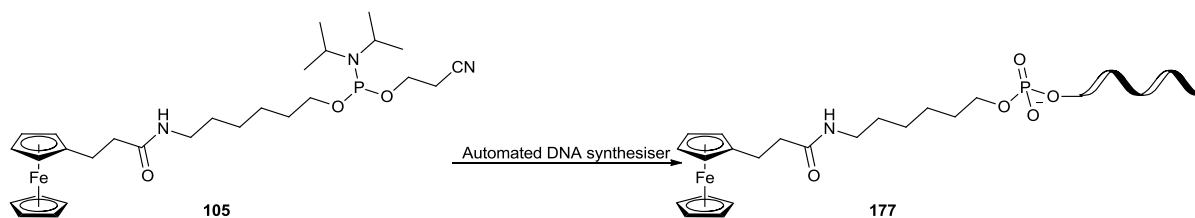


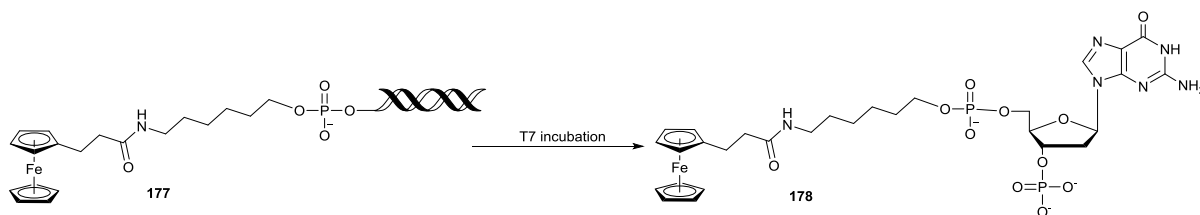
Figure 4.5: Chosen label 99 for duplex

99 was chosen as it was found to have an oxidation potential of 85 mV vs. Ag/AgCl which has a difference in oxidation potential of 190 mV compared to that of **98** which has an oxidation potential of 275 mV vs. Ag/AgCl.



Scheme 4.4: Synthesis of probe 177

The phosphoramidite **105** went through the conjugation to an oligonucleotide probe, however the efficiency of the coupling reaction was low (Scheme 4. 4). First of all the probe **177** was used in the synthetic target assay to analyse the probes behaviour in the assay and the T7 exonuclease reaction (Assay reaction volumes Table 1. Appendix). The assay was run and following the incubation with T7 exonucelase the assay runs were read on the electrode to detect for the probe digest product **178** (Scheme 4.5, Table 4.4, Figure 4.6).



Scheme 4.5: Hybridised probe 177 product incubation with T7 giving 178

Table 4.5: Electrochemical results of digest product 178

Run No.	Positive		Negative	
	Peak Position (mV vs. Ag/AgCl)	Peak Height (μ A)	Peak Position (mV vs. Ag/AgCl)	Peak Height (μ A)
1	65	4.28	/	/
2	83	4.86	/	/
3	68	3.34	/	/

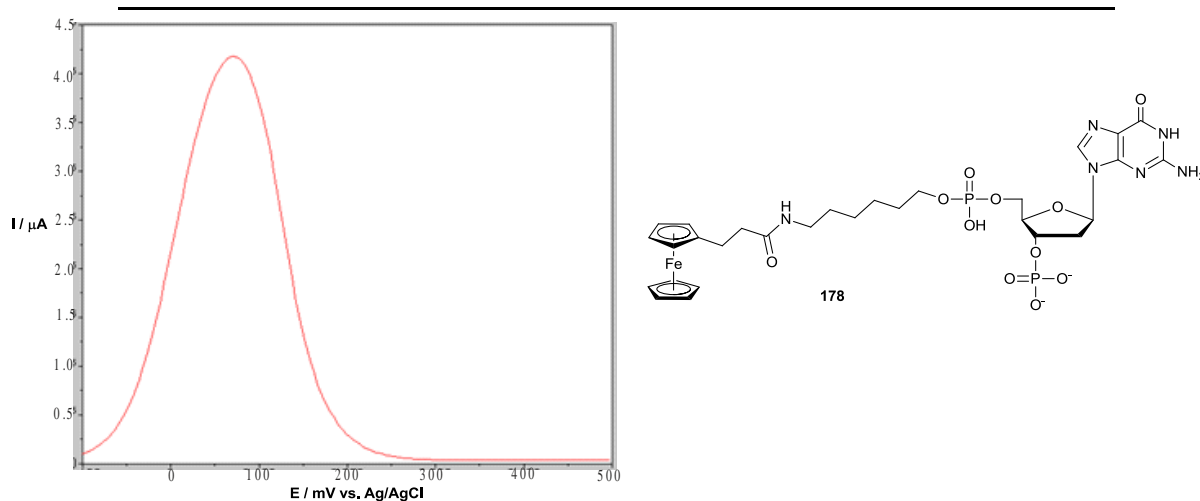


Figure 4.6: Voltammogram of the DPV scan of digest product 178

After the completion of the assay it was shown from the DPV analysis that **177** functions in the DNA detection assay. The fact that **177** functions well in the synthetic target assay, lead to **177** being used as the second probe in a duplex DNA detection assay along with **172**. The volumes of the reagents required for the duplex assay were calculated and the DNA detection assay was run (Table 4.5).

Table 4.5: Reagents for duplex assay between probes 172 and 177

Reagent	Positive 4 x rxn (μL)	Negative 4 x rxn (μL)
172	2.4	2.4
177	2.4	2.4
Synth target DNA	4	/
MgCl ₂	16	16
10x Atlas PCR buffer	8	8
T7	0.8	0.8
H ₂ O	46.4	52

Once the DNA detection assay had been carried out, the assay runs were read on the electrodes for the detection of the probe digest products *via* the use of probe **177** as the second redox-active probe in the duplex assay was successful, however the signal from probe digest product **178** was found to be less intense than that of the signal for probe digest product **174** (Table 4.6, Figure 4.7).

Table 4.7: Results of the duplex assay between 174 and 178 at the electrode

Run No.	Positive				Negative	
	Peak Position (mV vs. Ag/AgCl)	Peak Height (μA)	Peak Position (mV vs. Ag/AgCl)	Peak Height (μA)	Peak Position (mV vs. Ag/AgCl)	Peak Height (μA)
1	74	239	1.67	2.38	/	/
2	71	236	1.56	3.22	/	/
3	69	236	1.33	2.65	/	/

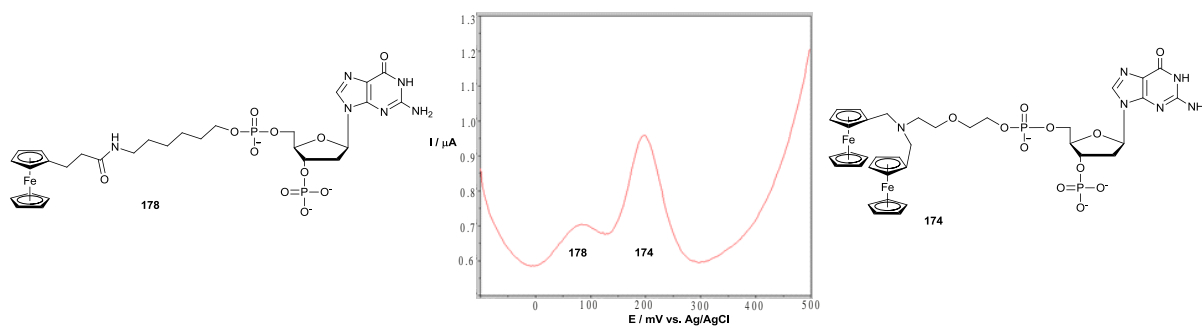


Figure 4.7: DPV scan of the duplex between 174 and 178

Figure 4.7 shows that the peak for digest product **178** does not make it back down to the baseline before the peak for probe digest product **174** starts to grow in, therefore considerable overlap between the two signals for the digest products was observed in the duplex assay. The fact that there is not clear separation between the signals received for the probe digest products of the duplex and the lower intensity of the signal for probe digest product **178** could affect the sensitivity of the duplex assay between these two labels. The use of probe **177** as a second label for a duplex assay with probe **172** as the lower intensity and overlap between the two peaks could lead to possible false negative results of the assay for probe **177**.

From the result of the duplex between probes **177** and **172**, it was shown that a duplex assay between a mono-ferrocenyl labelled probe and a di-ferrocenyl labelled probe was possible and successfully carried out. Therefore a triplex DNA detection assay was targeted between two of the mono-ferrocenyl labels presented in Chapter 2 and the di-ferrocenyl label **98**. Labels **118** and **127** were chosen as possible labels to be used in the synthesis of redox-active probes in a multiplex DNA detection assay. Labels **127** and **118** were targeted as their oxidation potentials of 114 mV vs. Ag/AgCl and 433 mV vs. Ag/AgCl respectively were found to be either side of the oxidation potential of **98** which was found to have an oxidation potential of 275 mV vs. Ag/AgCl (Figure 4.8).

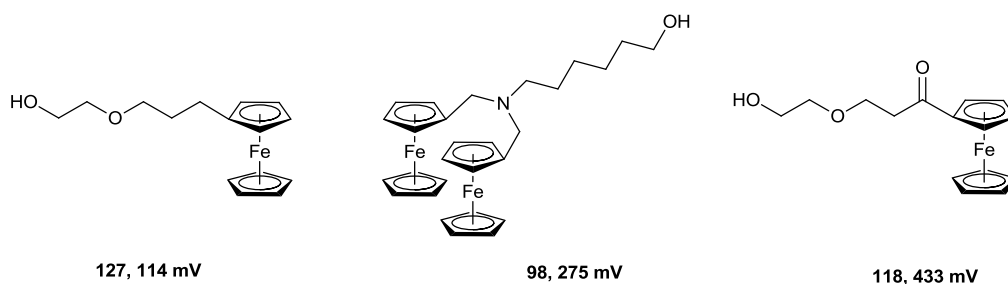
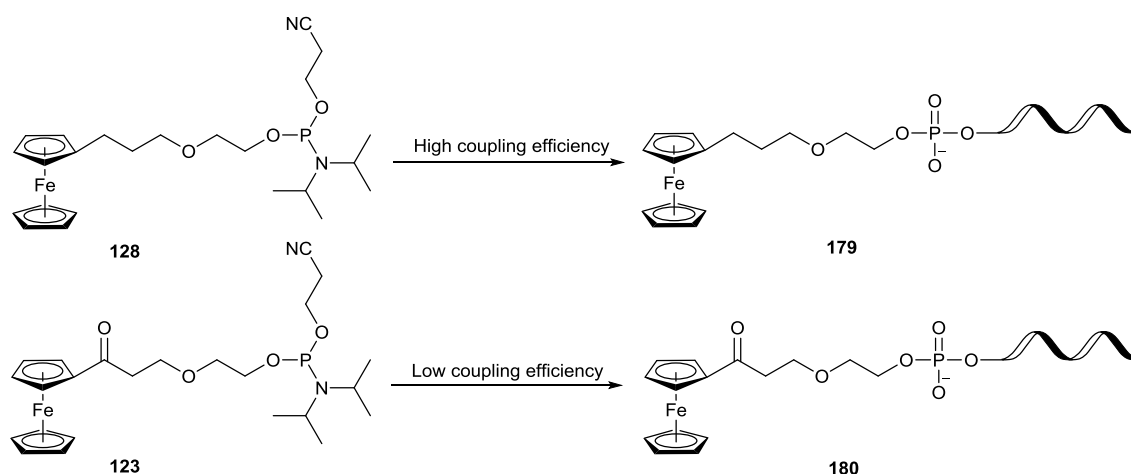


Figure 4.8: Labels and their oxidation potentials (vs. Ag/AgCl)

In the multiplex DNA detection assay the three phosphoramidite labels **171**, **123** and **128** were conjugated to three different probe strands. The aim was to conjugate the mono-labels to an internal control strand and the other to a second target strand in this case a Gonorrhoea probe. However upon conjugation **123** was found to have poor coupling efficiency to the oligonucleotide probe, were as **128** was found to have a high coupling efficiency to the oligonucleotide probe (Scheme 4.6). Therefore it was found that a triplex assay between **98**, **118** and **127** was not possible due to the poor coupling efficiency of **123** to the oligonucleotide. This lead to a duplex assay being run between probe **172** and probe **179**, with the mono-ferrocenyl probe being the internal control probe.



Scheme 4.6: Synthesis of probes 179 and 180

Probe **179** was first analysed in the DNA detection assay to investigate how it interacts within the DNA detection assay. The DNA detection assay run was the synthetic target assay (Assay volumes in appendix Table 2).

The reaction mixtures are made up to the desired volume without the addition of T7 in a master mix, the three positive and negative reaction mixes are then aliquoted into individual PCR tubes. The reaction mixture are then incubated using a PCR heating block to aid the hybridisation of the probe with the synthetic target DNA. The T7 is then added to each of the reaction tubes and the reaction mixtures are then incubated at 37°C which is the ideal temperature for the enzyme for 20 minutes to allow the T7 exonuclease reaction to take place and for the double-stranded DNA to be cleaved one base pair at a time from the 5' end of the DNA and the digest products were read on the electrode (Table 4.7).

Table 4.7: DPV results from the synthetic target assay detecting for probe digest product 181

Run No.	Positive		Negative	
	Peak Position (mV vs. Ag/AgCl)	Peak Height (µA)	Peak Position (mV vs. Ag/AgCl)	Peak Height (µA)
1	77	1.61e ⁻⁷	/	/
2	74	6.79e ⁻⁸	/	/
3	80	9.93e ⁻⁸	/	/

Probe **179** was found to function well in the synthetic target DNA detection assay. The digest product **181** when analysed *via* DPV it was found to have an oxidation potential of 75 mV vs. Ag/AgCl. The oxidation potential of **181** was found to be approximately 40 mV lower than that of label **128** which has an oxidation potential of 114 mV vs. Ag/AgCl (Figure 4.9). The shift in oxidation potential from the digest product **181** and the label **128** exhibited from this assay fits with the shifts in

oxidation potentials exhibited by other labels under the assay conditions such as label **149**.

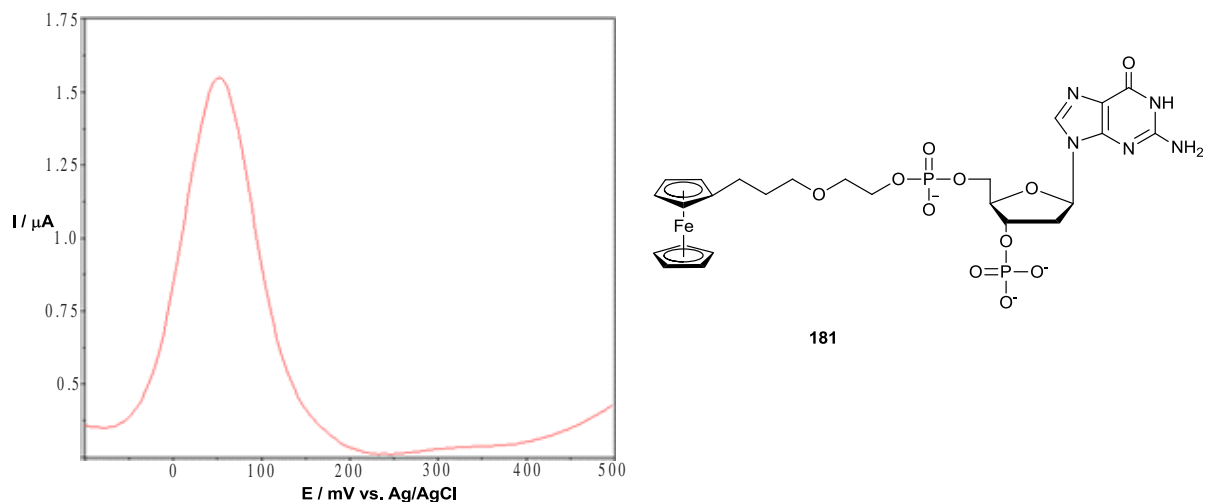


Figure 4.9: Voltammogram of the DPV scan of probe digest product **181**

The shift in the oxidation potential from **128** to the digest product **181** is thought to be due to the nucleotide base that is still coupled to the label post T7 cleavage, which is having an effect on the overall oxidation potential of the digest product. From the results showing that the probe has a good efficiency of hybridisation and also that the T7 exonuclease reaction works well on the hybridised product of this DNA probe shown in table 4.9, a duplex was carried out between the **179** probe and the current probe **172** used in the assay (Table of assay volumes in appendix Table 3). After the incubation with T7, the reactions were run on individual electrodes. It was found that the two peaks were in fact distinguishable from each other (Table 4.8, Figure 4.10).

Table 4.8: DPV results of duplex assay probe digest products 174 and 181

Run	Probe	Peak position (mV)	Peak Height (μA)
1	181	47	1.02
	174	245	8.23
2	181	43	3.07
	174	233	3.88
3	181	40	1.61
	174	217	3.11
4	181	43	1.09
	174	233	3.27

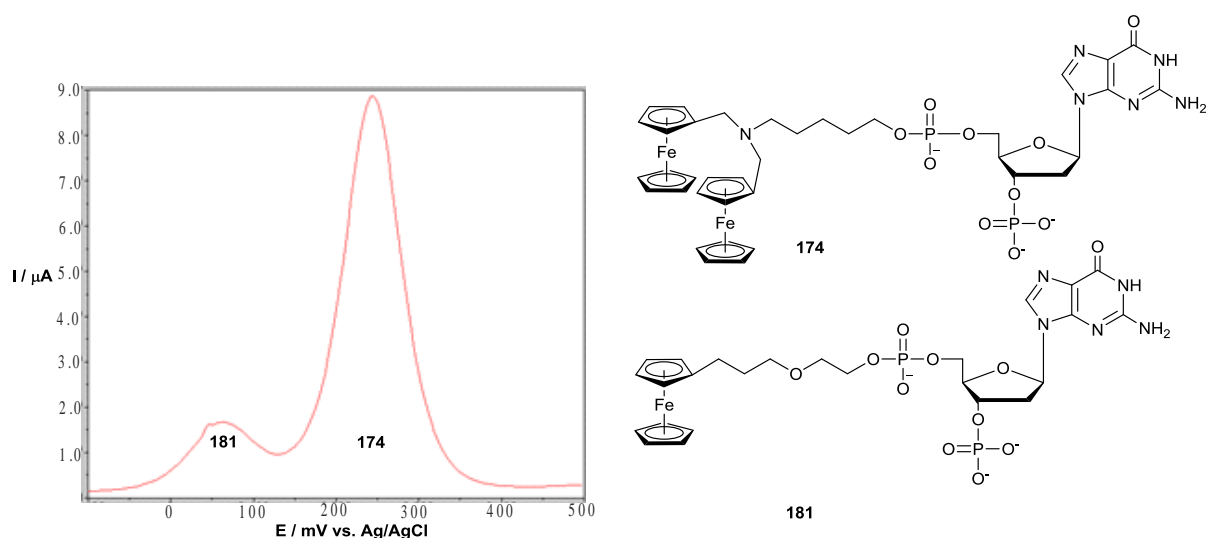


Figure 4.10: Voltammogram of the DPV scan of the product digest products 174 and 181

Figure 4.10 shows that the duplex between probe **181** and **174** is a viable duplex reaction with a greater level of separation between the two peaks than exhibited from the duplex between probe **177** and probe **172**. However as can be seen from figure 4.10 there is a large difference in the intensities observed for the two peaks. With the signal from **181** being less intense than that of the signal received from probe **174**, this was expected as previously mono-ferrocenyl labels have been shown to be less

intense than di-ferrocenyl labels. Therefore probe **179** would not be suitable for the detection of a second target DNA as the signal intensity is so much lower than the signal from probe **172**, this could lead to at lower concentrations of target DNA the loss of the signal from **181** under the start of the signal for **174**. As the signal for **181** is at a different oxidation potential to that of **174** and the signals exhibited by both digest products **181** and **174** are clearly separable it would be a suitable probe to be used as an internal control for the assay, therefore the concentration of the internal control target DNA would be at a constant concentration across all the assays.

With the duplex between probe **179** and probe **172** being found to be successful with **179** being used as the internal control probe in the assay and **172** being used as the Chlamydia probe. Therefore there was the need for a third label to be used as the label for the probe of another target. In the case of the multiplex DNA detection assay the third redox-active labelled probe is the probe for the detection of Gonorrhoea. **135** was chosen as the label to be used as the redox-active component of the Gonorrhoea probe (Figure 4.11), **135** was chosen as it has an oxidation potential of -80 mV vs. Ag/AgCl which is different to the oxidation potentials of both the other two redox-active probes going to be used in the multiplex DNA detection assay. **135** is another mono-ferrocenyl label, however as its oxidation potential is in such a unique region compared to the other two labels being used in the assay therefore there should not be any issue of overlap between the signal received for the probe labelled with **135** with the other two probes being used. **135** has been shown to be a viable label to be used in both duplex and triplex assays at the free alcohol stage.

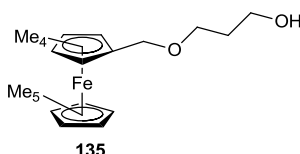
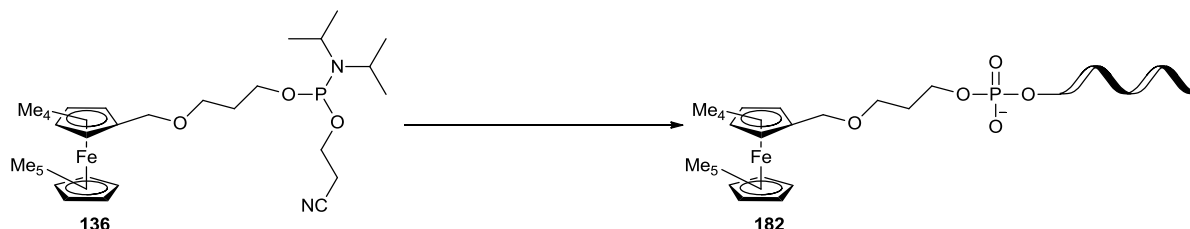


Figure 4.11: Label **135** to be used in a triplex assay with **98** and **128**

The phosphoramidite **136** went through the conjugation to the oligonucleotide successfully to give probe **182** (Scheme 4.7).



Scheme 4.7: Synthesis of probe **182**

Probe **182** was then taken through a triplex assay with probes **172** and **179**. The assay volume for one reaction is then calculated followed by the scale up to four reactions (Table 4.9). The assay mixture is then incubated to allow the probes to hybridise with their target DNA present in the assay mixture.

Table 4.9: Reagent volumes required for triplex assay between probes **172**, **179** and **182**

Reagent	Positive 4 x rxn (μL)	Negative 4 x rxn (μL)
172	4.5	4.5
179	4.5	4.5
182	4.5	4.5
Synth target DNA	7.45	/
MgCl ₂	16	16
10x Atlas PCR buffer	8	8
T7	0.8	0.8
H ₂ O	41.9	47.5

The T7 was then added to the reaction mediums which are incubated at 37°C for 20 minutes and the runs are then read on the electrodes (Figure 4.12, Table 4.10).

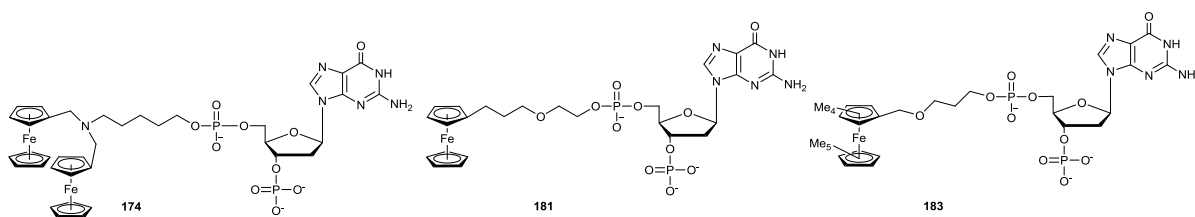


Figure 4.12: Digest products 174, 181 and 183 from the triplex assay

Table 4.10: DPV results of the triplex assay digest products 174, 181 and 183

Run		Peak Position (mV vs. Ag/AgCl)	Peak Height (μA)
1	183	-278	0.266
	181	42	0.504
	174	192	3.21
2	183	-278	0.271
	181	45	0.256
	174	192	3.73
3	183	-272	0.291
	181	45	0.514
	174	195	4.80

As shown from the data in table 4.10 all three of the peaks for the three probes used in the multiplex assay are distinguishable from each other, therefore showing that a commercial triplex DNA detection assay between these three probes is possible and can be carried out successfully. From table 4.14 it can be seen that the oxidation potentials from the three probe digest products have all shifted from the oxidation potential that the free labels were found to have. However as can be seen from figure 4.13 there is a large difference in the sensitivities between the two mono-ferrocenyl probes and the di-ferrocenyl probes (Figure 4.13). The signal for **174** was expected to be more intense than the signals for the other two mono-ferrocenyl probes **181** and **183**.

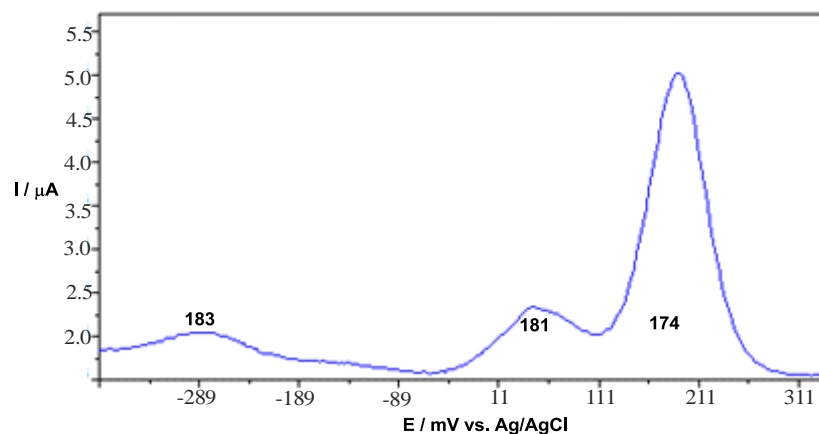


Figure 4.13: DPV scan of triplex assay of probe digest products 174, 181 and 183 at equimolar concentration

From the results in table 4.10 and from figure 4.13 it has been shown that the use of these three labels are able to be used in the detection of multiple DNA targets in a single commercial DNA detection assay. However the signal from the digest product **174** was found to have a significantly higher intensity than that of the two mono-ferrocenyl labelled probes digest products **181** and **183**, when the probes were in equimolar concentration in the assay medium. This result was found to support the findings on label sensitivities presented in chapters 2 and 3. The multiplex DNA detection assay was therefore carried out with probe **172** being at a third of the concentration in comparison to that of the two mono-ferrocenyl labelled probes which are in equimolar concentration with respect to each other (Assay volumes in appendix Table 4).

The T7 is then added to the reaction mixtures and they are incubated at 37°C for 20 minutes and the reactions are then read on the electrodes (Table 4.11).

Table 4.11: DPV results of the triplex assay of probe digest products 174, 181 and 183 with a lower concentration of probe 172

Run	Peak Position (mV vs. Ag/AgCl)	Peak Height (μA)
1	183	-272
	181	45
	174	201
2	183	-257
	181	45
	174	198
3	183	-272
	181	45
	174	201

As can be seen from the data in table 4.16 the signals received for the digest products of the probes are still all distinguishable from one another, however the signal received for the digest product **174** was still found to be more intense than the signals for the other two mono-labels (Figure 4.14). The greater intensity of the signal for the digest product **174** could not only be due to the label containing two redox-active moieties but also the possibility of the digest product **174** depositing on the electrode surface.

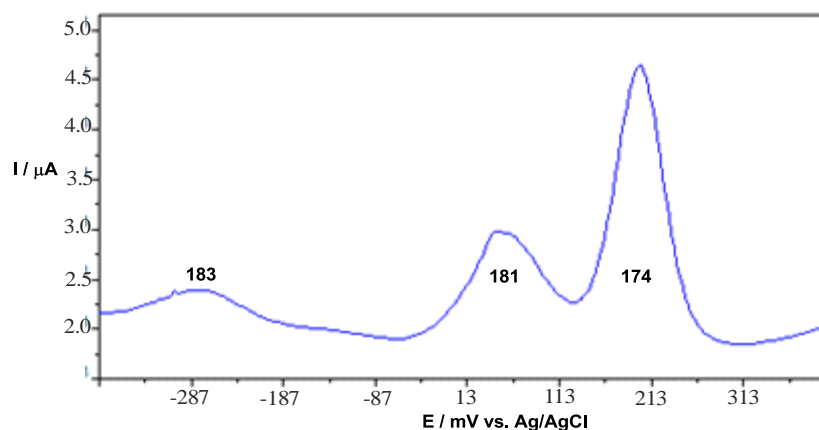


Figure 4.14: Voltammogram of the triplex assay digest products 174, 181 and 183 with probe 172 being at a third of the original concentration

The assay was then run with the **172** being at a ninth of the concentration compared to the probes **179** and **182** (Assay volumes in appendix Table 5). The assay is then run with the T7 being added post primary incubation and the assay reaction mixtures were then incubated for a further 20 minutes at 37°C, the samples are then run on the electrodes (Table 4.12).

Table 4.12: Electrochemical results of triplex assay

Run	Peak Position (mV)	Peak Height (μA)	
1	183	-281	3.29
	181	45	7.93
	174	195	6.16
2	183	-287	3.72
	181	45	8.83
	174	198	7.81
3	183	-289	2.73
	181	53	6.28
	174	197	6.14

As can be seen from the data on table 4.12 the intensities of the signals from the three probe digest products are almost all equal in intensity to one another, with the

peak for probe **183** still being lower than the signals for the other two probes (Figure 4.15).

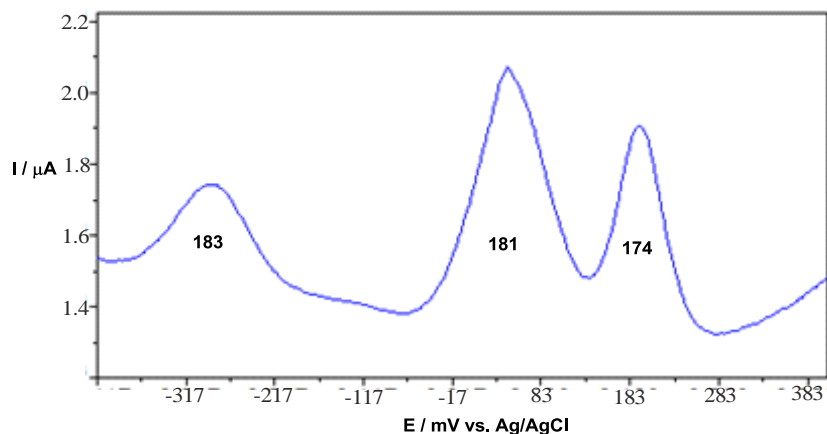
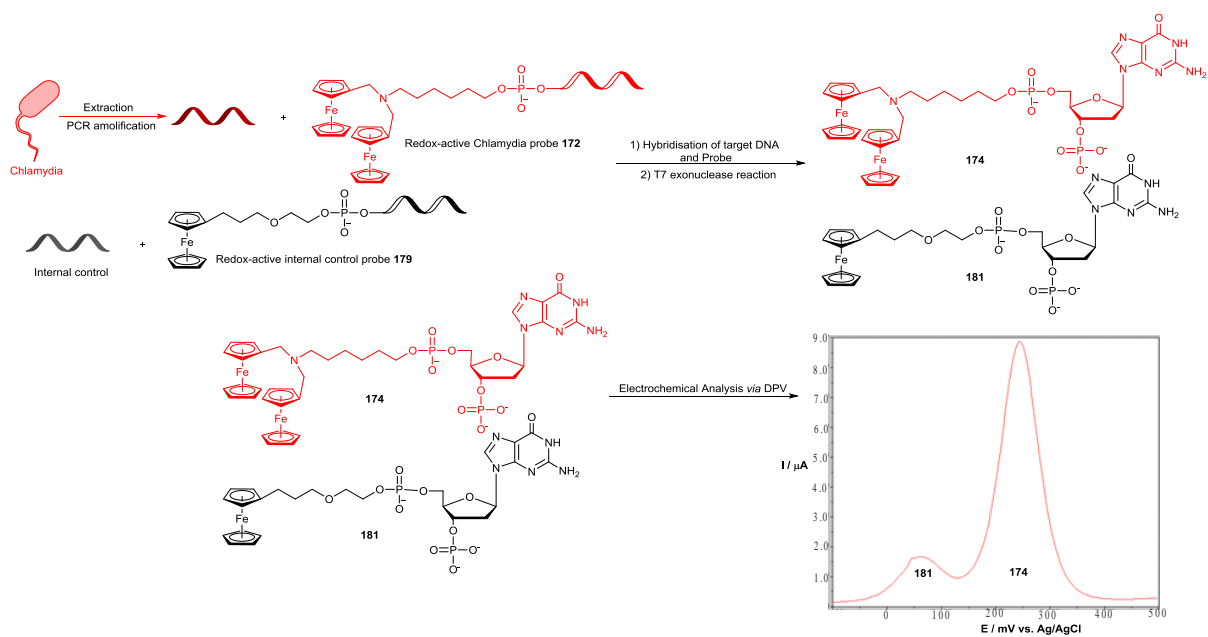


Figure 4.15: Voltammogram of the triplex assay digest products 174, 181 and 183 with probe 172 being at a ninth of the original concentration

Figure 4.15 shows that with probe **172** at a lower concentration there is clear separation between all the peaks from the probe digest products as well as all the peak intensities for the three probes being found to be similar in intensity to each other. Therefore this shows that a successful multiplex DNA detection assay has been carried out for the detection of two separate pathogenic DNA targets in the case of this triplex assay the two pathogenic DNA targets were Chlamydia and Gonorrhoea.

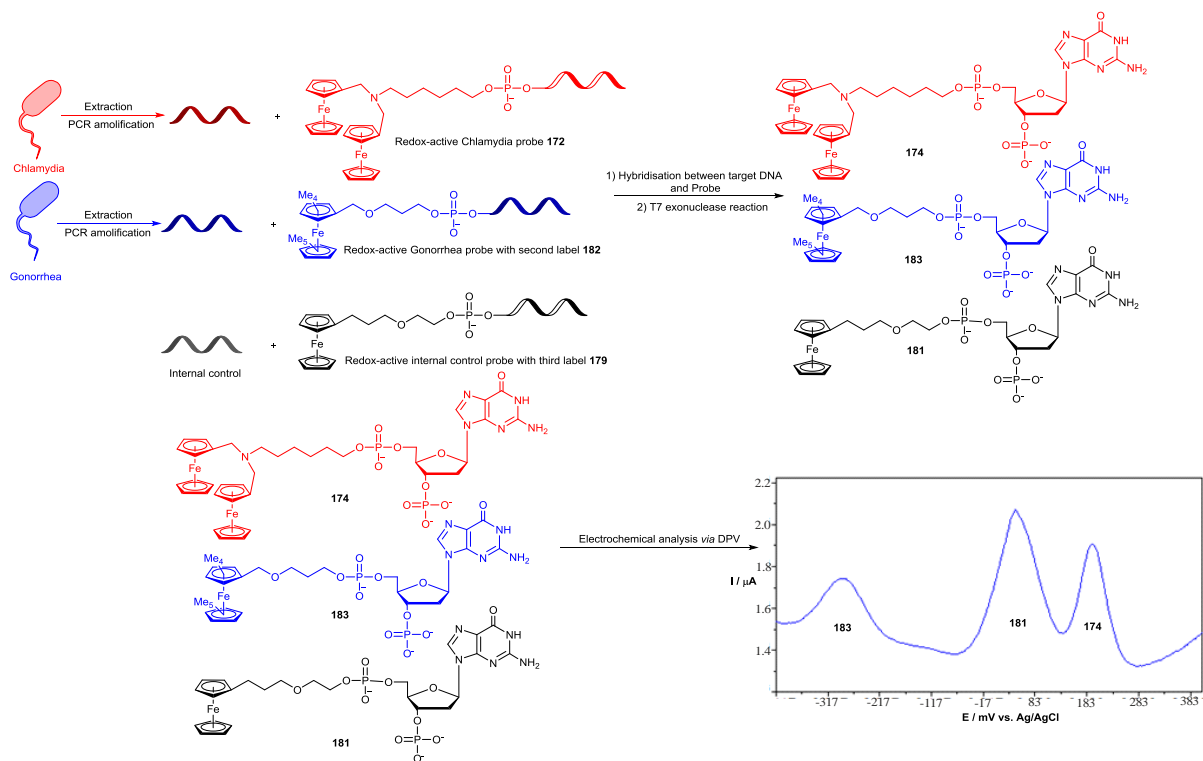
4.3 Conclusion

This chapter has shown the use of the labels synthesised in chapters 2 and 3 as labels for redox-active probes and their use in the Atlas DNA detection assay. It has been shown that through the labels synthesised a successful duplex DNA detection assay has been produced between probe **172** and probe **179** (Scheme 4.8).



Scheme 4.8: Schematic of the duplex DNA detection assay between probes 172 and 179

As well as the DNA duplex between probes **172** and **179**, it has been shown that a triplex DNA detection assay has been produced for the detection of two pathogens as well as an internal control probe (Scheme 4.9).



Scheme 4.9: Schematic of the multiplex DNA detection assay between probes 172, 179 and 182

The multiplex detection assay developed between probes **172**, **179** and **182** is now being utilised in the full commercial assay on the cartridges developed by Atlas Genetics (Figure 4.16).



Figure 4.16: Triples DNA detection assay developed being used on the commercial cartridge set up at Atlas

5 Chapter 5: The synthesis of 2-Oxazolines and The Ring-Opening Reaction for the use as an Analytical Tool for Carboxylic Acids

Summary of Chapter

This chapter details the synthesis of a range of functionalised oxazoline derivatives and their ring-opening reactions with a range of carboxylic acid derivatives. The direct conjugation of oxazolines and carboxylic acids has the potential application in the analytical detection of carboxylic acids which has been exhibited in this chapter through the use of oxazolines that have been functionalised with analytical reporter moieties.

5.1 Background

Oxazolines are a class of heterocycle, they are 5-membered rings that contain two different heteroatoms, a nitrogen and an oxygen. Oxazolines also contain a double bond and there are three possible positions the double bond can be in, leading to three different structural isomers (figure 5.1).¹²³

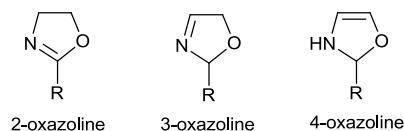
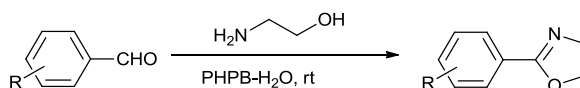


Figure 5.1: The three structural isomers of oxazolines

2-Oxazolines are of interest and importance in the area of organic chemistry due to their inclusion within a wide range of structures that show biological activity (Figure

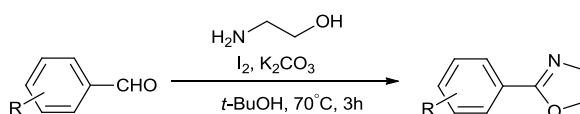
5.2),¹²⁴⁻¹²⁶ as ligands in catalytic reactions,¹²⁷ as well as being monomers for cationic ring-opening polymerisations (CROP).¹²⁸⁻¹³⁰

There are a number of synthetic routes towards the synthesis of 2-substituted 2-oxazolines, starting from a range of simple and commercially available compounds, such as carboxylic acids and derivatives,¹³¹⁻¹³³ acyl benzotriazoles¹³⁴ and nitriles.¹³⁵⁻¹³⁷ Recently there have been a number of publications reporting the synthesis of 2-oxazolines from aldehydes and alcohols using pyridinium hypobromide (PHPB) or molecular iodine. Sayama *et al*, reported the synthesis of 2-oxazolines using PHPB (Scheme 5.1).¹³⁸



Scheme 5.1: Conditions for the synthesis of oxazolines using PHPB-H₂O

The scope of the reaction tolerated a range of substituted benzaldehyde derivatives with ten examples, with yields ranging from 72-90%. Togo *et al*, published findings into the synthesis of 2-oxazolines starting from aldehydes as well as from benzylalcohols with the use of molecular iodine and potassium carbonate (Scheme 5.2).¹³⁹

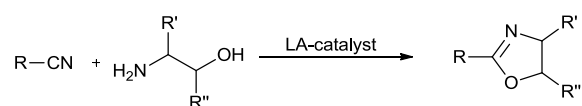


Scheme 5.2: Togo's conditions for the synthesis of oxazolines

The molecular iodine is in the reaction medium as an oxidising agent, in the case of the 2-oxazoline synthesis from the benzylalcohol derivatives the molecular iodine is thought to be involved in the generation of an aldehyde species *in situ*. Starting from benzaldehyde derivatives, with a range of functionality off the aldehyde such as substituted aryl rings, bicyclic derivatives and heteroaromatic derivatives are all

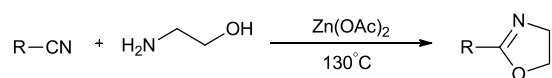
tolerated in the reaction. Eleven examples of 2-substituted 2-oxazolines were synthesised with yields up to 83%. The reaction system starting from the benzylalcohol derivatives also proved to be able to tolerate a range of functionality with eleven examples with yields up to 88%.

The synthesis of 2-oxazolines from nitrile compounds was first reported by Witte and Seeliger in 1974.¹³⁵ The reaction was carried out between the nitrile derivatives with an amino alcohol *via* the utilisation of a Lewis-acid catalyst (Scheme 5.3). The number of commercially available nitrile compounds makes this route for the synthesis of a range of 2-oxazolines *via* this method ideal for the synthesis of a range of 2-oxazoline derivatives.



Scheme 5.3: Seeliger synthesis of Oxazolines from nitriles

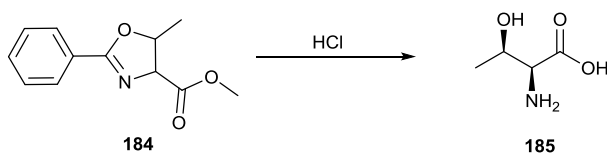
Schubert *et al*,¹⁴⁰ utilised the wide range of work into the synthesis of 2-substituted-2-oxazolines from nitriles using an automated parallel synthesiser to analyse the scope of the reaction. Using zinc acetate as a catalyst in chlorobenzene for the reaction between a range of nitrile derivatives and 2-aminoethanol, a total of eighteen 2-substituted-2-oxazolines were synthesised. A wide range of functionality from allyl to aromatic derivatives with yields for the synthesis of 2-oxazolines from 3-100% (Scheme 5.4).



Scheme 5.4: Schubert synthesis of oxazolines using zinc acetate as a catalyst

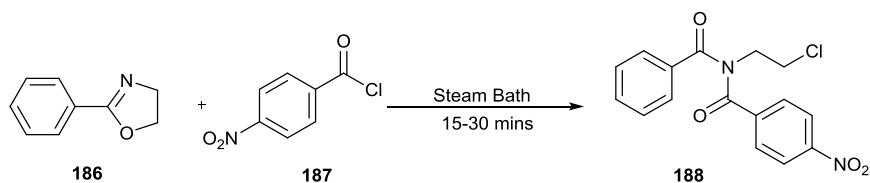
5.2 Ring-opening reactions of 2-oxazolines

The ring-opening of 2-oxazolines has been well documented and found to have a wide range of functions. For example, they have been used in polymerisation reactions as well as in the synthesis of novel amino acid derivatives. Tishler *et al.*,¹⁴¹ utilised this reaction of oxazolines to synthesise DL-threonine from 2-phenyl-5-methyl-4-carbomethoxy-2-oxazoline **184** (Scheme 5.5). This hydrolysis reaction afforded the amino acid **185** in a 70% yield.



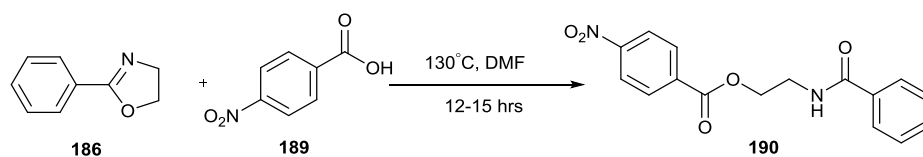
Scheme 5.5: Synthesis of DL-threonine from ring-opening reaction

When 2-phenyl-5-methyl-4-carbomethoxy-2-oxazoline underwent alkaline hydrolysis the DL-threonine was only afforded in a 20% yield. The position where a 2-substituted-2-oxazoline ring opens depends on which reagent is used and under what conditions the reactions are carried out. When 2-phenyl-2-oxazoline **186** is reacted with *p*-nitrobenzoyl chloride **187** it yields the compound *N*-(2-chloroethyl)-*N*-*p*-nitrobenzoyl benzamide **188** (Scheme 5.6).



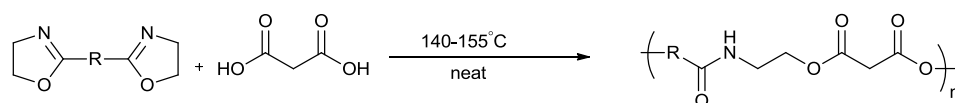
Scheme 5.6: 2-phenyl-2-oxazoline **186** ring-opening with *p*-nitrobenzoyl chloride **187**

However when 2-phenyl-2-oxazoline **186** is reacted with *p*-nitrobenzoic acid **189** at 120°C in DMF, the product 2-benzamidoethyl *p*-nitrobenzoate **190** is isolated (Scheme 5.7).¹⁴²



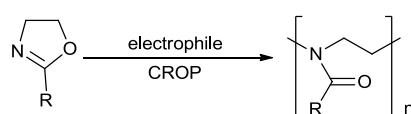
Scheme 5.7: 2-phenyl-2-oxazoline 186 ring-opening with *p*-nitrobenzoic acid 189

One of the main applications of 2-oxazoline ring-opening reactions is in the formation of polymers or as a functional handle on the side chain of polymers. When a bis-oxazoline ring containing compound, that are joined together at the 2-position by allyl, aromatic or hetrocyclic groups reacts with a dicarboxylic acid it is known to form polymers with a long chains that contain alternate ester and amide groups (Scheme 5.8).¹⁴³



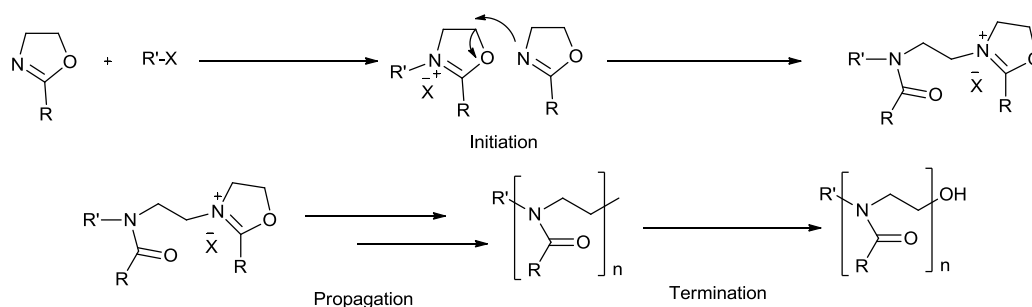
Scheme 5.8: Example of bis-oxazoline ring-opening polymerisation

Oxazolines with an unsubstituted backbone can undergo polymerisation in the presence of a cationic catalyst. Seeliger et al, showed that 2-propyl-2-oxazoline heated to 120-130°C for 15 hours in the presence of *p*-nitrobenzene-diazonium fluoroborate, yields a hard thermoplastic.¹⁴⁴ CROP that uses cationic catalyst or initiators for the ring-opening polymerisation of 2-oxazolines give poly(*N*-acylethylenimine)s. This reaction was first published in 1972, to afford the product poly(*N*-formylethylenimine) (Scheme 5.9).¹⁴⁵



Scheme 5.9: General procedure for CROP polymerisation of oxazolines

The mechanism of CROP is shown in scheme 5.10. An oxazoline is first of all activated using a cationic initiator to form the oxazolinium ion which then reacts with a second oxazoline through a nucleophilic addition from the nitrogen of the second oxazoline (Scheme 5.10).



Scheme 5.10: Mechanistic route for CROP polymerisation of 2-oxazolines

Schubert *et al*, reported the synthesis of polymers with large unsaturated fatty acid side chain, *via* CROP polymerisation of 2-oxazoline synthesised from soy bean fatty acid (Figure 5.2).

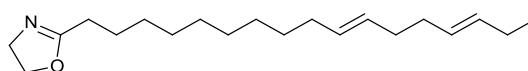
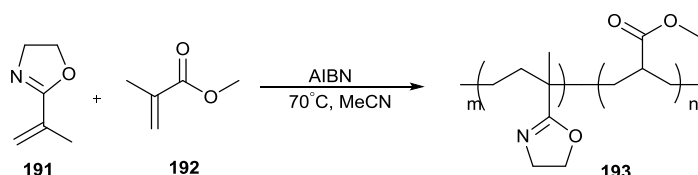


Figure 5.2: 2-Oxazoline monomer for CROP polymerisation, synthesised from soy bean carboxylic acid

The CROP polymerisation was initiated by methyl tosylate under micro-wave assisted conditions. The polymers with fatty acid side chains are sort after for the use in the synthesis of a wide range of applications, such as in the synthesis of rubbers and plastics, coatings and adhesives.

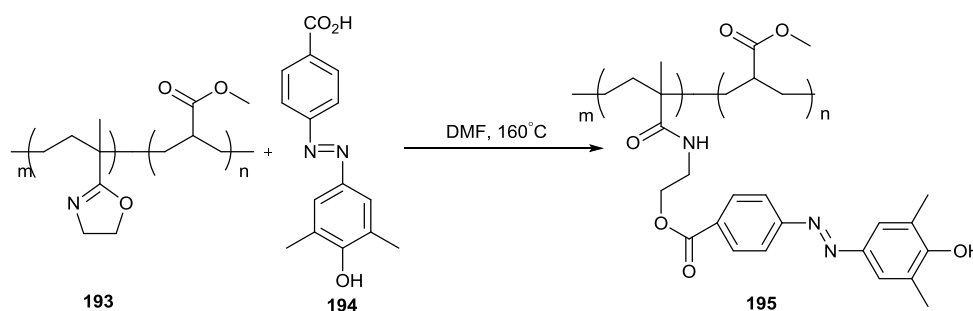
Vuluga *et al*,¹⁴⁶ reported the ring-opening of oxazoline side chains on an oxazoline-methyl methacrylate copolymers. The copolymers were synthesised from 2-

isopropenyl-2-oxazoline **191** with methyl methacrylate **192** in acetonitrile *via* a radical polymerisation using 2,2'-azobis(2-methylpropionitrile) (AIBN, Scheme 5.11).



Scheme 5.11: Block co-polymerisation of 2-isopropenyl-2-oxazoline and methyl methacrylate

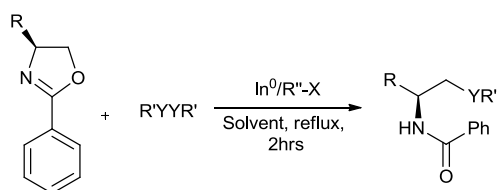
This led to the synthesis of copolymer **193** with alternating oxazoline and ester side chains. The polymer was then reacted with **194** under relatively harsh conditions, in DMF at 160°C the oxazoline is ring opened to yield a side chain containing an amide and ester linking moieties (Scheme 5.12).



Scheme 5.12: Functionalisation of oxazoline side-chain via carboxylic acid ring-opening

The ring-opened polymer products were found to have a decreased thermal stability compared to the oxazoline containing copolymer. The azobenzene containing polymers were analysed by fluorescence spectroscopy. Another application for the ring-opening reaction of 2-oxazolines is in the synthesis of novel amino acids and amide compounds. Vargas *et al*, published work into the synthesis of selenium or sulphur containing chiral β -chalcogen amides from the indium catalysed ring-

opening reaction of 2-oxazolines (Scheme 5.13).¹⁴⁷ Selenium and organoselenium derivatives are of interest as they have been found to possess anti-tumor, antioxidant and antiviral properties.



Scheme 5.13: General scheme for indium catalyzed synthesis of chiral β-chalcogen amide

A reaction optimisation was carried out to analyse the effect of the catalyst loading, temperature, solvent and loading of organoyl halide moiety on the ring-opening reaction. It was found that when the indium source was used in less than one equivalent of the catalyst the reaction either dropped in yield or the product was not obtained at all. With the optimised conditions in hand the scope of the reaction was investigated with a range of 2-oxazolines and organoselenium derivatives. The reaction conditions were found to tolerate a wide range of both derivatives with ten examples, with the yields ranging from 44-98%.

Yoon *et al*, described the synthesis of all four diastereomers of 3-mercaptoaspartic acid *via* both the hydrolytic ring-opening reaction as well as the nucleophilic ring-opening reaction of oxazoline-4,5-dicarboxylate. In the case of the nucleophilic ring-opening thioacetic acid was used as the nucleophile.¹⁴⁸ β-substituted aspartates are of synthetic interest due to numerous derivatives being incorporated in natural and synthetic biologically active compounds. By using both the hydrolytic ring-opening and the nucleophilic ring-opening reactions of oxazolines means that more control on the stereochemistry of the products can be included. When the oxazoline is ring-opened *via* the hydrolytic method using an aqueous acid source there is no change in the configuration at the C-5 position of the oxazoline.¹⁴⁹ However when the nucleophilic ring-opening is carried out there is inversion seen at the C-5 carbon in the product (Figure 5.3).¹⁵⁰

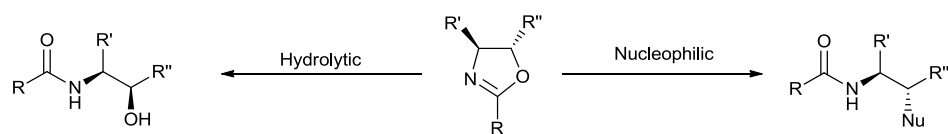
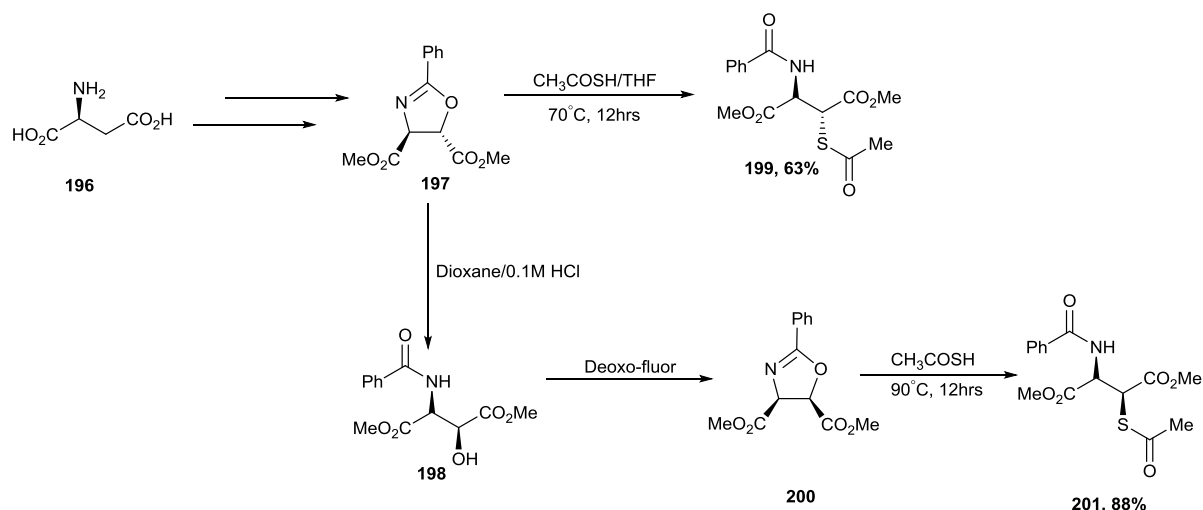


Figure 5.3: Products from the two different ring-opening reactions

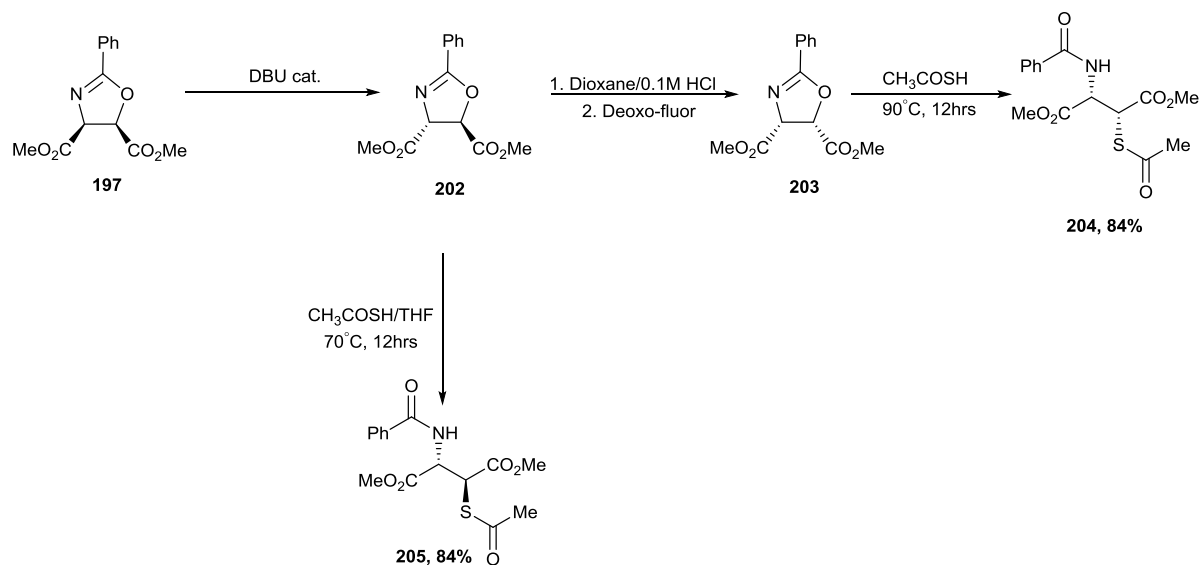
Starting from L-aspartic acid **196** they get through to the key intermediate for the synthesis of the four diastereomers *trans*-(4*S*, 5*S*)-oxazoline-4,5-dicarboxylate **197** as the only product. The oxazoline then undergoes either a nucleophilic ring-opening reaction to afford the first diastereomer *L-erythro*-(2*R*, 3*R*)-3-mercaptoaspartic acid **199** in a 68% yield. **197** can also undergo the hydrolytic ring-opening reaction with a mild acid, the product is then converted to the *cis*-(4*S*, 5*R*)-oxazoline-4,5-dicarboxylate **200**. **200** undergoes nucleophilic ring-opening to afford the second diastereomer *L-threo*-(2*R*,3*S*)-3-mercaptoaspartic acid **201** in an 88% yield (Scheme 5.14).



Scheme 5.14: Synthetic route to the two L-diastereoisomers of 3-mercaptoaspartic acid derivatives

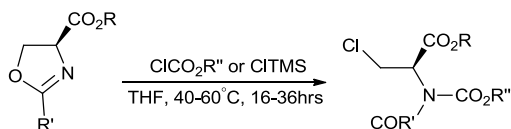
It was shown that the D-configuration could be synthesised *via* the same method as for the preparation of the two L-diastereomers by starting from D-aspartic acid,

however the remaining two diastereomers could also be synthesised *via* further manipulation of **197** *via* a base-induced epimerization of the C-4 position on the oxazoline which yielded the more stable *trans* derivative **202**. **202** could then undergo the same two pathways as the first key intermediate **197** and allow the synthesis of the two D-diastereomers **204** and **205** (Scheme 5.15).



Scheme 5.15: Synthetic route to the D-diastereoisomers of 3-mercaptoaspartic acid derivatives

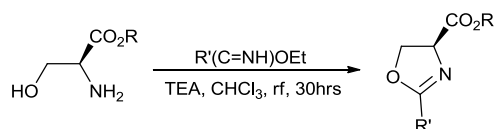
Juge *et al*, reported a new method for the preparation of N,(N)-protected β -halogeno α -aminoesters *via* an electrophilic ring-opening of oxazolines using a chloroformate or a trimethylsilyl halide as the electrophile (Scheme 5.16).¹⁵¹



Scheme 5.16: General reaction conditions for 2-oxazoline ring-opening

The oxazolines were synthesised by a previously published condensation method between amino esters and an iminoether hydrochloride (Scheme 5.17).¹⁵² The scope

of the reaction with chloroformates proved to tolerate a range of different functionality on the chloroformate affording the ring opening product in 48-89% yields over nine examples. With four examples of the electrophilic ring-opening reaction being carried out with various TMS-X derivatives, yields ranging from 30-86%.



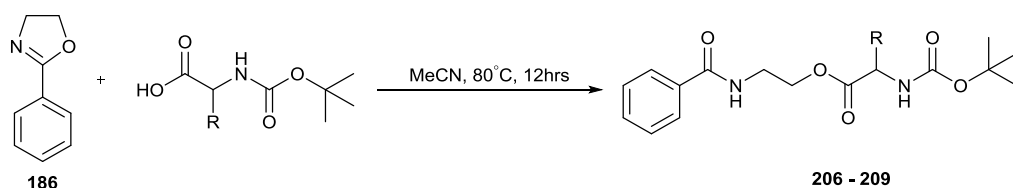
Scheme 5.17: Synthesis of 2-oxazolines from iminoether hydrochloride

5.3 Aims and Objectives

As presented in previous chapters an interest in bioconjugation has been exhibited through the synthesis of redox-active phosphoramidite derivatives and their conjugation to oligonucleotides. The aim of the research presented in this chapter is to utilise the direct conjugation of 2-oxazolines with carboxylic acids in the analytical detection carboxylic acids of interest, such as amino acids and drug compounds. The aim is to synthesise a range of oxazolines that have been derivatised with analytical reporter moieties for the analytical detection of carboxylic acids, such as: electrochemical, fluorescent and fluorine markers.

5.4 Results and Discussion

Phenyloxazoline was chosen as a simple starting material to investigate the scope of the ring opening reaction with *N*-boc amino acids being chosen as the carboxylic acid derivatives. The reactions were carried out in acetonitrile at 80°C and with no further additives (Table 5.1).



Scheme 5.18: General synthetic route to ring-opened products

Table 5.1: Yields from the ring-opening reactions of 2-phenyl-2-oxazoline

Product	Amino acid	Yield
206	Boc-Phe-OH	72
207	Boc-Ala-OH	89
208	Boc-Val-OH	65
209	Boc-Pro-OH	69

As shown in Scheme 5.18 the product formed *via* this ring opening reaction is the ester amide derivative. This is supported by the presence of an additional NH signal in the ^1H NMR spectrum. The yields exhibited for this reaction are good (Table 5.1). The reaction between Boc-valine and phenyloxazoline was used to explore the effect of various reaction parameters. First of all, the amount of Boc-valine was increased to two and three equivalents, to analyse the effect of the amount of carboxylic acid source present had on the yield of the ring-opening reaction (Table 5.2).

Table 5.2: Yields of 208 from ring-opening reactions with various quantities of carboxylic acid

Equivalents of carboxylic acid	Yield (%)
1	65
2	84
3	100

The results presented in Table 5.2 show that there is an increase in the yield as the equivalents of carboxylic acid moiety are increased within the reaction. When the reaction is carried out with three equivalents of Boc-valine the reaction goes to completion. This is a promising result, however if this reaction is going to be suitable for use in a bioconjugation capability the limiting reagent in the reaction would be the target, in this reaction that would be the presence of the carboxylic acid derivative. Therefore the reaction was tested with the number of equivalents of oxazoline present in the reaction mixture being varied while the equivalents of the carboxylic acid derivative, Boc-valine being kept constant. It was found that with increasing the equivalents of the oxazoline moiety had the same effect on the yield of the reaction and at three equivalents the reaction had gone to completion (Table 5.3).

Table 5.3: Ring-opening reactions with various quantities of 2-oxazoline to afford 208

Equivalents of phenyloxazoline	Yield
1	65
2	89
3	100

Taking the two equivalents of oxazoline as the conditions for further optimisation, the next aspect of the reaction to be studied was the effect temperature has on the reaction. As the reaction is currently being carried out at 80°C, close to the boiling point of MeCN. This temperature is also an unfavourable temperature for use in

bioconjugation. Therefore the conversion of the reaction at lower temperatures was investigated (Table 5.4).

Table 5.4: Yields of 208 at different temperature

Temperature (°C)	Yield (%)
Room temp	20
50	40
80	89

As can be seen from the results posted in Table 5.4 the reaction does take place at room temperature, an ideal temperature for conjugation is between room temperature and 40°C as this is the optimum temperature range for the biological component. However the reaction progressed at a slow rate, with only 20% conversion after 96 hours. The conversion of the reaction at 50°C was moderate so optimisation was continued. The effects of solvent on the reaction was next investigated using the conditions of two equivalents of phenyloxazoline at 50°C. These conditions were chosen as the conversion at this temperature in MeCN is at 40% and therefore any effect on the reaction from solvents will be easy to monitor. A range of non-polar and polar solvents, both protic and aprotic solvents were chosen (Table 5.5).

Table 5.5: Results from the solvent screen

Solvent	Yield (%)
Water	12
Toluene	26
Acetonitrile	40
Iso-butyl alcohol	39
Propionitrile	39
2-methyl THF	18
Acetonitrile/Water (1:1)	99 ^a

^a=reaction carried out at 80°C

As can be seen from the results in the Table 5.5 polar aprotic solvents were shown to give the best results, however with MeCN still giving the highest yield at 40%. From this result it was decided that MeCN would still be used as the solvent of choice for the examination of the effect of additives in the reaction medium. A range of Lewis acid and nucleophilic catalysts, at a 5 mol% loading were tested in the reaction to see if the addition of a catalyst would increase the yield of the reaction (Table 5.6).

Table 5.6: Yields from 5 mol% loading

Additive (5 mol%)	Yield (%)
Phenylboronic acid	45
Boric acid	41
DMAP	40
InCl ₃	45

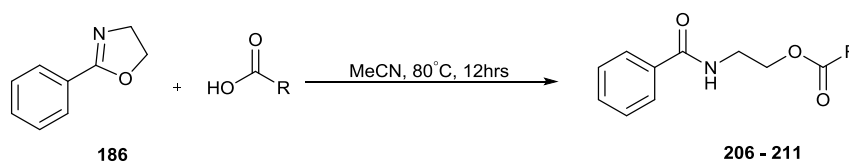
The addition of a Lewis acid or nucleophilic catalyst failed to give an increase in yield compared to the reaction carried out with no additive at a 5 mol% loading, the reactions were repeated at a 20 mol% loading to check it was not the loading being too low to have an effect in this case (Table 5.7).

Table 5.7: Yields from 20 mol% loading

Additive (20 mol%)	Yield (%)
Boric acid	42
DMAP	46
InCl ₃	47
ZnCl ₃	42

With the loading being at 20 mol% there is still only a minimal effect on the overall yield of the reaction, which could be in the range of experimental error. Therefore it was decided to take through the conditions of the oxazoline being at two equivalents and at 80°C in MeCN without the use of any additives.

The scope of the reaction was then tested under the optimised conditions with a range of carboxylic acid derivatives (Scheme 5.19, Table 5.8). The ring-opening reaction of phenyl-oxazoline was found to tolerate a wide range of functionalised carboxylic acid derivatives in good yield.

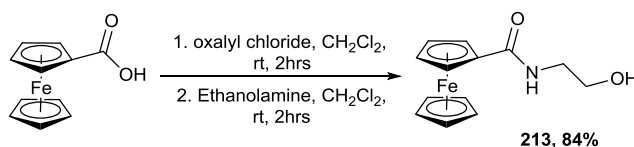


Scheme 5.19: Synthetic route to ring-open products 206-211

Table 5.8: Scope of the ring-opening reaction with 2-phenyl-2-oxazoline

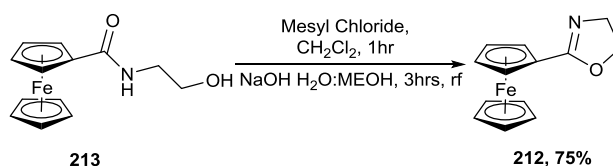
No.	Carboxylic acid	Yield (%)
206	Boc-phenylalanine	92
207	Boc-alanine	93
208	Boc-valine	89
209	Boc-proline	74
210	Sarcosine	95
211	3-bromopropionic acid	92

Next, a range of oxazolines were synthesised with different transducer elements such as fluorescent or electrochemical groups. Ferrocene-2-oxazoline **212** was the first target, which could be achieved by reacting ferrocenecarboxylic acid with ethanolamine *via* the in situ generation of the acid chloride with oxalyl chloride to yield the amide **213** (Scheme 5.20).



Scheme 5.20: Synthesis of N-(2-hydroxyethyl)ferrocenecarboxamide 211

The free hydroxyl group is then mesylated and under basic conditions the ring cyclisation occurs to install the oxazoline ring on the ferrocene moiety (Scheme 5.21).



Scheme 5.21: Synthesis of ferrocene-2-oxazoline

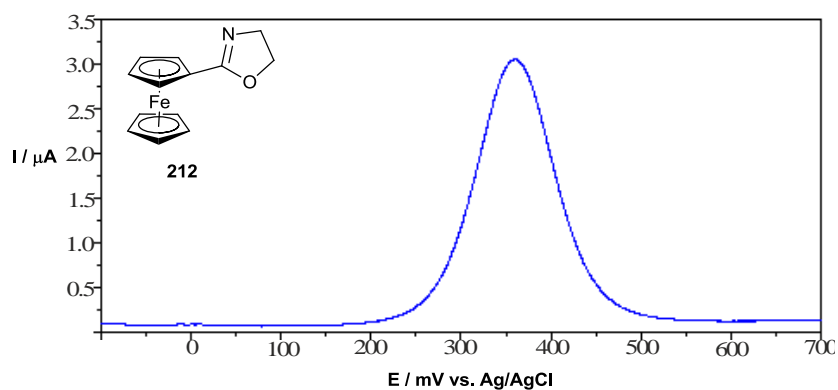
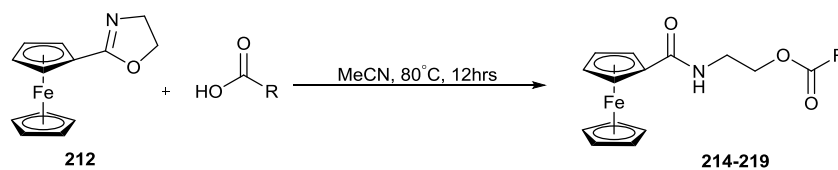


Figure 5.4: Voltammogram of the DPV scan of 212

212 was analysed *via* differential pulse voltammetry under the standard conditions shown in the experimental section, to analyse its oxidation potential. **212** was found to have an oxidation potential of 360 mV vs. Ag/AgCl (Figure 5.4, under the same conditions as used in the DNA label work). The scope of the reaction using ferroceneoxazoline was examined under the standard conditions with a range of carboxylic acid derivatives (Scheme 5.22, Table 5.9).



Scheme 5.22: Synthetic route to ring-open products 214-219

Table 5.9: Scope of ferrocene-2-oxazoline ring-opening reaction

No.	Carboxylic acid	Yield (%)
214	Boc-valine	76
215	Boc-phenylalanine	79
216	Boc-alanine	76
217	3,5-bis(trifluoromethyl)benzoic acid	88
218	Sarcosine	82
219	3-bromopropionic acid	93

It was found that the oxazoline ring opening reaction worked to a good to high yield with a range of carboxylic acids including amino acids, aromatic and simple alkyl carboxylic acids. To analyse the viability of the use of **212** in this reaction as a possible electrochemical analytical reporter for the use in the detection of carboxylic acids the oxidation potential of the boc-valine derivative was analysed to calculate the oxidation potential of compound **214**, which was found to be 430 mV vs. Ag/AgCl (Figure 5.5).

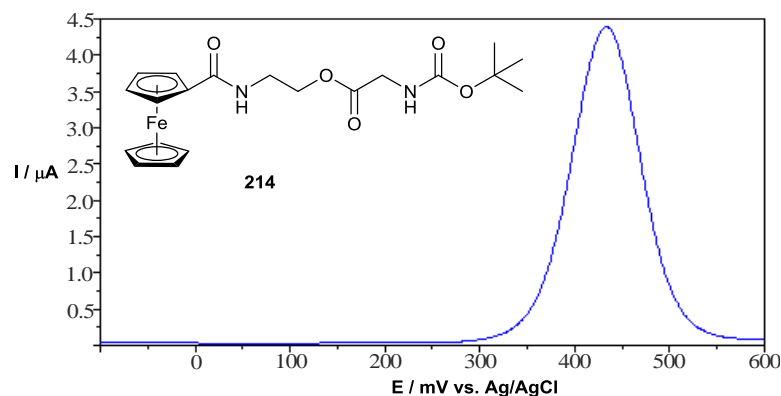


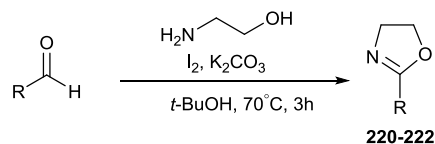
Figure 5.5: Voltammogram of the DPV scan of 214

For this system to be viable for the use in analytical detection of carboxylic acid derivatives there must be a distinguishable difference between the ferroceneoxazoline **212** and the ring opened product **214**. As can be seen from Table 5.11 there is an approximate shift of 70 mV between the ring opened product and the parent oxazoline derivative.

Table 5.11: Oxidation potential of ferrocene-2-oxazoline and the ring-opened product

No.	Oxidation potential (mV vs. Ag/AgCl)
212	360
214	430

Work carried out by Togo *et al.*,¹³⁹ into the synthesis of 2-oxazoline derivatives starting from aldehydes and aminoethanol, was utilised to synthesise a range of oxazolines starting from the parent aldehydes. Anthracenecarboxaldehyde and naphthalenecarboxaldehyde were used to prepare two fluorescent oxazolines for the use as potential fluorescent detection method. *p*-Bromophenyl-2-oxazoline was also synthesised as it can be further functionalised (Scheme 5.23, Table 5.12).

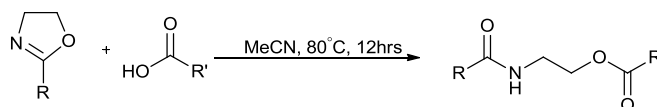


Scheme 2.23: Synthesis of 2-oxazolines from aldehydes

Table 5.12: 2-oxazolines synthesised from aromatic aldehydes

Aldehyde	Yield (%)
<i>p</i> -bromobenzaldehyde	74
1-naphthalenecarboxaldehyde	54
9-anthracenecarboxaldehyde	65

These oxazoline derivatives went through the ring opening reaction under the standard conditions and were found to all ring open with good yields (Scheme 5.24, Table 5.13).



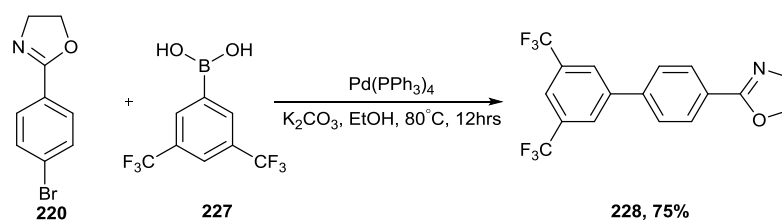
Scheme 5.24: Route to ring-opened products

Table 5.13: Yields from ring-opening reactions

R	R'	Product	Yield (%)
	Boc-valine	223	79
	Boc-valine	224	73
	Boc-phenylalanine	225	78
	Boc-valine	226	70

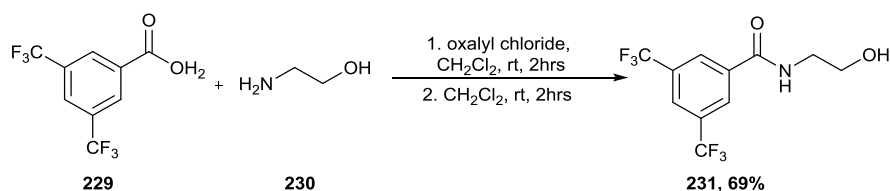
The *p*-bromophenyloxazoline can be used in further reactions to install functionality onto the aromatic ring, such as transition metal catalyst cross coupling reactions. One

method for functionalising the oxazoline is *via* a Suzuki cross-coupling reaction with a boronic acid. The *p*-bromophenyl oxazoline was taken through a Suzuki cross-coupling with a boronic acid with the functionality for the use as an analytical reporter moiety, in this case 3,5-bis(trifluoromethyl)phenylboronic acid was chosen for the use of the ^{19}F NMR as the analytical detection technique (Scheme 5.25).



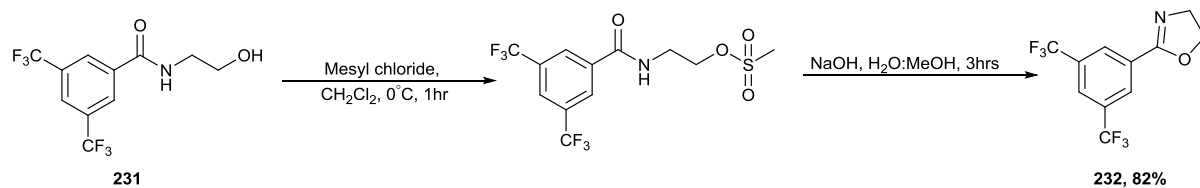
Scheme 5.25: Functionalisation of *p*-bromophenyl oxazoline *via* suzuki cross-coupling reaction

3,5-Bis(trifluoromethyl)benzoic acid was chosen as a possible starting material for the synthesis of an oxazoline derivative with the fluorine functionality in closer proximity to the oxazoline ring. Starting from 3,5-bis(trifluoromethyl)benzoic acid the amide derivative was synthesised using ethanolamine, *via* the generation of the acid chloride in situ using oxalyl chloride (Scheme 5.26).



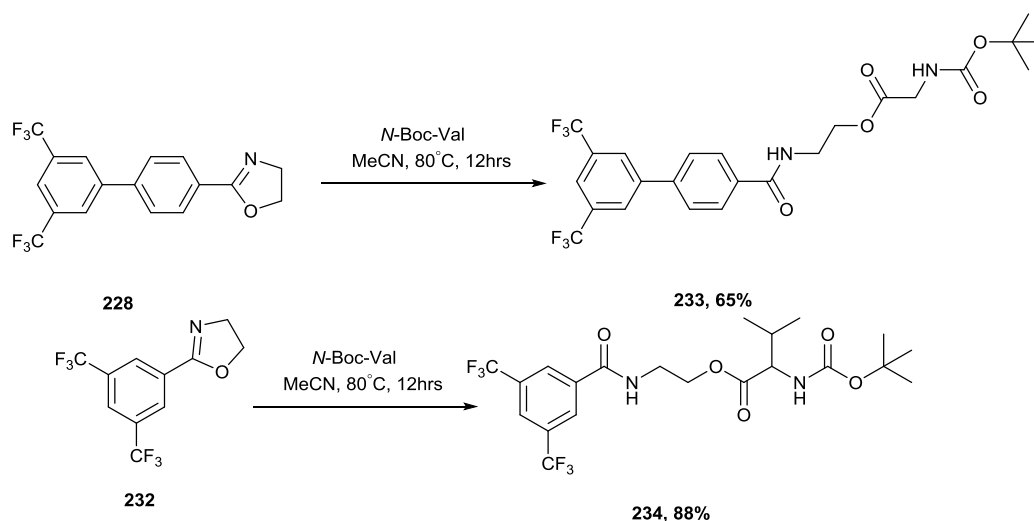
Scheme 5.26: Synthesis of N-(2-hydroxyethyl)-3,5-bis(trifluoromethyl)benzamide

231 was then converted to the oxazoline *via* the generation of the mesylate of the free hydroxyl group using methane sulfonyl chloride, which was then cyclised under basic conditions using sodium hydroxide by heating under reflux conditions (Scheme 5.27).



Scheme 5.27: Synthesis of 2-(3,5-bis(trifluoromethyl)phenyl)-2-oxazoline

232 was then taken through the optimised ring-opening reaction (Scheme 5.28), it afforded the **234** in a good yields. In comparison to **232**, **228** was also taken through the ring-opening reaction and afforded **233** in a good yield.



Scheme 5.28: Ring-opening of 228 and 232

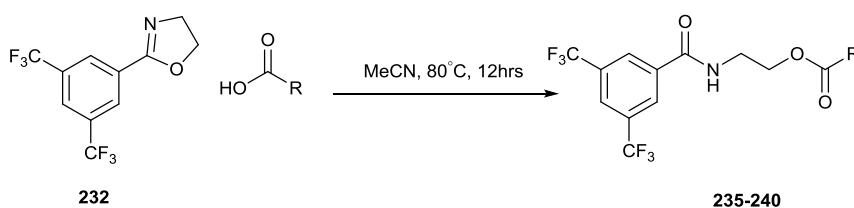
These two functionalised oxazolines were compared to assess which one would be suitable for use as an analytical reporter moiety for the analytical detection of carboxylic acids, for them to be suitable there would have to be a shift exhibited in the fluorine NMR spectra from the oxazoline to the ring-opened amide product (Table 5.14).

Table 5.14: Fluorine NMR signals for oxazoline and their ring-opened counterpart

Oxazoline	Ring-opened	Δ ^{19}F
228	233	0.1
-62.71	-62.80	
232	234	1.3
-61.94	-63.24	

Table 5.14 shows that there is not a shift in the fluorine NMR for the ring-opening of **228**, however there is a shift of approximately 1.3 ppm between **232** and **234**. Therefore **232** would be a valid analytical reporter for the detection of carboxylic acids.

The 3,5-bis(trifluoromethyl)phenyl oxazoline was taken through the ring opening reaction with a range of carboxylic acid derivatives (Scheme 5.29, Table 5.15), carboxylic acid derivatives ranging from amino acids, alkyl derivatives and aromatic carboxylic acids.



Scheme 5.29: Ring-opening of **232**

Table 5.15: Scope of 2-(3,5-bis(trifluoromethyl)phenyl)-2-oxazoline ring-opening reaction

No.	R	Yield (%)
235	Boc-valine	88
236	Boc-phenylalanine	91
237	Sarcosine	89
238	3-bromopropionic acid	79
239	<i>p</i> -bromobenzoic acid	83
240	Boc-alanine	86

As the table shows the ring opening reaction with the oxazoline derivative proceeded in very good yields across the scope of carboxylic acid derivatives used.

A number of drugs contain carboxylic acid functionality, the carboxylic acid groups in drugs are involved in specific charge-charge interaction and are often critical for the binding to the targets. Using the optimised conditions for the ring-opening reaction of oxazoline derivatives, the capability of the reaction to work under slightly more challenging conditions to detect the presence of the carboxylic acid derivative was investigated. Ibuprofen was chosen as the target due to its wide spread use and availability as an over the counter pain-relief medication (Figure 5.6).

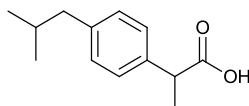
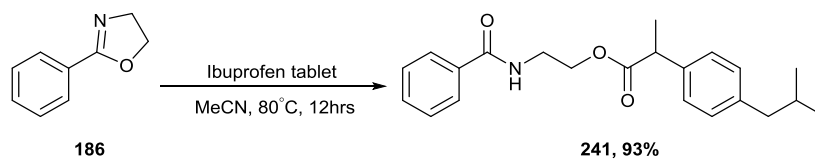


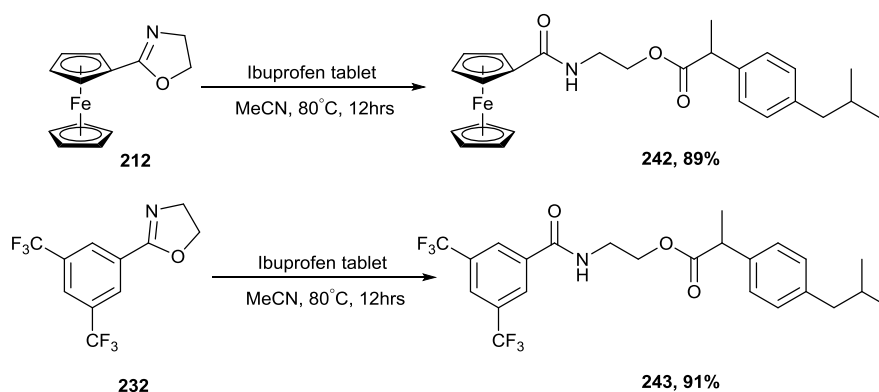
Figure 5.6: Ibuprofen

The reaction was carried out using ibuprofen tablets purchased over the counter from a supermarket. The tablets were then ground up and it was in this form that the ibuprofen tablet was used in the reaction. The direct formation of amides from carboxylic acid moieties of drugs in solution could be used to aid the analytical detection of drugs such as ibuprofen *via* techniques such as mass spectroscopy and other analytical methods (Scheme 5.30).



Scheme 5.30: 2-phenyl-2-oxazoline ring-opening reaction with Ibuprofen

The reaction proved to be highly efficient and high yielding. Interestingly, there was little interference in the reaction from any of the other compounds that make up the ibuprofen tablet such as sugars. The lack of interference on the reaction from the other components of the ibuprofen tablet, it is an important result in the analysis of this reaction as a conjugation tool of carboxylic acids for analytical detection. Functionalised 2-oxazolines were then used in the reaction, the ferroceneoxazoline and the 3,5-bis(trifluoromethyl)phenyloxazoline were chosen as two possible analytical reporters for this reaction (Scheme 5.31).



Scheme 5.31: Ring-opening reaction with Ibuprofen and sensing 2-oxazolines

Both the functionalised 2-oxazolines work to a good yield in the ring-opening conjugation reaction with ibuprofen. **212** allows the use of electrochemical detection methods in the analytical detection of ibuprofen. As stated previously the oxidation potential of **212** is 360 mV vs. Ag/AgCl, therefore using the shift in oxidation potential from the oxazoline **212** to the ring-opened form **242** allows for the analytical detection of the presence of ibuprofen in the solution. **242** was analysed *via* DPV and found to have an oxidation potential of 429 mV vs. Ag/AgCl (Figure 5.7).

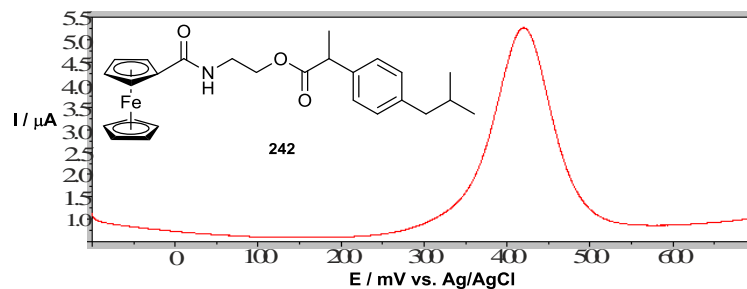


Figure: 5.3: DVP voltammogram of 242

The same principle would apply for **232** as an analytical reporter for the detection of carboxylic acids *via* ^{19}F NMR or mass spec.

5.5 Conclusion

This chapter has shown the synthesis of a range of 2-oxazolines with various functionality aimed towards conjugation with the goal of analytical detection of carboxylic acids, such as electrochemical, fluorescent and a fluoride marker. The ring-opening reaction was found to tolerate a wide range of carboxylic acid derivatives. The electrochemical analytical detection capability was analysed through the difference in the oxidation potential between ferrocene-2-oxazoline and the ring-opened form, which was found to have a 70 mV shift in oxidation potential. This reaction was analysed under more challenging conditions for the detection of ibuprofen from a tablet that contains a number of other compounds.

6 Future Work

The future work related to this project will be to further investigate the effects of substituting the ferrocene core of the redox-active labels with a wider range of functional groups as well as the use of different elements present in the functional groups such as sulfur and phosphorus. This will lead to the expansion of the range of labels that are currently available for the DNA detection assay as well as looking to increase the range of oxidation potentials available. This will allow for the development of a DNA detection assay capable of involving a larger number of labels than the triplex assay that was shown to be viable through the work carried out within this thesis. The ability to develop a DNA detection assay with a larger number of probes opens up the ability of the point of care device being developed by Atlas genetics to detect for a wider range of bacterial pathogens through one DNA detection assay.

However, in the immediate future the development of the mono-ferrocenyl labels currently being used in the triplex assay discussed in chapter 4, **127** and **135**, into di-ferrocenyl labels to match the third label **98** being used in the triplex assay. The importance of developing the current mono-ferrocenyl labels into di-ferrocenyl labels is to overcome the sensitivity issues that have been shown throughout the work presented in this thesis. This would lead to a triplex assay with a greater sensitivity than the current triplex being carried out in the DNA detection assay.

The future of DNA sensing could be seen to be developing into two different pathways; the first being the detection of infectious diseases and the second being in the sequencing for the detection of mutations as well as inherited genetic diseases such as Huntington's disease through technologies such as nanopores. The first pathway could be said to be caused by the rise in the requirement for the rapid, accurate and highly sensitive detection of infectious diseases such as sexually transmitted diseases. The rise has been driven by the attempt to cut down patient waiting times between being tested and receiving the results for the test with the aim

to increase the rapid treating and therefore reduce the infection rate of the disease. This is needed in both the developed and the developing world, which could see a rise in the development of smaller self-contained point of care devices for use at the patient interface. For example, the point of care device being developed by Atlas genetics which is currently designed to be used in GP's offices could be transformed to a robust handheld device to be used in the developing world for rapid and accurate diagnosis.

7 Experimental

7.1 General Considerations

Commercially available solvent and reagents were obtained from Sigma-Aldrich and Fisher Scientific Ltd and were used without any further purification. Deoxygenation of solvents and reagents when necessary were carried out by purging with nitrogen. The term Petrol refers to the fraction of petroleum ether that boils in the range of 40-60°C. Reactions carried out using anhydrous conditions used HPLC – grade solvent that was passed through an Innovative Technology Pure – Solv Solvent purification system (SPS).

Thin layer chromatography (TLC) was performed using commercially available aluminium backed plates coated with Merck kieselgel 60 0.20mm (ALUGRAM® sl G/UV₂₅₄) and visualised under UV or by staining. Melting points were calculated using a Büchi 535 melting point apparatus and are uncorrected. Mass spectra were obtained using the mass spectrometry service at the University of Bath, on a Bruker MicroTOF machine. Voltgrams were run on μ AUTOLAB, type II using GPES manager.

Chemical shifts (δ) are expressed in parts per million (ppm) and referenced to the internal SiMe₄ for ¹H-NMR and referenced to the relative solvent for ¹³C-NMR. NMR spectra were recorded on Bruker AV 250, AV 300, AV 400 or AV 500 spectrometers at 298K unless otherwise stated. Multiplicities of spectroscopic data are presented in the following manner: singlet (s), broad singlet (br.s), doublet (d), doublet of doublets (dd), triplet (t), quartet (q) and multiplet (m). The coupling constants (*J*) are expressed in Hertz.

7.2 General electrochemical procedure

Preparation of buffer solution

The buffer solution used for the electrochemical analysis of the ferrocene derivatives synthesised in this thesis was the same buffer solution as was used for the Atlas DNA detection assay, which is the Atlas 10x PCR buffer solution developed by Atlas genetics.

Preparation:

Tris(hydroxymethyl)aminomethane base (3.70 g) was dissolved in deionised water (500 mL) and Tris(hydroxymethyl)aminomethane HCl (3.07 g) was added and once dissolved the pH was checked to be 8.3. Potassium chloride (18.38 g) was then added and the solution was stirred until fully dissolved the final pH was checked to be 8.55.

Standard solutions and dilutions

General electrochemical solution:

Ferrocene (free alcohol) derivatives (5 mg) are dissolved in DMSO (1 mL), of which 25 μ L is diluted with Atlas 10x PCR buffer (600 μ L).

General electrochemical procedure and conditions:

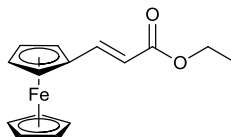
General electrochemical solution (10-20 μ L) was applied to a screen printed electrode and a scan is taken. Procedure repeated three times on separate electrodes.

Table 6.1: Conditions used for the DPV electrochemical analysis of ferrocene compounds

Differential Pulse Conditions	Measurement	Potential
Purge time (s): 0 Conditioning Potential (V): 0 Duration (s): 0 Deposition potential (V): 0 Duration (s): 0 Equilibration time (s): 0	Modulation time (s): 0.05 Interval time (s): 0.1	Initial potential (V): -0.1 End potential (V): 0.7 Step potential (V): 0.003 Modulation amplitude (V): 0.04995 Standby potential (V): 0.05

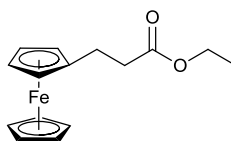
7.3 Synthesis of mono-ferrocenyl redox active labels

Ethyl-3-ferrocenyl acrylate **101**



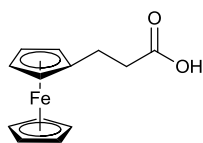
Triethylphosphonoacetate (0.86 mL, 4.22 mmol) was dissolved in dry THF (25 mL), to this solution *n*-butyl lithium (1.6M in THF, 1.69 mL, 4.22 mmol) was added dropwise *via* a pressure equalising dropping funnel and the reaction mixture was stirred at 0°C under nitrogen for two minutes. The reaction is then warmed up to room temperature and stirred for 30 mins. Ferrocenecarboxaldehyde (0.78 g, 3.52 mmol) in dry THF (10 mL) was added *via* a dropping funnel to the solution. The reaction was then stirred for another 15mins. The solvent was then removed *in vacuo*. The residue was taken up in diethyl ether (30 mL) and water (30 mL). The organic layer was separated and the aqueous fraction was then extracted with diethyl ether (30 mL). The organic fractions were combined dried over MgSO₄, the solvent was removed and the crude product was purified *via* column chromatography (9:1, hexanes:ethyl acetate) to yield the product as a waxy red solid (1.4 g, 75%). ¹H NMR (300 MHz; CDCl₃) δ 7.49 (1H, d, *J* = 15.5, CH), 6.31 (1H, d, *J* = 15.5, CH), 4.21 (2H, q, *J* = 6.25, CH₂) 4.13 (2H, s, FcH) 4.02 (7H, s, FcH) 1.38 (3H, t, *J* = 5.0, CH₃) ¹³C NMR (75.5 MHz; CDCl₃) δ 167.2, 145.6, 114.9, 77.5, 77.0, 76.6, 70.9, 69.8, 60.4, 21.0, 14.4. Data in accordance with literature.¹⁵³

Ethyl-3-ferrocenyl propanoate **102**



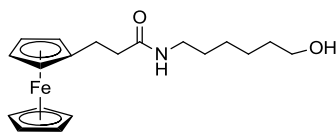
Ethyl-3-ferrocenyl acrylate (0.5 g, 1.76 mmol) was dissolved in absolute ethanol (20 mL) and 10% of palladium on activated carbon (0.19 g, 0.18 mmol) was added to the solution. Hydrogen gas is bubbled through the solution for 5 minutes, then the reaction is left to stir under a hydrogen (1 atm) for 2.5hrs. The reaction is then filtered through Celite 521. The solvent was then removed *in vacuo* to yield the product as an orange amorphous solid (0.49 g, 99%). **MP**; 30-31 °C. **¹H NMR** (300 MHz; CDCl₃) δ 4.20 (2H, q, *J* = 7.0, CH₂) 4.09 (2H, s, FcH) 4.02 (7H, s, FcH) 2.93-2.87 (2H, m, CH₂) 2.54-2.49 (2H, m, CH₂) 1.37 (3H, t, *J* = 7.0, CH₃). **¹³C NMR** (75.5 MHz, CDCl₃) δ 170.2, 77.5, 77.0, 76.6, 69.8, 61.3, 34.8, 23.2, 15.3. Data in accordance with literature.¹⁵⁴

3-ferrocenylpropanoic acid **103**



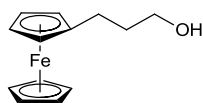
Ethyl-3-ferrocenyl propanoate (0.2 g, 0.69 mmol) was dissolved in ethanol (25 mL) and sodium hydroxide (0.16 g, 4.0 mmol). The solution was then heated to 50 °C and stirred for 18 hours. Acetic acid was then added until the solution reached a pH of 6.5. The product was extracted in CH₂Cl₂ (2 × 25 mL). The organic fraction was washed with brine (3 × 20 mL) and water (3 × 20 mL). The organic layer was dried over MgSO₄ and the solvent evaporated to afford the crude product, which was purified *via* column chromatography (7:3, hexanes : ethyl acetate) to yield the product as a dark yellow solid (1.36 g, 65%). **¹H NMR** (300 MHz; CDCl₃) δ 4.09 (2H, s, FcH) 4.02 (7H, s, FcH) 2.70 (2H, s, CH₂) 2.51 (2H, s, CH₂). **¹³C NMR** (75.5 MHz; CDCl₃) δ 170.2, 77.5, 77.0, 76.6, 70.9, 69.8, 24.1, **HRMS** (ESI) calcd for C₁₃H₁₄O₂Fe₁ *m/z* 258.0265 found C₁₃H₁₄O₂Fe₁Na₁ *m/z* 281.0254 Data in accordance with literature.¹⁵⁵

3-ferrocenyl-N-(6-hydroxyhexyl)propanamide **99**



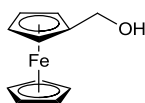
Oxalyl chloride (0.87 mL, 10.36 mmol) in dry CH_2Cl_2 (2 mL) was added dropwise *via* a pressure equalising dropping funnel to a stirred solution of 3-ferrocenylpropanoic acid (1.2 g, 4.78 mmol) in dry CH_2Cl_2 (100 mL) at 0 °C under N_2 . The reaction was warmed to room temperature and stirred for 2 hrs. Then the solvent was removed *en vacuo* and the acid chloride product was taken up in dry CH_2Cl_2 (75 mL) and cooled to 0 °C. 6 – amino hexan – 1 – ol (0.56 g, 4.78 mmol) in dry CH_2Cl_2 (75 mL) was added dropwise *via* a dropping funnel under N_2 . The reaction was then stirred for 2 hrs while warming to room temperature. The solution was then washed with NaHCO_3 (sat.) (100 mL) and 1M HCl (aq.) (100 mL). The organic fractions were dried over MgSO_4 and the solvent was removed to yield the crude product, which was purified *via* column chromatography (7:3, hexanes : ethyl acetate) to yield the product as a yellow solid (1.68 g, 80%). **IR** (cm^{-1}): 3259, 3101, 2972, 2934, 2204, 2049, 1729, 1654, 1576, 1425 **^1H NMR** (300 MHz; CDCl_3) δ 4.12 (2H, s, FcH), 4.09 (7H, s, FcH), 3.60 (1H, s, OH), 3.52 (2H, t, $J = 4.0$, CH_2), 3.00 (2H, s, CH_2), 2.85 (2H, s, CH_2), 2.30 (2H, s, CH_2), 1.56–1.25 (8H, m, CH_2). **^{13}C NMR** (75.5 MHz; CDCl_3) δ 173.3, 77.8, 77.4, 76.9, 62.0, 38.85, 35.4, 32.0, 30.6, 26.7, 26.3, 25.4, 25.4. **HRMS** (ESI) calcd for $\text{C}_{19}\text{H}_{27}\text{N}_1\text{O}_2\text{Fe}_1$ m/z : 357.1321 found $\text{C}_{19}\text{H}_{28}\text{N}_1\text{O}_2\text{Fe}_1$: 358.1213.

3-ferrocenylpropan-1-ol **104**



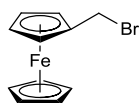
Lithium aluminium hydride (0.15 g, 0.15 mL, 3.87 mmol) was dissolved in ether (40 mL) in a two necked round bottomed flask. 3-ferrocenylpropanoic acid (0.5 g, 1.94 mmol) in ether (10 mL) was added dropwise and the solution was stirred at 0°C for 10mins. The solution was then refluxed for 2 hours, the reaction mixture was then quenched with water (10 mL) then NaOH 20% solution (15 mL). Water (12 mL) was then added and the ether layer was decanted and the solvent was removed to afford the product as an orange oil (0.44 g, 88%). **¹H NMR** (300 MHz; CDCl₃) δ 4.19 (9H, s, FcH), 4.65 (2H, t, *J* = 6.0, CH₂), 2.55 (2H, d, *J* = 5.0, CH₂), 1.70 (2H, t, *J* = 5.5, CH₂). **¹³C NMR** (75.5 MHz; CDCl₃) δ 77.8, 77.6, 77.4, 76.9, 63.4, 38.5, 29.4. **HRMS** (ESI) calcd for C₁₃H₁₆O₁Fe₁ *m/z* 244.0435 found 244.0434 Data in accordance with literature.¹⁵⁶

Ferrocenylmethanol **138**



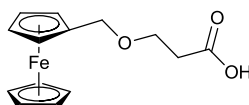
A solution of ferrocenecarboxaldehyde (0.5 g, 2.31 mmol) in EtOH : dioxane (50 mL, 4:1) was added NaBH₄ (0.25 g, 6.76 mmol) in a round bottomed flask. The solution was stirred for 1 hour. Water was then added and the product extracted with ether (30 mL). The organics were washed with water (2 × 25 mL) and the organic layer was dried over MgSO₄. The solvent was removed *in vacuo* to afford the product as a yellow solid without any further purification (0.5 g, 99%). **¹H NMR** (300 MHz; CDCl₃) δ 4.34 (2H, s, CH₂), 4.28 (2H, s, FcH), 4.13 (7H, s, FcH), 3.60 (1H, s, OH). **¹³C NMR** (75.5 MHz; CDCl₃) δ 77.8, 77.4, 76.9, 69.7, 68.7. Data in accordance with literature.¹⁵⁷

(Bromomethyl)ferrocene **168**



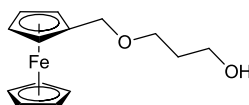
Ferrocene methanol (0.4 g, 1.85 mmol) was dissolved in ether (30 mL) and cooled to 0°C in an ice bath, phosphorous tribromide (0.74 g, 0.3 mL, 2.77 mmol) was then added dropwise to the reaction mixture once addition was complete the solution was allowed to warm up to room temperature and stirred for 14 hrs. The reaction mixture was then re-cooled to 0°C in an ice bath and the reaction was quenched with water (20 mL). The product was then extracted into ether (20 mL) and dried over MgSO₄ and the solvent evaporated to afford the product as a dark red oil (0.39 g, 99%). **IR** (cm⁻¹): 3009, 2204, 2049, 1729, 1634, 1576, 1435 **¹H NMR** (300 MHz; CDCl₃) δ 4.59 (2H, s, CH₂), 4.34 (2H, s, FcH), 4.28 (2H, s, FcH), 4.13 (5H, s, FcH). **¹³C NMR** (75.5 MHz; CDCl₃) δ 77.8, 77.4, 76.9, 69.7, 40.3. **HRMS** (ESI) calcd for C₁₁H₁₁O₁Fe₁Br₁ *m/z* 277.9315 found 277.9317.

3-(Ferrocenylmethoxy)propanoic acid **139**



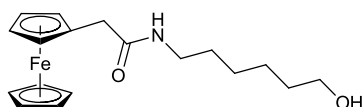
Sodium hydride (0.11 g, 4.62 mmol) was added to a solution of ferrocene methanol (0.5 g, 2.31 mmol) in THF (20 mL) and allowed to stir for 2hrs in an ice bath. To this suspension was added 3-bromopropanoic acid (0.4 g, 2.31 mmol), the reaction was stirred at room temperature for 2 hrs. Water (20 mL) was then added and the product was extracted with ether (20 mL). The organic fraction was dried over MgSO_4 and the solvent was removed to yield the crude product as a yellow solid. The product was purified *via* column chromatography (6:4, hexanes : ethyl acetate) to afford the title compound as a yellow oil (0.4 g, 50%). **IR** (cm^{-1}): 3101, 2972, 2934, 2204, 2049, 1729, 1634, 1566, 1435. **^1H NMR** (300 MHz; CDCl_3) δ 4.86 (2H, s, CH_2) 4.82 (2H, s, FcH), 4.57 (2H, s, FcH), 4.28 (5H, s, FcH), 3.76 (2H, t, $J = 6.5$, CH_2), 3.33 (2H, t, $J = 6.5$, CH_2). **^{13}C NMR** (75.5 MHz; CDCl_3) δ 173.6, 77.6, 77.1, 76.8 69.9, 69.2, 63.3, 35.0. **HRMS** (ESI) calcd for $\text{C}_{14}\text{H}_{16}\text{O}_3\text{Fe}_1$ m/z 288.0449 found 288.0449.

3-(ferrocenylmethoxy)propan-1-ol **140**



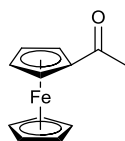
Lithium aluminium hydride (0.5 g, 1.38 mmol) was dissolved in dry ether (20 mL) in a two necked round bottomed flask. 3-(ferrocenylmethoxy)propanoic acid (0.2 g, 0.69 mmol) in ether (5 mL) was added dropwise and the solution was stirred at 0 °C for 30 mins. The solution was then refluxed for 2 hrs. The solution was then quenched by the addition of water (5 mL) then NaOH (aq.) (10 mL). Water (12 mL) was then added and the ether layer was separated and the solvent was removed. The product was purified *via* column chromatography (8:2, hexanes : ethyl acetate) and the product was afforded as a yellow oil (0.12 g, 59%). **IR** (cm⁻¹): 3254, 3101, 2204, 2049, 17001, 1622, 1476. **¹H NMR** (300 MHz; CDCl₃) δ 4.82 (2H, s, FcH), 4.57 (2H, s, FcH), 4.28 (5H, s, FcH), 3.66 (2H, t, *J* = 6.75Hz, CH₂), 3.45 (2H, t, *J* = 6.5Hz, CH₂), 3.32 (2H, t, *J* = 6.5, CH₂) 1.75 (2H, t, *J* = 6.75, CH₂). **¹³C NMR** (75.5 MHz, CDCl₃) δ 72.6, 70.1, 69.9, 69.2, 67.2, 66.1, 58.2, 32.4. **HRMS** (ESI) calcd for C₁₄H₁₈O₂Fe₁ *m/z* 274.0578 found 274.0579.

2-ferrocenyl-*N*-(6-hydroxyhexyl)acetamide **147**



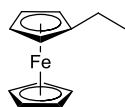
Ferroceneacetic acid (0.5 g, 4.35 mmol) was dissolved in dry CH_2Cl_2 (15 mL) and was treated with oxalyl chloride (0.7 mL, 8.69 mmol) under an inert atmosphere and was stirred at room temperature for 30 mins to obtain a red solution. Excess oxalyl chloride was removed under vacuum. The residue was re-dissolved in dry CH_2Cl_2 (15 mL) and cooled to 0 °C. 6-Aminohexan-1-ol (0.4 g, 4.35 mmol) in dry CH_2Cl_2 (20 mL) was added dropwise followed by triethylamine (0.6 mL, 4.35 mmol) and the reaction was left to stir overnight. The reaction mixture was then treated with NH_4Cl (sat) (30 mL) and extracted with CH_2Cl_2 (30 mL). The organic layer was washed with water (30 mL) and dried over MgSO_4 and solvent was removed to yield the crude product, which was purified *via* column chromatography (7:3, hexanes : ethyl acetate) to yield the product as an orange solid (0.65g, 72%). **IR** (cm^{-1}): 3101, 2972, 2934, 1729, 1634, 1566, 1428 **^1H NMR** (300 MHz; CDCl_3) δ 4.12 (2H, s, FcH), 4.09 (7H, s, FcH), 3.60 (1H, s, OH), 3.52 (2H, t, $J = 4$, CH_2), 3.00 (2H, s, CH_2), 2.85 (2H, s, CH_2), 2.30 (2H, s, CH_2), 1.56–1.25 (8H, m, CH_2). **^{13}C NMR** (75.5 MHz; CDCl_3) δ 173.3, 77.8, 77.4, 76.9, 62.0, 38.8, 35.4, 32.0, 30.6, 26.7, 25.4, 25.4. **HRMS** (ESI) calcd for $\text{C}_{18}\text{H}_{25}\text{N}_1\text{O}_2\text{Fe}_1$ m/z : 343.1207 found $\text{C}_{18}\text{H}_{26}\text{N}_1\text{O}_2\text{Fe}_1$: 344.1253.

Acetylferrocene **107**



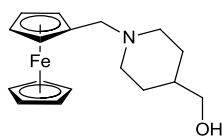
Ferrocene (1 g, 5.3 mmol) was dissolved in dry CH_2Cl_2 (25 mL) in a two-necked flask equipped with a condenser. The solution is cooled to 0°C in an ice bath then acetyl chloride (0.5 mL, 6 mmol) was added to the reaction mixture. Aluminum chloride (1.1 g, 8.2 mmol) is then added portionwise and the reaction mixture was then stirred at room temperature for 30mins. The solution was then poured into an ice water bath and extracted with CH_2Cl_2 (25 mL) and the organic layer was washed with water (25 mL). The organic fraction was then dried over MgSO_4 and the solvent removed to yield the product as an orange crystalline solid (0.78g, 75% yield). **^1H NMR** (300 MHz; CDCl_3) δ 4.72 (2H, s, FcH), 4.53 (2H, s, FcH), 4.13 (5H, s, FcH), 2.31 (3H, s, CH_3). **^{13}C NMR** (75.5 MHz; CDCl_3) δ 201.0, 80.7, 77.8, 77.3, 76.9, 73.6, 70.9, 27.6. **HRMS** (ESI) calcd for $\text{C}_{12}\text{H}_{12}\text{O}_1\text{Fe}_1$ m/z: 229.0314 found 229.0315 and $\text{C}_{12}\text{H}_{12}\text{O}_1\text{Fe}_1\text{Na}_1$: 251.0135. Data in accordance with literature.¹⁵⁸

Ethylferrocene **244**



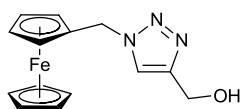
Acetylferrocene (0.18 g, 0.78 mmol) was dissolved in THF (5 mL) and treated with BMS (0.78 mL, 0.78 mmol). The reaction mixture was stirred at room temperature for 3hrs. The reaction mixture was then quenched with aqueous NH_4Cl (sat, 20 mL) and the aqueous layer was then extracted with EtOAc (15 mL). The combined organic layers were dried over MgSO_4 and the solvent was removed to yield the crude product as a yellow solid, that was purified by column chromatography (9:1, hexanes:EtOAc) to afford the crude product as a yellow amorphous solid (0.55, 50%). $^1\text{H NMR}$ (300 MHz; CDCl_3) δ 4.23 (2H, s, FcH), 4.19 (2H, s, FcH), 4.13 (5H, s, FcH), 2.75 (2H, s, CH_2) 1.26 (3H, s, CH_3). $^{13}\text{C NMR}$ (75.5 MHz; CDCl_3) δ 80.6, 76.9, 73.6, 70.8, 28.9, 11.8 **HRMS** (ESI) calcd for $\text{C}_{12}\text{H}_{14}\text{Fe}_1$ m/z: 214.0367 found 214.0370. Data in accordance with literature.¹⁵⁹

(1-(ferrocenylmethyl)piperidin-4-yl)methanol **137**



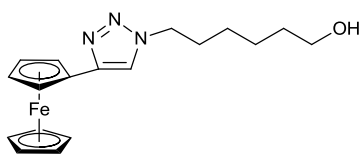
Ferrocene carboxaldehyde (0.6 g, 1.75 mmol) and piperidine-4-methanol (0.2 g, 1.75 mmol) were dissolved in dry THF (20 mL) to which sodium triacetoxyborohydride (1 g, 3.52 mmol) was added portionwise the suspension was then stirred at room temperature under an inert atmosphere for 12hrs. The reaction mixture is then partitioned between EtOAc (20 mL) and 1M NaOH (20 mL). The organic fraction was then dried over MgSO₄ and the solvent was evaporated to yield the crude product as a pale orange oil. The crude product was purified *via* column chromatography (7:3, hexanes : EtOAc) to afford the desired product as a yellow solid (0.45g, 75%). **IR** (cm⁻¹): 3256, 3121, 2214, 2050, 17001, 1622, 1476 **¹H NMR** (300 MHz; CDCl₃) δ 4.18 (2H, s, FcH), 4.17 (2H, s, FcH), 4.13 (5H, s, FcH), 3.66 (4H, t, *J* = 6.25, CH₂), 3.48 (2H, s, CH₂), 1.48-1.17 (5H, m, CH₃, CH). **¹³C NMR** (75.5 MHz; CDCl₃) δ 88.2, 77.8, 77.4, 77.1, 76.6, 69.6, 68.5, 67.5, 60.6, 58.5, 52.7, 46.0, 38.3, 28.6, 25.6. **HRMS** (ESI) calcd for C₁₇H₃₂N₁O₁Fe₁ *m/z* 312.1921 found 312.1922.

(1-(ferrocenylmethyl)-1*H*-1,2,3-triazol-4-yl)methanol **142**



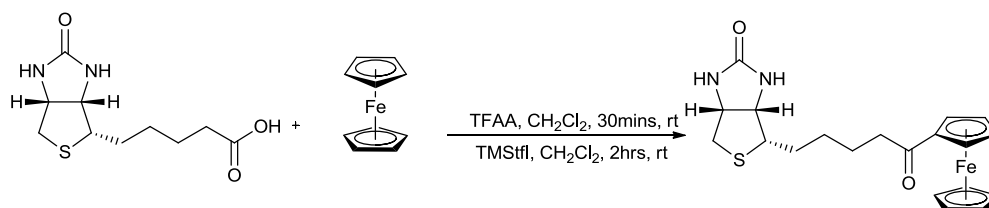
DBU (0.16 mL, 1.07 mmol) and DPPA (0.16 mL, 0.74 mmol) were added to a stirred solution of ferrocene methanol (0.1 g, 0.5 mmol) in dry toluene (6 mL). The reaction mixture was stirred at room temperature for 12hrs. The product was not isolated as was used sequentially. Propargyl alcohol (0.05 g, 0.05 mL, 0.86 mmol) was added to then added to the reaction mixture followed by copper acetate (50 mg, 5 mol%) and sodium ascorbate (80 mg, 10 mol%). The reaction was then left to stir at room temperature overnight. The product was extracted using CH₂Cl₂ (20 mL) and washed with NaHCO₃ (sat, 20 mL). The organic fractions were dried over MgSO₄ and the solvent was removed to yield the crude product as a dark yellow solid. The crude product was purified *via* column chromatography (7:3, hexanes : EtOAc) to afford the product as a dark yellow solid (0.11 g, 73%). ¹H NMR (300 MHz; CDCl₃) δ: 7.48 (1H, s, CHC=C), 5.39 (2H, t, *J* = 1.75, CH₂), 4.82 (2H, t, *J* = 2.65, CH₂), 4.21 (2H, s, FcH), 4.17 (2H, s, FcH) 4.16 (5H, s, FcH). ¹³C NMR (75.5 MHz; CDCl₃) δ 143.2, 123.1, 72.9, 72.5, 70.1, 69.9, 54.1, 52.6. Data in accordance with literature.¹⁶⁰

6-(4-ferrocenyl-1*H*-1,2,3-triazol-1-yl)hexan-1-ol **143**



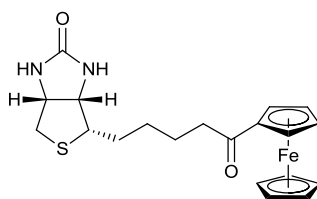
6-Bromohexan-1-ol (0.1 g, 0.6 mmol) was dissolved in Butanol : water (1:1, 1.5 mL) solvent mixture. Sodium azide (0.04 g, 0.6 mmol) was added and the reaction mixture was stirred at room temperature for 12hrs. The product was not isolated as it was used sequentially. Ethynylferrocene (0.09 g, 0.428 mmol) was added to the reaction mixture followed by copper acetate (40 mg, 5 mol%) and sodium ascorbate (80 mg, 10 mol%). The reaction was then left to stir at room temperature overnight. The product was extracted using CH₂Cl₂ (20 mL) and washed with NaHCO₃ (sat) (20 mL). The organic fractions were dried over MgSO₄ and the solvent was removed to yield the crude product as a dark yellow solid. The crude product was purified *via* column chromatography (7:3, hexanes:EtOAc) to afford the product as a dark yellow solid (0.21 g, 83%). **IR** (cm⁻¹): 3256, 3121, 2214, 2050, 17001, 1622, 1476. **¹H NMR** (300 MHz; CDCl₃) δ 7.59 (1H, s, CHC=C) 4.16 (2H, s, FcH), 4.14 (2H, s, FcH), 4.12 (5H, s, FcH), 3.66 (2H, t, *J* = 6.25, CH₂), 3.53 (2H, t, *J* = 6, CH₂), 1.74–1.28 (8H, m, CH₂). **¹³C NMR** (75.5 MHz, CDCl₃) δ 148.5, 130.2, 73.5, 72.4, 72.3, 70.5, 68.8, 52.5, 32.2, 28.2, 27.5, 25.3. **HRMS** (ESI) calcd for C₁₈H₂₃N₃O₁Fe₁ *m/z* 368.2740 found 368.2741.

General procedure A: Synthesis of 4-(5-(ferrocenyl)-5-oxopentyl)tetrahydro-1*H*-thieno[3,4-*d*]inidazol-2(3*H*)-ones



To a solution of biotin (1 mmol) in dry dichloromethane (5 mL) was added trifluoroacetic anhydride (TFAA, 1 mmol) and the reaction mixture was stirred at room temperature for 30 mins or until the biotin has fully dissolved. Ferrocene derivative (1 mmol) and trimethylsilyl trifluoromethane sulfonate (TMSTf, 1 mmol) were added and the reaction mixture was stirred at room temperature for two hours. Water (25 mL) was then added to quench the reaction and extracted with dichloromethane (3 x 25 mL). The combined organic fractions were dried over MgSO₄ and the solvent was removed. The crude product was purified using column chromatography (2% MeOH in dichloromethane).

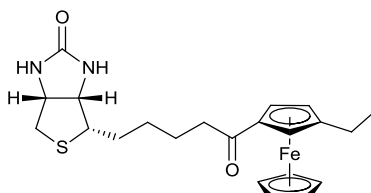
4-(5-(ferrocenyl)-5-oxopentyl)tetrahydro-1*H*-thieno[3,4-*d*]inidazol-2(3*H*)-one **110**



Biotin (0.244 g, 1 mmol), TFAA (0.21 g, 150 μ L, 1 mmol), ferrocene (0.186 g, 1 mmol) and TMSTf (0.22 g, 180 μ L, 1 mmol) reacted under general condition. (98% yield). ¹H NMR (300 MHz; CDCl₃) δ 6.53 (1H, br s, NH), 6.43 (1H, brs, NH), 4.85 (2H, t, *J* = 1.8, FcH), 4.62 (2H, t, *J* = 1.8, FcH), 4.37 (1H, dd, *J* = 7.6, 5.3, CH), 4.28 (5H, s, FcH), 4.23-4.21 (1H, m, CH), 2.91 (2H, t, *J* = 7.3, CH₂), 2.78 (2H, t, *J* = 7.3, CH₂), 1.73-1.42 (6H, m, CH₂). ¹³C NMR (75.5 MHz; CDCl₃) δ 203.4, 162.7, 79.1, 72.0, 69.5, 69.0, 61.1, 59.2, 55.5, 39.8, 38.7, 28.4, 24.2, 24.1. HRMS (ESI)

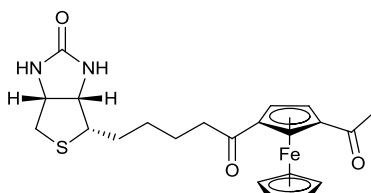
calcd for $C_{18}H_{23}N_3O_1Fe_1S_1$ m/z 412.0913 found 412.0913. Data in accordance with literature.¹⁶¹

4-(5-(ethylferrocenyl)-5-oxopentyl)tetrahydro-1*H*-thieno[3,4-*d*]imidazole-2(3*H*)-one
113



Biotin (0.244 g, 1 mmol), TFAA (0.21 g, 150 μ L, 1 mmol), ethylferrocene (0.228 g, 1 mmol) and TMS₂Stf (0.22 g, 180 μ L, 1 mmol). Reacted under the general reaction conditions. (0.35 g, 92%). **IR** (cm^{-1}): 3121, 2214, 2050, 1729, 1713, 1622, 1476. **¹H NMR** (300 MHz; $CDCl_3$) δ 6.51 (1H, br s, NH), 6.42 (1H, brs, NH), 4.83 (1H, s, FcH), 4.63 (2H, t, $J = 1.8$, FcH), 4.34 (1H, dd, $J = 7.6, 5.3$, CH), 4.29 (5H, s, FcH), 4.24-4.22 (1H, m, CH), 2.92 (2H, t, $J = 7.25$, CH_2), 2.78 (2H, t, $J = 7.25$, CH_2), 2.69 (2H, t, $J = 5.5$, CH_2), 1.73-1.45(6H, m, CH_2), 1.28 (3H, s, CH_3). **¹³C NMR** (75.5 MHz; $CDCl_3$) δ 203.4, 162.7, 79.1, 72.0, 69.5, 69.0, 61.1, 59.2, 55.5, 39.8, 38.7, 28.4, 24.2, 24.1, 14.3 **HRMS** (ESI) calcd for $C_{22}H_{28}N_2O_2Fe_1S_1$ m/z 440.1221 found 440.1222.

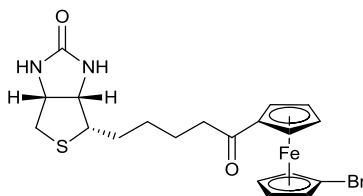
4-(5-(acetylferrocenyl)-5-oxopentyl)tetrahydro-1*H*-thieno[3,4-*d*]imidazole-2(3*H*)-one
112



Biotin (0.244 g, 1 mmol), TFAA (0.21 g, 150 μ L, 1 mmol), acetylferrocene (0.228 g, 1 mmol) and TMS₂Stf (0.22 g, 180 μ L, 1 mmol). Reacted under the general reaction conditions. (0.37 g, 92%). **IR** (cm^{-1}): 3121, 2214, 2050, 1729, 1713, 1622, 1476. **¹H**

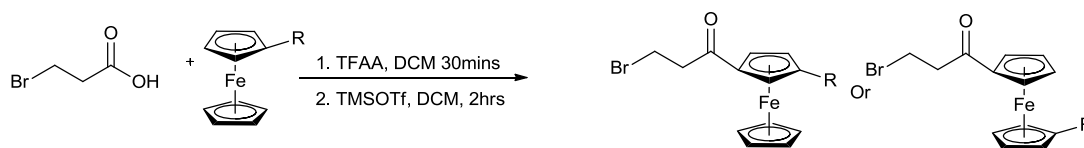
NMR (300 MHz; CDCl₃) δ 6.51 (1H, br s, NH), 6.42 (1H, brs, NH), 4.83 (1H, s, FcH), 4.62 (2H, t, *J* = 1.8, FcH), 4.34 (1H, dd, *J* = 7.6, 5.3, CH), 4.28 (5H, s, FcH), 4.24-4.22 (1H, m, CH), 2.92 (2H, t, *J* = 7.25, CH₂), 2.78 (2H, t, *J* = 7.25, CH₂), 2.69 (2H, t, *J* = 5.5, CH₂), 1.73-1.45(6H, m, CH₂), 1.28 (3H, s, CH₃). **¹³C NMR** (75.5 MHz; CDCl₃) δ 203.4, 201.4, 162.7, 79.1, 72.0, 69.5, 69.0, 61.1, 59.2, 55.5, 39.8, 38.7, 28.4, 24.2, 24.1, 14.3 **HRMS** (ESI) calcd for C₂₂H₂₈N₂O₂Fe₁S₁ *m/z* 454.1014 found 454.1015.

4-(5-(1'-bromoferrocenyl)-5-oxopentyl)tetrahydro-1*H*-thieno[3,4-*d*]imidazole-2(3*H*)-one **111**



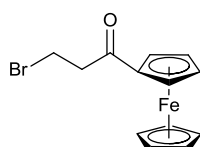
Biotin (0.244 g, 1 mmol), TFAA (0.21 g, 150 μL, 1 mmol), bromoferrocene (0.264 g, 1 mmol) and TMS₂Stf (0.22 g, 180 μL, 1 mmol). Reacted under the general reaction conditions. (0.45 g, 90%). **IR** (cm⁻¹): 3122, 2214, 2050, 1727, 1713, 1622, 1476. **¹H NMR** (300MHz, CDCl₃) δ 6.55 (1H, br s, NH), 6.47 (1H, brs, NH), 4.76 (2H, t, *J*=4, FcH), 4.54 (2H, t, *J*=4, FcH), 4.46 (2H, t, *J*=4, FcH), 4.36 (1H, dd, *J* = 7.6, 5.3, CH), 4.22-4.19 (1H, m, CH), 4.15 (2H, t, *J*=4, FcH), 2.94 (2H, t, *J* = 7.3, CH₂), 2.73 (2H, t, *J* = 7.2, CH₂), 1.73-1.42 (6H, m, CH₂). **¹³C NMR** (75.5 Hz, CDCl₃) δ 203.4, 162.7, 79.1, 72.0, 69.5, 69.0, 61.1, 59.2, 55.5, 39.8, 38.7, 28.4, 24.2, 24.1. **HRMS** (ESI) calcd for C₁₈H₂₂N₃O₁Fe₁Br₁S₁ *m/z* 490.0035 found C₁₈H₂₃N₃O₁Fe₁Br₁S₁ *m/z* 491.1274.

General Procedure B: Synthesis of 3-bromo-1-ferrocenylpropan-1-ones



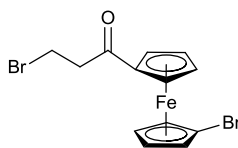
3-bromopropionic acid (0.152 g, 1 mmol) was dissolved in dry CH₂Cl₂ (5 mL), to which trifluoroacetic anhydride (150 μL, 1 mmol) was added and the reaction mixture was stirred at room temperature for 30mins. An appropriate Ferrocene derivative (1 mmol) was then added along with trimethylsilyl trifluoromethanesulfonate (180 μL, 1 mmol) and the reaction mixture was stirred for two hours at room temperature. The reaction was then quenched with water (20 mL), the organic layer was then separated and the aqueous layer was then extracted with CH₂Cl₂ (20 mL). The combined organic layers were dried over MgSO₄ and then the solvent was removed to yield the crude product. The crude product was purified *via* silica column chromatography (9:1, hexanes:ethylacetate) to yield product.

3-bromo-1-ferrocenylpropan-1-one **115**



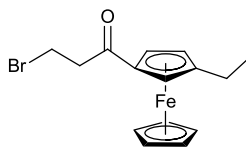
3-bromopropionic acid (0.76 g, 5 mmol), TFAA (1.05 g, 0.69 mL, 5 mmol), ferrocene (0.93 g, 5 mmol) and TMSOTf (1.11 g, 0.9 mL, 5 mmol) were reacted under general procedure B. Product afforded as a red crystalline solid (1.6 g, 95%). ¹H NMR (250 MHz, CDCl₃) δ 4.82 (2H, s, FcH), 4.57 (2H, s, FcH), 4.28 (5H, s, FcH), 3.76 (2H, t, *J* = 6.5, CH₂), 3.33 (2H, t, *J* = 6.5, CH₂). ¹³C NMR (75.5 MHz, CDCl₃) δ 200.6, 72.6, 70.1, 69.9, 69.2, 42.3, 26.0. HRMS (ESI) calcd for C₁₃H₁₃O₁Fe₁Br₁ m/z: 319.9421 found 319.9422.

3-bromo-1-(bromoferrocenyl)propan-1-one **116**



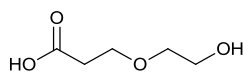
3-bromopropionic acid (0.152 g, 1 mmol), TFAA (0.15 mL, 1 mmol), Bromoferrocene (0.264 g, 1 mmol) and TMStf (0.18 mL, 1 mmol) were reacted under the general procedure B. Product yield (0.06g, 65%). $^1\text{H NMR}$ (300 MHz, CDCl_3) δ : 4.74 (2H, t, $J=3.75$, FcH), 4.50 (2H, t, $J=3.75$, FcH), 4.41 (2H, t, $J=3.75$, FcH), 4.14 (2H, t, $J=1.75$, FcH), 3.66 (2H, t, $J=6.75$, CH_2), 3.27 (2H, t, $J=6.75$, CH_2). $^{13}\text{C NMR}$ (75.5 MHz, CDCl_3) δ 200.0, 79.9, 74.7, 72.5, 72.4, 69.0, 42.6, 25.8. **HRMS** (ESI) calcd for $\text{C}_{13}\text{H}_{12}\text{O}_1\text{Fe}_1\text{Br}_2$ m/z : 397.8526 found 397.8527.

3-bromo-1-(3-ethylferrocenyl) propan-1-one **117**



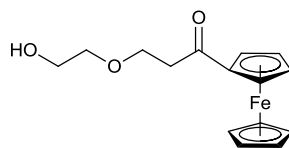
3-bromopropionic acid (0.152 g, 1 mmol), TFAA (0.15 mL, 1 mmol), Ethylferrocene (0.214 g, 1 mmol) and TMStf (0.18 mL, 1 mmol) were reacted under general procedure B. Product yield (0.18 g, 65%). $^1\text{H NMR}$ (500 MHz; CDCl_3) δ 4.22 (2H, s, FcH), 4.16 (1H, s, FcH), 4.09 (5H, s, FcH), 3.69 (2H, t, $J = 1.75$, CH_2), 3.66–3.62 (4H, m, CH_2), 2.75 (2H, t, $J = 1.75$, CH_2), 1.26 (3H, s, CH_3). $^{13}\text{C NMR}$ (75.5 MHz; CDCl_3) δ 198.3, 72.7, 72.6, 70.1, 69.9, 69.7, 65.6, 61.7, 26.7, 22.4, 14.2. **HRMS** (ESI) calcd for $\text{C}_{15}\text{H}_{17}\text{O}_1\text{Fe}_1\text{Br}_1$ m/z : 347.9734 found $\text{C}_{15}\text{H}_{17}\text{O}_1\text{Fe}_1\text{Br}_1\text{Na}_1$ m/z 370.8732.

2-(3-hydroxyethoxy)propanoic acid **120**



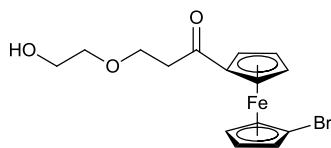
Ethylene glycol (0.9 mL, 16.13 mmol) was dissolved in dry THF (20 mL) under an inert atmosphere and the solution was cooled down to 0°C in an ice bath. To this sodium hydride (0.38 g, 16.13 mmol) was added and the reaction mixture was stirred at 0 °C for 2 hours. The reaction mixture was then re-cooled using an ice bath and 3-bromopropionic acid (2.45 g, 16.13 mmol) was added to the reaction mixture in a solution of THF (2 mL). The reaction mixture was then stirred at room temperature for 6 hours. Water (25 mL) was then added and the reaction mixture was extracted using ether (2 × 25 mL). The combined organic layers were then dried over MgSO₄ and the solvent was removed to yield the crude product as an off white solid. The crude product was then purified *via* column chromatography (8:2, hexanes:EtOAc) to afford the compound as an amorphous off white solid (2.24 g, 65%). **IR** (cm⁻¹): 3258, 3121, 2214, 2050, 1728, 1712, 1612, 1476. **¹H NMR** (250 MHz, CDCl₃) δ 3.72 (2H, t, *J* = 6.6, CH₂), 3.51 (2H, t, *J* = 6.6, CH₂), 2.92 (2H, t, *J* = 6.6, CH₂). **¹³C NMR** (75.5 MHz, CDCl₃) δ 175.8, 67.5, 63.5, 37.4, 25.5, 25.2. **HRMS** (ESI) calcd for C₅H₁₀O₄ *m/z*: 134.0579 found 134.0579.

1-ferrocenyl-3-(2-hydroxyethoxy) propan-1-one **118**



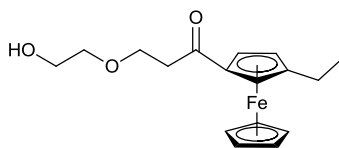
3-(2-hydroxyethoxy)propanoic acid (0.130 g, 1 mmol) was dissolved in dry CH_2Cl_2 (5 mL), to which trifluoroacetic anhydride (150 μL , 1 mmol) was added and the reaction mixture was stirred at room temperature for 30mins. Ferrocene (0.186 g, 1 mmol) was then added along with trimethylsilyl trifluoromethanesulfonate (180 μL , 1 mmol) and the reaction mixture was stirred for two hours at room temperature. The reaction was then quenched with water (20 mL), the organic layer was then separated and the aqueous layer was then re-washed with CH_2Cl_2 (20 mL). The combined organic layers were dried over MgSO_4 and then the solvent was removed to yield the crude product as a brown oil. The crude compound was then purified silica column chromatography (8:2, hexanes:EtOAc) to afford the compound as a red oil (0.27g,85%). **IR** (cm^{-1}): 3258, 3121, 2214, 2050, 1728, 1712, 1612, 1476. **^1H NMR** (300 MHz, CDCl_3) δ : 4.73 (2H, t, $J=3.75$, FcH), 4.45 (2H, t, $J=3.75$, FcH), 4.16 (5H, s, FcH), 3.83 (2H, t, $J=6.25$, CH_2), 3.68 (2H, s, CH_2), 3.58 (2H, t, $J=5.75$, CH_2), 2.93 (2H, t, $J=6.25$, CH_2). **^{13}C NMR** (75.5 MHz, CDCl_3) δ 202.5, 72.9, 72.5, 70.1, 69.9, 69.7, 69.3, 65.6, 61.7, 38.6. **HRMS** (ESI) calcd for $\text{C}_{15}\text{H}_{18}\text{O}_3\text{Fe}_1$ m/z : 302.0672 found 303.0673 and $\text{C}_{15}\text{H}_{18}\text{O}_3\text{Fe}_1\text{Na}_1$ m/z 325.0519

1-bromoferrocenyl-3-(2-hydroxyethoxy)propan-1-one **121**



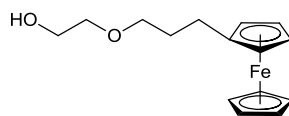
3-(2-hydroxyethoxy)propanoic acid (0.130 g, 1 mmol) was dissolved in dry CH_2Cl_2 (5 mL), to which trifluoroacetic anhydride (150 μL , 1 mmol) was added and the reaction mixture was stirred at room temperature for 30 mins. Bromoferrocene (0.264 g, 1 mmol) was then added along with trimethylsilyl trifluoromethanesulfonate (180 μL , 1 mmol) and the reaction mixture was stirred for two hours at room temperature. The reaction was then quenched with water (20 mL), the organic layer was then separated and the aqueous layer was then extracted with CH_2Cl_2 (20 mL). The combined organic layers were dried over MgSO_4 and then the solvent was removed to yield a brown oil. The compound was then purified *via* column chromatography (8:2, hexanes : EtOAc) to afford the product as a deep red oil (0.25g, 65%). **IR** (cm^{-1}): 3256, 3121, 2214, 2050, 1728, 1622, 1476. **^1H NMR** (250 MHz, CDCl_3) δ : 4.86 (2H, t, $J=2.5$, FcH), 4.62 (2H, t, $J=2.5$, FcH), 4.52 (2H, t, $J=2.5$, FcH), 4.26 (2H, t, $J=2.5$, CH_2), 3.97 (2H, t, $J=7.25$, CH_2), 3.81 (2H, s, CH_2), 3.68 (2H, t, $J=5.75$, CH_2) 3.08 (2H, t, $J=7.25$, CH_2). **^{13}C NMR** (75.5 MHz, CDCl_3) δ 203.58, 72.94, 72.57, 70.11 69.89, 69.73, 69.35, 65.66, 61.73, 38.69 **HRMS** (ESI) calcd for $\text{C}_{15}\text{H}_{17}\text{O}_3\text{Fe}_1\text{Br}_1$ m/z: 379.9723 found $\text{C}_{15}\text{H}_{17}\text{O}_3\text{Fe}_1\text{Br}_1\text{Na}_1$ m/z 402.9617.

1-(4-ethylferrocenyl)-3-(2-hydroxy)propan-1-one **122**



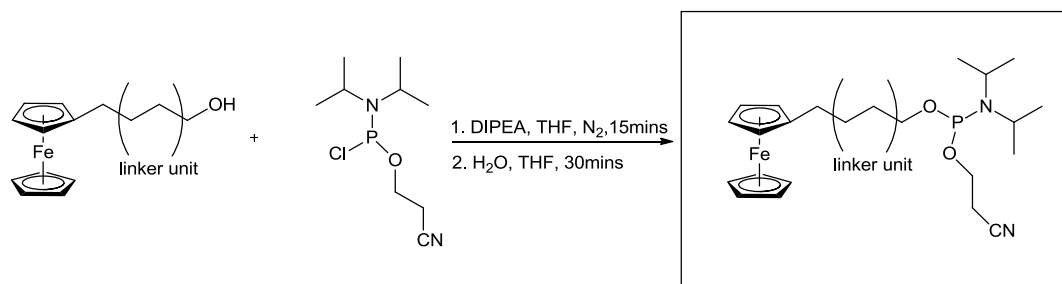
3-(2-hydroxyethoxy)propanoic acid (0.130 g, 1 mmol) was dissolved in dry CH₂Cl₂ (5 mL), to which trifluoroacetic anhydride (150 μL, 1 mmol) was added and the reaction mixture was stirred at room temperature for 30mins. Ethylferrocene (0.264 g, 1 mmol) was then added along with trimethylsilyl trifluoromethanesulfonate (180 μL, 1 mmol) and the reaction mixture was stirred for two hours at room temperature. The reaction was then quenched with water (20 mL), the organic layer was then separated and the aqueous layer was then extracted with CH₂Cl₂ (20 mL). The combined organic layers were dried over MgSO₄ and then the solvent was removed to yield a brown oil. The compound was then purified *via* column chromatography (99:1, hexanes : EtOAc) to afford the compound as a red oil (0.05g, 65%). **IR** (cm⁻¹): 3256, 3121, 2214, 2050, 1729, 1622, 1476. **¹H NMR** (500 MHz, CDCl₃) δ 4.21 (2H, s, FcH), 4.15 (1H, s, FcH), 4.13 (5H, s, FcH), 3.67 (2H, t, *J* = 1.75, CH₂), 3.64 – 3.60 (4H, m, CH₂), 2.69–2.62 (4H, m, CH₂), 1.26 (3H, t, *J* = 6.5, CH₃). **¹³C NMR** (75.5 MHz, CDCl₃) δ 198.1, 72.8, 72.6, 70.1, 69.9, 69.7, 65.6, 61.7, 38.6, 22.5, 14.3. **HRMS** (ESI) calcd for C₁₇H₂₁O₃Fe₁ *m/z*: 329.1918 found 329.1919.

Synthesis of 2-(3-ferrocenylpropoxy) ethanol **127**



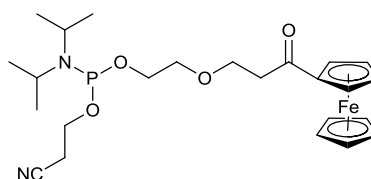
1-ferrocenyl-3-(2-hydroxyethoxy)propan-1-one (0.2 g, 0.66 mmol) was dissolved in dry CH_2Cl_2 (20 mL) to which BMS (0.3 mL, 1.5 mL) the reaction mixture was then stirred at room temperature until completion. The reaction was monitored by TLC (9:1, petrol:ethylacetate). When the reaction was complete, NH_4Cl (sat, 30 mL) was used to quench the reaction. The aqueous layer was then extracted with ethyl acetate (25 mL) and then the combined organic layers are dried using MgSO_4 and the solvent was removed to yield the product as an orange/yellow oil (0.19 g, 96%). **IR** (cm^{-1}): 3256, 3131, 2221, 2065, 1932, 1712, 1622, 1476 **$^1\text{H NMR}$** (300 MHz; CDCl_3) δ : 4.63 (2H, t, $J=3.75$, FcH), 4.34 (2H, t, $J=3.75$, FcH), 4.25 (5H, s, FcH), 3.95 (2H, t, $J=6$, CH_2), 3.83 (2H, t, $J=6.25$, CH_2), 3.68 (2H, s, CH_2), 3.58 (2H, t, $J=6$, CH_2), 2.93 (2H, t, $J=6$, CH_2). **$^{13}\text{C NMR}$** (75.5 MHz, CDCl_3) δ 72.9, 72.5, 70.1, 69.9, 69.7, 69.3, 65.6, 61.7, 38.6, 36.3. **HRMS** (ESI) calcd for $\text{C}_{15}\text{H}_{19}\text{O}_2\text{Fe}_1$ m/z : 287.1553 found $\text{C}_{15}\text{H}_{20}\text{O}_2\text{Fe}_1$ m/z 288.0987.

General synthetic procedure for phosphoramidite synthesis



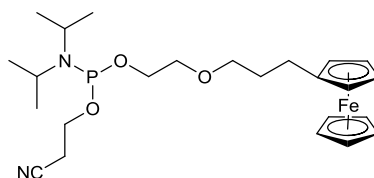
N, N – diisopropylethylamine (0.4 mL, 8.4 mmol) was added to a stirred solution of the ferrocene derivative (2.1 mmol) in dry THF (25 mL) under a nitrogen atmosphere. 2 – cyanoethyl diisopropylchlorophosphoramidite (0.2 ml, 3.15 mmol) was added dropwise and the resulting mixture was stirred for 15 mins. MilliQ filtered water (200 mL) was added and the solution was stirred for a further 30 mins. Ethyl Acetate – Triethylamine (1:1, 25 mL) was added, a precipitate formed. The mixture was washed with saturated NaHCO₃ (25 mL) and MilliQ filtered water (25 mL). The organic fraction was dried over MgSO₄ and the solvent was removed under *vacuo*. The crude product was then purified *via* column chromatography (9:1, hexanes : EtOAc).

2-cyanoethyl(2(3-ferrocenyl-3-oxopropoxy)ethyl)diisopropylphosphoramidite **123**



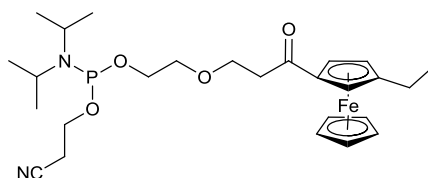
¹H NMR (500 MHz, CDCl₃) δ 4.23 (2H, s, FcH), 4.18 (2H, s, FcH), 4.13 (5H, s, FcH), 3.61 (2H, t, *J* = 1.75, CH₂), 3.58 (4H, m, CH₂), 3.41 (2H, t, *J* = 6.5, CH₂), 3.33 (2H, t, *J* = 6.5, CH), 2.65 (2H, t, *J* = 6.5, CH₂), 0.86 (12H, t, *J* = 7, CH₃). ¹³C NMR (75.5 MHz, CDCl₃) δ 198.6, 117.3, 79.3, 79.2, 78.7, 76.9, 71.2, 65.3, 64.7, 58.4, 51.3, 51.1, 40.8, 24.8, 20.3. ³¹P NMR (DEC) (202.5 MHz, CDCl₃) δ 147.16.

2-cyanoethyl(2-(3-ferrocenylpropoxy)ethyl)diisopropylphosphoramidite **128**



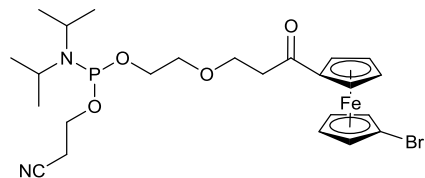
¹H NMR (500 MHz, CDCl₃) δ 4.32 (2H, s, FcH), 4.22 (2H, s, FcH), 4.15 (5H, s, FcH), 3.75 (2H, t, *J* = 1.75, CH₂), 3.64 (4H, m, CH₂), 3.52 (2H, t, *J*=6, CH₂), 3.34 (2H, t, *J* = 6.5, CH), 2.75 (2H, t, *J* = 6.5, CH₂), 2.59 (2H, q, *J* = 6.5, CH₂), 0.98 (12H, t, *J* = 7, CH₃). **¹³C NMR** (75.5 MHz, CDCl₃) δ 116.8, 79.5, 79.3, 78.9, 76.3, 71.6, 71.4, 64.3, 58.0, 51.9, 51.8, 35.6, 27.6, 24.4, 24.3. **³¹P NMR** (DEC) (202.5 MHz, CDCl₃) δ 147.23.

2-cyanoethyl(2-(3-ethylferrocenyl)-3-oxopropoxy)ethyl)diisopropylphosphoramidite **125**



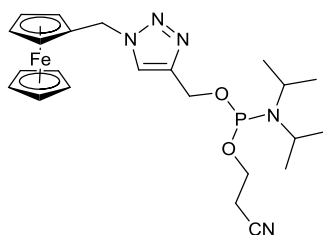
¹H NMR (500 MHz, CDCl₃) δ 4.26 (2H, s, FcH), 4.16 (2H, s, FcH), 4.12 (5H, s, FcH), 3.65 (2H, t, *J* = 1.75, CH₂), 3.60 (4H, m, CH₂), 3.57 (2H, t, *J*=6, CH₂), 3.35 (2H, t, *J* = 6.5, CH), 2.69 (2H, t, *J* = 6.5, CH₂), 1.26 (3H, t, *J* = 6, CH₃), 0.86 (12H, t, *J* = 7, CH₃). **¹³C NMR** (75.5 MHz, CDCl₃) δ 197.4, 114.6, 79.8, 79.6, 78.4, 76.9, 71.3, 65.3, 64.1, 58.3, 51.7, 51.6, 40.4, 32.7, 24.5, 20.6, 11.8. **³¹P NMR** (DEC) (202.5 MHz, CDCl₃) δ 147.27.

2-cyanoethyl(2-(1'-bromoferrocenyl)-3-oxopropoxy)ethyl)diisopropylphosphoramidite **124**



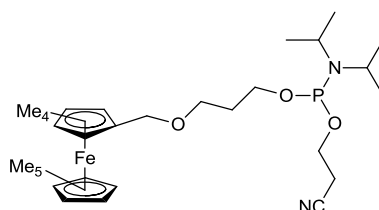
¹H NMR (500 MHz, CDCl₃) δ 4.78 (2H, t, *J*=3.5, FcH), 4.56 (2H, t, *J*=3.75, FcH), 4.44 (2H, t, *J*=3.5, FcH), 4.18 (2H, t, *J*=1.75, FcH), 3.65 (2H, t, *J* = 1.75, CH₂), 3.60 (4H, m, CH₂), 3.57 (2H, t, *J*=6, CH₂), 3.35 (2H, t, *J* = 6, CH), 2.69 (2H, t, *J* = 6, CH₂), 0.86 (12H, t, *J* = 7, CH₃). **¹³C NMR** (75.5 MHz, CDCl₃) δ 197.6, 115.3, 81.4, 79.8, 79.6, 78.5, 76.4, 71.3, 65.6, 64.3, 59.1, 51.7, 42.7, 24.7, 21.0. **³¹P NMR** (DEC) (202.5 MHz, CDCl₃) δ 147.27.

2-cyanoethyl((1-ferrocenylmethyl)-1*H*-1,2,3-triazol-4-yl)methyl)diisopropylphosphoramidite **245**



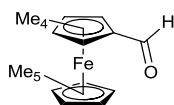
¹H NMR (500 MHz, CDCl₃) δ 7.48 (1H, s, CHC=C), 5.39 (2H, t, *J* = 1.75 Hz, CH₂), 4.26 (2H, s, FcH), 4.16 (2H, s, FcH), 4.12 (5H, s, FcH), 3.65 (2H, t, *J* = 1.75, CH₂), 3.60 (4H, m, CH₂), 3.57 (2H, t, *J*=6, CH₂), 3.35 (2H, t, *J* = 6.5, CH), 2.69 (2H, t, *J* = 6.5, CH₂), 1.26 (3H, t, *J* = 6, CH₃), 0.86 (12H, t, *J* = 7, CH₃). **¹³C NMR** (75.5 MHz, CDCl₃) δ 142.4, 122.4, 111.9, 61.2, 58.3, 51.9, 51.7, 24.6, 22.4. **³¹P NMR** (DEC) (202.5 MHz, CDCl₃) δ 147.31.

2-Cyanoethyl(2-(nonamethylferrocenylmethoxy)diisopropylphosphoramidite **136**



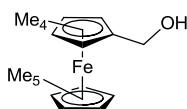
¹H NMR (500 MHz, CDCl₃) δ 4.06 (2H, s, CH₂), 3.69-3.46 (7H, m, CH₂, CH), 3.36-3.29 (3H, q, *J* = 7.2, CH₂), 2.52 (2H, t, *J* = 6.0, CH₂), 1.62 (6H, s, CH₃Fc), 1.59 (6H, s, CH₃Fc), 1.56 (15H, s, CH₃Fc). **¹³C NMR** (75.5 MHz, CDCl₃) δ 79.5, 79.1, 78.3, 76.9, 65.4, 65.3, 64.9, 60.2, 59.9, 58.0, 57.8, 42.5, 42.3, 31.3, 31.1, 23.7, 23.6, 23.5, 19.7, 19.6, 14.3, 8.5, 8.4, 8.2. **³¹P NMR** (DEC) (202.5 MHz, CDCl₃) δ 147.89.

Nonamethylferrocenecarboxaldehyde **130**



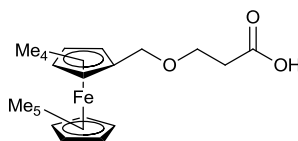
Decamethylferrocene (2.5 g, 7.66 mmol) was added to a solution of ground barium manganate (9.81 g, 38.30 mmol) in benzene : ether (1:1, 40 mL) and placed in an ultrasound bath for 10-15 mins. The reaction mixture was then heated at 45°C for 18hrs before being cooled to room temperature and the barium manganate residues being removed by suction filtration. The solvent was evaporated under reduced pressure and the crude product as a deep red solid. The crude product was purified *via* column chromatography (9:1, hexanes:EtOAc) to afford the product as a red solid (1.4 g, 63%). **¹H NMR** (300 MHz, CDCl₃) δ 9.91 (1H, s, CHO), 1.94 (6H, s, c(CHO)C(CMe)₂), 1.70 (6H, s, c(CHO)C(CMe)₂), 1.59 (15H, s, C(CMe)₅). **¹³C NMR** (75.5 MHz, CDCl₃) δ 196.2, 86.4, 83.3, 81.1, 73.4, 9.6, 9.2. **HRMS** (ESI) calcd for C₂₀H₂₈O₁Fe₁ *m/z* 340.1484 found 340.1485. Data in accordance with literature.¹¹⁹

Nonamethylferrocene methanol **133**



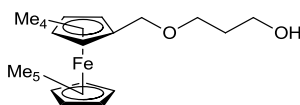
A solution of nonamethylferrocenecarboxaldehyde (0.5 g, 1.47 mmol) in EtOH : dioxane (4:1, 50 mL) was added sodium borohydride (0.05 g, 1.47 mmol) in a round bottomed flask. The solution was stirred for 1 hour. Water (30 mL) was then added and then extracted with ether (30 mL). Re – extracted with water and the organic solution was dried with MgSO₄. The solvent was removed *in vacuo* to afford the product as a yellow solid (0.5 g, 99%). **IR** (cm⁻¹): 3256, 3121, 2214, 1654, 1622, 1476 **¹H NMR** (300 MHz, CDCl₃) δ, 3.49 (2H, t, *J* = 6.4, CH₂) 1.91 (6H, s, c(CHO)C(CMe)₂), 1.63 (6H, s, c(CHO)C(CMe)₂), 1.56 (15H, sm, C(CMe)₅). **¹³C NMR** (75.5 MHz, CDCl₃) δ 87.5, 84.6, 82.3, 73.4, 63.2 9.4, 9.1. **HRMS** (ESI) calcd for C₂₀H₃₀O₁Fe₁ *m/z* 342.1646 found C₂₀H₃₀O₁Fe₁Na₁: 365.1203.

6-(nonamethylferrocenylmethoxy)propanoic acid **134**



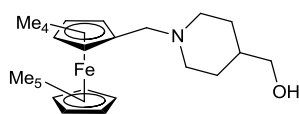
Sodium hydride (0.042 g, 1.75 mmol) was added to a solution of nonamethylferrocene methanol (0.3 g, 0.88 mmol) in THF (20 mL) and allowed to stir for 2 hours in an ice bath. To the formed suspension 3-bromopropanoic acid (0.11 g, 0.88 mmol) was added and the reaction was stirred at room temperature for 2 hours. Water (20 mL) was then added and the product was extracted with ether (20 mL). The organic fraction was dried over MgSO_4 and the solvent was evaporated to yield the crude product as a yellow solid. The crude product was purified *via* column chromatography (7:3, hexanes : EtOAc) to afford the product as a yellow powder (0.14g, 40%). **IR** (cm^{-1}): 3256, 3121, 2214, 2050, 1728, 1652, 1621, 1476 **$^1\text{H NMR}$** (300 MHz, CDCl_3) δ 3.76 (2H, t, $J = 6.5\text{Hz}$, CH_2), 3.59 (2H, t, $J = 6.75$, CH_2), 3.33 (2H, t, $J = 6.5\text{Hz}$, CH_2), 1.94 (6H, s, $\text{C}(\text{CMe})_2$), 1.70 (6H, s, $\text{c}(\text{CHO})\text{C}(\text{CMe}_2)$), 1.59 (15H, sm, $\text{C}(\text{CMe})_5$). **$^{13}\text{C NMR}$** (75.5 MHz, CDCl_3) δ 176.2, 86.4, 83.3, 81.1, 73.4, 9.4, 9.1. **HRMS** (ESI) calcd for $\text{C}_{23}\text{H}_{35}\text{O}_3\text{Fe}_1$ m/z 414.1284 found 414.1285.

3-(nonamethylferrocenylmethoxy)propan-1-ol **135**



Lithium aluminium hydride (0.06 g, 1.74 mmol) was dissolved in ether (20 mL) in a two necked round bottomed flask. 6-(nonamethylferrocenylmethoxy)propanoic acid (0.36 g, 0.87 mmol) in ether (5 mL) was added dropwise and the solution was stirred at 0 °C for 30 mins. The solution was then refluxed for 2 hours. The solution was then quenched with water (3 mL) then NaOH 20% solution. Water (12 mL) was then added and the ether layer was decanted and the solvent was evaporated. (0.219 g, 60%). **IR** (cm^{-1}): 3258, 3021, 2214, 2150, 1701, 1622, 1476 **$^1\text{H NMR}$** (300 MHz, CDCl_3) δ 3.56 (2H, t, $J = 6.5$, CH_2), 3.41 (2H, t, $J = 6.75$, CH_2), 3.23 (2H, t, $J = 6.75$, CH_2), 1.94 (6H, s, $\text{C}(\text{CMe}_2)$), 1.75 (2H, t, $J = 7$, CH_2), 1.70 (6H, s, $\text{c}(\text{CHO})\text{C}(\text{CMe}_2)$), 1.59 (15H, s, $\text{C}(\text{CMe})_5$). **$^{13}\text{C NMR}$** (75.5 MHz, CDCl_3) δ 86.4, 84.5, 83.3, 81.1, 73.4, 58.4, 32.2, 9.7, 9.4. **HRMS** (ESI) calcd for $\text{C}_{23}\text{H}_{35}\text{O}_2\text{Fe}_1$ m/z 399.1986 found 399.1986. Anal. Calcd. $\text{C}_{23}\text{H}_{35}\text{O}_2\text{Fe}_1$: C, 69.17% H, 8.83% found C, 69.17% H, 9.10%.

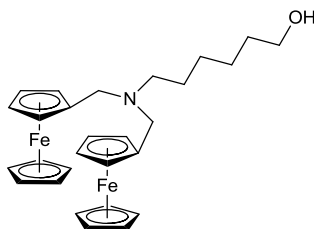
(nonamethylferrocenyl-1-methyl-piperidin-4-yl) methanol **132**



Nonaferrocene carboxaldehyde (0.6 g, 1.75 mmol) and piperidine-4-methanol (0.2 g, 1.75 mmol) were dissolved in dry THF (20 mL) to which sodium triacetoxyborohydride (1 g, 3.52 mmol) was added portionwise and stir at room temperature under an inert atmosphere for 12hrs. The reaction mixture is then extracted between EtOAc and 1N NaOH. The organic fraction was then dried over MgSO₄ and the solvent was removed to yield the crude product as a orange/brown soild. The crude product was purified *via* column chromatography (7:3, hexanes:EtOAc) to afford the product as a yellow solid (0.45 g, 55%). **IR** (cm⁻¹): 3256, 3121. 2214, 2050, 17001, 1622, 1476, 1465. **¹H NMR** (300 MHz, CDCl₃) δ 3.66 (4H, t, *J* = 6.25, CH₂), 2.21(6H, s, CH₃), 2.11 (6H, s, CH₃), 1.92 (15H, s, CH₂) 1.84-1.17 (5H, m, CH₂, OH).). **¹³C NMR** (75.5 MHz, CDCl₃) δ 86.4, 84.5, 83.3, 81.1, 73.4, 58.4, 32.2, 9.7, 9.4. **HRMS** (ESI) calcd for C₂₀H₄₁N₁O₁Fe₁ *m/z* 438.2543 found 438.2543.

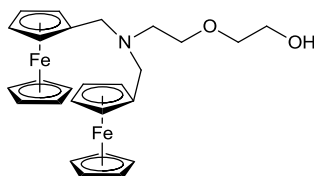
7.4 Synthesis of di-ferrocenyl redox active labels

6-(bis(ferrocenylmethyl)amino)hexan-1-ol **98**



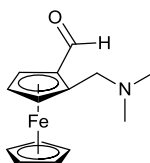
Ferrocene carboxaldehyde (2.1 g, 9.81 mmol) and 6 – aminohexan - 1 – ol (0.5 g, 4.27 mmol) in dry THF (25 mL) were added to an oven dried flask. Sodium triacetoxyborohydride (2.3 g, 10.90 mmol) was added portionwise to the solution. The reaction was left overnight. The reaction was taken up in ethyl acetate (40 mL), the organic layer was washed with NaCO₃ (20 mL), Brine (20 mL) and MilliQ water (20 mL). The organic fraction was then dried over MgSO₄ and the solvent removed *en vacuo*. The crude product was then purified *via* column chromatography (9:1-7:3, hexanes:EtOAc) to afford the product as a dark orange solid (2.21 g, 85%). **IR** (cm⁻¹): 3101, 2972, 2934, 2204, 2049, 1700, 1632, 1466, 1395. **¹H NMR** (300 MHz, CDCl₃) δ 4.18 (4H, s, FcH), 4.17 (4H, s, FcH), 4.13 (10H, s, FcH), 3.66 (4H, t, *J* = 6.25, CH₂), 3.48 (2H, s, CH₂), 2.20 (2H, t, *J* = 6.25, CH₂), 1.59 – 1.31 (8H, m, CH₂). **¹³C NMR** (75.5 Hz, CDCl₃) δ 77.8, 77.4, 76.9, 70.5, 68.8, 63.3, 53.0, 52.1, 33.1, 27.4, 25.8. **HRMS** (ESI) calcd for C₂₈H₃₃N₁O₁Fe₂ *m/z* 519.1430 found 519.1430. Anal. Calcd. C₂₈H₃₃N₁O₁Fe₂: C, 65.52% H, 6.87% N, 2.73% found C, 65.51% H, 6.94% N, 2.62%.

(diferrocenyl – 2 – aminoethoxy) ethanol **149**



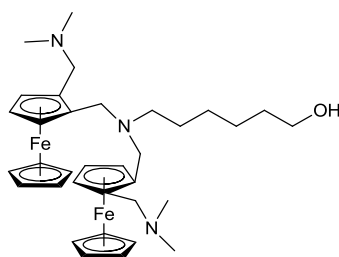
Ferrocene carboxaldehyde (2.1 g, 9.81 mmol) and (aminoethoxy) ethanol (0.5 g, 4.27 mmol) in dry THF (25 mL) were added to an oven dried flask. Sodium triacetoxyborohydride (2.3 g, 10.90 mmol) was added portionwise to the solution. The reaction was left overnight. The reaction was taken up in ethyl acetate (40 mL), the organic layer was washed with NaCO₃ (20 mL), Brine (20 mL) and MilliQ water (20 mL). The organic fraction was then dried over MgSO₄ and the solvent was removed. The crude product was then purified *via* column chromatography (9:1-7:3, hexanes:EtOAc) to afford the product as an orange amorphous solid (2.0 g, 78%). **IR** (cm⁻¹): 3241, 2972, 2934, 2204, 2049, 1700, 1632, 1466, 1395, 1364. **¹H NMR** (300 MHz, CDCl₃) δ 4.18 (4H, s, FcH), 4.17 (4H, s, FcH), 4.13 (10H, s, FcH), 3.66 (4H, t, *J* = 6.25, CH₂), 3.60–3.52 (4H, m, CH₂), 3.48 (2H, s, CH₂), 2.20 (2H, t, *J* = 6.25, CH₂). **¹³C NMR** (75.5 MHz, CDCl₃) δ 77.8, 77.4, 76.9, 70.5, 68.8, 63.3, 53.0, 52.1, 33.1, 27.4, 25.8. **HRMS** (ESI) calcd for C₂₆H₃₃N₁O₂Fe₂ *m/z* 501.1430 found 501.1438.

2-((dimethylamino)methyl)ferrocene carboxaldehyde **156**



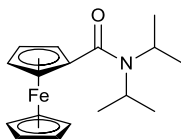
n-Butyl lithium (3.1 mL, 32.63 mmol) was added to a stirring solution of ((Dimethylamino)methyl) ferrocene (1 g, 4.11 mmol) in dry ether (40 mL). The reaction mixture was stirred at room temperature for 16 hours. DMF (0.41 mL, 5.36 mmol) was then added and the reaction mixture was stirred for four hours, water (30 mL) was then added and the product was extracted with ether (30 mL). The organic fraction was dried over MgSO₄ and the solvent was removed to afford the crude product as a dark orange solid. The crude product was purified *via* column chromatography (ethyl acetate:hexane 1:9) to afford the product as an orange solid (1.25 g, 75%). **¹H NMR** (300 MHz, CDCl₃) δ 9.98 (1H, s, CHO), 4.81 (1H, s, FcH), 4.62 (1H, s, FcH), 4.56 (1H, s, FcH) 4.21 (5H, s, FcH), 3.85 (2H, s, CH₂), 2.16 (6H, s, CH₃). **¹³C NMR** (75.5 MHz, CDCl₃) δ 190.8, 72.8, 72.4, 70.9, 69.5, 66.3, 58.8, 46.1. **HRMS** (ESI) calcd for C₂₈H₃₃N₁O₁Fe₂ *m/z* 271.1634 found C₂₈H₃₄N₁O₁Fe₁: 272.1701 (with H⁺). Data in accordance with literature.¹⁶²

Di – (dimethylamino)methylferrocenyl – 6 – aminohexanol **154**



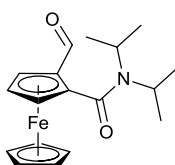
(dimethylamino)methyl ferrocenecarboxaldehyde (1.1 g, 4.04 mmol) was dissolved in dry THF (30 mL). 6 – aminohexan – 1 – ol (0.25 g, 2.13 mmol) was added. Then Sodium triacetoxyborohydride (1.3 g, 6.16 mmol) was added to the reaction mixture. The solution was stirred under nitrogen at room temperature overnight. Ethyl acetate (20 mL) and 1N NaOH (20 mL) were then added and the organic layer was then extracted with NaCO₃ (25mL), Brine (25 mL) and Milli Q filtered water (25 mL) then dried over MgSO₄ and the solvent removed to afford the crude product as an orange oil, which was purified *via* column chromatography (9:1-6:4, Hexanes:EtOAc) to afford the product as an orange oil (0.95 g, 75%). **IR** (cm⁻¹): 3252, 3201, 3164, 3101, 2972, 2204, 2049, 1700, 1632, 1446. **¹H NMR** (300 MHz, CDCl₃) δ 4.24 (2H, s, FcH), 4.21 (2H, s, FcH), 4.19 (2H, s, FcH), 4.15 (10H, s, FcH), 3.86 (4H, s, CH₂), 3.66 (4H, t, *J* = 6.25Hz, CH₂), 3.48 (2H, s, CH₂), 2.20 (2H, t, *J* = 6, CH₂), 2.17 (12H, s, CH₃) 1.59 – 1.31 (6H, m, CH₂). **¹³C NMR** (75.5 MHz, CDCl₃) δ 77.4, 77.2, 76.8, 70.5, 64.6, 62.7, 62.6, 58.1, 47.3, 32.2, 28.6, 26.4, 25.2, 23.2. **HRMS** (ESI) calcd for C₃₄H₄₉N₃O₁Fe₂ *m/z* 627.3012 found 627.3013.

N,N-Diisopropylferrocenecarboxamide **86**



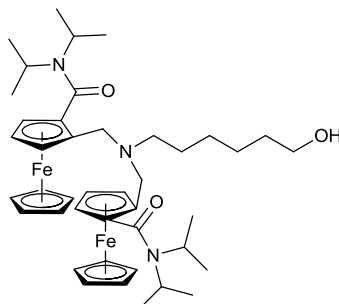
Ferrocenecarboxylic acid (1 g, 4.35 mmol) was dissolved in dry CH_2Cl_2 (15 mL) and was treated with oxalyl chloride (1.1 g, 0.7 mL, 8.69 mmol) under an inert atmosphere and was stirred at room temperature for 30 mins to obtain a red solution. Excess oxalyl chloride was removed under vacuum. The residue was re-dissolved in CH_2Cl_2 (15 mL) and cooled to 0°C . Diisopropylamine (0.4 g, 0.6 mL, 4.35 mmol) in dry CH_2Cl_2 was added dropwise followed by triethylamine (0.44 g, 0.6 mL, 4.35 mmol) and the reaction was left to continue over night. The reaction mixture was treated with NH_4Cl (30 mL) and extracted with CH_2Cl_2 (30 mL). The organic layer was washed with water (30 mL) and dried over MgSO_4 and solvent was removed to yield an off yellow solid (0.92 g, 66%). $^1\text{H NMR}$ (300 MHz, CDCl_3) δ 4.53 (2H, s, FcH), 4.25 (2H, s, FcH), 4.21 (5H, s, FcH), 3.89 (2H, m, CH), 1.50 (12H, s, CH_3). $^{13}\text{C NMR}$ (75.5 MHz, CDCl_3) δ 171.6, 72.8, 72.4, 70.9, 68.8, 54.6, 21.3. Data is in accordance with literature.¹⁶³

2-Formyl-*N,N*-diisopropylferrocenecarboxamide **158**



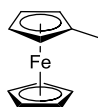
n-Butyl lithium (1.69 mL, 17.33 mmol) was added to a stirring solution of *N,N*-diisopropylferrocenecarboxamide (1 g, 4.11 mmol) in dry ether (40 mL). The reaction mixture was stirred at room temperature for 16 hours. DMF (0.41 mL, 5.36 mmol) was then added and the reaction mixture was stirred for four hours, water (30 mL) was then added and the product was extracted with ether (30 mL). The organic fraction was dried over MgSO₄ and the solvent was removed to yield the crude product as a dark orange solid. The crude product was purified by column chromatography (ethyl acetate:hexane 1:9) to afford the product as an orange solid (1.18g, 56%). **IR** (cm⁻¹): 3212, 3201, 3164, 3101, 2972, 2934, 2204, 2049, 1729, 1727, 1700, 1634, 1458. **¹H NMR** (300 MHz, CDCl₃) δ 9.88 (1H, s, CHO), 4.47 (1H, s, FcH), 4.24 (1H, s, FcH), 4.20 (1H, s, FcH), 4.18 (5H, s, FcH), 3.92 (2H, m, CH₂), 1.53 (12H, s, CH₃). **¹³C NMR** (75.5 MHz, CDCl₃) δ 194.7, 171.7, 72.3, 72.0, 70.8, 68.8, 54.6, 21.1. **HRMS** (ESI) calcd for C₁₈H₂₃N₁O₂Fe₁ *m/z* 341.1078 found 341.1079.

2,2'-(6-Hydroxyhexylazanedy)bis(methylene)bis(*N,N*-diisopropylferrocenecarboxamide) **157**



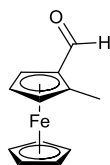
2-formyl-*N,N*-diisopropylferrocenecarboxamide (1 g, 4.04 mmol) was dissolved in dry THF (30 mL). 6-aminohexan-1-ol (0.25 g, 2.13 mmol) was added. Then Sodium triacetoxyborohydride (1.3 g, 6.16 mmol) was added to the reaction mixture. The solution was stirred under nitrogen at room temperature overnight. Ethyl acetate (20 mL) and 1N NaOH (20 mL) were then added and the organic layer was then extracted with NaCO₃ (25 mL), Brine (25 mL) and Milli Q filtered water (25 mL) then dried over MgSO₄ and the solvent removed unvacuo to afford the crude product, the crude product was then purified *via* column chromatography (9:1-7:3, hexanes:EtOAc) to afford the product as an orange oil (0.96 g, 75%). **IR** (cm⁻¹): 3215, 3207, 3164, 3111, 2970, 2930, 2214, 2047, 1753 1700, 1632. **¹H NMR** (300 MHz, CDCl₃) δ 4.34 (2H, s, FcH), 4.29 (2H, s, FcH), 4.25 (2H, s, FcH), 4.19 (10H, s, FcH), 3.91 (2H, m, CH) 3.63 (4H, t, *J* = 6, CH₂), 3.46 (2H, s, CH₂), 2.23 (2H, t, *J* = 6, CH₂), 2.17 (12H, s, CH₃) 1.56 – 1.30 (6H, m, CH₂). **¹³C NMR** (75.5 MHz, CDCl₃) δ 172.4, 77.6, 77.5, 76.7, 70.5, 63.3, 62.6, 59.2, 58.4, 33.1, 28.7, 25.5, 22.9, 21.6. **HRMS** (ESI) calcd for C₃₄H₄₉N₃O₁Fe₂ *m/z* 627.3012 found 627.3013.

Methylferrocene **152**



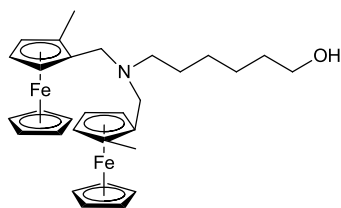
n-Butyl lithium (1.69 mL, 17.33 mmol) was added dropwise to a stirring solution of ferrocene (0.5 g, 2.68 mmol) in dry ether (30 mL). The reaction mixture was stirred at room temperature for 16hrs, then iodomethane (0.17 mL, 2.68 mmol) was added and the reaction was left for a further 4hrs. Water (30 mL) was then added and the product was extracted with ether (30 mL). The organic fraction was dried over MgSO₄ and the solvent was removed to yield the crude product, which was then purified *via* column chromatography (9:1, hexanes:EtOAc) to afford the product as an orange powder (0.59 g, 68%). **¹H NMR** (300 MHz, CDCl₃) δ 4.15 (2H, s, FcH), 4.12 (2H, s, FcH), 4.09 (5H, s, FcH), 2.32 (3H, s, CH₃). **¹³C NMR** (75.5 MHz, CDCl₃) δ 72.8, 72.4, 70.9, 68.8, 14.2. **HRMS** (ESI) calcd for C₁₁H₁₂Fe₁ *m/z* 200.0532 found 200.0533. Data in accordance with literature.¹⁶⁴

Methylferrocenecarboxaldehyde **153**



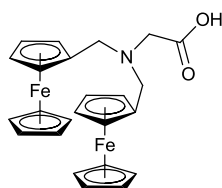
n-Butyl lithium (1.69 mL, 17.33 mmol) was added dropwise to a stirring solution of methylferrocene (0.5 g, 2.68 mmol) in dry ether (30 mL). The reaction mixture was stirred at room temperature for 16hrs, then DMF (0.17 mL, 2.68 mmol) was added and the reaction was left for a further 4hrs. Water (30 mL) was then added and the product was extracted with ether (30 mL). The organic fraction was dried over MgSO₄ and the solvent was removed to yield the crude product (0.6 g, 73%). **¹H NMR** (300 MHz, CDCl₃) δ 9.91(1H, s, CHO) 4.15 (2H, s, FcH), 4.12 (2H, s, FcH), 4.09 (5H, s, FcH), 2.36 (3H, s, CH₃). **¹³C NMR** (75.5 MHz, CDCl₃) δ 192.0 72.8, 72.4, 71.5, 70.9, 68.8, 14.2. **HRMS** (ESI) calcd for C₁₂H₁₃O₁Fe₁ *m/z* 228.1052 found 228.1052.

6-(bis((2-methylferrocenyl)methyl)amino)hexan-1-ol **151**



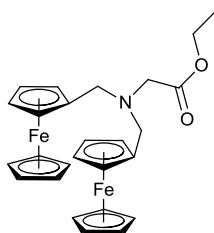
Methylferrocenecarboxaldehyde (1 g, 5 mmol) was dissolved in dry THF (30 mL). 6-aminohexan-1-ol (0.25 g, 2.13 mmol) was added. Then Sodium triacetoxyborohydride (1.3 g, 6.16 mmol) was added to the reaction mixture. The solution was stirred under nitrogen at room temperature overnight. Ethyl acetate (20 mL) and 1N NaOH (20 mL) were then added and the organic layer was then extracted with NaCO₃ (25 mL), Brine (25 mL) and Milli Q filtered water (25 mL) then dried over MgSO₄ and the solvent removed to afford the crude product as an orange oil, which was purified *via* column chromatography (6:4, hexanes, EtOAc) to afford the product as a dark orange oil (0.95 g, 65%). **IR** (cm⁻¹): 3226, 3207, 3167, 3099, 2976, 2964, 2204, 2049, 1632, 1466. **¹H NMR** (300 MHz, CDCl₃) δ 4.21 (2H, s, CH₂), 4.18 (2H, s, FcH), 4.17 (2H, s, FcH), 4.13 (10H, s, FcH), 3.63 (4H, t, *J* = 6.25, CH₂), 3.42 (2H, s, CH₂), 2.41 (6H, s, CH₃), 2.28 (2H, t, *J* = 6.25, CH₂), 1.47 – 1.28 (8H, m, CH₂). **¹³C NMR** (75.5 MHz, CDCl₃) δ 76.7, 76.4, 74.6, 72.8, 72.4, 65.2, 63.1, 58.6, 33.1, 28.7, 25.6, 23.2, 18.6. **HRMS** (ESI) calcd for C₃₀H₄₇N₁O₁Fe₂ *m/z* 539.8232 found 539.8233.

2-(bis(ferrocenylmethyl)amino)acetic acid **160**



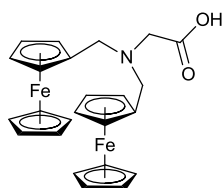
Ferrocene carboxaldehyde (2.1 g, 9.81 mmol) was added to a round bottomed flask containing dry THF (20 mL). Glycine (0.5 g, 6.66 mmol) was added to the solution and the reaction was stirred under N₂. Sodium triacetoxyborohydride (2.3 g, 10.90 mmol) was added portionwise to the stirring solution. The reaction was stirred overnight. The solution was then partitioned between ethyl acetate (40 mL) and 1M aqueous sodium hydroxide (40 mL). The organic fraction was washed with saturated aqueous NaHCO₃ (20 mL), brine (40 mL) and water (40 mL). The organic fraction was dried using MgSO₄ and the solvent was removed to afford the crude product as an dark orange solid. The crude product was purified *via* column chromatography (7:3, hexanes:EtOAc) to afford the product as an orange solid (1.66 g 64%). **IR** (cm⁻¹): 3212, 3201, 3164, 3101, 2972, 2934, 2204, 2049, 1729, 1632, 1466 **¹H NMR** (250 MHz, CDCl₃) δ 4.09 (2H, s, FcH), 4.05 (2H, s, FcH), 4.02 (12H, s, FcH), 3.55 (4H, t, *J* = 6.75, CH₂), 3.35 (2H, s, CH₂), 1.979 (1H, s, OH). **¹³C NMR** (75.5 MHz, CDCl₃) δ 171.5, 78.0, 77.5, 77.1, 68.9, 67.4, 61.1. **HRMS** (ESI) calcd for C₂₄H₂₅N₁O₂Fe₂ m/z: 477.3974 found 477.3973.

Ethyl 2-(bis(ferrocenylmethyl)amino)acetate **164**



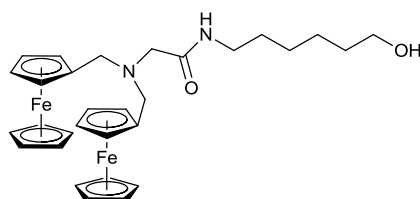
To a stirred solution of ferrocenecarboxaldehyde (1 g, 4.67 mmol) in dry THF (40 mL) was added glycine ethyl ester (0.32 g, 2.34 mmol) and TEA (1.6 mL, 11.50 mmol) the reaction mixture was stirred at room temperature for 5 minutes. Sodium triacetoxyborohydride (1.055 g, 5 mmol) was then added and the reaction mixture was stirred at room temperature for 12 hours. The reaction mixture was quenched with water (40 mL) and extracted with EtOAc (2 x 30 mL). The combined organic fractions were then washed with saturated aqueous NaHCO₃ (30 mL) and brine (30 mL). The organic fraction was dried over MgSO₄ and the solvent was removed to yield the crude product as deep orange oil. The crude product was purified *via* column chromatography (9:1, hexanes:EtOAc – 7:3, hexanes:EtOAc) to afford the product as an orange solid (1.28 g, 97%). ¹H NMR (300 MHz, CDCl₃) δ 4.21 (4H, s, FcH), 4.11 (6H, m, CH₂), 4.07 (10H, s, FcH), 3.63 (4H, s, CH₂), 3.16 (2H, s, CH₂), 1.24 (3H, t, *J* = 6.5, CH₃). ¹³C NMR (75.5 MHz, CDCl₃) δ 171.5, 83.10, 70.17, 68.55, 68.06, 60.22, 52.97, 14.35. HRMS (ESI) calcd for C₂₆H₂₉N₁O₂Fe₂ m/z: 499.1884 found C₂₆H₃₀N₁O₂Fe₂ m/z 500.1019. Data in accordance with literature¹⁶⁵

Alternative preparation of 2-(bis(ferrocenylmethyl)amino)acetic acid **160**



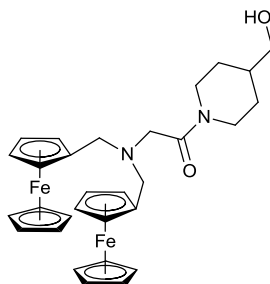
Ethyl 2-(bis(ferrocenylmethyl)amino)acetate (1 g, 2 mmol) was dissolved in ethanol (40 mL) and sodium hydroxide (0.24 g, 6.0 mmol). The solution was then heated to 50°C and stirred for 18 hours. Acetic acid was then added until the solution reached a pH of 6.5. The product was extracted in DCM (2x25 mL). The organic fraction was washed with brine (3x20 mL) and MilliQ filtered water (3x20 mL). The organic layer was dried over MgSO₄ and the solvent removed to afford the crude product, which was purified *via* column chromatography (7:3, hexanes:ethylacetate) to yield the product as a dark yellow solid (0.87 g, 85%). **¹H NMR** (250 MHz, CDCl₃) δ 4.09 (2H, s, FcH), 4.05 (2H, s, FcH), 4.02 (10H, s, FcH), 3.54 (4H, t, *J* = 6.75, CH₂), 3.34 (2H, s, CH₂), 1.99 (1H, s, OH). **¹³C NMR** (75.5Hz, CDCl₃) δ 171.5, 78.0, 77.5, 77.1, 68.9, 67.4, 61.1. **HRMS** (ESI) calcd for C₂₄H₂₅N₁O₂Fe₂ m/z: 477.3974 found 477.3974.

2-(bis(ferrocenylpentylmethyl)amino)-*N*-(6-hydroxyhexyl)acetamide **161**



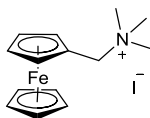
Oxalyl chloride (0.87 mL, 8.69 mmols) in dry CH_2Cl_2 (2 mL) was added dropwise *via* a pressure equalising dropping funnel to a stirred solution of 2-(bis(ferrocenylmethyl)amino)acetic acid (1 g, 4.35 mmol) in dry CH_2Cl_2 (100 mL) at 0°C under N_2 . The reaction warmed to room temperature and stirred for 2hrs. Then the solvent was removed and the acid chloride product was taken up in dry CH_2Cl_2 (75 mL). 6 – amino hexan – 1 – ol (0.56 g, 4.78 mmols) in dry CH_2Cl_2 (75 mL) was added dropwise *via* a dropping funnel at 0°C under N_2 . The reaction was then stirred for 2hrs while warming to room temperature. The solution was then washed with NaHCO_3 (100 mL) and 1.0M HCL (100 mL). The organic fraction was dried over MgSO_4 then the solvent was removed to afford the crude product as a dark orange solid, which was purified by column chromatography (7:3-hexanes:EtOAc) to afford the product as a dark yellow solid (1.23 g, 79%). **IR** (cm^{-1}): 3222, 3205, 3174, 3111, 2972, 2934, 2204, 2049, 1700, 1632, 1466. **^1H NMR** (250MHz, CDCl_3) δ 4.16 (4H, t, $J = 6$, FcH), 4.13 (4H, t, $J = 6$, FcH), 4.11 (10H, s, Fc), 3.55 (4H, t, $J = 6.25$, CH_2), 3.31 (2H, s, CH_2), 1.48 – 1.18 (8H, m, CH_2). **^{13}C NMR** (75.5Hz, CDCl_3) δ 173.3, 77.8, 77.3, 76.9, 62.1, 38.8, 35.4, 32.0, 30.6, 26.7, 25.5, 25.4. **HRMS** (ESI) calcd for $\text{C}_{24}\text{H}_{25}\text{N}_1\text{O}_2\text{Fe}_2$ m/z: 576.0988 found 576.0988.

2-(bis(ferrocenylmethyl)amino)-1-(4-(hydroxymethyl)piperidin-1-yl)ethanone **165**



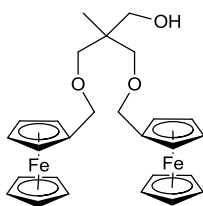
Oxalyl chloride (0.87 mL, 8.69 mmols) in dry CH_2Cl_2 (2 mL) was added dropwise *via* a pressure equalising dropping funnel to a stirred solution of 2-(bis(ferrocenylmethyl)amino)acetic acid (1 g, 4.35 mmol) in dry CH_2Cl_2 (100 mL) at 0°C under N_2 . The reaction warmed to room temperature and stirred for 2hrs. Then the solvent was removed and the acid chloride product was taken up in dry CH_2Cl_2 (75 mL). 4-piperidene methanol (0.56 g, 4.78 mmols) in dry CH_2Cl_2 (75mL) was added dropwise *via* a dropping funnel at 0°C under N_2 . The reaction was then stirred for 2hrs while warming to room temperature. The solution was then washed with NaHCO_3 (100 mL) and 1.0M HCL (100 mL). The organic fraction was dried over MgSO_4 then the solvent was removed to afford the crude product as an orange solid. The crude product was purified *via* column chromatography (8:2-6:4, hexanes:EtOAc) to afford the product as a light orange oil (1.31 g, 85%). **IR** (cm^{-1}): 3212, 3201, 3164, 3101, 2972, 2934, 2204, 2049, 1700, 1495. **^1H NMR** (250MHz, CDCl_3) δ 4.19 (2H, s, FcH), 4.15 (2H, s, FcH), 4.11 (10H, s, FcH), 3.65 (4H, t, $J = 6.0$, CH_2), 3.55 (2H, s, CH_2), 1.48 – 1.18 (5h, m, CH_2). **^{13}C NMR** (75.5 MHz, CDCl_3) δ 173.3, 77.8, 77.9, 76.9, 62.1, 38.8, 35.4, 32.0, 30.7, 26.5, 25.5, 25.4. **HRMS** (ESI) calcd for $\text{C}_{24}\text{H}_{25}\text{N}_1\text{O}_2\text{Fe}_2$ m/z: 576.0988 found 576.1264

1-(ferrocenyl)-*N,N,N*-trimethylmethanaminium iodide **170**



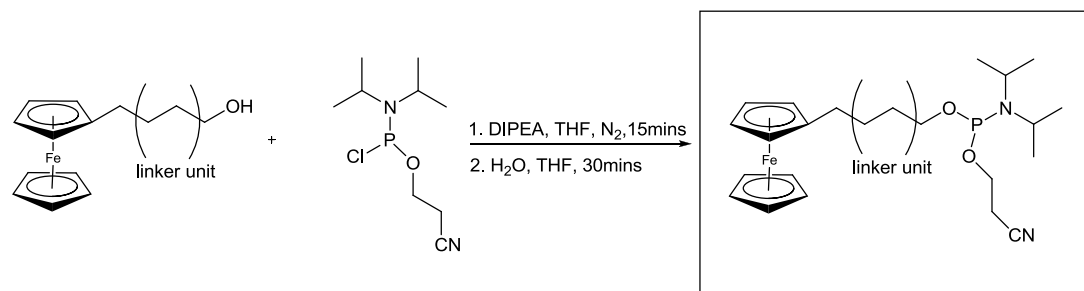
To a stirred solution of ((dimethylamino)methyl)ferrocene (3 g, 12.09 mmol) in MeOH (20 mL) was added methyl iodide (2.55 g, 18.02 mmol) and the reaction mixture was stirred at room temperature for 1 hour. The reaction mixture was then evaporated to dryness, the residue was taken up in MeOH and Et₂O was added and the product was filtered off. The filtrate was washed with cooled Et₂O (2 x 25 mL). The product was dried under reduced pressure to afford a pale orange crystalline solid (5.68 g, 99%). ¹H NMR (300 MHz, CDCl₃) δ 4.86 (2H, m, CH₂), 4.59 (2H, s, FcH), 4.34 (2H, s, FcH), 4.31 (5H, s, FcH), 3.31 (9H, s, CH₃) ¹³C NMR (75.5 MHz, CDCl₃) δ 77.7, 77.5, 76.3, 75.4, 70.4, 55.3. Data in accordance with literature¹⁶⁶

3-ferrocenylmethyl-2-(ferrocenylmethyl)-2-methylpropan-1-ol **167**



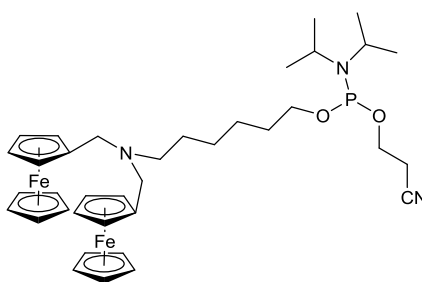
Trimethyl(ferrocenylmethyl) ammonium iodide (3.2 g, 8 mmol), 1,1 – tris(hydroxymethyl) – ethane (0.5 g, 4 mmol) and potassium carbonate (1g, 8 mmol) were dissolved in dry acetonitrile (100 mL) and refluxed for 6hrs. The solvent was then removed in vacuo and the residue was portioned between water (30 mL) and dichloromethane (30 mL). The aqueous layer was re-washed with dichloromethane. The combined organic fractions were dried over MgSO_4 , filtered and the solvent was removed to afford the product as a yellow powder (2.5 g, 84%). $^1\text{H NMR}$ (300 MHz, CDCl_3) δ 4.17 (4H, s, FcH), 4.16 (4H, s, FcH), 4.11 (10H, s, FcH), 3.79 (4H, s, CH_2), 3.45 (2H, s, CH_2), 1.05 (4H, m, CH_2), 0.93 (3H, s, CH_3). $^{13}\text{C NMR}$ (75.5 MHz, CDCl_3) δ 77.8, 77.4, 76.9, 75.9, 70.5, 67.7, 64.1, 39.6, 15.8. **HRMS** (ESI) calcd for $\text{C}_{27}\text{H}_{32}\text{O}_3\text{Fe}_2$ m/z 546.1523 found $\text{C}_{27}\text{H}_{32}\text{O}_3\text{Fe}_2\text{Na}_1$ m/z 569.1487.

General synthetic procedure for phosphoramidite synthesis



N, N – diisopropylethylamine (0.4 mL, 8.4 mmol) was added to a stirred solution of the ferrocene derivative (2.1 mmol) in dry THF (25 mL) under a nitrogen atmosphere. 2 – cyanoethyldiisopropylchlorophosphoramidite (0.2 ml, 3.15 mmol) was added dropwise and the resulting mixture was stirred for 15mins. MilliQ filtered water (200 mL) was added and the solution was stirred for a further 30mins. Ethyl Acetate – Triethylamine (1:1, 25 mL) was added, a precipitate formed. The mixture was washed with saturated NaHCO₃ (25 mL) and MilliQ filtered water (25 mL). The organic fraction was dried over MgSO₄ and the solvent was removed under vacuo. The crude product was then purified by silica gel chromatography (petroleum ether: ethyl acetate 9:1).

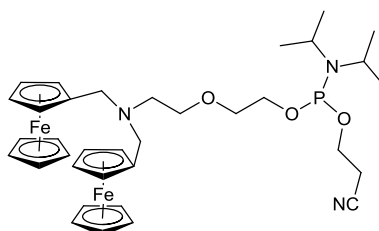
6-(bis(ferrocenylmethyl)amino)hexyl(2-cyanoethyl)diisopropylphosphoramidite **171**



¹H NMR (500 MHz, CDCl₃) δ 4.23 (4H, s, FcH), 4.18 (4H, s, FcH), 4.13 (10H, s, FcH), 3.61 (4H, t, *J* = 1.75, CH₂), 3.58 (2H, s, CH₂), 3.41 (2H, s, CH₂), 3.35 (2H, s, CH₂), 3.33 (2H, t, *J* = 6.5, CH), 2.65 (2H, t, *J* = 6.5, CH₂), 1.26 – 1.18 (8H, m, CH₂), 0.86 (12H, t, *J* = 7, CH₃). ¹³C NMR (75.5 MHz, CDCl₃) δ 111.6, 77.2, 77.0,

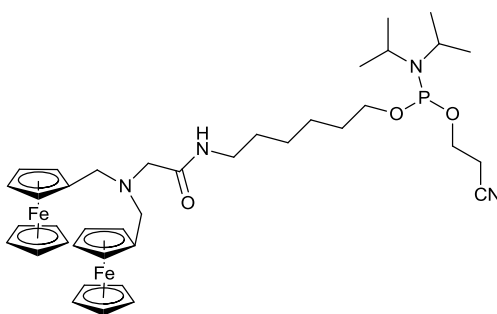
76.7, 68.5, 67.8, 52.5, 42.9, 25.7, 23.6, 22.5, 21.4, 14.1. ^{31}P NMR (DEC) (202.5Hz, CDCl_3) δ 147.32. HRMS (ESI) calcd for $\text{C}_{37}\text{H}_{50}\text{N}_3\text{O}_3\text{Fe}_2\text{P}_1$ m/z: 711.2354 found 711.2354.

2-(2-(bis(ferrocenylmethyl)amino)ethoxy)ethyl(2-cyanoethyl)diisopropylphosphoramidite **150**



^1H NMR (500 MHz, CDCl_3) δ 4.20 (4H, s, FcH), 4.18 (4H, s, FcH), 4.15 (10H, s, FcH), 3.66 (4H, t, $J = 6.5$, CH_2), 3.60–3.52 (4H, m, CH_2), 3.48 (2H, s, CH_2), 2.71 (2H, t, $J = 6.5$, CH_2), 2.20 (2H, t, $J = 6.5$, CH_2), 0.86 (12H, t, $J = 7$, CH_3). ^{13}C NMR (75.5 MHz, CDCl_3) δ 171.1, 112.6, 77.2, 77.0, 76.7, 68.5, 67.8, 52.5, 42.9, 21.0, 14.3. ^{31}P NMR (DEC) (202.5Hz, CDCl_3) δ 148.28. HRMS (ESI) calcd for $\text{C}_{37}\text{H}_{50}\text{N}_3\text{O}_3\text{Fe}_2\text{P}_1$ m/z: 711.2354 found 711.2254.

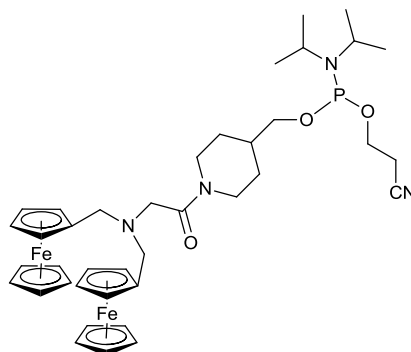
6-(2-(bis(ferrocenylmethyl)amino)acetamido)hexyl(2-cyanoethyl)diisopropylphosphoramidite **162**



^1H NMR (500MHz, CDCl_3) δ 4.16 (4H, t, $J = 6$, FcH), 4.13 (4H, t, $J = 6$, FcH), 4.11 (10H, s, Fc), 3.61 (2H, t, $J = 1.75$, CH_2), 3.55 (4H, t, $J = 6$, CH_2), 3.41 (2H, s, CH_2), 3.31 (2H, s, CH_2), 3.28 (2H, t, $J = 6$, CH), 2.65 (2H, t, $J = 6.5$, CH_2), 1.48 – 1.18 (8H, m, CH_2), 0.86 (12H, t, $J = 7$, CH_3). ^{13}C NMR (75.5 MHz, CDCl_3) δ

171.1, 111.6, 77.2, 77.0, 76.5, 68.0, 67.8, 52.5, 42.9, 21.4, 14.9. ^{31}P NMR (DEC) (202.5 MHz, CDCl_3) δ 147.24. HRMS (ESI) calcd for $\text{C}_{33}\text{H}_{43}\text{N}_3\text{O}_3\text{Fe}_2\text{P}_1$ m/z: 776.2534 found 776.25534.

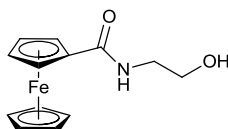
(1-(2-(bis(ferrocenylmethyl)amino)piperidin-4-yl)methyl(2-cyanoethyl)diisopropylphosphoramidite **246**



^1H NMR (500 MHz, CDCl_3) δ 4.23 (2H, s, Cp), 4.18 (2H, s, Cp), 4.13 (15H, s, Cp), 3.90-3.82 (2H, m, CH_2), 3.71-3.54 (4H, m, CH_2), 3.44 (4H, s, CH_2), 2.64 (2H, t, $J = 6$, CH_2), 2.35 (2H, t, $J = 6.5$, CH_2), 1.69 – 1.35 (5H, m, CH_2 , CH), 1.23 (12H, t, $J = 7$, CH_3). ^{13}C NMR (75.5 MHz, CDCl_3) δ 171.1, 111.7, 7.26, 77.0, 76.7, 68.5, 67.8, 52.5, 42.9, 21.0, 14.2. ^{31}P NMR (DEC) (202.5 MHz, CDCl_3) δ 148.43. HRMS (ESI) calcd for $\text{C}_{39}\text{H}_{53}\text{N}_4\text{O}_3\text{Fe}_2\text{P}_1$ m/z: 768.0973 found 768.1254.

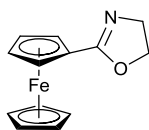
7.5 Synthesis of Oxazolines

N-(2-hydroxyethyl)ferrocenecarboxamide **213**



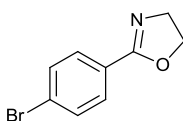
A solution of ferrocene carboxylic acid (1 g, 4.347 mmol) in dry dichloromethane (20 mL) was cooled to 0°C in an ice bath, to this solution oxalyl chloride (1.09 g, 0.72 mL, 8.694 mmol) was added and the reaction mixture was warmed to room temperature and stirred for 2 hrs. Excess oxalyl chloride was then removed *en vacuo*, the residue was then taken up in dry dichloromethane (20 mL). To which TEA (1.2 mL, 8.694 mmol) and ethanol amine (0.3 mL, 4.918 mmol) were added and the reaction mixture was stirred at room temperature overnight. The reaction mixture was diluted with dichloromethane (100 mL) and washed with water (2 x 25 mL). The organic fractions were combined and dried over MgSO₄ and the solvent was removed to yield a dark brown solid. The crude product was purified *via* column chromatography (7:3, dichloromethane:MeOH) to afford the product as an orange powder (1.08 g, 84%). ¹H NMR (300 MHz, CDCl₃) δ 6.17 (1H, s, NH), 4.62 (2H, s, FcH), 4.29 (2H, s, FcH), 4.15 (5H, s, FcH), 3.74 (2H, q, *J* = 4.5, CH₂), 3.49 (2H, q, *J* = 4.5, CH₂). ¹³C NMR (75.5 MHz, CDCl₃) δ 171.9, 71.5, 70.6, 69.8, 68.2, 62.9, 42.6. Data in accordance with literature.¹⁶⁷

2-Ferrocenyloxazoline **212**



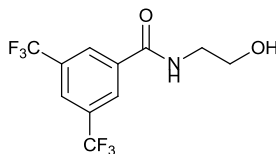
To an ice cold solution of N-(2-hydroxyethyl)ferrocenecarboxamide (0.5 g, 1.937 mmol) in dry dichloromethane (10 mL) was added TEA (0.39 g, 0.53 mL, 3.875 mmol) followed by methane sulfonyl chloride (0.22g, 0.149 mL, 1.937 mmol). The reaction mixture was stirred at 0°C for 1 hr, the reaction mixture was then diluted with dichloromethane (100 mL) and washed with water (2 x 50 mL). The organic fractions were combined and dried over MgSO₄ and the solvent was removed to afford deep red oil that was used without further purification. The oil residue was taken up in a 0.5M sodium hydroxide solution in water/MeOH (1:1, 50 mL) and the reaction mixture was refluxed for 3 hrs. The reaction mixture was then allowed to cool to room temperature, diluted with water (50 mL) and extracted with dichloromethane (3 x 25 mL). The combined organic fractions were dried over MgSO₄ and the solvent was removed to yield the crude product as a brown solid. The crude product was purified *via* column chromatography (8:2, hexanes:EtOAc) to afford the product as a dark orange solid (0.37, 75%). **¹H NMR** (300 MHz, CDCl₃) δ 4.67 (2H, s, FcH), 4.27 (4H, at, *J* = 9.6, FcH, CH₂), 4.13 (5H, s, FcH) 3.83 (2H, t, *J* = 9.3, CH₂). **¹³C NMR** (75.5 MHz, CDCl₃) δ 167.2, 70.5, 70.2, 70.1, 69.8, 69.6, 68.9, 6.3, 54.7, 53.4. Data in accordance with literature.¹⁶⁸

2-(4-Bromophenyl)-4,5-dihydrooxazole **220**



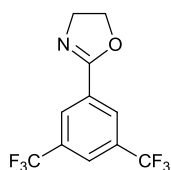
To a solution of *p*-bromobenzaldehyde (1.5 g, 8.1 mmol) in *tert*-butyl alcohol (80 mL) was added ethanol amine (0.49 g, 0.49 mL, 8.1 mmol). The reaction mixture was stirred at room temperature for 30 mins under an inert atmosphere, then K_2CO_3 (3.35 g, 24.3 mmol) and iodine (4.09 g, 16.2 mmol) were added to the reaction mixture and the solution was heated at 70°C for 18 hrs. After the reaction mixture had been cooled to room temperature the reaction mixture was quenched with saturated Na_2SO_3 until the iodine colour had almost disappeared and was extracted with ether (3 x 25 mL). the combined organic fractions were washed with brine (2 x 20 mL) and dried over Na_2SO_4 . The solvent was then removed to yield the crude product as an off white solid. The crude product was purified *via* column chromatography (8:2, hexanes:EtOAc) to afford the product as a white powder (1.43 g, 72%). MP: 95-97°C. 1H NMR (300 MHz, $CDCl_3$) δ 7.74 (2H, d, $J = 8.7$, ArCH), 7.47 (2H, d, $J = 8.7$, ArCH), 4.36 (2H, t, $J = 9.6$, CH_2), 3.98 (2H, t, $J = 9.6$, CH_2). ^{13}C NMR (75.5 MHz, $CDCl_3$) δ 163.9, 131.6, 129.7, 126.6, 125.9, 61.8, 54.9. Data in accordance with literature.¹³⁹

N-(2hydroxyethyl)-3,5-bis(trifluoromethyl)benzamide **231**



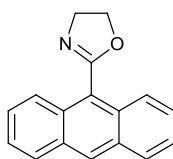
To a solution of 3,5-bistrifluorobenzoic acid (3 g, 11.63 mmol) in dry dichloromethane (50 mL) was added amino ethanol (0.7 mL, 11.63mmol), EDCI (1.9 g, 12.78 mmol), HOBT (1.7 g, 12.78 mmol) and triethylamine (3.2 mL, 22.77 mmol) and the reaction mixture was stirred at room temperature for 12 hours. The reaction mixture was then filtered and washed with water (30 mL), the organic fraction was dried over MgSO₄ and the solvent was removed to afford the crude product as an off white solid, which was purified *via* column chromatography (95:5, CH₂Cl₂:MeOH) to afford the product as a white solid (2.55 g, 69%). **¹H NMR** (300 MHz, CDCl₃) δ 8.34 (2H, s, ArCH), 7.90 (1H, s, ArCH), 4.44 (2H, t, *J* = 10.2, CH₂), 4.05 (2H, t, *J* = 10.2, CH₂). **¹³C NMR** (75.5 MHz, CDCl₃) δ 162.2, 132.6, 132.1, 131.7, 131.2, 129.9, 128.3, 128.3, 124.7, 124.6, 124.6, 124.5, 121.1, 117.5, 68.3, 55.1. **¹⁹F NMR** (376 MHz; CDCl₃) δ -63.41. Data in accordance with literature.¹⁶⁹

2-(-3,5-Bis(trifluoromethyl)phenyl)-2-oxazoline **232**



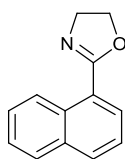
N-(2-hydroxyethyl)-3,5-bis(trifluoromethyl)benzamide (1.2 g, 3.99 mmol) was dissolved in dry dichloromethane (20 mL) and cooled to 0 °C. To which methane sulfonyl chloride (0.3 mL, 3.99 mmol) and triethylamine were added and the reaction mixture was stirred at 0 °C for 1 hours. The solution was then diluted with dichloromethane (100 mL) and washed with water (2 x 50 mL). The organic fraction was dried over MgSO₄ and the solvent was removed. The crude colourless oil residue was then dissolved in 0.5M sodium hydroxide (50 mL, 1:1 H₂O:MeOH) and the reaction mixture was refluxed for 3 hours. The reaction mixture was allowed to cool to room temperature and diluted with water (50 mL) and extracted with dichloromethane (3 x 25 mL), the combined organic fractions were dried over MgSO₄ and the solvent was removed to afford the crude product as a white product. The crude product was purified *via* column chromatography (7:3, hexanes:EtOAc) to afford the product as a white product (0.98 g, 82%). **IR** (cm⁻¹): 2968, 2924, 2234, 2167, 1701, 1632, 1466. **¹H NMR** (300 MHz; CDCl₃) δ 8.34 (2H, s, ArCH), 7.90 (1H, s, ArCH), 4.44 (2H, t, *J* = 10.2, CH₂), 4.05 (2H, t, *J* = 9.3, CH₂). **¹³C NMR** (75.5 MHz; CDCl₃) δ 162.21, 132.64, 132.19, 131.74, 129.92, 128.32, 124.78, 68.30, 55.11. **¹⁹F NMR** (376 MHz, CDCl₃) δ -61.94.

2-(anthracen-9-yl)-2-oxazoline **222**



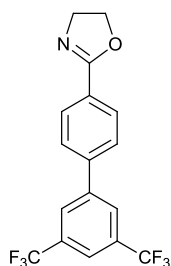
To a solution of 9 – anthracenecarboxaldehyde (0.406 g, 2 mmol) in *tert*-butyl alcohol (20 mL) was added aminoethanol (0.12 mL, 2 mmol). The mixture was stirred at room temperature under an inert atmosphere for 30 mins. Potassium carbonate (0.828 g, 6 mmol) and iodine (1.012 g, 4 mmol) were then added and the reaction mixture was heated at 70°C for 18 hours. The reaction mixture was then allowed to cool to room temperature and was quenched with satd aq Na₂SO₃, until the iodine colour was lost and was extracted with Et₂O (25 mL). The organic layer was washed with brine (20 mL) and dried over Na₂SO₄. The solvent was removed and the product was purified *via* column chromatography (8:2, hexanes:EtOAc) to afford the product as a dark orange oil (0.34, 65%). ¹H NMR (300 MHz; CDCl₃) δ 8.53 (1H, m, ArH), 7.90 (4H,d, *J* = 7.5, ArH), 7.43 (4H, d, *J* = 7.5, ArH), 3.96 (2H, t, *J* = 6.2, CH₂), 3.46 (2H, t, *J* = 6.2, CH₂). ¹³C NMR (75.5 MHz; CDCl₃) δ 164.2, 138.2, 131.9, 128.4, 128.2, 127.4, 125.3, 123.9, 64.8, 58.6.

2-(Naphthalene-1-yl)oxazoline **221**



To a solution of 1-naphthalenecarboxaldehyde (0.2 g, 1.2 mmol) in *tert*-butyl alcohol (10 mL) was added aminoethanol (0.07 mL, 1.2 mmol) and the solution was stirred at room temperature for 30 mins under an inert atmosphere. Potassium carbonate (0.49 g, 3.6 mmol) and iodine (0.6 g, 2.4 mmol) were added and the reaction mixture was heated at 70°C for 18 hours. After cooling to room temperature the reaction was quenched with Na₂SO₃ and extracted with Et₂O. The organic fraction was washed brine (20 mL) and dried over Na₂SO₄ and the solvent was removed to afford the crude product as an oil, which was purified by column chromatography (8:2, hexanes:EtOAc) to afford the product as a colourless oil (0.14 g, 69%). ¹H NMR (300 MHz, CDCl₃) δ 9.13 (1H, d, *J* = 8.5, ArH), 8.08 (1H, dd, *J* = 7.2, 0.3, ArH), 7.92 (1H, d, *J* = 8.2, ArH), 7.84 (1H, d, *J* = 8.2, ArH), 7.60-7.55 (1H, m, ArH), 7.50-7.43 (2H, m, ArH) 4.39 (2H, t, *J* = 9.2, CH₂), 4.17 (2H, t, *J* = 9.2, CH₂). ¹³C NMR (75.5 MHz, CDCl₃) δ 164.2, 133.5, 131.4, 131.2, 128.5, 128.1, 127.3, 126.4, 126.0, 124.2, 124.0, 66.4, 55.7. Data in accordance with literature.¹³⁹

2-(3',5'-nistrifluoromethyl)-[1,1'-biphenyl]-4-yl)-oxazoline **228**



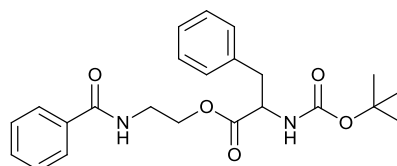
To an oven dried carousel tube was added 2-(4-bromophenyl)oxazoline (0.2 g, 0.88 mmol) and the flask was purged with argon for 30 mins. 3,5-bis(trifluoromethyl)benzeneboronic acid (0.25 g, 1.32 mmol), Pd(PPh₃)₄ (0.101 g, 0.088 mmol), K₂CO₃ (0.24 g, 1.76 mmol) and ethanol (4 mL) were added under an atmosphere of argon. The reaction mixture was then heated at 80°C for 12 hours. Upon cooling to room temperature the reaction mixture was passed through a pad of celite and the celite pad was washed with EtOAc (30 mL). the organics were then washed with water (15 mL) and dried over MgSO₄. The solvent was removed to yield the crude compound as an off white solid. The crude product was purified *via* column chromatography (8:2, hexanes:EtOAc) to afford the compound as a white powder (0.45 g, 74%). **IR** (cm⁻¹): 3101, 2972, 2954, 2199, 2053, 1701, 1648, 1421. **¹H NMR** (400 MHz, CDCl₃) δ 8.09 (1H, d, *J* = 5.25, ArH), 7.91-7.82 (1H, m, ArH), 7.74-7.49 (5H, m, ArH), 4.52 (2H, t, *J* = 9.2, CH₂), 4.15 (2H, t, *J* = 9.2, CH₂). **¹³C NMR** (75.5 MHz, CDCl₃) δ 164.3, 142.4, 141.0, 133.0, 132.1, 131.9, 131.5, 130.4, 129.5, 128.6, 128.4, 127.4, 127.1, 124.5, 124.5, 124.0, 123.9, 67.7, 55.0. **¹⁹F NMR** (376 MHz, CDCl₃) δ -62.71. **HRMS** (ESI) calcd for C₁₇H₁₁F₆N₁O₁ m/z: 359.0745 found 359.0746.

General procedure:



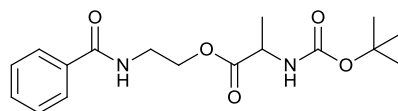
To a solution of oxazoline (3.0 mmol) in dry acetonitrile (3 mL) was added carboxylic acid (1.5 mmol) and heated at 80°C for 18 hours. The reaction mixture was then allowed to cool to room temperature and diluted with water (25 mL) and extracted with dichloromethane (3 x 25 mL), the combined organic fractions were dried over MgSO₄ and solvent removed.

2-((*tert*-Butoxycarbonyl)amino)-3-phenylpropanamido)ethyl benzoate **206**



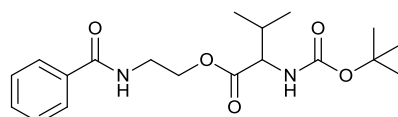
Phenylloxazoline (0.39 mL, 3.0 mmol), boc-phenylalanine (0.4 g, 1.5 mmol). Purified *via* column chromatography (7:3, hexanes:EtOAc) to yield the compound as a colourless oil (0.72 g, 92%). **IR** (cm⁻¹): 3167, 3111, 3025, 2949, 2901, 2211, 2023, 1729, 1648, 1436 **¹H NMR** (300 MHz, CDCl₃) δ 7.78 (2H, d, *J* = 7.2, ArCH), 7.45-7.33 (3H, m, ArH), 7.22-7.07 (5H, m, ArH), 4.95 (1H, d, *J* = 6.6, CH), 4.26-4.23 (2H, m, CH₂), 3.67-3.52 (2H, m, CH₂), 2.99 (2H, d, *J* = 6.9, CH₂), 1.32 (9H, s, CH₃) **¹³C NMR** (75.5 MHz, CDCl₃) δ 172.3, 162.4, 155.4, 135.8, 134.1, 131.5, 129.1, 128.7, 125.5, 127.2, 127.1, 80.3, 64.3, 55.0, 39.0, 38.0, 28.2. **HRMS** (ESI) calcd for C₂₃H₂₈N₂O₅ *m/z* 412.1998 found C₂₃H₂₉N₂O₅ *m/z* 413.1999.

2-(2-((*tert*-butoxycarbonyl)amino)propanamido)ethyl benzoate **207**



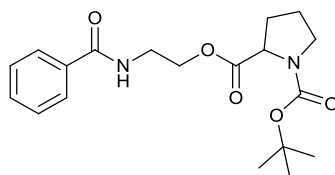
Phenyloxazoline (0.39 mL, 3.0 mmol), boc-alanine (0.28 g, 1.5 mmol). Purified *via* column chromatography (7:3, hexanes:EtOAc), to yield the title compound as a colourless oil (0.64 g, 93%). **IR** (cm^{-1}): 3168, 3107, 2967, 2938, 2209, 2053, 1728, 1727, 1723, 1636, 1459. **^1H NMR** (300 MHz, CDCl_3) δ 8.02 (2H, d, $J = 7.3$, ArH), 7.67-7.59 (3H, m, ArH), 4.37-4.32 (2H, m, CH_2), 4.29 (1H, d, $J = 6.5$, CH), 3.85-3.82 (2H, m, CH_2), 2.21-2.18 (1H, m, CH), 1.45 (3H, s, CH_3), 1.30 (9H, s, CH_3). **^{13}C NMR** (75.5 MHz, CDCl_3) δ 173.8, 167.5, 155.3, 134.3, 132.7, 128.5, 127.31 79.6, 62.6, 61.3, 38.3, 30.3, 28.9, 17.3. **HRMS** (ESI) calcd for $\text{C}_{17}\text{H}_{24}\text{N}_2\text{O}_5$ m/z 336.1685 found 336.1685.

2-(2-((*tert*-butoxycarbonyl)amino)-3-methylbutanamido)ethyl benzoate **208**



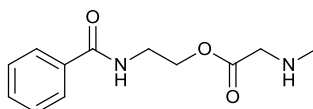
Phenyloxazoline (0.39 mL, 3.0 mmol), boc-valine (0.33 g, 1.5 mmol). Purified *via* column chromatography (7:3, hexanes:ethyl acetate) to afford the title compound as a colourless oil (0.064 g, 89%). **IR** (cm^{-1}): 3164, 3101, 2972, 2934, 2204, 2049, 1731, 1726, 1724, 1632, 1466. **^1H NMR** (300 MHz, CDCl_3) δ 8.03 (2H, d, $J = 7.1$, ArH), 7.65-7.58 (3H, m, ArH), 4.35-4.30 (2H, m, CH_2), 4.27 (1H, d, $J = 6.0$, CH), 3.81 (2H, m, CH_2), 2.21 (1H, m, CH), 1.31 (9H, s, CH_3), 0.89 (6H, dd, $J = 5.5$). **^{13}C NMR** (75.5 MHz, CDCl_3) δ 172.8, 167.3, 155.7, 134.2, 132.5, 128.0, 127.3, 79.7, 62.3, 61.3, 38.4, 30.2, 28.9, 18.7. **HRMS** (ESI) calcd for $\text{C}_{19}\text{H}_{28}\text{N}_2\text{O}_5$ m/z 364.1998 found 364.1997.

Tert-butyl 2-((2-(benzoyloxy)ethyl)carbamoyl)pyrrolidine-1-carboxylate **209**



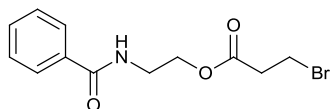
Phenyloxazoline (0.39 mL, 3.0 mmol), boc-proline (0.32 g, 1.5 mmol). Purified *via* column chromatography (7:3, hexanes:EtOAc), to yield the title compound as a colourless oil (0.53 g, 74%). **IR** (cm⁻¹): 3163, 3101, 2974, 2934, 2204, 2048, 1733, 1727, 1724, 1632, 1467. **¹H NMR** (300 MHz, CDCl₃) δ 8.03 (2H, d, *J* = 7.1, ArH), 7.65-7.58 (3H, m, ArH), 4.31 (2H, t, *J* = 6.25 CH₂), 4.27 (1H, s, CH), 3.82 (2H, t, *J* = 6.25, CH₂), 3.41-3.32 (2H, t, *J* = 7.0, CH₂) 1.73-1.46 (4H, m, CH₂), 1.38 (9H, s, CH₃). **¹³C NMR** (75.5 MHz, CDCl₃) δ 172.6, 167.5, 155.3, 134.5, 132.2, 128.3, 127.1, 79.4, 66.5, 62.3, 49.3, 38.6, 30.4, 28.2, 24.5. **HRMS** (ESI) calcd for C₁₉H₂₆N₂O₅ *m/z* 362.1842 found 362.1842.

2-(2-(Methylamino)acetamido)ethyl benzoate **210**



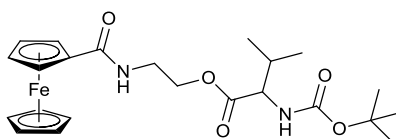
Phenyloxazoline (0.39 mL, 3.0 mmol), sarcosine (0.13 g, 1.5 mmol). Purified *via* column chromatography (7:3, hexanes:EtOAc), to yield the compound as a colourless oil (0.5 g, 95%). **IR** (cm⁻¹): 3031, 2972, 2934, 2204, 2049, 1731, 1727, 1724, 1632, 1495. **¹H NMR** (300 MHz, CDCl₃) δ 8.04 (2H, d, *J* = 7.1, ArH), 7.63-7.56 (3H, m, ArH), 4.34 (2H, t, *J* = 6.0 CH₂), 3.96 (3H, s, CH₃), 3.43 (2H, t, *J* = 7, CH₂), 3.23 (2H, s, CH₂). **¹³C NMR** (75.5 MHz, CDCl₃) δ 173.3, 166.2, 134.6, 133.2, 129.4, 128.3, 78.1, 63.5, 57.3, 38.2. **HRMS** (ESI) calcd for C₁₂H₁₆N₂O₃ *m/z* 236.1161 found 237.1160.

2-(3-bromopropanamido)ethyl benzoate **211**



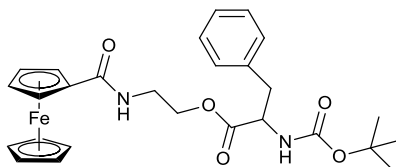
Phenyloxazoline (0.39 mL, 3.0 mmol), 3-bromopropionic acid (0.23 g, 1.5 mmol). Purified *via* column chromatography (7:3, hexanes:EtOAc), to yield the compound as a colourless oil (0.57 g, 92%). **IR** (cm^{-1}): 3164, 3087, 2972, 2934, 2206, 2049, 1727, 1724, 1720, 1632, 1466. **$^1\text{H NMR}$** (300 MHz, CDCl_3) δ 8.04 (2H, d, $J = 7.1$, ArH), 7.63-7.56 (3H, m, ArH), 4.34 (2H, t, $J = 7.5$ CH_2), 3.59 (2H, t, $J = 6.0$ CH_2), 3.48 (2H, t, $J = 7.5$, CH_2), 2.66 (2H, t, $J = 6.0$, CH_2). **$^{13}\text{C NMR}$** (75.5 MHz, CDCl_3) δ 176.6, 166.4, 133.6, 132.2, 128.4, 127.3, 63.6, 38.5, 38.2, 28.3. **HRMS** (ESI) calcd for $\text{C}_{12}\text{H}_{14}\text{N}_1\text{O}_3\text{Br}_1$ m/z 299.0156 found 299.0156.

2-(2-(*tert*-Butoxycarbonyl)amino)-3-methylbutanamido)ethyl ferrocenecarboxylate **214**



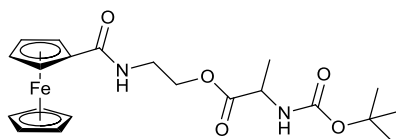
Ferroceneoxazoline (0.76 g, 3.0 mmol), boc-Val-OH (0.33 g, 1.5 mmol). Purified *via* column chromatography (7:3, hexanes: EtOAc), to yield the compound as an orange oil (0.83 g, 76%). **IR** (cm^{-1}): 3231, 3164, 3101, 2972, 2934, 2204, 2049, 1731, 1724, 1722, 1632, 1459. **$^1\text{H NMR}$** (300 MHz, CDCl_3) δ 4.55-4.43 (2H, m, CH_2), 4.27 (1H, d, $J = 6.0$, CH), 4.19 (2H, s, FcH), 4.15 (2H, s, FcH), 4.09 (5H, s, FcH), 3.83-3.76 (2H, m, CH_2), 2.23-2.12 (1H, m, CH), 1.33 (9H, s, CH_3), 0.86 (6H, dd, $J = 5.6$, CH_2). **$^{13}\text{C NMR}$** (75.5 MHz, CDCl_3) δ 172.8, 167.3, 155.7, 79.7, 78.4, 77.3, 77.2, 76.3, 62.3, 61.3, 38.4, 30.2, 28.9, 18.7. **HRMS** (ESI) calcd for $\text{C}_{23}\text{H}_{31}\text{N}_2\text{O}_5\text{Fe}_1$ m/z 471.1582 found $\text{C}_{23}\text{H}_{32}\text{N}_2\text{O}_5\text{Fe}_1$ m/z 472.1623.

2-(2-((*tert*-butoxycarbonyl)amino)-3-phenylpropanamido)ethyl ferrocenecarboxylate
215



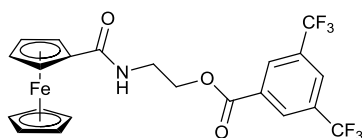
Ferroceneoxazoline (0.76 g, 3.0 mmol), boc-Phe-OH (0.4 g, 1.5 mmol). Purified *via* column chromatography (7:3, hexanes: EtOAc), to yield the compound as an orange oil (0.91 g, 79%). **IR** (cm^{-1}): 3164, 3101, 3012, 2972, 2934, 2204, 2049, 1731, 1726, 1724, 1632, 1466. **$^1\text{H NMR}$** (300 MHz, CDCl_3) δ 7.21-7.13 (5H, m, ArH), 4.97 (1H, d, $J = 6.6$, CH), 4.26-4.23 (2H, m, CH_2), 4.18 (2H, s, FcH), 4.16 (2H, s, FcH), 4.03 (5H, s, FcH), 3.67-3.52 (2H, m, CH_2), 2.94 (2H, d, $J = 6.6$, CH_2), 1.32 (9H, s, CH_3) **$^{13}\text{C NMR}$** (75.5 MHz, CDCl_3) δ 172.3, 166.9, 155.4, 135.8, 134.6, 131.5, 129.1, 128.7, 80.3, 77.8, 77.4, 76.7, 76.2, 64.3, 55.0, 39.0, 38.0, 28.2. **HRMS** (ESI) calcd for $\text{C}_{27}\text{H}_{31}\text{N}_2\text{O}_5\text{Fe}_1$ m/z 519.1583 found 519.1582.

2-(2-((*tert*-butoxycarbonyl)amino)propanamido)ethyl ferrocenecarboxylate **216**



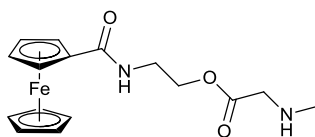
Ferroceneoxazoline (0.76 g, 3.0 mmol), boc-Ala-OH (0.28 g, 1.5 mmol). Purified *via* column chromatography (7:3, hexanes: ethyl acetate), to yield the compound as an orange oil (0.64 g, 76%). **IR** (cm^{-1}): 3173, 3121, 2982, 2912, 2200, 2050, 1728, 1724, 1722, 1633, 1462. **$^1\text{H NMR}$** (300 MHz, CDCl_3) δ 4.37-4.34 (2H, m, CH_2), 4.27 (1H, d, $J = 6.5$, CH), 4.17 (2H, s, FcH), 4.14 (2H, s, FcH), 4.10 (5H, s, FcH), 3.87-3.83 (2H, m, CH_2), 2.23-2.16 (1H, m, CH), 1.47 (3H, s, CH_3), 1.33 (9H, s, CH_3). **$^{13}\text{C NMR}$** (75.5 MHz, CDCl_3) δ 173.8, 167.5, 155.3, 79.6, 77.5, 77.1, 76.8, 76.4, 62.6, 61.3, 38.3, 30.3, 28.9, 17.3. **HRMS** (ESI) calcd for $\text{C}_{21}\text{H}_{27}\text{N}_2\text{O}_5\text{Fe}_1$ m/z 443.1270 found $\text{C}_{21}\text{H}_{28}\text{N}_2\text{O}_5\text{Fe}_1$ m/z 444.1341.

2-(3,5-bis(trifluoromethyl)benzamido)ethyl ferrocenecarboxylate **217**



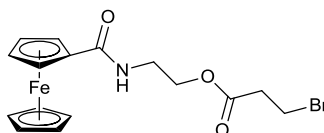
Ferroceneoxazoline (0.76 g, 3.0 mmol), 3,5-bis(trifluoromethyl)benzoic acid (0.38 g, 1.5 mmol). Purified *via* column chromatography (7:3, hexanes: EtOAc), to yield the compound as an orange oil (1.0 g, 88%). **IR** (cm^{-1}): 3172, 3102, 2973, 2939, 2214, 2044, 1730, 1727, 1724, 1632, 1476. **$^1\text{H NMR}$** (300 MHz, CDCl_3) δ 8.52 (2H, s, ArH), 8.02 (1H, s, ArH), 4.75 (2H, s, FcH), 4.35 (2H, s, FcH), 4.21 (2H, t, $J = 6.25$, CH_2), 4.09 (5H, s, FcH), 3.89 (2H, t, $J = 6.25$, CH_2). **$^{13}\text{C NMR}$** (75.5 MHz; CDCl_3) δ 172.3, 164.3, 132.5, 132.2, 132.0, 129.9, 126.7, 124.2, 70.9, 70.0, 68.4, 65.2, 39.8. **HRMS** (ESI) calcd for $\text{C}_{22}\text{H}_{17}\text{N}_1\text{O}_3\text{Fe}_1\text{F}_6$ m/z 513.0462 found 513.0461.

2-(2-methylamino)acetamido)ethyl ferrocenecarboxylate **218**



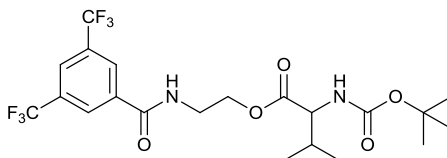
Ferroceneoxazoline (0.76 g, 3.0 mmol), sarcosine (0.13 g, 1.5 mmol). Purified *via* column chromatography (7:3, hexanes: EtOAc), to yield the compound as an orange oil (0.68 g, 76%). **IR** (cm^{-1}): 3167, 3103, 2976, 2929, 2208, 2052, 1735, 1728, 1723, 1629, 1476. **$^1\text{H NMR}$** (300 MHz, CDCl_3) δ 4.36 (2H, t, $J = 6.25$ CH₂), 4.18 (2H, s, FcH), 4.12 (2H, s, FcH), 4.08 (5H, s, FcH), 3.96 (3H, s, CH₃), 3.42 (2H, t, $J = 7$, CH₂), 3.25 (2H, s, CH₂). **$^{13}\text{C NMR}$** (75.5 MHz, CDCl_3) δ 173.3, 166.2, 78.1, 77.7, 77.3, 76.8, 76.2, 63.5, 57.3, 38.2. **HRMS** (ESI) calcd for $\text{C}_{16}\text{H}_{19}\text{N}_2\text{O}_3\text{Fe}_1$ m/z 343.0745 found $\text{C}_{16}\text{H}_{20}\text{N}_2\text{O}_3\text{Fe}_1$ m/z 344.1432.

2-(3-bromopropanamido)ethyl ferrocenecarboxylate **219**



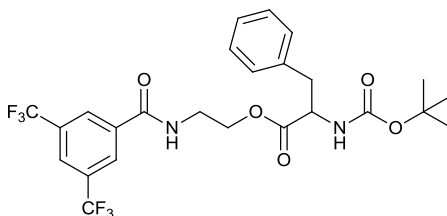
Ferroceneoxazoline (0.76 g, 3.0 mmol), 3-bromopropionic acid (0.23 g, 1.5 mmol). Purified *via* column chromatography (7:3, hexanes: ethyl acetate), to yield the compound as an orange oil (0.74 g, 93%). **IR** (cm^{-1}): 3101, 2972, 2934, 2204, 2049, 1737, 1725, 1722, 1635, 1469. **$^1\text{H NMR}$** (300 MHz, CDCl_3) δ 4.32 (2H, t, $J = 7.25$ CH₂), 4.16 (2H, s, FcH), 4.12 (2H, s, FcH), 4.09 (5H, s, FcH), 3.60 (2H, t, $J = 6.25$ CH₂), 3.52 (2H, t, $J = 7.25$, CH₂), 2.63 (2H, t, $J = 6.25$, CH₂). **$^{13}\text{C NMR}$** (75.5 MHz, CDCl_3) δ 176.6, 166.4, 77.6, 77.1, 76.7, 76.2, 63.6, 38.5, 38.2, 28.3. **HRMS** (ESI) calcd for $\text{C}_{16}\text{H}_{19}\text{N}_1\text{O}_3\text{Br}_1\text{Fe}_1$ m/z 407.9741 found 407.9742.

2-(2-((*tert*-butoxycarbonyl)amino)-3-methylbutanamido)ethyl-3,5-bis(trifluoromethyl)benzoate **235**



2-(3,5-Bis(trifluoromethyl)phenyl)-2-oxazoline (0.84 g, 3.0 mmol), boc-Val-OH (0.33 g, 1.5 mmol). Purified *via* column chromatography (7:3, hexanes: ethyl acetate), to yield the compound as a colourless oil (0.84 g, 88%). **IR** (cm^{-1}): 3162, 3110, 2970, 2935, 2201, 2053, 1733, 1724, 1632, 1462. **$^1\text{H NMR}$** (300 MHz, CDCl_3) δ 8.34 (2H, s, ArH), 7.91 (1H, s, ArH), 4.36-4.32 (2H, m, CH_2), 4.29 (1H, d, $J = 7.0$, CH), 3.79-3.72 (2H, m, CH_2), 2.19-2.05 (1H, m, CH), 1.34 (9H, s, CH_3), 0.91 (6H, dd, $J = 6.5$, CH_3). **$^{13}\text{C NMR}$** (75.5 MHz, CDCl_3) δ 172.8, 167.3, 155.7, 131.2, 130.8, 128.4, 127.2, 79.4, 62.7, 61.3, 38.6, 30.6, 28.7, 18.2. **$^{19}\text{F NMR}$** (376 MHz, CDCl_3) δ -63.24. **HRMS** (ESI) calcd for $\text{C}_{21}\text{H}_{26}\text{N}_2\text{O}_5\text{F}_6$ m/z 500.1746 found $\text{C}_{21}\text{H}_{27}\text{N}_2\text{O}_5\text{F}_6$ m/z 501.1649.

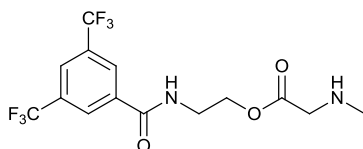
2-(2-((*tert*-butoxycarbonyl)amino)-3-phenylpropanamido)ethyl 3,5-bis(trifluoromethyl)benzoate **236**



2-(3,5-Bis(trifluoromethyl)phenyl)-2-oxazoline (0.84 g, 3.0 mmol), boc-Phe-OH (0.4 g, 1.5 mmol). Purified *via* column chromatography (7:3, hexanes: EtOAc), to yield the compound as a colourless oil (0.93 g, 91%). **IR** (cm^{-1}): 2982, 2924, 2209, 2009, 1731, 1726, 1724, 1629, 1501. **$^1\text{H NMR}$** (300 MHz, CDCl_3) δ 8.34 (2H, s,

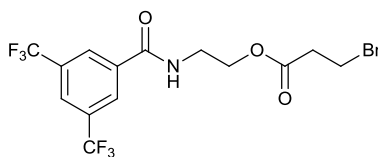
ArH), 7.93 (1H, s, ArH), 7.24-7.13 (5H, m, ArH), 4.96 (1H, d, $J = 6.6$, CH), 4.27-4.23 (2H, m, CH₂), 3.67-3.52 (2H, m, CH₂), 2.83 (2H, d, $J = 6.6$, CH₂), 1.32 (9H, s, CH₃) **¹³C NMR** (75.5 MHz, CDCl₃) δ 172.3, 167.4, 155.4, 135.8, 134.1, 131.5, 129.1, 128.7, 125.5, 127.2, 127.1, 80.3, 64.3, 55.0, 39.0, 38.0, 28.2. **¹⁹F NMR** (376 MHz, CDCl₃) δ -63.41 **HRMS** (ESI) calcd for C₂₅H₂₆N₂O₅F₆ m/z 548.1746 found C₂₅H₂₇N₂O₅F₆ m/z 549.1824.

2-(2-(methylamino)acetamido)ethyl 3,5-bis(trifluoromethyl)benzoate **237**



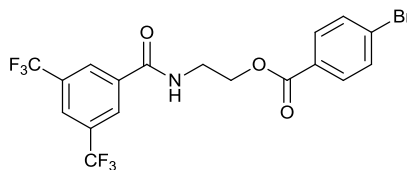
2-(3,5-Bis(trifluoromethyl)phenyl)-2-oxazoline (0.84 g, 3.0 mmol), sarcosine (0.13 g, 1.5 mmol). Purified *via* column chromatography (7:3, hexanes: ethyl acetate), to yield the compound as a colourless oil (0.67 g, 89%). **IR** (cm⁻¹): 3101, 2972, 2934, 2204, 2049, 1731, 1726, 1724, 1632, 1466. **¹H NMR** (300 MHz, CDCl₃) δ 8.36 (2H, s, ArH), 7.93 (1H, s, ArH), 4.41 (2H, t, $J = 6.25$, CH₂), 3.99 (3H, s, CH₃), 3.46 (2H, t, $J = 6.25$, CH₂), 3.25 (2H, s, CH₂). **¹³C NMR** (75.5 MHz, CDCl₃) δ 173.3, 166.2, 131.2, 130.4, 128.6, 127.6, 78.3, 63.1, 57.5, 38.1. **¹⁹F NMR** (376 MHz, CDCl₃) δ -63.36. **HRMS** (ESI) calcd for C₁₄H₁₄N₂O₃F₆ m/z 372.0909 found C₁₄H₁₅N₂O₃F₆ m/z 373.1233.

2-(3-bromopropanamido)ethyl 3,5-bis(trifluoromethyl)benzoate **238**



2-(-3,5-Bis(trifluoromethyl)phenyl)-2-oxazoline (0.84 g, 3.0 mmol), 3-bromopropionic acid (0.23 g, 1.5 mmol). Purified *via* column chromatography (7:3, hexanes: EtOAc), to yield the compound as a colourless oil (0.68 g, 79%). **IR** (cm^{-1}): 3101, 2972, 2934, 2204, 2049, 1731, 1726, 1724, 1632, 1466. **^1H NMR** (300 MHz, CDCl_3) δ 8.35 (2H, s, ArH), 7.94 (1H, s, ArH), 4.36 (2H, t, $J = 7.25$ CH_2), 3.61 (2H, t, $J = 5.5$ CH_2), 3.46 (2H, t, $J = 7.25$, CH_2), 2.64 (2H, t, $J = 5.5$, CH_2). **^{13}C NMR** (75.5 MHz, CDCl_3) δ 176.6, 166.4, 131.7, 130.4, 128.6, 127.4, 63.6, 38.5, 38.2, 28.3. **^{19}F NMR** (376 MHz, CDCl_3) δ -63.32. **HRMS** (ESI) calcd for $\text{C}_{14}\text{H}_{12}\text{N}_1\text{O}_3\text{Br}_1\text{F}_6$ m/z 434.9905 found 434.9905.

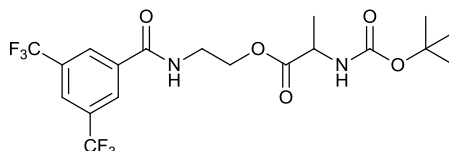
2-(4-bromobenzamido)ethyl 3,5-bis(trifluoromethyl)benzoate **239**



2-(-3,5-Bis(trifluoromethyl)phenyl)-2-oxazoline (0.84 g, 3.0 mmol), *p*-nitrobenzoic acid (0.25 g, 1.5 mmol). Purified *via* column chromatography (7:3, hexanes: EtOAc), to yield the compound as a colourless oil (0.73 g, 83%). **^1H NMR** (300 MHz, CDCl_3) δ 8.45 (2H, s, ArH), 7.91 (1H, s, ArH), 7.74 (2H, d, $J = 8.7$, ArCH), 7.47 (2H, d, $J = 8.7$, ArCH), 4.26 (2H, t, $J = 7.0$, CH_2), 3.67 (2H, t, $J = 7.0$, CH_2). **^{13}C NMR** (75.5 MHz, CDCl_3) δ 172.3, 164.3, 135.8, 134.1, 131.5, 129.1, 128.7, 125.5, 127.2, 127.1, 80.3, 55.0, 39.0. **^{19}F NMR** (376 MHz, CDCl_3) δ -63.64. **HRMS** (ESI) calcd for $\text{C}_{17}\text{H}_{32}\text{N}_1\text{O}_1\text{Fe}_1$ m/z 312.1921 found 312.1921.

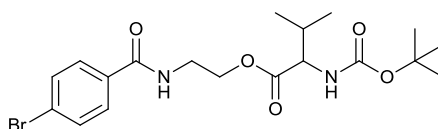
2-(2-((*tert*-butoxycarbonyl)amino)propanamido)ethyl
bis(trifluoromethyl)benzoate **240**

3,5-



2-(3,5-Bis(trifluoromethyl)phenyl)-2-oxazoline (0.84 g, 3.0 mmol), boc-Ala-OH (0.28 g, 1.5 mmol). Purified *via* column chromatography (7:3, hexanes: EtOAc), to yield the compound as a colourless oil (0.78 g, 86%). **IR** (cm^{-1}): 3106, 2976, 2934, 2211, 20496, 1731, 1728, 1718, 1632, 1459. **^1H NMR** (300 MHz, CDCl_3) δ 8.36 (2H, s, ArH), 7.89 (1H, s, ArH), 4.41-4.37 (2H, m, CH_2), 4.30 (1H, d, $J = 6.25$, CH), 3.87-3.83 (2H, m, CH_2), 2.19-2.13 (1H, m, CH), 1.47 (3H, s, CH_3), 1.35 (9H, s, CH_3). **^{13}C NMR** (75.5 MHz, CDCl_3) δ 173.8, 167.5, 155.3, 131.6, 130.4, 128.6, 127.4, 78.9, 62.3, 61.6, 38.2, 30.4, 28.6, 18.2. **^{19}F NMR** (376 MHz, CDCl_3) δ -64.21 **HRMS** (ESI) calcd for $\text{C}_{19}\text{H}_{22}\text{N}_2\text{O}_5\text{F}_6$ m/z 472.1433 found $\text{C}_{19}\text{H}_{23}\text{N}_2\text{O}_5\text{F}_6$ m/z 473.1536.

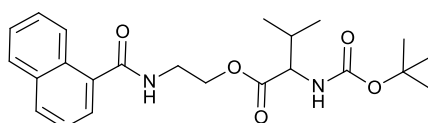
2-(2-((*tert*-butoxycarbonyl)amino)-3-methylbutanamido)ethyl 4-bromobenzoate **223**



P-bromophenyl oxazoline (0.67 g, 3.0 mmol), boc-Val-OH (0.33 g, 1.5 mmol). Purified *via* column chromatography (7:3, hexanes: EtOAc), to yield the compound as a colourless oil (0.78 g, 79%). **IR** (cm^{-1}): 3111, 2952, 2844, 2214, 2029, 1731, 1726, 1724, 1632, 1466. **^1H NMR** (300 MHz, CDCl_3) δ 7.74 (2H, d, $J = 8.7$, ArCH), 7.47 (2H, d, $J = 7.1$, ArCH), 4.37-4.33 (2H, m, CH_2), 4.29 (1H, d, $J = 6.25$,

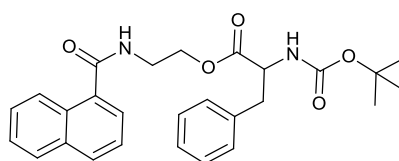
CH), 3.81-3.75 (2H, m, CH₂), 2.28-2.21 (1H, m, CH), 1.37 (9H, s, CH₃), 0.91 (6H, dd, $J = 6.5$). ¹³C NMR (75.5 MHz, CDCl₃) δ 172.8, 167.3, 155.7, 131.6, 129.7, 126.6, 125.9, 79.7, 62.3, 61.3, 38.4, 30.2, 28.9, 18.7. HRMS (ESI) calcd for C₁₉H₂₇N₂O₅Br₁ m/z 442.1103 found C₁₉H₂₈N₂O₅Br₁ m/z 443.1232.

2-(2-((*tert*-butoxycarbonyl)amino)-3-methylbutanamido)ethyl 1-naphthoate **224**



2-(Naphthalene-1-yl)oxazoline (0.59 g, 3.0 mmol), boc-Val-OH (0.33 g, 1.5 mmol). Purified *via* column chromatography (7:3, hexanes: EtOAc), to yield the compound as a colourless oil (0.67 g, 73%). IR (cm⁻¹): 3101, 2972, 2936, 2209, 2055, 1731, 1723, 1644, 1446. ¹H NMR (300 MHz, CDCl₃) δ 9.12 (1H, d, $J = 8.3$, ArH), 8.11 (1H, dd, $J = 7.5, 0.4$, ArH), 7.94 (1H, d, $J = 8.3$, ArH), 7.86 (1H, d, $J = 8.3$, ArH), 7.75 (2H, d, $J = 7.5$, ArCH), 7.63-7.57 (1H, m, ArH), 4.95 (1H, d, $J = 6.6$, CH), 4.26-4.23 (2H, m, CH₂), 3.67-3.52 (2H, m, CH₂), 2.75 (2H, d, $J = 6.6$, CH₂), 1.34 (9H, s, CH₃), 0.87 (6H, dd, $J = 7.25$). ¹³C NMR (75.5 MHz, CDCl₃) δ 172.3, 164.3, 155.4, 135.8, 134.1, 133.5, 131.5, 131.4, 131.2, 129.2, 128.7, 128.5, 128.1, 127.3, 127.1, 126.4, 126.0, 124.2, 124.0, 80.3, 64.3, 55.0, 39.0, 38.0, 28.2. HRMS (ESI) calcd for C₂₃H₃₀N₂O₅ m/z 414.2155 found C₂₃H₃₀N₂O₅Na₁ m/z 437.1934.

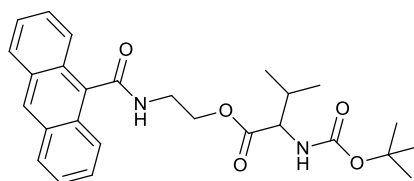
2-(2-((*tert*-butoxycarbonyl)amino)-3-phenylpropanamido)ethyl 1-naphthoate **225**



2-(Naphthalene-1-yl)oxazoline (0.59 g, 3.0 mmol), boc-phenylalanine (0.4 g, 1.5 mmol). Purified *via* column chromatography (7:3, hexanes: EtOAc) to yield the

compound as a colourless oil (0.77, 78%). **IR** (cm^{-1}): 3107, 2969, 2954, 2210, 2055, 1736, 1723, 1724, 1632, 1436. **$^1\text{H NMR}$** (300 MHz, CDCl_3) δ 9.13 (1H, d, $J = 8.5$, ArH), 8.08 (1H, dd, $J = 7.2, 0.3$, ArH), 7.92 (1H, d, $J = 8.2$, ArH), 7.84 (1H, d, $J = 8.2$, ArH), 7.78 (2H, d, $J = 7.2$, ArCH), 7.60-7.55 (1H, m, ArH), 7.49-7.41 (5H, m, ArH), 4.91 (1H, d, $J = 6.5$, CH), 4.26-4.22 (2H, m, CH_2), 3.68-3.54 (2H, m, CH_2), 2.88 (2H, d, $J = 6.5$, CH_2), 1.32 (9H, s, CH_3). **$^{13}\text{C NMR}$** (75.5 MHz, CDCl_3) δ 172.3, 167.5, 155.4, 135.8, 134.1, 131.5, 129.1, 128.7, 127.4, 125.5, 80.3, 64.2, 55.2, 39.0, 38.6, 28.6. **HRMS** (ESI) calcd for $\text{C}_{27}\text{H}_{30}\text{N}_2\text{O}_5$ m/z 462.2155 found 462.2155.

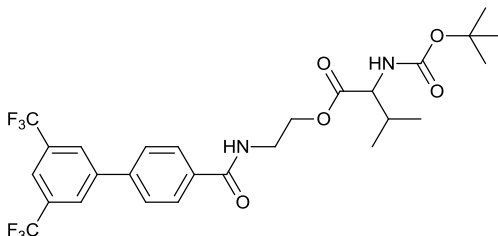
2-(2-((*tert*-butoxycarbonyl)amino)-3-methylbutanamido)ethyl anthracene-9-carboxylate **226**



2-(anthracen-9-yl)-2-oxazoline (0.74 g, 2.25 mmol), Boc-Val-OH (0.33 g, 1.5 mmol). Purified *via* column chromatography (7:3, hexanes: ethyl acetate), to yield the compound as a colourless oil (0.75 g, 70%). **IR** (cm^{-1}): 3104, 2971, 2941, 2208, 2046, 1731, 1726, 1722, 1632, 1446. **$^1\text{H NMR}$** (300 MHz, CDCl_3) δ 8.42 (3H, d, $J = 6.25$, ArH), 7.63-7.56 (2H, m, ArH), 7.31-7.24 (4H, m, ArH), 4.93 (1H, d, $J = 6$, CH), 4.26-4.23 (2H, m, CH_2), 3.67-3.52 (2H, m, CH_2), 2.99 (2H, d, $J = 6$, CH_2), 1.32 (9H, s, CH_3), 0.86 (6H, dd, $J = 7.5$, CH_3). **$^{13}\text{C NMR}$** (75.5 MHz, CDCl_3) δ 172.3, 155.4, 135.8, 134.1, 131.5, 129.1, 128.7, 125.5, 127.5, 127.1, 80.6, 64.2, 55.2, 39.0, 38.2, 28.6. **HRMS** (ESI) calcd for $\text{C}_{28}\text{H}_{34}\text{N}_2\text{O}_5$ m/z 464.2311 found 464.2312.

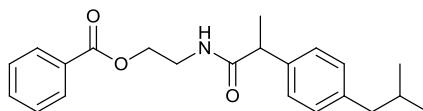
2-(2-((*tert*-butoxycarbonyl)amino)-3-methylbutanamido)ethyl bis(trifluoromethyl)-[1,1'-biphenyl]-4-carboxylate **233**

3',5'-



2-(3',5'-nistrifluoromethyl)-[1,1'-biphenyl]-4-yl)-oxazoline (1.07 g, 3.0 mmol), boc-Val-OH (0.33 g, 1.5 mmol). Purified *via* column chromatography (7:3, hexanes: ethyl acetate), to yield the compound as a colourless oil (0.91 g, 65%). **IR** (cm^{-1}): 2972, 2934, 2204, 2049, 1731, 1726, 1724, 1632, 1466 **$^1\text{H NMR}$** (300 MHz; CDCl_3) δ 8.09 (1H, d, $J = 5.25$, ArH), 7.91-7.82 (1H, m, ArH), 7.74-7.49 (5H, m, ArH), 4.35-4.30 (2H, m, CH_2), 4.27 (1H, d, $J = 6.0$, CH), 3.81 (2H, m, CH_2), 2.21 (1H, m, CH), 1.31 (9H, s, CH_3), 0.89 (6H, dd, $J = 5.5$, CH_3). **$^{13}\text{C NMR}$** (75.5 MHz; CDCl_3) δ 172.3, 164.5, 155.4, 135.8, 134.1, 131.5, 129.1, 128.7, 127.1, 124.5, 124.2, 80.3, 64.3, 55.0, 39.0, 38.0, 28.2. **$^{19}\text{F NMR}$** (376 MHz, CDCl_3) δ -62.81. **HRMS** (ESI) calcd for $\text{C}_{27}\text{H}_{30}\text{N}_2\text{O}_5\text{F}_6$ m/z 576.2059 found $\text{C}_{27}\text{H}_{31}\text{N}_2\text{O}_5\text{F}_6$ m/z 577.1934.

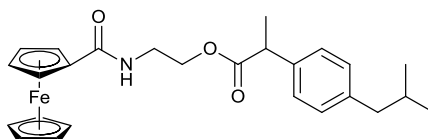
2-(2-(4-isobutylphenyl)propanamido)ethyl benzoate **241**



Phenyloxazoline (0.39 mL, 3.0 mmol), ibuprofen tablet (0.25 g, 1.5 mmol). Purified *via* column chromatography (7:3, hexanes: ethyl acetate), to yield the compound as a colourless oil (0.51 g, 93%). **$^1\text{H NMR}$** (300MHz, CDCl_3) δ 8.12 (2H, d, $J = 7.2$, ArCH), 7.65-7.59 (3H, m, ArH), 7.21 (2H, d, $J = 7.5$, ArH), 7.06 (2H, d, $J = 7.5$, ArH), 4.38 (2H, t, $J = 6.5$, CH_2), 3.78-3.69 (1H, m, CH), 3.39 (2H, t, $J = 6.5$, CH_2),

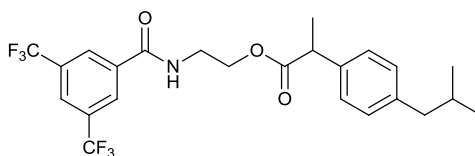
2.43 (2H, s, CH₂), 1.82-1.78 (1H, m, CH), 1.51 (3H, s, CH₃), 0.89 (6H, s, CH₃). ¹³C NMR (75.5 MHz, CDCl₃) δ 173.2, 167.5, 140.2, 134.6, 132.1, 132.0, 128.9, 127.5, 64.1, 44.5, 40.1, 38.7, 29.0, 22.1, 14.2. HRMS (ESI) calcd for C₂₂H₂₇N₁O₃ *m/z* 353.1991 found 354.1834.

2-(2-(4-isobutylphenyl)propanamido)ethyl ferrocenecarboxylate **242**



Ferroceneoxazoline (0.76 g, 3.0 mmol), ibuprofen tablet (0.25 g, 1.5 mmol). Purified *via* column chromatography (7:3, hexanes: ethyl acetate), to yield the compound as an orange oil (0.68 g, 89%). ¹H NMR (300MHz, CDCl₃) δ 7.22 (2H, d, *J* = 6.25, ArH), 7.08 (2H, d, *J* = 6.25, ArH), 4.36 (2H, t, *J* = 6.0, CH₂), 4.18 (2H, s, FcH), 4.14 (2H, s, FcH), 4.09 (5H, s, FcH) 3.77-3.70 (1H, m, CH), 3.42 (2H, t, *J* = 6.0, CH₂), 2.29 (2H, s, CH₂), 1.85-1.81 (1H, m, CH), 1.53 (3H, s, CH₃), 0.90 (6H, s, CH₃) ¹³C NMR (75.5 Hz, CDCl₃) δ 172.36, 167.5, 140.2, 134.6, 132.1, 132.0, 128.9, 127.5, 72.7, 72.3, 71.6, 70.8, 64.5, 45.0, 41.3, 39.1, 29.6, 22.3, 14.5. HRMS (ESI) calcd for C₂₆H₃₁N₁O₃Fe₁ *m/z* 461.1653 found 461.1655.

2-(2-(4-isobutylphenyl)propanamido)ethyl 3,5-bis(trifluoromethyl)benzoate **243**



2-(3,5-Bis(trifluoromethyl)phenyl)-2-oxazoline (0.84 mL, 3.0 mmol), ibuprofen tablet (0.25 g, 1.5 mmol). Purified *via* column chromatography (7:3, hexanes: ethyl acetate), to yield the compound as a colourless oil (0.80 g, 91%). ¹H NMR (300MHz, CDCl₃) δ 8.37 (2H, s, ArCH), 7.86 (1H, s, ArH), 7.24 (2H, d, *J* = 7.5,

ArH), 7.16 (2H, d, $J = 7.5$, ArH), 4.34 (2H, t, $J = 5.5$, CH₂), 3.74-3.66 (1H, m, CH), 3.42 (2H, t, $J = 5.5$, CH₂), 2.45 (2H, s, CH₂), 1.84-1.79 (1H, m, CH), 1.54 (3H, s, CH₃), 0.88 (6H, s, CH₃). ¹³C NMR (75.5 Hz, CDCl₃) δ 172.5, 167.8, 140.4, 134.3, 132.6, 132.3, 132.0, 128.7, 127.3, 124.2, 64.3, 44.1, 40.3, 38.9, 29.3, 22.5, 14.6. **HRMS** (ESI) calcd for C₂₄H₂₅N₁O₃F₆ m/z 489.1739 found 489.1738.

8 References

1. Terry, L. A.; White, S.F.; Tigwell, L. J. *Journal of Agricultural and Food Chemistry*. **2005**, 53, 1309–1316.
2. Pohanka, M.; Skladal, P.; Kroea, M. *Defence Science Journal*. **2007**, 57, 185–193.
3. Dorst, B. V.; Mehta, J.; Bekaert, K.; Rouah-Martin, E.; Coen, W. D.; Dubruel, P.; Blust, R.; Robbens, J. *Biosensors and Bioelectronics*. **2010**, 26, 1178–1194.
4. Vo-Dinh, T.; Cullum, B.; *Fresenius J. Anal. Chem.* **2000**, 366, 540–551
5. Thevenot, D. R.; Toth, K.; Durst, R. A.; Wilson, G. S. *Biosensors and Bioelectronics*, **2001**, 16, 121–131.
6. Malhotra, B.D.; Chaubey, A. *Sensors and Actuators B: Chemical*. **2003**, 91, 117–127.
7. Lhong, J. H. T.; Male, K. B.; Glennon, J. D. *Biotechnology Advances*, **2008**, 26, 492–500.
8. Ronkainen, N. J.; Halsall, H. B.; Heineman, W. R. *Chem. Soc. Rev.* **2010**, 39, 1747–1763.
9. Ligler, F. S. *Anal. Chem*, **2009**, 81, 519–526.
10. Ivnitski, D.; Abdel-Hamid, I.; Atanasov, P.; Wilkins, E. *Biosensors and Bioelectronics*, **1999**, 14, 599–624.
11. Newman, J. D.; Seford, S. J. *Molecular Biotech.* **2006**, 32, 249–268.
12. Caygill, R. L.; Blair, G. E.; Millner, P. A. *Analytica Chimica acta*. **2010**, 681, 8–15.
13. Palecek, E.; Bartosik, M. *Chem. Rev.* **2012**, 112, 3427–3481.
14. Struss, A.; Pasini, P.; Ensor, C. M.; Raut, N.; Daunet, S. *Anal Chem*. **2010**, 82, 4457–4463.
15. Gruhl, F. J.; Rapp, B. E.; Lunge, K. *Adv. Biochem. Engin/ Biotechnol.* **2012**, 1–34.
16. Strianese, M.; Staiano, M.; Ruggiero, G.; Labella, T.; Pellicchic, C.; D'Auria, S. *Spectroscopic Methods of Analysis*. **2012**, 875, 193–216.

17. Drummond, G. T.; Hill, M. G.; Barton, J. K. *Nature Biotech.* **2003**, 21, 1192–1199.
18. Palecek, E.; Fojta, m.; Jelen, F. *Bioelectrochemistry.* **2002**, 56, 85–90.
19. Saiki, R. K.; Bugawan, T. L.; Horn, G. T.; Mullis, K. B. *Nature.* **1986**, 324, 163–166.
20. Embury, S. H.; Scherf, S. J.; Saiki, R. K.; Gholson, M. A.; Golbus, M.; Arnheim, N.; Erlich, H. A. *N. Engl. J. Med.* **1987**, 316, 656–661.
21. Wang, J.; Liu, G.; Polsky, R.; Merkoci, A. *Electrochem Commun.* **2002**, 4, 722–726.
22. Popovich, N. D.; Thorp, H. H. *Interface.* **2002**, 11, 30–34.
23. Palecek, E. *Electroanalysis.* **1996**, 8, 7–14.
24. De-los-Santos-Alvarez, P.; Lobo-Castanon, M. J.; Miranda-Oridieres, A. J.; Tunon-Blanco, P. *Anal. Chem.* **2002**, 74, 3342–3347.
25. Wang, J.; Kawde, A.-N. *Analytica Chimica Acta.* **2001**, 431, 219–224.
26. Wang, J, Xu, D.; Polsky, R. *J. Am. Chem. Soc.* **2002**, 124, 4208–4209.
27. Thorp, H. H.; Ropp, P. A.; Yang, I. V. *Anal. Chem.* **2002**, 74, 347–354.
28. Kannan, B.; Williams, D. E.; Booth, M. A.; Travas-Sejdic, J. *Anal. Chem.* **2011**, 83, 3415–3421.
29. Millan, K. M.; Mikkelsen, S. R. *Anal. Chem.* **1993**, 65, 2317–2323.
30. Garcia, T.; Revenga-Parra, M.; Abruna, H. D.; Pariante, F.; Lorenzo, E. *Anal. Chem.* **2008**, 80, 77–84.
31. Cranshaw, J. M.; Gravas, D. E.; Denny, W. A.; *Biochemistry.* **1995**, 34, 13682–13687.
32. Ferguson, L. R.; Denny, W. A.; *Mutation Research/Fundamental and Molecular Mechanisms of Mutagenesis.* **2007**, 623, 14–23.
33. Chen, J.; Zhang, J.; Huang, L.; Lin, X.; Chen, G. *Biosensors and Bioelectronics.* **2008**, 24, 349–355.
34. Gao, Z.; Tansil, N. *Anal. Chemi. Acta.* **2009**, 636, 77–82.
35. Wong, E. L. S.; Gooding, J. J. *Anal. Chem.* **2006**, 78, 2138–2144.
36. Hvastkov, E. G.; Buttry, D. A. *Anal. Chem.* **2007**, 79, 6922–6926.
37. Jelen, F.; Erdem, A.; Palecek, E. *Bioelectrochemistry.* **2002**, 55, 165–167.
38. Giovannageli, C.; Montenay-Garestier, T.; Rougee, M.; Classignol, M.; Thuong, N.T.; Helene, C. *J. Am. Chem. Soc.* **1991**, 113, 7775–7777.

39. Gross, A.; Husken, N.; Schur, J.; Raszeja, L.; Ott, I.; Metzler-Nolte, N. *Bioconjugate Chemistry*. **2012**, *23*, 1764–1774.
40. Duwensee, H.; Mix, M.; Broer, I.; Flechsig, G. –U. *Electrochemistry commun.* **2009**, *11*, 1487–1491.
41. Hocek, M.; Fojta, M. *Chem. Soc. Rev.* **2011**, *40*, 5802–5814.
42. Wanninger-Weiss, C.; Wagenknecht, H. –A. *Eur. J. Org. Chem.* **2008**, 64–71.
43. Fencft, L.A.; Bouamied, I.; Thoni, S.; Amoit, N.; Stulz, E. *J. Am. Chem. Soc.* **2002**, *129*, 15319–15329.
44. Weizman, H.; Tor, Y. *J. Am. Chem. Soc.* **2002**, *124*, 1568–1569.
45. Verhijen, J. C.; van der Marel, G. A.; van Boom, J. H.; Metzler-Nolte, N. *Bioconjugate Chemistry*. **2000**, *11*, 741–743.
46. Mitra, R.; Ganesh, K. N.; *J. Org. Chem.* **2012**, *77*, 5696–5704.
47. Gross, A.; Husken, N.; Schur, J.; Raszeja, L.; Ott, I.; Metzler-Nolte, N. *Bioconjugate Chem.* **2012**, *23*, 1764–1774.
48. Hu, X.; Smith, G. D.; Sykora, M.; Lee, S. J.; Grinstaff, M. W. *Inorg. Chem.* **2000**, *39*, 2500–2504.
49. Zhang, J.; Qi, H.; Li, Y.; Yang, J.; Gao, Q.; Zhang, C. *Anal. Chem.* **2008**, *80*, 2888–2894.
50. Kumamoto, S.; Watanabe, M.; Kowakami, N.; Nakamura, M.; Yamana, K. *Bioconjugate Chem.* **2008**, *19*, 65–69.
51. Yamana, K.; Mitsui, T.; Yoshioka, J.; Isuno, T.; Nakano, N. *Bioconjugate Chem.* **1996**, *7*, 715–720.
52. Hu, X.; Tierney, M. T.; Grinstaff, M. W. *Biocnjugate Chem.* **2002**, *13*, 83–89.
53. Liu, S.; Hu, Y.; Jin, J.; Zhang, H.; Cai, C. *Chem Commun.* **2009**, *45*, 1635–1637.
54. Tierney, M. T.; Grinstaff, M. W. *J. Org. Chem.* **2000**, *65*, 5355–5359.
55. Ricci, F.; Lai, R. Y.; Plaxco, K. W. *Chem Commun.* **2007**, 3768–3770.
56. Jacobsen, M. F.; Ferapontova, E. E.; Gothelf, K. V. *Org. Biomol. Chem.* **2009**, *7*, 905–908.
57. Wu, J.; Huang, C.; Cheng, G.; Zhang, F.; He, P.; Fang, Y. *Electrochemistry Comm.* **2009**, *11*, 177–180.

58. Kim, D. -K.; Yoo, S. M.; Park, T. J.; Yoshikawa, H.; Tamiya, E.; Park, J. Y.; Lee, S. Y. *Anal. Chem.* **2011**, 83, 6215–6222.
59. Wang, J. *Analyst.* **2005**, 130, 421–426.
60. Li, Y.; Schlusener, H. J.; Xu, S. *Gold Bulletin.* **2010**, 43, 29–41.
61. Pingarron, J. M.; Yanez-Sedeno, P.; Gonzalez-Cortes, A. *Electrochimica Acta.* **2008**, 53, 5848–5866.
62. Cheng, Y.; Stakenborg, T.; Dorpe, P. V.; Lagae, L.; Wang, M.; Chen, H.; Borghs, G. *Anal. Chem.* **2011**, 83, 1307–1314.
63. Wang, J.; Lin, G.; Merkoci, A. *J. Am. Chem. Soc. Commun.* **2003**, 125, 3214–3215.
64. Kwon, S. J.; Bard, A. J. *J. Am. Chem. Soc.* **2012**, 134, 10777–10779.
65. Sassolas, A.; Leca-Bouvier, B. D.; Blum, L. S. *Chem. Rev.* **2008**, 108, 109–139.
66. Peng, L.; Wollenberger, U.; Kinne, H.; Hofrichter, M.; Ulleich, R.; Scheibner, K.; Fischer, A.; Scheller, F. W. *Biosensors and Bioelectronics.* **2010**, 26, 1432–1436.
67. Miranda-Castro, R.; Lobo-Castanon, M. J.; Miranda-Ordieres, A. J.; Tunon-Blanco, P. *Electroanalysis.* **2010**, 22, 1297–1305.
68. He, W.; Yang, Q.; Liu, Z.; Yu, X.; Xu, D. *Anal. Lett.* **2005**, 38, 2567–2578.
69. Manrao, E. A.; Darrington, I. M.; Leszlo, A. H.; Langford, K. W.; Hopper, M. K.; Gillgren, N.; Pavlenok, M.; Niederweis, M.; Gandlach, J. M. *Nature Biotech.* **2012**, 30, 349–353.
70. Ashkenasy, N.; Sanchez-Quesada, J.; Bayley, H.; Ghadiri, M. R. *Angew. Chem. Int. Ed.* **2005**, 44, 1401–1404.
71. Schneider, G. F.; Kowalczyk, S. W.; Calado, V. E.; Pandraud, G.; Zandbergen, H. W.; Vandersypen, L. M. K.; Dekker, C. *Nanoletts.* **2010**, 10, 3163–3167.
72. Dekker, C. *Nat. Nanotechnol.* **2007**, 2, 209–215.
73. Fischkein, M. D.; Drndic, M. *Appl. Phys. Lett.* **2008**, 93, 11307–11309.
74. Cheley, S.; Gu, L. O. Q.; Bayley, H. *Chem. Biol.* **2002**, 9, 829–838.
75. Bayley, H.; Cremer, P. S. *Nature.* **2001**, 413, 226–230.
76. Choi, Y. -E.; Kwak, J. -W.; Park, J. W. *Sensors.* **2010**, 10, 428–435.
77. Vercootere, W.; Winters-Hilt, S.; Olsen, H.; Deamer, D.; Haussler, D.; Akeson, M. *Nature Biotech.* **2001**, 19, 248–252.

78. Shendure, J.; Mitra, R. D.; Varma, C.; Church, G. M. *Nature Reviews*. **2004**, 5, 335–344.
79. Branton, D.; Deamer, D. W. *Acc. Chem. Res.* **2002**, 35, 817–825.
80. Harrell, C. C.; Choi, Y.; Horne, L. P.; Baker, L. A.; Siwy, Z. S.; Martin, C. R. *Langmuir*. **2006**, 22, 10837–10843.
81. Novoselov, K. S.; Jiang, Z.; Zhang, Y.; Morozov, S. V.; Stormer, H. L.; Zeitler, V.; Maan, J. C.; Boebinger, G. S.; Kim, P.; Geim, A. K. *Science*. **2008**, 315, 1379–1382.
82. Fischbein, M. D.; Drndic, M. *App. Phys. Lett.* **2008**, 93, 113107–113109.
83. Garaj, S.; Hubbard, W.; Riena, A.; Kong, J.; Branton, D.; Golovchenko, J. A. *Nature Lett.* **2010**, 467, 190–193.
84. Merchant, C. A.; Healy, K.; Wanunu, M.; Ray, V.; Peterman, N.; Bartel, J.; Fischbein, M. D.; Venta, K.; Luo, Z.; Johnson, A. T. C.; Drndic, M. *Nanolett.* **2010**, 10, 2915–2921.
85. Atkinson, R. C. J.; Gibson, V. C.; Long, N. J. *Chem. Soc. Rev.* **2004**, 33, 313–328.
86. Arrayas, R. G.; Adrio, J.; Carretero, J. C. *Angew. Chem. Int. Ed.* **2006**, 45, 7674–7715.
87. Lucarelli, F.; Tombelli, S.; Minunni, M.; Marrazza, G.; Mascini, M. *Anal. Chimi. Acta.* **2008**, 609, 139–159.
88. Silva, M. E. N. P. R. A.; Pomborio, A. J. L. *J. Org. Chem.* **1994**, 480, 81–85.
89. Wang, J. *Electroanalysis.* **2001**, 13, 983–988.
90. Patwa, A. N.; Gonnade, R. G.; Kumar, V. A.; Bhadbhade, M. M.; Ganesh, K. N. *J. Org. Chem.* **2010**, 75, 8705–8709.
91. Nguyen, H. V.; Sallustrau, A.; Male, L.; Thornton, P. J.; Tucker, J. H. R. *Organometallics.* **2011**, 30, 5284–5290.
92. Ong, C-W.; Jeng, J-Y.; Juang, S-S.; Chen, C-F. *Bioorganic Med. Chem.* **1992**, 2, 929–932.
93. Takenaka, S.; Uto, Y.; Saita, H.; Yokoyama, M.; Kondo, H.; Wilson, W. D. *Chem Commun.* **1998**, 1111–1112.
94. Sato, S.; Takenaka, S. J. *J. Organomet. Chem.* **2008**, 693, 1177–1185.
95. Takenaka, S.; Uto, Y.; Kondo, H.; Ihara, T.; Takagi, M. *Anal. Biochem.* **1994**, 218, 436–443.

96. Wang, X.; Dong, P.; Yun, W.; Xu, Y.; He, P.; Fang, Y. *Biosensors and Bioelectronics*. **2009**, *24*, 3288–3292.
97. Kang, D.; Zuo, X.; Yang, R.; Xia, F.; Plaxco, K. W.; White, R. J. *Anal. Chem.* **2009**, *81*, 9109–9113.
98. Zuo, X.; Song, S.; Zhang, J.; Pan, D.; Wang, L.; Fan, C. *J. Am. Chem. Soc. Commun.* **2007**, *129*, 1042–1043.
99. Umek, R. M.; Lin, S. W.; Vielmetter, J.; Terbrueggen, R. H.; Irvine, B.; Yu, C. J.; Keyyem, J. F.; Yowanto, H.; Blackburn, G. F.; Chen, Y. -P.; Farkas, D. H. *J. molecular Diagnostics*. **2001**, *3*, 74–84.
100. Hausen, M. N.; Farjami, E.; Kristiansen, M.; Clima, L.; Pederson, S. V.; Dausjerg, K.; Ferapontova, E. E.; Gothelf, K. V. *J. Org. Chem.* **2010**, *75*, 2474–2481.
101. Chatelain, C.; Chaix, C.; Brisset, H.; Moustrou, C.; Fayes, F.; Mandrand, B. *Sensors and Actuators B*. **2008**, *132*, 439–442.
102. Broude, N. E. *Trends in Biotechnology*. **2002**, *20*, 249–256.
103. Guo, J.; Ju, J.; Turro, N. J. *Analytical and Bioanalytical Chemistry*. **2012**, *402*, 3115–3125.
104. Chatelain, G.; Ripert, M.; Farre, C.; Ansanay-Alex, S.; Chaix, C. *Electrochimica Acta*. **2012**, *59*, 57–63.
105. Meade, T. J.; Bertin, P. A. *Tet. Let.* **2009**, 5409–5412.
106. Husken, N.; Gebala, M.; Schuhmann, W.; Meltzler-Nolte, N. *ChemBioChem*. **2010**, *11*, 1175–1761.
107. Zhang, Y.; Wang, Y.; Wang, H.; Jiang, J.-H.; Shen, G. L.; Yu, R.-Q, Li, J. *Anal. Chem.* **2009**, *81*, 1982–1987.
108. Yang, W.; Lai, R. Y. *Electrochemistry Comm.* **2011**, *12*, 989–992.
109. Yu, C. J.; Wan, Y.; Yowanto, H.; Li, J.; Tao, C.; James, M. D.; Tan, C. L.; Blackburn, G. F.; Meade, T. J. *J. Am. Chem. Soc.* **2001**, *123*, 11155–11161.
110. Beilstein, A. E.; Grinstaff, M. W. *J. Organomet. Chem.* **2001**, *637-639*, 398–406.
111. Pearce, D. M.; Shenton, D. P.; Holden, J.; Gaydos, C. A. *IEEE Transactions on Biomedical Engineering*. **2011**, *58*, 755–758.
112. Hillier, S. C.; Frost, C.G.; Jenkins, A. T. A.; Flower, S.E.; Keay, R.; Braven, H.; Clarkson, J. *Bioelectrochemistry*. **2004**, *63*, 307–310.

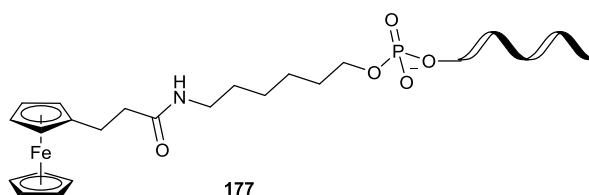
113. Hillier, S. C.; Frost, C.G.; Jenkins, A. T. A.; Flower, S.E.; Keay, R.; Braven, H.; Clarkson, J. *Electrochem. Comm.* **2004**, 6, 1227–1232.
114. Chahima, M'L.; Lee, J. S.; Kraatz, H-B. *J. Organomet. Chem.* **2002**, 648, 81–86.
115. Batterjee, S. M.; Marzouk, M. I.; Aazab, M. E.; El-Hashash, M. A. *Appl. Organometal. Chem.* **2003**, 17, 291–297.
116. Wilkinson, G.; Rosenblum, M.; Whiting, M. C.; Woodward, R. B. *J. Am. Chem. Soc.* **1952**, 74, 2125–2126.
117. Rosenblum, M.; Brawn, N.; Papenmeier, J.; Applebaum, M. *J. Organomet. Chem.* **1966**, 6, 173–180.
118. Plazuk, D.; Zakrzewski, J.; Salmain, M. *Org. Biomol. Chem.* **2011**, 9, 408–417.
119. Kelly, A. K.; Katif, N.; James, T. D.; Marken, F. *New. J. Chem.* **2010**, 34, 1225–1492.
120. El – Sagheer, A. H.; Brown, T. *Chem. Soc. Rev.* **2010**, 39, 1388–1405.
121. Bolton, E. S.; Pauson, P. L.; Sandhu, M. A.; Watts, W. E. *J. Chem. Soc.* **1962**, 26, 2260–2263.
122. Lednicer, D.; Hauser, C. R. *Org. Synth.* **1960**, 40, 31–34.
123. Frump, J.A. *Chem. Rev.* **1971**, 71, 483–505.
124. Genet, J. P.; Thorimbert, S.; Touzin, A. M. *Tetrahedron Lett.* **1993**, 34, 1159-1162
125. Mohammadpoor-Baltork, I.; Khosropour, A. R.; Hojati, S. F. *Synlett.* **2005**, 2747-2750
126. Ishihara, M.; Togo, H. *Synlett.* **2006**, 227-230
127. Guirg, P. J.; McManus, H. A. *Chem. Rev.* **2004**, 104, 4151-4202
128. Wiesbrock, F.; Hoogenboom, R.; Leenen, M. A. M.; Meier, M. A. R.; Schubert, U. S. *Macromolecules.* **2005**, 38, 5025-5034
129. Hoogenboom, R.; Schubert, U. S. *Green Chem.* **2006**, 8, 895-899
130. Hoogenboom, R. *Macromol. Chem. Phys.* **2007**, 208, 18-25
131. Vorbruggen, H.; Krolkiewicz, K. *Tetrahedron.* **1993**, 49, 9353-9372
132. Whelligan, D. K.; Bolm, C. *J. Org. Chem.* **2006**, 71, 4609-4618
133. Kangani, C. O.; Kelley, D. E.; Day, B. W. *Tetrahedron Lett.* **2006**, 47, 6497-6499

134. Katritzky, A. R.; Cai, C. M.; Suzuki, K.; Singh, S. K. *J. Org. Chem.* **2004**, *69*, 811-814
135. Witte, H.; Seeliger, W. *Liebigs. Ann. Chem.* **1974**, 996-1009
136. Anastassiadou, M.; Baziard-Mouysset, G.; Payard, M. *Synthesis.* **2000**, 1814-1819
137. Wu, J.; Sun, X.; Xia, H. *Tetrahedron Lett.* **2006**, *47*, 1509-1511
138. Suyama, S. *Synlett*, **2006**, *10*, 1479-1484
139. Ishihara, M.; Togo, H. *Tetrahedron*, **2007**, *63*, 1474-1480
140. Kempe, K.; Lobert, M.; Hoogenboom, R.; Schubert, U. S. *J. Comb. Chem.* **2009**, *11*, 274-280
141. Pfister, K.; Robinson, C. A.; Schabic, A. C.; Tishler, M. *J. Amer. Chem. Soc.* **1949**, *71*, 1101-1105
142. Lambert, R. F.; Kristofferson, C. E. *J. Org. Chem.* **1965**, *30*, 3938-3943.
143. Kagiya, T.; Narisawa, S.; Maeda, T.; Fukui, K. *J. Polym. Sci, Part B.* **1966**, *4*, 257-260.
144. Seeliger, W. *Chem. Abstr.* **1966**, *65*, 7383-7386.
145. Saegusa, T.; Fujii, H.; Ikeda, H. *J. Polym. Chem.* **1972**, *3*, 35-39
146. Jerca, V. V.; Nicolescu, F. A.; Baran, A.; Anghel, D. F.; Vasilescu, D. S.; Vuluga, D. M. *Reactive and Functional Polymers.* **2010**, *70*, 827-835
147. Braga, A. L.; Galetto, F. Z.; Taube, P. S.; Paixão, M. W.; Silveira, C. C.; Singh, D.; Vargas, F. *J. Organomet. Chem.* **2008**, *693*, 3563-3566
148. Lee, S. -H.; Bok, J.; Qi, X.; Kim, S. K.; Lee, Y.-S.; Yoon, J. *Tetrahedron Letts.* **2007**, *48*, 7309-7312
149. Fernandez-Megia, E.; Paz, M. M.; Sardina, F. T. *J. Org. Chem.* **1994**, *59*, 7643-7647
150. Charvillon, F. B.; Amouroux, R. *Synth. Commun.* **1997**, *27*, 395-399.
151. Laaziri, A.; Uziel, J.; Jugé, S. *Tetrahedron Assym.* **1998**, *9*, 437-447
152. Huang, Y.; Dalton, D. R.; Carroll, P. J. *J. Org. Chem.* **1997**, *62*, 372-376.
153. Catusus, M.; Bueno, A.; Mayano, A.; Maestro, M. A.; Mahia, J. *J. Organomet. Chem.* **2002**, *642*, 212-216.
154. Navarro, A.-E.; Spinelli, N.; Moustrou, C.; Chaix, C.; Mandrand, B.; Brisset, H. *Nucleic Acids Research.* **2004**, *32*, 5310-5319.
155. Galangau, O.; Dumas-Verdes, C.; Schmidt, E. Y.; Trofimov, B. A.; Clavier, G. *Organometallics.* **2011**, *30*, 6476-6481.

156. Long, B.; Liang, S.; Xin, D.; Yang, Y.; Xiang, J. *Eur. J. Medicinal Chem.* **2009**, *44*, 2572–2576.
157. Kalita, D.; Morisue, M.; Kobuke, Y. *New. J. Chem.* **2006**, *30*, 77–92.
158. Bejblova, M.; Zones, S. I.; Cejka, J. *Applies Catalysis.* **2007**, *327*, 255–260.
159. Routaboul, L.; Chiffre, J.; Balavoine, G. G. A.; Daran, J.-C.; Manoury, E. *J. Organomet. Chem.* **2001**, *637*, 364–371.
160. SaiSudhir, V.; PhaniKumar, N. Y.; Chandrasekaran, S. *Tetrahedron.* **2010**, *66*, 1327–1334.
161. Plazuk, D.; Zakrzewski.; Salmain, M. *Org. Biomol. Chem.* **2011**, *9*, 408–417.
162. Delavaux-Nicot, B.; Guari, Y.; Mathieu, R. *J. Organomet. Chem.* **1995**, *489*, 87–89.
163. Tsukazaki, M.; Tinkl, M.; Roglans, A.; Chapell, B. J.; Taylor, N. J.; Snieckus, V. *J. Am. Chem. Soc.* **1996**, *118*, 685–686.
164. Zhang, H.; Bian, Z. *J. Organomet. Chem.* **2007**, *692*, 5687–5689.
165. Khrushcheva, N. S.; Sokolov, V. I. *Russian Chemical Bulletin Int. Ed.* **2004**, *53*, 830–833.
166. Lednicer, D.; Hauser, C. R. *Org. Synth.* **1960**, *40*, 31–34.
167. Richards, C. J.; Damalidis, T.; Hibbs, D. E.; Hursthouse, M. B. *Synlett.* **1995**, 74–76.
168. Richards, C. J.; Mulvaney, A. W. *Tet. Ass.* **1996**, *7*, 1419–1430.
169. Kita, Y.; Nishii, Y.; Higuchi, T.; Mashima, K. *Angew. Chem. Int. Ed.* **2012**, *51*, 5723–5726.

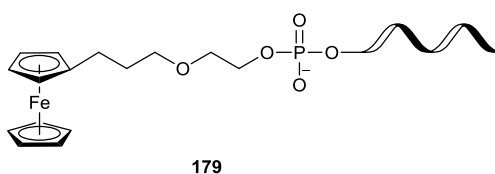
9 Appendix

Table 1. Assay volumes for probe 177



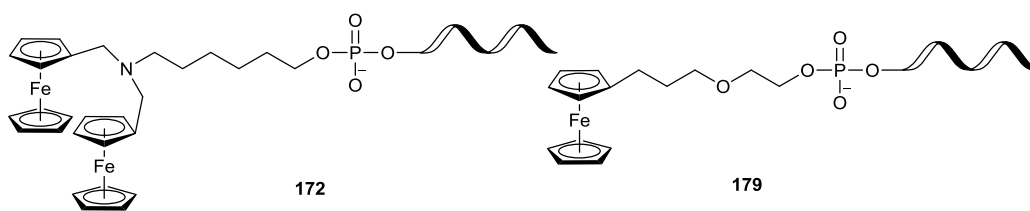
Reagent	1 x rxn (μL)	Positive 4 x rxn (μL)	Negative 4 x rxn (μL)
177	0.6	2.4	2.4
Synth target DNA	1	4	/
MgCl₂	4	16	16
10x Atlas PCR buffer	2	8	8
T7	0.2	0.8	0.8
H₂O	12.2	46.4	52

Table 2. Assay volumes for probe 179



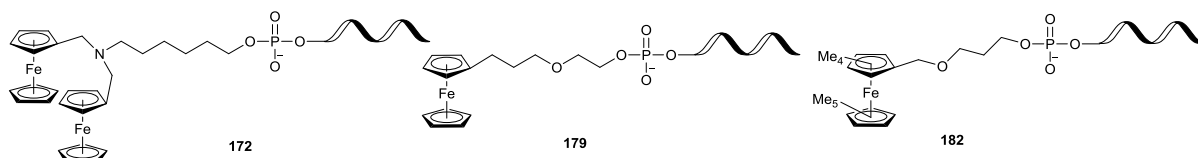
Reagent	+ve rxn (μL)	-ve 4x rxn (μL)
179	2.4	2.4
Synth. Target DNA	4	0
MgCl₂	16	16
10x Atlas PCR buffer	8	8
T7	0.8	0.8
H₂O	48.8	52

Table 3. Assay reaction volumes for the duplex between probes 172 and 179



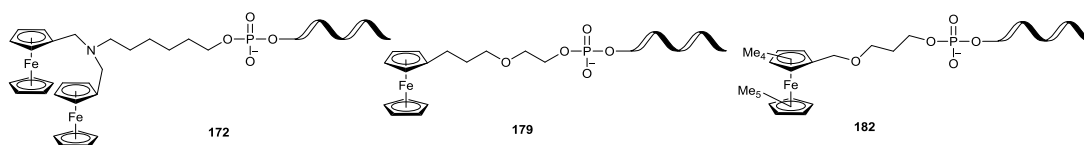
Reagent	Positive 4 x rxn (μL)	Negative 4 x rxn (μL)
172	2.4	2.4
179	2.4	2.4
Synth target DNA	4	/
MgCl ₂	16	16
10x Atlas PCR buffer	8	8
T7	0.8	0.8
H ₂ O	46.4	52

Table 4. Assay reaction volumes for the triplex between probes 172, 179 and 182



Reagent	Positive 4 x rxn (μL)	Negative 4 x rxn (μL)
172	1.5	1.5
179	4.5	4.5
182	4.5	4.5
Synth target DNA	7.45	/
MgCl ₂	16	16
10x Atlas PCR buffer	8	8
T7	0.8	0.8
H ₂ O	44.9	50.5

5. Assay reaction volumes for the triplex between probes 172, 179 and 182



Reagent	Positive 4 x rxn (μL)	Negative 4 x rxn (μL)
172	0.5	0.5
179	4.5	4.5
182	4.5	4.5
Synth target DNA	7.45	/
MgCl ₂	16	16
10x Atlas PCR buffer	8	8
T7	0.8	0.8
H ₂ O	45.9	51.5